Advances in Atom and Single Molecule Machines
Series Editor: Christian Joachim

Francesca Moresco
Christian Joachim *Editors*

Single Molecule Mechanics on a Surface

Gears, Motors and Nanocars

Springer

Advances in Atom and Single Molecule Machines

Series Editor

Christian Joachim, GNS, CNRS, Toulouse Cedex, France

Editorial Board

Leonhard Grill, Institut für Chemie, Karl-Franzens-Universität Graz, Graz, Steiermark, Austria

Fedor Jelezko, Institute of Quantum Optics, Ulm University, Ulm, Baden-Württemberg, Germany

Masanori Koshino, Chemistry and Materials, National Institute of Advanced Industrial Science and Technology, Tsukuba, Ibaraki, Japan

David Martrou, Nanosciences Group, Centre d'Élaboration de Matériaux et d'Etudes Structurales, Toulouse, France

Tomonobu Nakayama, National Institute for Materials Science, Tsukuba, Ibaraki, Japan

Gwénaël Rapenne, Centre d'Élaboration de Matériaux et d'Etudes Structurales, Toulouse, France

Françoise Remacle, Chemistry, University of Liege, Liège, Belgium

Advances in Atom and Single Molecule Machines is the first comprehensive series of books dealing specifically with single atom and molecule machines. Derived from a number of long-term European Commission Future and Emerging Technologies (FET) projects including AtMol, Elfos, Focus, Diamant, Artist, PAMS and MEMO, volumes in this series comprise topical reviews, lecture-course derived textbooks and re-worked proceedings of workshops.

Francesca Moresco · Christian Joachim
Editors

Single Molecule Mechanics on a Surface

Gears, Motors and Nanocars

Springer

Editors
Francesca Moresco
Centre for Advancing Electronics Dresden
Technische Universität Dresden
Dresden, Sachsen, Germany

Christian Joachim
Pico-Lab CEMES-CNRS
Centre d'Élaboration de Matériaux et
d'Etudes Structurales
Toulouse, France

ISSN 2193-9691 ISSN 2193-9705 (electronic)
Advances in Atom and Single Molecule Machines
ISBN 978-3-031-16929-8 ISBN 978-3-031-16930-4 (eBook)
https://doi.org/10.1007/978-3-031-16930-4

© The Editor(s) (if applicable) and The Author(s), under exclusive license to Springer Nature Switzerland AG 2023
This work is subject to copyright. All rights are solely and exclusively licensed by the Publisher, whether the whole or part of the material is concerned, specifically the rights of translation, reprinting, reuse of illustrations, recitation, broadcasting, reproduction on microfilms or in any other physical way, and transmission or information storage and retrieval, electronic adaptation, computer software, or by similar or dissimilar methodology now known or hereafter developed.
The use of general descriptive names, registered names, trademarks, service marks, etc. in this publication does not imply, even in the absence of a specific statement, that such names are exempt from the relevant protective laws and regulations and therefore free for general use.
The publisher, the authors, and the editors are safe to assume that the advice and information in this book are believed to be true and accurate at the date of publication. Neither the publisher nor the authors or the editors give a warranty, expressed or implied, with respect to the material contained herein or for any errors or omissions that may have been made. The publisher remains neutral with regard to jurisdictional claims in published maps and institutional affiliations.

This Springer imprint is published by the registered company Springer Nature Switzerland AG
The registered company address is: Gewerbestrasse 11, 6330 Cham, Switzerland

Preface

Mechanics with a single molecule starts with a dimer: vibrating, rotating, flying randomly and possibly dissociating in the gas phase. Adsorbed on a surface, such a dimer can also vibrate, rotate, desorb or dissociate. Preserving the dimer integrity on the surface requires that its electronic wave function is intrinsically coherent while its mechanical di-nuclear wave function can be preserved or not. On a surface, this mechanical wave function becomes semi-classical by decoherence. Here, vibration and rotation are therefore becoming classical.

This book is about the mechanics of larger multi-atomic molecules, large enough that their collective mechanical motions become almost classical by themselves. Going from a dimer to such large molecule opens the path to design single molecule mechanical machinery. When adsorbed on a proper metallic surface, it is known that already a single PF3 molecule can alone works like a single molecule-gear (See Volume 13 of this series). While remaining well below the number of atoms entering in the chemical composition of a protein but increasing this number in a covalent manner from the PF3 molecule to, for example, 50 to 100 atoms, then a single molecule can become alone on a surface a molecule-wheel, a molecule-gear, a molecular train of gears, a molecule-motor, a molecule-car or even a molecular mechanical calculator.

This book presents different examples of single molecule mechanical machinery, each molecule functioning one at a time while adsorbed on a surface. This functioning (random or not?) can be made possible by the energy extracted from the surface by the molecule alone or using part of the energy provided using the atomic apex of the tip of a scanning tunneling microscope. This book results from the MEMO workshop "Single Molecule Machines on a Surface Gears, Train of Gears, Motors, and Cars" held in Toulouse (France) during November 24–25, 2021. It also results from the second International Nanocar Race II organized in Toulouse by MEMO during the March 24–25, 2022. Mechanics with molecules (MEMO) was an H2020 FET European project from 2017 to 2022.

We have regrouped in this volume general considerations concerning single molecule mechanics on a surface like unidirectional motion, the corresponding molecular synthesis and the required surface adsorption calculations. Four teams

having participated to Nanocar Race II are presenting their molecule-vehicles and the story related to their design. We are honored to have received the contribution of the two winners of the race describing their design and their driving on the Au(111) surface. Finally, we have chosen three possible topical applications of single molecule mechanics on a surface: the functioning of a molecular mechanical calculator, the simulation of what will be the transmission of rotation between a solid-state nanogear and a molecule-gear and finally one possible 2D self-assembly architecture for single molecule machinery, each molecule being well isolated in the surface nanoporous molecular network.

We expect that this new volume of the series concerning single molecule mechanics and its related functioning machinery will encourage the readers to enter in the design of new molecules or molecular machinery. This will be a good opportunity to explore the mixing between quantum and semi-classical design of mechanical nanomachines and may be to propose new molecular structures of molecule-vehicles for Nanocar Race III.

We thank the European Commission H2020 FET program for the MEMO and Nanocar Race II financial supports, the C'Nano for the co-organization of the November 2021 Toulouse workshop at The P. Baudis congress center. A very special thanks to the CEMES-CNRS and TU-Dresden personnel for their contribution to the organization of Nanocar Race II in March 2022 and certainly to the Webcast IN2P3-CNRS teams (and their affiliates) for their fantastic job before (November 2021), during and after Nanocar Race II in handling the live HD transmission of the competition.

Dresden, Germany — Francesca Moresco
Toulouse, France — Christian Joachim

Contents

Unidirectional Motion of Single Molecules at Surfaces 1
Grant J. Simpson and Leonhard Grill

DMBI—from n-Type Dopant to Molecular Machines 29
Oumaima Aiboudi and Franziska Lissel

Assembly, Diffusion and Rotation of Organic Molecules on a Gold Surface 41
Roberto Robles, Vladimír Zobač, and Nicolás Lorente

From Early Prototypes to On-Surface Drivable Single Molecule Nano-vehicles 59
Henri-Pierre Jacquot de Rouville, Sonia Adrouche, Xavier Bouju, Jean-Pierre Launay, Gwénaël Rapenne, and Christian Joachim

On-Surface Translational Activity of Porphyrin Chromophore Molecules 83
Jonathan P. Hill, Daniel T. Payne, Kewei Sun, Yoshitaka Matsushita, Ayako Nakata, Puneet Mishra, Takashi Uchihashi, Waka Nakanishi, Katsuhiko Ariga, Tomonobu Nakayama, and Shigeki Kawai

Controlled Driving of a Single-Molecule Anthracene-Based Nanocar on a Metal Surface 105
Ana Barragán, Koen Lauwaet, Tomás Nicolás-García, Ana Sánchez-Grande, José Ignacio Urgel, Jonas Björk, Emilio M. Pérez, and David Écija

Azulene Based Nanocars 121
Tim Kühne, Kwan Ho Au-Yeung, Suchetana Sarkar, and Francesca Moresco

Towards a Molecular Mechanical Calculator 141
We-Hyo Soe and Christian Joachim

Atomistic Modelling of Energy Dissipation in Nanoscale Gears 157
Huang-Hsiang Lin, Alexander Croy, Rafael Gutierrez,
and Gianaurelio Cuniberti

Molecular Networks and Surface Engineering for Single Molecule Studies: From Spatial Separation to Emergent Properties 177
R. S. Koen Houtsma and Meike Stöhr

Unidirectional Motion of Single Molecules at Surfaces

Grant J. Simpson and Leonhard Grill

Abstract It is a basic concept of physical chemistry that in thermal equilibrium every individual process is compensated by its reverse process, which is called microscopic reversibility. It is therefore a challenge to realize unidirectional motion of atoms and molecules. Here, various examples of unidirectional motion at surfaces are presented, which cover both rotation and translation of single molecules. Two ways to achieve unidirectionality are discussed. First, the presence of a local gradient that deforms the potential energy surface and leads to unidirectionality. This can be caused by the tip of a scanning tunneling microscope, which is also a very suitable instrument to follow the motion of individual molecules. Second, intrinsic unidirectionality of a molecule-surface system, which is of particular interest to be employed in molecular machines for useful work at the atomic scale.

Keywords Unidirectionality · Microscopic reversibility · Surfaces · Molecular motors · Rotation · Translation · Scanning tunneling microscopy (STM) · Single-molecule manipulation · Adsorption · Single-crystals · Surface-molecular-beam · Potential energy surface · Molecular machines · Mechanics with molecules

1 Unidirectionality Caused by Local Gradients

The motion of molecules at solid surfaces is dictated by the potential energy surface (PES) that is determined by the interaction between adsorbate and substrate. In the case of the commonly used single-crystal surfaces, which are well-defined and thus facilitate molecular dynamics studies of model systems, the PES shape reflects their periodic lattice. Scanning tunneling microscopy (STM) is a very suitable method to study such systems. One the one hand, this is because it can image single molecules with high spatial resolution to reveal intramolecular details. On the other hand, it can be used to controllably deform the potential energy surface via the forces that are

G. J. Simpson · L. Grill (✉)
Department of Physical Chemistry, University of Graz, Heinrichstrasse 28, Graz, Austria
e-mail: leonhard.grill@uni-graz.at

© The Author(s), under exclusive license to Springer Nature Switzerland AG 2023

F. Moresco and C. Joachim (eds.), *Single Molecule Mechanics on a Surface*,
Advances in Atom and Single Molecule Machines,
https://doi.org/10.1007/978-3-031-16930-4_1

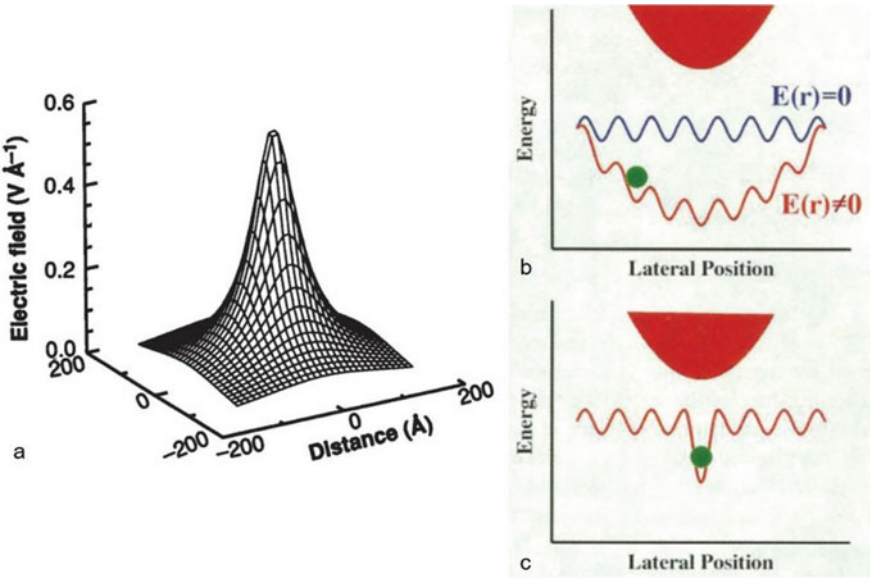

Fig. 1 **a** Calculated electric field under an STM tip. **b**, **c** Schematic of the potential energy of an adsorbate (green) under an STM tip (red) as a function of its position on the surface. **b** The tip causes a broad deformation for an adsorbate with an electric dipole moment while (**c**) only a narrow potential well is created by attractive chemical forces from the tip in the absence of a dipole moment. Reprinted with permission from Ref. [1], copyright (1991) American Association for the Advancement of Science (AAAS)

applied by the STM tip. Despite the relatively low bias voltage (of about 1 V) applied between tip and surface, a strong electric field of roughly 0.5 V/Å (Fig. 1a), which corresponds to 5×10^7 V/cm, exists in the junction. This leads to a broad deformation of the PES in the vicinity of the STM tip (as sketched in Fig. 1b in comparison to the situation without an electric field). However, even in the absence of a bias voltage, chemical forces between tip and adsorbate are still active, but—due to their short-range character in comparison to the electric field—they produce correspondingly local deformations of the PES (Fig. 1c). By controlling the deformation via the STM tip location relative to the molecule (both in terms of lateral position and vertical distance), unidirectional motion of molecules on a surface can achieved.

1.1 Rotation

Molecular rotation on a surface is defined as the motion of a molecule around a fixed axis. This fixed axis can come about due to a strong bond between molecule and surface [2] or can be as a result of preferred adsorption configurations on a surface [3]. This fixed axis can be thought of as a pivot point between a mobile

rotor (in this case a single molecule) and an immobile stator (the surface). Molecular rotors are analogous to macroscale objects such as turbines or propellers, however, the actuation of a rotor on the single molecule scale is much more challenging and difficult to control because their motion is dictated by probabilistic quantum processes. By understanding these processes in detail, we can start to conceive molecular machines capable of performing meaningful work at the nanoscale. Indeed, progress has already been made in, the transfer of motion between rotating gear-like molecules [4–7], light-driven molecular motors [8–10], as well as chemically fuelled rotary motion [11, 12]. While rotation is found in many systems, we restrict the discussion here to molecules adsorbed at surfaces.

Rotation is found in various molecule-surface systems [3, 14–17] and was first studied in detail at the single molecule level by Ho and co-workers [13]. Their molecule of choice was a single O_2 molecule adsorbed on a Pt(111) surface (Fig. 2a) which, dictated by the symmetry of the surface, displayed three equivalent adsorption positions. Single rotation events could be recorded by positioning the STM tip above an individual molecule and measuring the tunneling current at a constant bias (Fig. 2b). After some time, a sharp drop in the current indicates that the molecule below the tip has moved and, by imaging before (Fig. 2c) and after (Fig. 2d) this event, one determines that a rotation has occurred.

The physical process of rotation could be understood by the creation of an adsorbate induced resonance due to the inelastic tunnelling of electrons from the STM tip [18]. This transiently occupied resonance then transfers energy to a hindered rotational mode of the molecule at a current dependent rate. In fact, the same reasoning

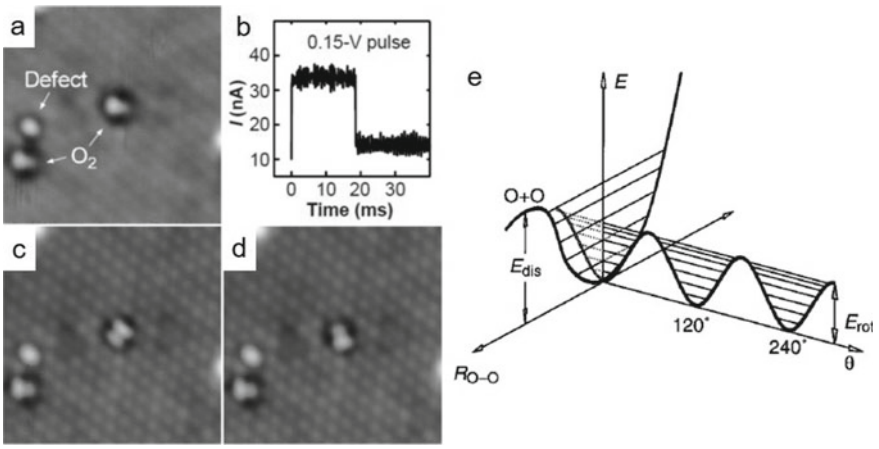

Fig. 2 **a** STM image identifying two O_2 molecules adsorbed on the Pt(111) surface with a defect nearby. **b** Current as a function of time showing a sudden step at 20 ms indicative of a rotation event. **c**, **d** STM images before and after a rotation of the O_2 molecule has occurred. **e** Schematic of simple one-dimensional potential wells along the molecular stretch, R_{O-O}, and angular, θ, coordinates. Reprinted with permission from Ref. [13], copyright (1998) American Association for the Advancement of Science (AAAS)

can be used to explain the dissociation of O_2 on Pt(111) where energy is instead transferred to the O–O stretch vibration. It may also be that, after activation of this stretch vibration, subsequent coupling to rotation is a possible route to energy dissipation as illustrated by the potential energy surface in Fig. 2e.

Through measurements of the rate of rotation at various tip-surface distances, the number of inelastically scattering electrons required to activate the molecule can be determines. By repeating this process for a series of voltages, the activation energy of a single rotational hop event could be determined. This system did not display any directionality and the three rotational states were accessed in a stochastic manner.

Another study with a considerably higher degree of chemical complexity investigated the rotational and constitutional dynamics of noncovalently bound dynamers confined in a porous 2D coordination network [19]. Here, the host network consisted of a highly ordered hexagonal array of Co atoms coordinated with *para*-sexiphenyl-dicarbonitrile linkers (Fig. 3a) which provided pores with well-defined symmetry (sixfold) and area (24 nm^2). With a slight stoichiometric excess of the linker units, it was found that the pores can accommodate self-assembled aggregates of such monomers which, more often than not, formed trimers (Fig. 3b). These trimers were found in both left- and right-handed chiralities stabilised by weak attraction between the -CN end-groups and phenyl moieties.

With an onset temperature of approximately 60 K, it was found that rotations of the trimers was triggered as shown in Fig. 3c, d. These rotations were interpreted to be collective and concerted meaning that the three constituent molecules of the timer moved as one entity from one stable configuration to the next energetically equivalent one with no reorganisation or intermediate adsorption sites one the way. With increasing temperature, the rotation rate increased in the typical Arrhenius fashion (Fig. 3e) for both chiral forms whereupon the STM imaging showed a superposition of all equivalent orientations (Fig. 3f, g). At temperatures above ~ 70 K transitions between the two chiral states could be observed.

This study shows how rather complex systems can be constructed in a well-defined manner and which then result in rotational motion. Due to the thermal activation of this process, the second law of thermodynamics dictates that any directionality in the sense of rotation should not be observed as was the case (with both chiral forms) in this work.

We would like to turn our attention to molecule-surface systems which display some degree of unidirectionality where we can define the degree of directionality, D, with the following expression:

$$D = 100\% \times \frac{N_{cw} - N_{ccw}}{N_{cw} + N_{ccw}}$$

where N_{cw} and N_{ccw} refer to the number of clockwise and counter-clockwise rotations, respectively. In these terms, a directionality of 100% would refer to the case where a molecule rotates exclusively clockwise, -100% exclusively counter-clockwise, and 0% would mean that the rotation is completely random. Whether that degree is 100% or somewhere below and why that is the case will be discussed.

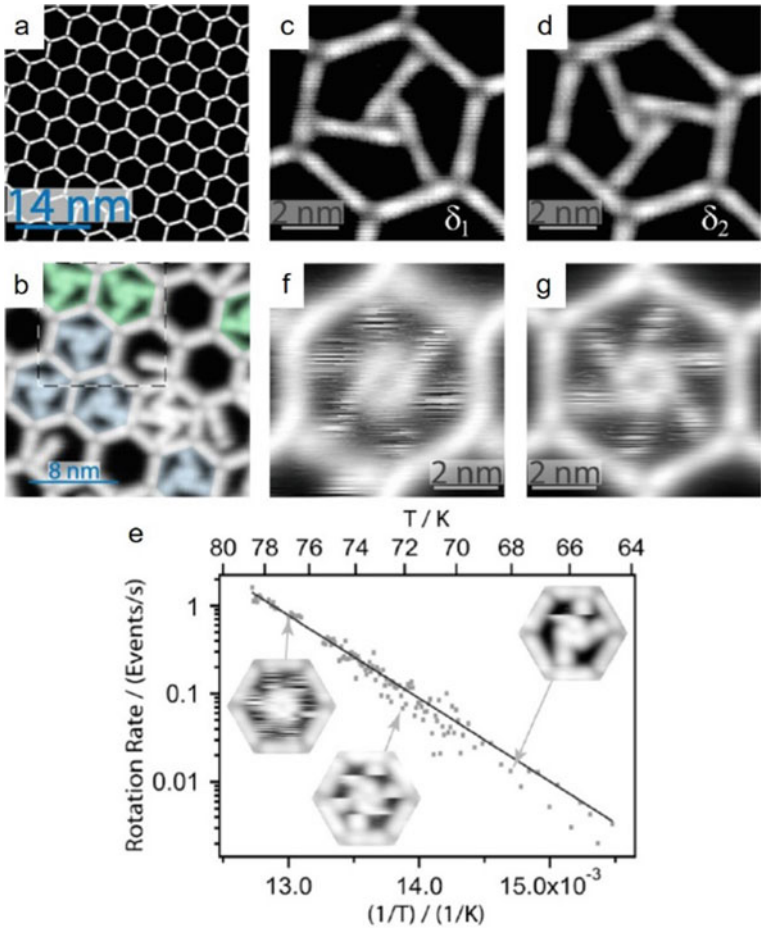

Fig. 3 **a** Nanoporous host lattice formed on Ag(111). **b** Self-assembled supramolecular trimers occupying the individual pores showing both chiral orientations (blue and green). **c**, **d** 60° rotation of a caged supramolecular dynamer of one chirality. **e** Arrhenius plot of rotation rate as a function of temperature with an extracted rotational activation energy of 187 ± 8 meV. **f**, **g** Rapid fluctuation of rotors leads to a superposition of all orientations, for both chiral forms, due to the relatively slow scan rate of the STM tip. Reprinted with permission from Ref. [19], copyright (2010) National Academy of Sciences

It is also useful to make a distinction between rotation which is induced due to some external gradient and rotation which is intrinsic to the molecule and requires no external gradient. In the former case, a deformation of the potential energy surface can be achieved, for example, using the strong electric field between the tip of a scanning tunnelling microscope (STM) and the electrically biased substrate below (Fig. 1a) [1]. In this manner, the barriers for a rotational event can be modified in a way that makes the forward process more probable than the reverse process

(Fig. 1b). In the latter case, the molecule itself, due to some property of its chemical structure, possesses some asymmetry which results in the forward and backward rotation processes being unequally favoured. This property may be imparted by, for example, chirality or by some irreversible isomerisation event.

As already discussed, one chiral form of a molecular rotor does not lead to preferential rotation in one direction when the system is thermally activated. However, chirality appears to play an important role when the presence of an STM tip is considered. This was the case for butyl methyl sulphide (BuSMe) molecules which form a sulphur-metal rotation centre when adsorbed on a Cu(111) surface (Fig. 4a) [20]. Despite being achiral in the gas phase BuSMe is prochiral when adsorbed on a metal surface. Correspondingly, two chiral forms of this molecule, (R) and (S), are seen when adsorbed on a surface depending on which sulphur lone pair forms a bond with the surface and can be distinguished in STM images when rapidly rotating around this pivot point. Individual rotation events can be monitored based on the current signal (Fig. 4b) when the tip is placed at an asymmetric position (Fig. 4b inset). Six different current levels are found based on the six different possible orientations due to the symmetry of the surface. Using non-perturbative tunnelling conditions (i.e. below the voltage threshold for rotation activation), these current states (and hence rotation) were monitored upon thermal activation at 8 K, 0.2 V. As expected, and in line with the study from Barth et al., no directionality was found, confirming the prediction from thermodynamics. However, through excitation of a C–H stretch vibration which then coupled to rotation, electrically driven rotation (5 K, 0.38 V) displayed a directionality of up to 5% for the S chiral form (but not the other). Additionally, an increased incidence of 60° rotations observed for R whereas S showed homogeneous distribution of hop angles.

Despite the degree of directionality being rather low, it was found to be statistically significant (number of events recorded $> 10^3$) and thus was termed a motor rather than simply a rotor (which would display no directionality). The difference in directionality between enantiomers was attributed to the presence and chirality of the STM tip. A previous study showed that STM tips can be chiral and can affect the rate of rotation [21]. Both R and S forms were investigated (schematic shown in Fig. 4c, d) with a number of different tips and showed varying degrees of directionality (as well as non-directionality) depending on the tip state.

The basis for the observed directionality is based on Brownian ratchets operating under thermal fluctuations [22, 23] (Fig. 4e, f). Having a ground state ratchet potential for rotation with much lower barrier [24] than the C–H stretch which is excited upon electron tunnelling means that the system is brought to an energy state far above the ground state. Through intramolecular energy redistribution into lower-lying modes the molecule makes rotations in both directions. Importantly however, despite the barrier heights being equal for cw and ccw rotation, the probabilities for relaxation onto the ground state potential are unequal and hence directionality is observed. The reason for these apparent unequal probabilities stem from symmetry matching between a chiral tip and one of the surface enantiomers.

The stochastic nature of molecular excitations can lead to a high degree of randomness in the direction of rotation. However, the strong electric field in the

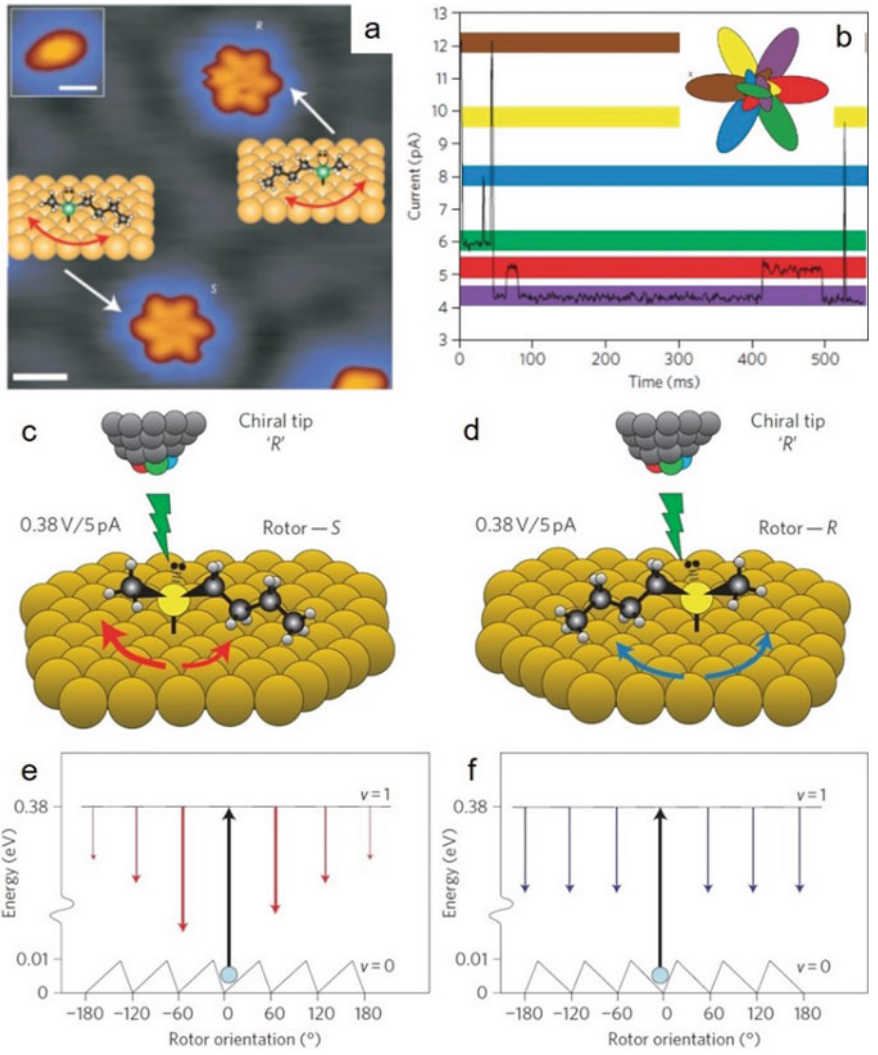

Fig. 4 **a** STM image of the two enantiomeric forms of BuSMe, R and S, adsorbed on Cu(111) with accompanying schematic models. The molecules are rotating rapidly during the scan whereas the inset shows a stationary molecule. **b** Current versus time traces measured over a single molecule showing six different current levels corresponding to six different BuSMe orientations (inset). **c**, **d** Schematics of the S and R rotors electrically excited by the same chiral STM tip. **e**, **f** Ratchet mechanism in which excitation of a C–H stretch leads to excitation (black arrow) followed by energy redistribution (red, blue arrows) to the ground potential energy landscape. Reprinted with permission from Ref. [20], copyright (2011) Springer Nature

tunnelling junction of an STM can also be used to direct rotation with a very high degree of precision. In such an example [25], 2,5-di(ethynyladamantanyl) − 4-(dimethylamino)nitrobenzene (DDNB) molecules possess a strong permanent dipole moment due to the electron withdrawing/donating properties of the -NO_2/-$N(CH_3)_2$ functional groups attached to its central carbon ring (Fig. 5a). In addition, the dipole moment in the central section of the molecule is lifted off of the surface by two peripheral adamatyl moieties to alleviate any possible strong molecule-surface interaction.

While using low scanning bias (< 1 V), DDNB could be imaged without being perturbed. When the bias is increased (and hence also the electric field in the tunnelling junction) a rotation of the molecule by 60° is observed (Fig. 5b, c). Subsequent repeated voltage pulses reveals that there are (like other systems discussed) 6 different orientations due to the symmetry of the underlying Ag(111) surface. A fixed pivot point around which these rotations occur was also identified and is due to the interaction of an oxygen atom with one of the silver surface atoms is a manner similar to that seen in the BuSMe case. By mapping the rotation direction as well as the probability (Fig. 5c, d) it was found that, depending on whether the tip is

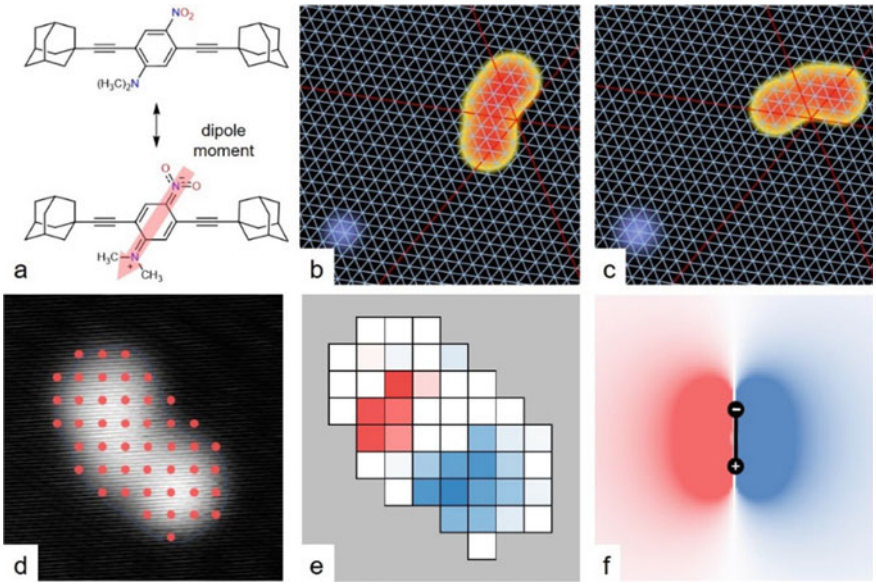

Fig. 5 **a** Chemical structure of DDNB showing the electrical dipole moment. STM images of DDNB on Ag(111) before (**b**) and after (**c**) a rotation event. Gridlines indicate the Ag(111) lattice and the crossing point of the red lines indicates the pivot point of rotation. **d** STM image of DDNB with 46 positions of the tip voltage pulses. **e** Rotational map measured at − 1.3 V. Blue and red colours represent clockwise and counter-clockwise rotations, respectively, and the intensity relates to the likelihood of rotation. **f** Simulation of the torque acting on an electrical dipole (shown in black) from a positive test charge as a function of position. Reprinted with permission from Ref. [25], copyright (2019) Springer Nature

located on one side of the molecular dipole or the other, the sense of rotation could be controlled. Indeed, through simple modelling of the torque acting on a dipole due to a nearby test charge (Fig. 5f), the experimental data showed that the interaction of the electric field in the tunnel junction with the molecular dipole moment was the reason for such high (100%) directionality. By destabilizing the pivot point for the molecule, a combination of rotation and translation was observed. It is worth noting that even higher bias voltages and hence stronger electric fields are sufficient to overcome the O-Ag interaction and allows for directed translations [26].

1.2 Translation

The translation of molecules at surfaces is key in various fields, for instance film growth processes [27], heterogeneous catalysis [28, 29], on-surface polymerization [30], device fabrication in organic electronics [31] or the assembly of two-dimensional materials [32]. Thermal diffusion of molecules on a surface is typically a random process, consisting of uncorrelated hops on the atomic surface lattice. The motion of molecules on surfaces can be followed indirectly via scattering of ^{3}He atoms from the surface [33]. Direct visualization of the molecules by scanning tunneling microscopy (STM) is a very suitable method to study the translation of adsorbed molecules as it can image single molecules with high spatial resolution and follow their pathway during motion. The hopping rate, given by Arrhenius' law, is determined by the rate of individual hops and the potential barrier that needs to be overcome by the particle to reach the neighboring site. Hopping of molecules typically occurs to the adjacent lattice sites [34, 35] with diffusion properties that depend on their chemical structure and the substrate [36]. Larger displacements were also predicted to occur [37] and, indeed, molecules were observed to show mean-squared displacements of 4 lattice constants over the surface, a value that is increased to 7 when reducing the molecule-surface interaction [38]. In addition and as another remote stimulus, also light can be used to induce molecular motion at a surface [39, 40].

In the absence of thermally or light-induced translation, the tip of a scanning tunneling microscope can be used to induce molecular displacement by applying force to the molecule, i.e. by deforming the potential energy landscape around the molecule and creating a local gradient. This can be done via the applied bias voltage and the resulting electric field in the junction or via interatomic forces that are active between the STM tip and the molecule (see Fig. 1b, c, respectively). The former acts over rather large surface areas in the range of hundreds of Å (Fig. 1a), which has been recently used to move single molecules over large distances across a surface [42]. The latter is only short-ranged and is active only in the vicinity of the STM tip (Fig. 1c). By applying different forces, a single molecule can be moved controllably over a surface as has been shown in many examples since the 1990s [43–46], for instance for CO molecules [47] as being the first case in which the molecular hopping motion was revealed via the response of the molecular motion on the STM junction (i.e.

either the tip height or the tunneling current for constant-current and constant height manipulation modes, respectively [48]). In the following, some examples will be given for the manipulation of molecules that exhibit rather complex structures and/or internal degrees of freedom. One case is the so-called Lander molecule (Fig. 6a) [41]. These molecules are equipped with four side groups that are designed to lift the central board from the surface and are rotatable around their C–C bond to the board. If such a molecule is manipulated laterally on a corrugated Cu(211) surface, it can be displaced controllably as shown in Fig. 6b, c where the molecule follows the pathway of the STM tip during manipulation (indicated by a black arrow), parallel to the surface steps in $[01\bar{1}]$ direction. Inspecting the current signal during this (constant-height) manipulation reveals that the motion was a typical hopping process with a periodicity of 2.6 Å that matches with the lattice constant of the Cu(211) surface (2.55 Å). This shows that during the manipulation process the molecule hops from one adsorption site to the next one along the Cu rows, being pushed (rather than pulled, which would lead to an inverted sawtooth-shaped signal [48]) by the STM tip. This very simple signal shape is remarkable as the molecule exhibits various degrees of freedom for internal motion, but rather seems to move as a rigid object.

This local deformation of the potential energy surface obviously defines the direction of the gradient and therefore of the acting force. Consequently, the direction of translation can typically be controlled very well in STM manipulation, leading to unidirectional motion. In order to clearly distinguish between unidirectionality and directionality: the former describes the motion in one direction only (i.e. from A to B on a straight line), while the latter stands for motion in one dimension (i.e. along a straight line with two possible directions of motion). An example for the first case was the motion of single molecules along a pre-defined course in the first molecular nanocar race [49]. By controlling the direction of motion in every step and thus achieving unidirectionality, a rather long pathway of straight and curved sections with a total distance of 150 nm could be successfully completed by using suitable molecules and manipulation modes [26]. The second case was reported recently when sending (and receiving) single molecules, which move along straight lines on a Ag(111) surface, over very large distances of up to 150 nm with a single voltage pulse [42]. Note however that repulsion was done in a way that can result in two possible directions of motion along this straight line, thus being ‘directional’ and not ‘unidirectional’ in its character.

The fact that a single molecule can be moved on a pre-defined line was used by L. Gross et al. to trap single atoms on a surface and displace them with the molecule. Such a sequence is shown in Fig. 7a–e where at the start several copper adatoms were place in a row on a Cu(111) surface. When laterally moving a HB-HPB molecule towards the first adatom in the row, the molecule is stabilized there and can be imaged with the (invisible) copper adatom underneath it (Fig. 7b). Interestingly, upon further manipulation events along the row, the molecule is moved from one atom to another and takes the captured adatoms with it. Hence, the manipulation mechanism can be used to trap and transport copper atoms on a surface with a single molecule. Note that the noise on the images is rather high in (b) and is then reduced as more adatoms are picked up. This results from the very low tunneling currents (5 pA in Fig. 7b, c

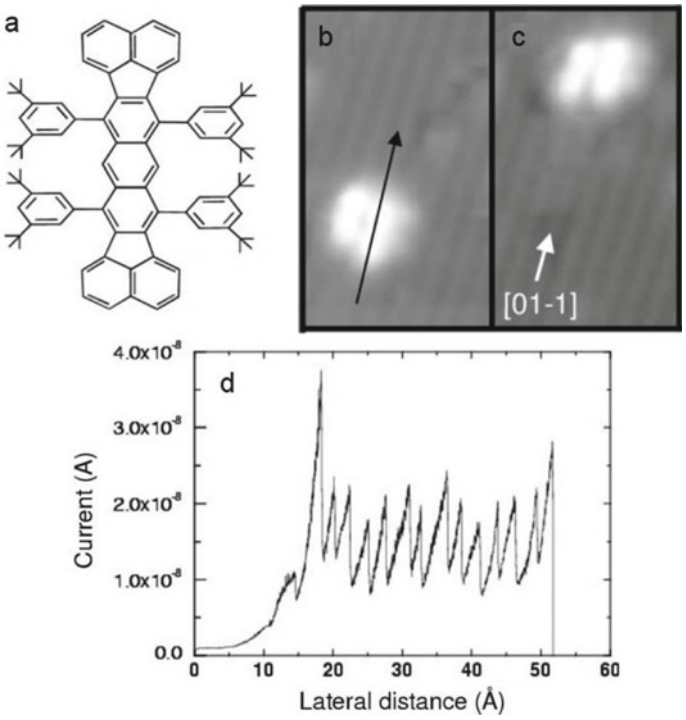

Fig. 6 **a** Chemical structure of the Lander molecule ($C_{90}H_{98}$), consisting of a central polyaromatic board and four spacer legs to elevate the central board from the surface. **b**, **c** STM images of a single Lander molecule on Cu(211) before and after a lateral manipulation (indicated by the black arrow) along the intrinsic steps of the surface with **d** the corresponding current signal. Reprinted with permission from Ref. [41], copyright (2005) Elsevier

as compared to 0.1 nA in the other images) that must be used for stable imaging of the HB-HPB with only one adatom underneath as otherwise the molecule would be displaced during imaging. Upon trapping more adatoms, the molecule is stabilized and higher tunneling currents can be employed, leading to less noise in the images. At the end of the sequence where five copper atoms where trapped, the HB-HPB molecule was picked up by the STM tip, leaving a Cu_5 cluster on the surface that is visible in the subsequent STM image (Fig. 7g).

STM manipulation of molecules leads to hopping motion, either in a pulling or pushing mechanism, depending whether the active force is attractive or repulsive, respectively [48]. This is in contrast to the macroscopic world, where objects not only hop or slide from one place to another, but rolling is often the mechanism of choice, due to the reduced friction. On the atomic scale, such a motion has been observed for triptycene dimers (Fig. 8a) [51], acting as molecular 'wheels', on the corrugated Cu(110) surface as shown schematically in Fig. 8b. Not only due to the tip motion, but also due to the rolling mechanism, this process is unidirectional as it allows one direction of motion. It is obvious that the STM images before and after molecular

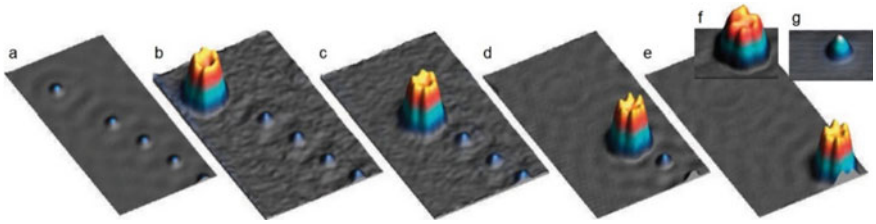

Fig. 7 Hexa-t-butyl-hexaphenylbenzene (HB-HPB) molecules on Cu(111). A sequence of (pseudo-3D) STM images of the very same surface area is shown in **a**–**e** where initially five copper adatoms were placed on purpose in a row **a**. Afterwards, a single HB-HPB molecule is moved across this row, trapping and moving one copper adatom after another on the surface. **f** HB-HPB molecule with five Cu atoms underneath and **g** the same area after picking up the molecule where a Cu_5 cluster is left on the surface. Reprinted with permission from Ref. [50], copyright (2005) Springer Nature

displacement cannot identify the kind of motion and in fact, are identical for hopping and rolling motions. They differ only in the displacement distance, which is a result of the mechanism that can be restored for hopping, but not for rolling (see Fig. 8e) [51]. Hence, it is crucial to study the current signal during the molecular motion, which reveals characteristic differences as can be seen in Fig. 8c, d: A hopping motion (occurring at rather small tip-molecule distances during the manipulation) is reflected in the typical sawtooth-shaped signal (c) that is known from adatoms [47] or molecules (Fig. 1d) [41]. The rolling motion instead (achieved only a large tip-molecule distances) shows a very different current signal, which is approximately symmetric (d). This is due to the particular rolling mechanism as sketched in Fig. 8e: Interatomic forces between tip and molecular wheel cause a rotation (described in (1)-(3)), because the rather large tip height leads to an increased torque as compared to smaller tip heights. Accordingly, only one (120°) rotation of the molecular wheel occurs and no further motion can be induced in the same process since the tip is located behind the molecule after the event, moving away from the molecule. This is in stark contrast to the hopping motion (Fig. 8c) where the tip is located in front of the molecule after each hopping event. Another kind of molecular motion across a surface, which goes beyond the pure hopping mechanism, is the 'walking' mode [34, 52], even carrying a CO_2 molecule as 'cargo' [53] directionally along a straight line.

An alternative way of defining the directionality of motion for molecules on a surface is the edge of a molecular island (Fig. 9) [54]. As the HB-NPB molecule moves only along the island edge during a sequence of various STM manipulation steps (Fig. 9c–h), its motion is unidirectional along one line. This experiment thus reflects a 'rack-and-pinion' mechanism (Fig. 9a) with the island being the 'rack' and the moving molecule the 'pinion', which "rolls" along the molecular island and hence includes both rotation and translation of a single molecule. The chemical structure of the molecule includes a chemical tag (pyrimidyl group in the chemical structure; Fig. 9a), which allowed to assign an orientation to the molecule (indicated

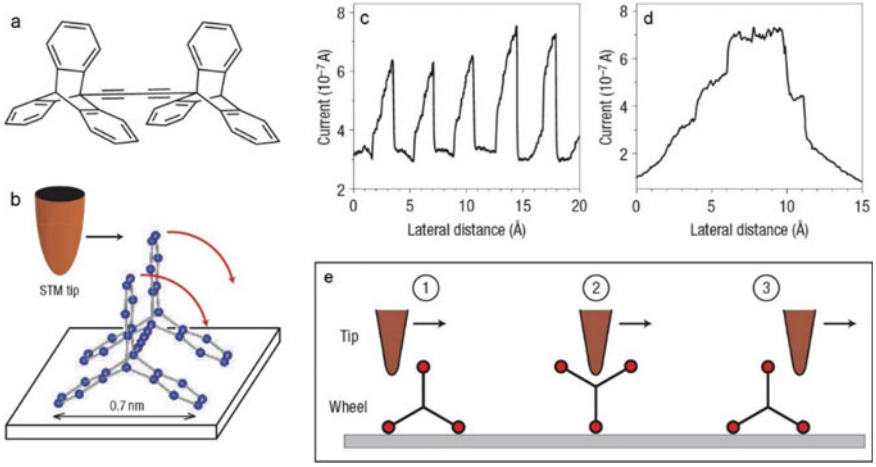

Fig. 8 **a** Chemical structure of the wheel-dimer molecule ($C_{44}H_{24}$). **b** Manipulation scheme to induce a rolling motion (arrows indicate the rotation of the wheels). **c**, **d** Current signals during constant-height manipulation for (**c**) hopping and (**d**) rolling motion. **e** Scheme of the rolling mechanism (see main text). Reprinted with permission from Ref. [51], copyright (2007) Springer Nature

by a white arrow in the STM images) and therefore to prove to molecular rotation during translation.

STM tip-induced translation of molecules is typically limited to hops from one lattice site to the next, thus small distances below 1 nm [26, 47, 51, 54–56]. Longer

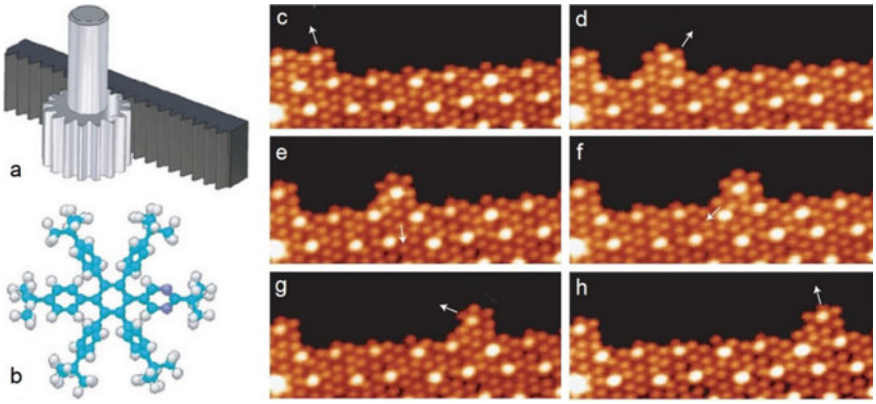

Fig. 9 **a** 'Rack-and-pinion' mechanism. **b** Chemical structure of the hexa-t-butyl–pyrimidopentaphenylbenzene (HB–NPB, $C_{64}N_2H_{76}$) molecule. **c**–**h** STM images (13 × 6 nm^2) of the same surface area during a sequence of manipulation steps (between the images). The white arrow indicates the molecular orientation. Reprinted with permission from Ref. [54], copyright (2007) Springer Nature

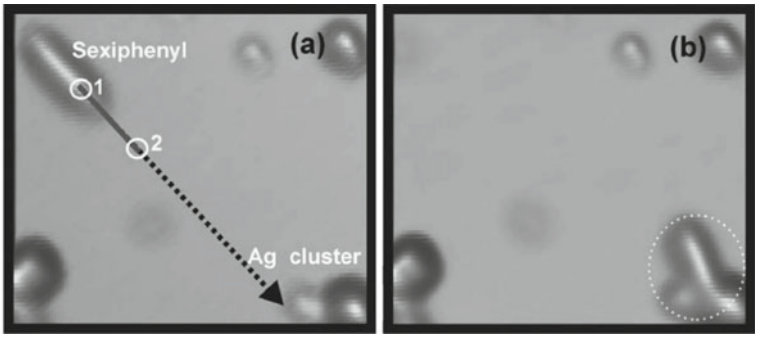

Fig. 10 STM images ($11 \times 9.5\,nm^2$) of the same surface area with sexiphenyl molecules on Ag(111) (**a**) before and (**b**) after a manipulation with the STM tip. The tip moves during manipulation from 1 to 2 (in **a**) and is then withdrawn while the molecule, which is found at the bottom right (dashed circle in **b**) afterwards, continues to move along the dashed arrow (in **a**). Reprinted with permission from Ref. [57], copyright (2004) American Physical Society

distances have been achieved by Hla et al. with sexiphenyl molecules on Ag(111) that are first dragged with the STM tip and continue to move further across the surface after the tip is retracted [57]. This process is presented in Fig. 10 where initially (a) a single sexiphenyl molecule is located at the top left of the imaged surface area as indicated. The STM tip is then used to laterally dislocate the molecule by approaching it vertically towards the surface over the molecule (indicated as 1 in (a)), then moving it laterally along its long axis in a close-packed direction of the surface from 1 to 2 where the tip is vertically retracted from the surface.

In a usual experiment, the molecule would stop its movement as soon as the cause of motion, i.e. the STM tip at a close distance, is removed. Accordingly, the sexiphenyl molecule can be expected to be located top left of the centre in the STM image taken after the manipulation (Fig. 10b). Instead, the surface is empty in that area and the molecule is found at the bottom right. Hence, in this particular case, the molecule continues to move even in the absence of the STM tip. It is important that initial lateral dragging of the molecules over the surface (with the STM) occurrs since this results in flipping of the phenyl rings and consequently translational motion of the molecules, which is key for this observation. Another example of molecular motion after tip retraction has been recently found by Polanyi and co-workers after CF_3 dissociation on Cu(110) [58]. The thus produced CF_2 moves exactly along one atomic line on this slightly corrugated surface for distances up to about 5 nm, with average displacements of about 2 nm, due to recoil from electron-induced bond dissociation [59], which is discussed below in Sect. 2.2 (Fig. 14).

2 Intrinsic Unidirectionality

It is one of the major topics of physical chemistry to describe how processes are directed. Lewis has formulated in 1925 "*Corresponding to every individual process there is a reverse process, and in a state of equilibrium the average rate of every process is equal to the average rate of its reverse process*" [60] and it was R. C. Tolman in the same year to name this principle microscopic reversibility [61]. Applied to the atomic or molecular scale, this means that for any potential energy surface in equilibrium, forward and backward processes compensate each other. Hence, an asymmetric potential energy landscape is not sufficient and unidirectional motion of molecules is impossible in thermal equilibrium as this would violate the 2nd law of thermodynamics.

On the theoretical side, this effect has been described quite in detail (see e.g. [23, 63, 64]) and it was found that unidirectional motion can be induced if a *potential energy surface is modulated in time and space* [22, 62, 65]. An example is given in Fig. 11 where the on/off switching of an asymmetric sawtooth potential can do work against an external force: A particle distribution (shown in red) is spatially confined if the system is in the "on" state (top) and broadens when the potential is switched off (shown at the centre of Fig. 11). When the potential is switched on again (bottom), the particles become trapped again – importantly with a higher probability in the well at the right of its initial position (than at the left). Hence, the *asymmetry* of the potential in combination with its *modulation* in time results in unidirectional motion to the right, although the external force (i.e. net potential gradient) points to the left.

Despite a detailed theoretical picture, only little experimental work exists on microscopic reversibility, due to the difficulty in measuring such a property. Directional motion via modulated potential landscapes was studied with micrometer

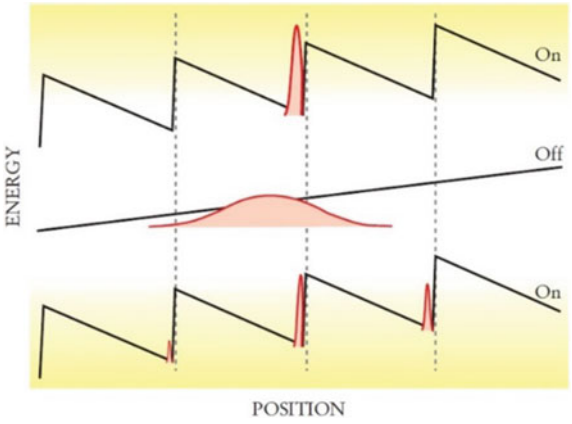

Fig. 11 Scheme how switching a saw-tooth potential can cause unidirectional motion. Reprinted with permission from Ref. [62], copyright (2002) American Institute of Physics

objects, thus far beyond the atomic scale [66, 67]. At the atomic scale, a molecular ratchet [68] has been synthesized and studied by NMR. The rotation was found to be non-directional, which proves the concept of microscopic reversibility. Bartels and co-workers could show for the first time at the level of single molecules and in real space that microscopic reversibility is preserved for molecular diffusion on a surface in the absence of PES modulation [69]. He has also shown the importance of statistical analysis of these individually observed events, i.e. the 'law of large numbers': By examining about 1300 molecular movements, a forward/backward ratio of 1.009, i.e. less than 1% deviation from unity, was found, in perfect agreement with the principle of microscopic reversibility.

2.1 Rotation

In contrast to the molecular rotors discussed until now, where some influence of the STM tip played a role in imparting directionality, there exist systems in which directionality is encoded into the structure and directionality is not dependent on some external source. An example of this is seen in a molecular propeller consisting of three indazole groups arranged in a tripodal manner attached to a five spoked stator (p-bromophenylene substituted cyclopentalienyl) via a central Ru atom (Fig. 12a) [70]. Upon adsorption onto Au(111) with the stator in contact with the surface, the three blades of the rotor are seen in STM images in a chiral arrangement. Through DFT calculations, the arrangement of the phenyl rings on the stator are found to be tilted in the same direction due to steric interactions between the individual rings (shown schematically in Fig. 12b). This arrangement of the stator then dictates the chirality observed in the upper portion of the molecule and causes the indazole groups to adopt a pseudo-helical arrangement similar to a propeller. The combined geometry of the molecule then now constitutes a ratchet shaped molecular gear which imposes a preferred directionality on the rotation of the propeller with respect to the stator.

Indeed, when tunnelling with voltages exceeding 1 V, it was found that left-handed molecules rotated with preference in the clockwise direction (Fig. 12c–e) and the opposite direction was observed for the other chirality. In addition, the authors were able to show that rotations of the molecule could be activated using inelastic electron tunnelling as well as the STM electric field. Statistically, when activated using the electric field, a 78.6% directionality was found (Fig. 12f).

Through mechanical actuation of the molecular rotor (in a manner similar to molecular wheels [51]), by bringing the STM tip into close proximity with one of the propeller blades and pushing it, a characteristic signal is seen when the stepwise rotation of the molecule occurs. While the reverse mechanical rotation was also possible, it required a stronger force and hence demonstrates the intrinsic directionality of the system.

As a number of the examples discussed have shown, a symmetry breaking achieved through some chiral arrangement of the molecule can confer rotational directionality. In a surprisingly simple system, this concept was reversed whereby

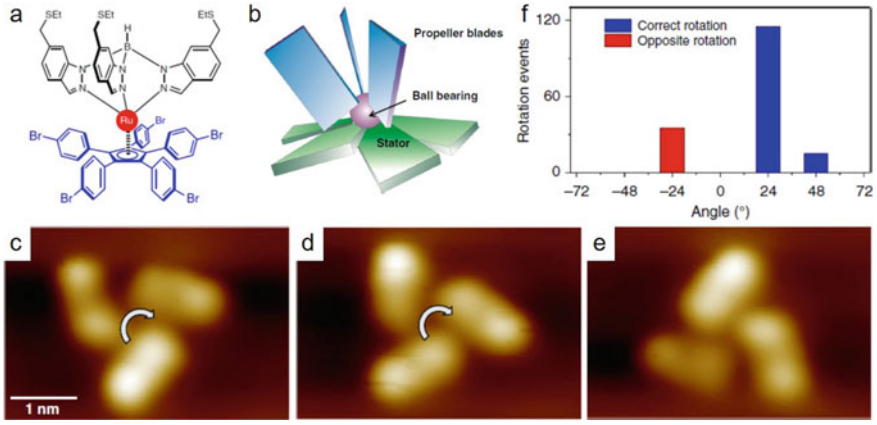

Fig. 12 **a** Chemical structure of the chiral molecular propeller. **b** Schematic representation of the shape adopted upon adsorption onto the Au(111) surface showing chirality of the stator. **c**–**e** STM images of the left-handed propeller after sequential clockwise rotations. **f** Distribution of clockwise and counter-clockwise rotations upon activation with the electric field of the STM tip. Reprinted with permission from Ref. [70], copyright (2019) Springer Nature

a highly symmetric small molecule (acetylene, C_2H_2) was adsorbed on a non-centrosymmetric PdGa surface and displayed a high degree of directionality. A unit cell of the PdGa surface consists of three Pd atoms in a triangular arrangement coordinated to six second-layer Ga atoms and three third layer Pd atoms which absent of inversion symmetry and shown in Fig. 13a [71]. This termination (termed Pd_3) acts as the stator onto which single molecules adsorb in one of three equivalent orientations, R_A, R_B, and R_C, and are imaged using STM as double lobed features (Fig. 13b).

Measuring the current as a function of time over a single molecule led to a remarkable observation: the acetylene molecule rotated repetitively through the states $R_A \rightarrow R_B \rightarrow R_C \rightarrow R_A \ldots$ with perfect counter-clockwise directionality indicated by the three distinct current levels in Fig. 13c. Due to the independence of tip position on directionality, the authors conclude that it is solely the stator which dictates the rotation direction of C_2H_2. As expected, the degree of directionality decreases with increasing temperature up to about 20 K, where the rotation direction becomes completely random. Additionally, a decrease in the directionality at tunnelling biases above 30 mV was also observed. Both of these parametric dependencies are well described by a Langevin kinetic model.

In the classical regime, rotation mechanism was understood by considering a biased Brownian motion on a ratchet shaped potential energy surface [72, 73]. From the parametric dependence on temperature, two dissimilar kinetic energies for overcoming the barrier to the left and right are deduced (Fig. 13d). Then, based on the energy input from a single inelastic tunnelling event, three trajectory regimes are defined (Fig. 13d, right): (1) $E_L < E_R < E_{kin}$, where the rotational kinetic energy is sufficient to overcome either barrier resulting in undirected rotation, (2) $E_L < E_{kin} <$

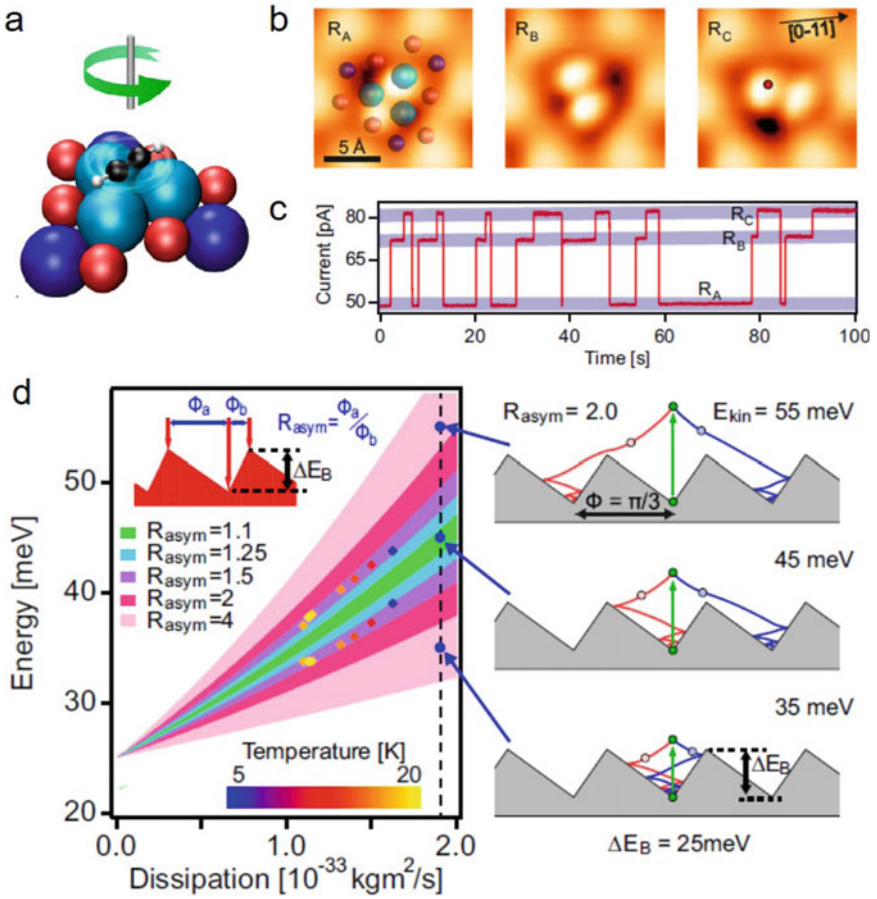

Fig. 13 **a** Sketch of the acetylene (C_2H_2) on Pd_3 motor. **b** STM images of the acetylene rotor in all three of its rotational configurations R_A, R_B, and R_C. The Pd_3 trimer stator is shown superimposed for reference. **c** Tunneling current as a function of time measured at the position marked in red in (**b**) showing a clear repetitive sequence of $R_A \rightarrow R_B \rightarrow R_C$. **d** Schematic representation of rotation dynamics based on the Langevin model. (Left) The range of transferred kinetic energy as a function of energy dissipation for several R_{asym} for the ratchet potential as defined in the inset. (Right) The three regimes from top to bottom: undirected rotation, directed rotation, and no rotation. Reprinted with permission from Ref. [71], copyright (2020) National Academy of Sciences

E_R, where the only one barrier is surmounted resulting in unidirectional motion, and (3) $E_{kin} < E_L < E_R$, where no barrier is overcome and no rotation occurs.

The high degree of directionality was preserved for the tunnelling regime whereby the C_2H_2 molecule tunnels though the barrier between configurations R_A, R_B, and R_C. Although not fully understood, it was presumed that the STM tip plays a crucial role in driving the system out of equilibrium in this regime.

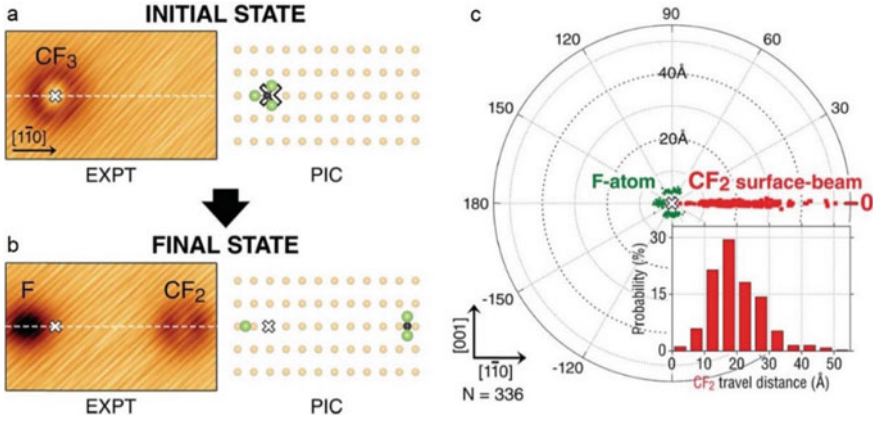

Fig. 14 **a–b** STM images (left) and schemes (right) of the generation of a CF_2 surface-molecular-beam from the electron-induced dissociation of CF_3 on Cu(110) at 4.6 K (the dashed line marks a close-packed copper row of the surface). The white cross indicates the CF_3 position prior to the dissociation. **c** Distance and angle distributions as a polar plot for the two products of the CF_3 dissociation, a F atom and a CF_2 molecule. Reprinted with permission from Ref. [59], copyright (2019) Royal Society of Chemistry

2.2 Translation

Inducing unidirectional translation of molecules by a local deformation of the potential energy surface with the STM tip (as described in Sect. 1.1) is a very versatile process that can be realized with any molecule that is free to move in all directions and does not follow other pathways (e.g. chemisorption or transfer to the STM tip) when the tip is in close vicinity. It is much more challenging to achieve unidirectionality as an intrinsic property of the molecules and, accordingly, the number of cases is very limited. One example is to use chemical fuel as energy source for the translation of CF_2 molecules on a corrugated Cu(110) surface (Fig. 14) [58, 59, 74]. In their work, Polanyi and co-workers obtained a 'surface-molecular-beam' from a chemisorbed CF_3 molecule (that was created by the adsorption of CF_3I on Cu(110) where the C-I bond is broken, resulting in the CF_3 species). By applying voltage pulses of at least 0.9 V, the C-F bond is broken and the two products of the reaction, a F atom and a CF_2 molecule move on the surface as can be seen in Fig. 14a, b that show the same surface area before and after such an event.

Calculations have shown that one of the C-F bonds of the initial CF_3 molecule is oriented along the close-packed row of copper atoms underneath (horizontal lines in the schemes of Fig. 14a, b). After bond dissociation, the two products (F and CF_2) are recoiled along the direction of this C-F bond, thus along the surface atomic row as indicated by a dashed line in the STM images of Fig. 14, but in opposite directions: the F atom moves to the left, while the CF_2 'projectile' moves unidirectionally to the right, i.e. in the opposite direction of the initial C-F bond.

While the displacement of the F atom is with 3.8 Å on average rather small (green dots in the polar plot of Fig. 14c), the CF_2 molecules (red dots in Fig. 14c) move much further. The average displacement was 19.7 Å, but even distances up to 52.6 Å have been observed. This surprisingly large translation on the surface occurred unidirectionally on a straight line. It was explained by a 'ratcheting motion' where the internal energy transfer between the C atom and the pair of F atoms in the CF_2 'projectile' is more efficient than the energy dissipation to the surface. Consequently, the CF_2 molecule remains 'hot' and can travel long distances on the surface without further supply of energy on its way.

The most important class of molecules for intrinsic unidirectional motion are molecular motors, which are defined as molecules with a motor unit, while a molecular motor converts electrical, optical, or chemical energy into *controlled* motion. Note that they are not simple analogues of their macroscopic counterparts, due to the dominance of thermal Brownian motion and viscous forces while at the same time inertia becomes irrelevant [75]. While molecular motors are known in nature [76, 77], their artificial counterparts have seen enormous developments in the last decades [78–81], which was awarded with the Nobel Prize in Chemistry 2016. They are well established in solution [82–88], but much less is known for their motion on surfaces, despite various advantages: (1) fixed point of reference for motion, which is important for useful work; (2) large quantities of equally oriented molecular motors are achievable; (3) ability to suppress Brownian motion; (4) use of scanning probe microscopy to image single molecular motors with high spatial resolution.

Ben Feringa and co-workers have developed a type of molecular motor that is based on a combination of isomerization and helix inversion steps [8]. The key property is the photo-excited state, reached by light absorption, that allows transition of the highest energy barrier of the ground state in few ps [90]. While most studies of this molecule were done in solution, they have also been studied adsorbed on gold nanoparticles [9], although without knowledge about the structure of the nanoparticle and without microscopy that could offer single-molecule information. A little bit later, Feringa, Ernst and coworkers could image and excite single molecular motors adsorbed on a flat single-crystal surface by using STM as shown in Fig. 15 [89]. These molecules consist of a central axle with alkane side groups and four rotary motor units at the periphery (Fig. 15a). It was found that the molecule moves over the surface upon voltage pulses from the STM tip and a dislocation distance of about 6 nm could be achieved by 10 translation steps in the sequence of Fig. 15b–d. Importantly, although the molecule does not move in a straight line, it clearly shows unidirectional motion as it translates from the bottom right to the centre of the imaged surface area during this experiment as evident in the schematic trajectory plotted between Fig. 15b and c. It is obvious from the chemical structure that the possibility to excite either one or various motor units as well as different combinations of them in each step leads to deviations from a straight line. Since voltage pulses were always applied to the centre of the molecule, i.e. approximately above the central axle, it is not known which of the four motor units were triggered in each step.

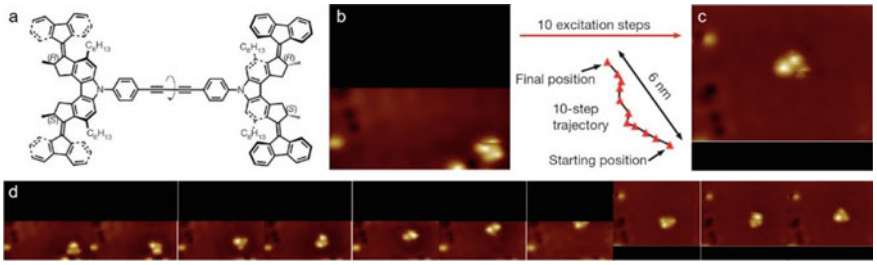

Fig. 15 **a** Chemical structure of a molecule, equipped with four motor units. **b–c** STM images (10.2×9.3 nm^2) of a single molecule on Cu(111) before and after ten excitation steps, as sketched in the centre, with STM images during this sequence shown in **d**. Reprinted with permission from Ref. [89], copyright (2011) Springer Nature

In their pioneer study, Ernst, Feringa and co-workers could for the first time follow a single molecule on its unidirectional pathway that is caused by an intrinsic property of the molecule [89], which was stimulated locally with the STM tip. They used molecules that contain four motor units, in contrast to other studies of motors molecules at well-defined surfaces where only one motor unit is incorporated [91–94]. One example is presented in Fig. 16 [92] where it has been shown how a molecular motor can be stimulated on a surface by light as a remote stimulus, which addresses many molecules at the same time, while characterization was done on the single molecule level. This requires very stable experimental conditions, because the STM tip has to be removed vertically after the first STM image far above the surface in order to avoid tip enhancement of the light as well as shadowing effects. Typically, removal distances of several mm have been used, which can challenge the reproducibility of the lateral tip position upon re-approach (after illumination), because the same surface area must be found again. Only this procedure allows imaging of the very same molecular motors and thus a reasonable analysis of the ongoing processes. If the procedure can be done reliable, difference images (as in Fig. 16a, b) can be obtained to directly visualize the motion of each individual molecules.

A systematic study at various sample temperatures and with (and without) different light sources in the UV and visible range revealed details about the molecular motor motion on the surface [92]: the hopping rate, which is the number of molecules moving per second, depends on the sample temperature, but does not show any differences if light is used or not (Fig. 16c). However, this parameter contains only information about *how many* molecules move, but not *how far* they go. This property is quantified in the tracer diffusion, plotted in Fig. 16e, which reveals clear differences with larger values for higher photon energies. This fits to the absorption bands of the motor units below 400 nm [92]. Importantly, the experiments were compared with the same setups by using a 'control molecule' that is similar to the nanoroadster molecules in its chemical structure, but lacks a motor unit. Accordingly, it allows to analyze the role of the motor unit for the molecular dynamics (Fig. 16d, f). The results do not show any influence of the light, in particular for the translation distance (Fig. 16f).

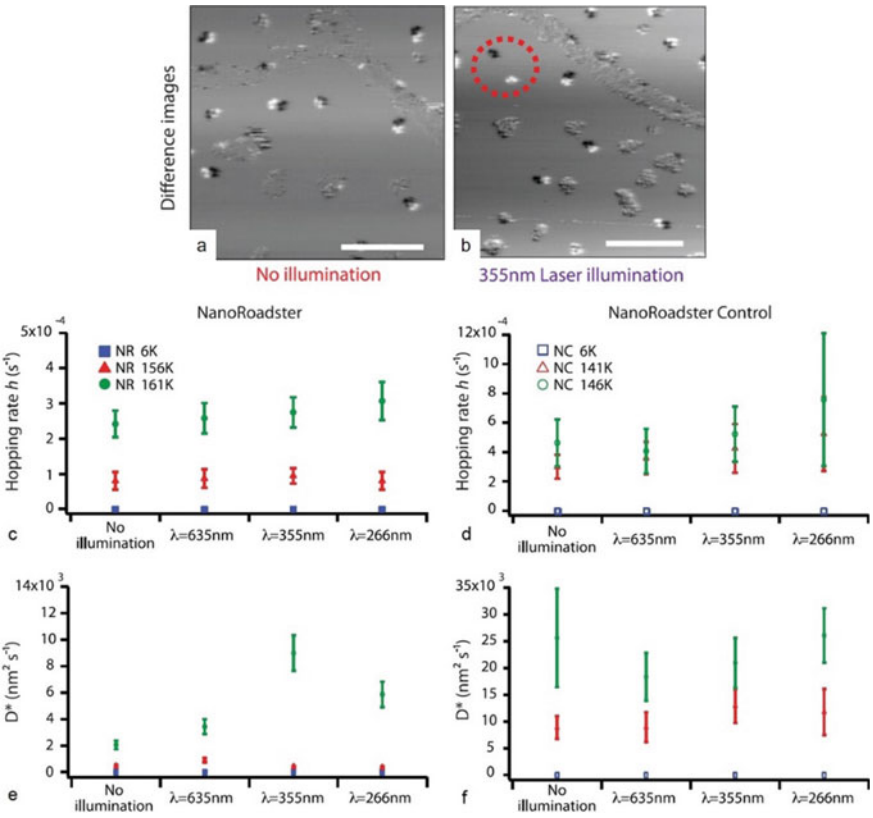

Fig. 16 **a**, **b** STM difference images of nanoroadster molecules on Cu(111), obtained at 161 K sample temperature from a subtraction of two STM images of the very same surface area taken before and after a manipulation experiment (scale bars: 20 nm), without and with illumination as indicated. **c–f** Statistical analysis of the hopping rate (**c–d**) and the tracer diffusion D* (**e–f**) for the nanoroadster (at the left) and the control molecule (at the right). Reprinted with permission from Ref. [92], copyright (2016) American Chemical Society

Note that elevated sample temperatures (around 160 K) were used in these experiments, because at 6 K no motion was observed. This agrees with the design of the 'Feringa' motors as it is the combination of both—heat and light—that is needed to trigger optimal motor motion. Hence, it can be concluded that it is the motor unit in the molecular structure that is responsible for the enhanced light-induced motion. While the number of moving molecules is determined by the temperature, it is the light that seems to give the molecules a 'kick' (in addition to thermal diffusion) which results in larger dislocations on the surface.

It should be mentioned that the surface plays an important role in the unidirectional translation of molecules: On the one hand for the directionality that might be supported or at least affects by the surface topography, in the simplest picture by troughs or rows (see Fig. 14) that keep them on a straight line. On the other

hand, the electronic interaction can alter molecular properties as for instance excited states, which are involved in the motor mechanism, could be quenched on a surface as compared to solution or the gas phase. Non-metallic oxide surfaces are attractive in this regard, but the adsorption and dynamics become much more complex there [93]. In addition, it should be considered that adsorption can drastically change the potential energies of the various molecular conformations that are involved in the motor mechanism, which can even invert their stability as compared to the gas phase [94].

Acknowledgements Financial support from the European Commission via the MEMO project (FET open project no. 766864) is gratefully acknowledged.

References

1. Stroscio, J.A., Eigler, D.M.: Atomic and molecular manipulation with the scanning tunneling microscope. Science **254**, 1319 (1991)
2. Baber, A.E., Tierney, H.L., Sykes, E.C.H.: A quantitative single-molecule study of thioether molecular rotors. ACS Nano **2**, 2385–2391 (2008)
3. Gimzewski, J.K., Joachim, C., Schlittler, R.R., Langlais, V., Tang, H., Johannsen, I.: Rotation of a single molecule within a supramolecular bearing. Science **281**, 531–533 (1998)
4. Soe, W.-H., Srivastava, S., Joachim, C.: Train of single molecule-gears. J. Phys. Chem. Lett. **10**, 6462–6467 (2019)
5. Soe, W.-H., Kleinwächter, M., Kammerer, C., Rapenne, G., Joachim, C.: Mechanics of molecule-gears with six long teeth. J. Phys. Chem. C **124**, 22625–22630 (2020)
6. Yeung, K.H.A., Kühne, T., Eisenhut, F., Kleinwächter, M., Gisbert, Y., Robles, R., Lorente, N., Cuniberti, G., Joachim, C., Rapenne, G., Kammerer, C., Moresco, F.: Transmitting stepwise rotation among three molecule-gear on the Au(111) surface. J. Phys. Chem. Lett. **11**, 6892–6899 (2020)
7. Lin, H.-H., Croy, A., Gutierrez, R., Joachim, C., Cuniberti, G.: Mechanical transmission of rotational motion between molecular-scale gears. Phys. Rev. Appl. **13**, 034024 (2020)
8. Koumura, N., Zijistra, R.W.J., Delden, R.A.V., Harada, N., Feringa, B.L.: Light-driven monodirectional molecular rotor. Nature **401**, 152–155 (1999)
9. Delden, R.A.V., Wiel, M.K.J.T., Pollard, M.M., Vicario, J., N. Koumura, B.L. Feringa, Unidirectional molecular motor on a gold surface. Nature **437**, 1337–1340 (2005)
10. Ruangsupapichat, N., Pollard, M.M., Harutyunyan, S.R., Feringa, B.L.: Reversing the direction in a light-driven rotary molecular motor. Nat. Chem. **3**, 53–60 (2011)
11. Hernandez, J.V., Kay, E.R., Leigh, D.: A reversible synthetic rotary molecular motor. Science **306**, 1532–1537 (2004)
12. Erbas-Cakmak, S., Fielden, S.D.P., Karaca, U., Leigh, D.A., McTernan, C.T., Tetlow, D.J., Wilson, M.R.: Rotary and linear molecular motorsdriven by pulses of a chemical fuel. Science **358**, 340–343 (2017)
13. Stipe, B.C., Rezaei, M.A., Ho, W.: Inducing and viewing the rotational motion of a single molecule. Science **279**, 1907 (1998)
14. Ohmann, R., Meyer, J., Nickel, A., Echeverria, J., Grisolia, M., Joachim, C., Moresco, F., Cuniberti, G.: Supramolecular rotor and translator at work: on-surface movement of single atoms. ACS Nano **9**, 8394–8400 (2015)
15. Shchadilova, Y.E., Tikhodeev, S.G., Paulsson, M., Ueba, H.: Rotation of a single acetylene molecule on Cu(001) by tunneling electrons in STM. Phys. Rev. Lett. **111**, 186102 (2013)

16. Eisenhut, F., Meyer, J., Krüger, J., Ohmann, R., Cuniberti, G., Moresco, F.: Inducing the controlled rotation of single o-MeO-DMBI molecules anchored on Au(111). Surf. Sci. **678**, 177–182 (2018)
17. Perera, U.G.E., Ample, F., Kersell, H., Zhang, Y., Vives, G., Echeverria, J., Grisolia, M., Rapenne, G., Joachim, C., Hla, S.-W.: Controlled clockwise and anticlockwise rotation switching of a molecular motor. Nat. Nanotech. **8**, 46–51 (2013)
18. Teillet-Billy, D., Gauyacq, J.P., Persson, M.: Molecular rotation induced by inelastic electron tunneling. Phys. Rev. B **62**, 13306-13309(R) (2000)
19. Kuhne, D., Klappenberger, F., Krenner, W., Klyatskaya, S., Ruben, M., Barth, J.V.: Rotational and constitutional dynamics of caged supramolecules. Proc. Natl. Acad. Sci. U.S.A. **107**, 21332–21336 (2010)
20. Tierney, H.L., Murphy, C.J., Jewell, A.D., Baber, A.E., Iski, E.V., Khodaverdian, H.Y., McGuire, A.F., Klebanov, N., Sykes, E.C.H.: Experimental demonstration of a single-molecule electric motor. Nat. Nanotech. **6**, 625–629 (2011)
21. Tierney, H.L., Murphy, C.J., Sykes, E.C.H.: Regular scanning tunneling microscope tips can be intrinsically chiral. Phys. Rev. Lett. **106**, 010801 (2011)
22. Astumian, R.D.: Thermodynamics and kinetics of a Brownian motor. Science **276**, 917–922 (1997)
23. Reimann, P., Hänggi, P.: Introduction to the physics of Brownian motors. Appl. Phys. A **75**, 169–178 (2002)
24. Jewell, A.D., Tierney, H.L., Baber, A.E., Iski, E.V., Laha, M.M., Sykes, E.C.H.: Time-resolved studies of individual molecular rotors. J. Phys. Condens. Matter **22**, 264006 (2010)
25. Simpson, G.J., García-López, V., Boese, A.D., Tour, J.M., Grill, L.: How to control single-molecule rotation. Nature Comm. **10**, 4631 (2019)
26. Simpson, G.J., Garcia-Lopez, V., Petermeier, P., Grill, L., Tour, J.M.: How to build and race a fast nanocar. Nat. Nanotech. **12**, 604–606 (2017)
27. Barth, J.V., Costantini, G., Kern, K.: Engineering atomic and molecular nanostructures at surfaces. Nature **437**, 671–679 (2005)
28. Ertl, G.: Reactions at Surfaces: From Atoms to complexity (nobel lecture). Angew. Chem. Int. Ed. **47**, 3524–3535 (2008)
29. Henß, A.-K., Sakong, S., Messer, P.K., Wiechers, J., Schuster, R., Lamb, D.C., Groß, A., Wintterlin, J.: Density fluctuations as door-opener for diffusion on crowded surfaces. Science **363**, 715–718 (2019)
30. Grill, L., Hecht, S.: Covalent on-surface polymerization. Nat. Chem. **12**, 115–130 (2020)
31. Witte, G., Wöll, C.: Growth of aromatic molecules on solid substrates for applications in organic electronics. J. Mater. Res. **19**, 1889 (2004)
32. Patera, L.L., Bianchini, F., Africh, C., Dri, C., Soldano, G., Mariscal, M.M., Peressi, M., Comelli, G.: Real-time imaging of adatom-promoted graphene growth on nickel. Science **359**, 1243–1246 (2018)
33. Rotter, P., Lechner, B.A.J., Morherr, A., Chisnall, D.M., Ward, D.J., Jardine, A.P., Ellis, J., Ellison, W., Eckhardt, B., Witte, G.: Coupling between diffusion and orientation of pentacene molecules on an organic surface. Nat. Mater. **15**, 397–400 (2016)
34. Kwon, K.-Y., Wong, K.L., Pawin, G., Bartels, L., Stolbov, S., Rahman, T.S.: Unidirectional adsorbate motion on a high-symmetry surface: "walking" molecules can stay the course. Phys. Rev. Lett. **95**, 166101 (2005)
35. Miwa, J.A., Weigelt, S., Gersen, H., Besenbacher, F., Rosei, F., Linderoth, T.R.: Azobenzene on Cu(110): adsorption site-dependent diffusion. J. Am. Chem. Soc. **128**, 3164–3165 (2006)
36. Barth, J.V.: Transport of adsorbates at metal surfaces: from thermal migration to hot precursors. Surf. Sci. Rep. **40**, 75–149 (2000)
37. Dobbs, K.D., Doren, D.J.: Dynamics of molecular surface diffusion: origins and consequences of long jumps. J. Chem. Phys. **97**, 3722–3735 (1992)
38. Schunack, M., Linderoth, T.R., Rosei, F., Laegsgaard, E., Stensgaard, I., Besenbacher, F.: Long jumps in the surface diffusion of large molecules. Phys. Rev. Lett. **88**, 156102 (2002)

39. Bartels, L., Wang, F., Möller, D., Knoesel, E., Heinz, T.F.: Real-space observation of molecular motion induced by femtosecond laser pulses. Science **305**, 648–651 (2004)
40. Mehlhorn, M., Gawronski, H., Morgenstern, K.: Diffusion and dimer formation of CO molecules induced by femtosecond laser pulses. Phys. Rev. Lett. **104**, 076101 (2010)
41. Alemani, M., Gross, L., Moresco, F., Rieder, K.-H., Wang, C., Bouju, X., Gourdon, A., Joachim, C.: Recording the intramolecular deformation of a 4-legs molecule during its STM manipulation on a Cu(211) surface. Chem. Phys. Lett. **402**, 180 (2005)
42. Civita, D., Kolmer, M., Simpson, G.J., Li, A.-P., Hecht, S., Grill, L.: Control of long-distance motion of single molecules on a surface. Science **370**, 957–960 (2020)
43. Meyer, G., Repp, J., Zöphel, S., Braun, K.-F., Hla, S.W., Fölsch, S., Bartels, L., Moresco, F., Rieder, K.-H.: Controlled manipulation of atoms and small molecules with a low temperature scanning tunneling microscope. Single Mol **1**, 79 (2000)
44. Moresco, F.: Manipulation of large molecules by Low-Temperature STM: model systems for molecular electronics. Phys. Rep. **399**, 175 (2004)
45. Grill, L.: Imaging and manipulation of single molecules by scanning tunneling microscopy. In: Mikhailov, A.S., Ertl, G. (eds.) Engineering of chemical complexity, pp. 27–49. World Scientific Publishing Co., (2013)
46. Morgenstern, K., Lorente, N., Rieder, K.-H.: Controlled manipulation of single atoms and small molecules using the scanning tunnelling microscope. Phys. Status Solidi B **250**, 1671–1751 (2013)
47. Bartels, L., Meyer, G., Rieder, K.-H.: Basic steps of lateral manipulation of single atoms and diatomic clusters with a scanning tunnelling microscope tip. Phys. Rev. Lett. **79**, 697 (1997)
48. Grill L.: Functionalized molecules studied by STM: motion, switching and reactivity. J. Phys. Condens. Matter **20**, 053001 (2008)
49. Rapenne, G., Joachim, C.: The first nanocar race. Nat. Rev. Mat. **2**, 17040 (2017)
50. Gross, L., Rieder, K.-H., Moresco, F., Stojkovic, S.M., Gourdon, A., Joachim, C.: Trapping and moving metal atoms with a six-leg molecule. Nature Mater. **4**, 892–895 (2005)
51. Grill, L., Rieder, K.-H., Moresco, F., Rapenne, G., Stojkovic, S., Bouju, X., Joachim, C.: Rolling a single molecular wheel at the atomic scale. Nat. Nanotech. **2**, 95–98 (2007)
52. Haq, S., Wit, B., Sang, H., Floris, A., Wang, Y., Wang, J., Perez-Garcia, L., Kantorovitch, L., Amabilino, D.B., Raval, R.: A small molecule walks along a surface between porphyrin fences that are assembled in situ. Angew. Chem. Int. Ed. **54**, 7101–7105 (2015)
53. Wong, K.L., Pawin, G., Kwon, K.-Y., Lin, X., Jiao, T., Solanki, U., Fawcett, R.H.J., Bartels, L., Stolbov, S., Rahman, T.S.: A molecule carrier. Science **315**, 1391–1393 (2007)
54. Chiaravalloti, F., Gross, L., Rieder, K.-H., Stojkovic, S.M., Gourdon, A., Joachim, C., Moresco, F.: A rack-and-pinion device at the molecular scale. Nat. Mater. **6**, 30–33 (2007)
55. Beton, P.H., Dunn, A.W., Moriarty, P.: Manipulation of C_{60} molecules on a Si surface. Appl. Phys. Lett. **67**, 1075 (1995)
56. Jung, T.A., Schlittler, R.R., Gimzewski, J.K., Tang, H., Joachim, C.: Controlled room-temperature positioning of individual molecules: molecular flexure and motion. Science **217**, 181 (1996)
57. Hla, S.-W., Braun, K.-F., Wassermann, B., Rieder, K.-H.: Controlled low-temperature molecular manipulation of sexiphenyl molecules on Ag(111) using scanning tunneling microscopy. Phys. Rev. Lett. **93**, 208302 (2004)
58. Anggara, K., Leung, L., Timm, M.J., Hu, Z., Polanyi, J.C.: Approaching the forbidden fruit of reaction dynamics: Aiming reagent at selected impact parameters, Sci. Adv. **4**, eaau2821 (2018)
59. Anggara, K., Leung, L., Timm, M.J., Hu, Z., Polanyi, J.C.: Electron-induced molecular dissociation at a surface leads to reactive collisions at selected impact parameters. Faraday Discuss. **214**, 89–103 (2019)
60. Lewis, G.N.: A new principle of equilibrium. Proc. Nat. Acad. Sci. **11**, 179–183 (1925)
61. Tolman, R.C.: The principle of microscopic reversibility. Proc. Nat. Acad. Sci. **11**, 436–439 (1925)
62. Astumian, R.D., Hänggi, P.: Brownian motors. Phys. Today **55**, 33–39 (2002)

63. Onsager, L.: Reciprocal relations in irreversible processes I. Phys. Rev. **37**, 405–426 (1931)
64. Astumian, R.D.: Microscopic reversibility as the organizing principle of molecular machines. Nat. Nanotech. **7**, 684–688 (2012)
65. Astumian, R.D.: Protein conformational fluctuations and free-energy transduction. Appl. Phys. A **75**, 193–206 (2002)
66. Rousselet, J., Salome, L., Ajdari, A., Prost, J.: Directional motion of brownian particles induced by a periodic asymmetric potential. Nature **370**, 446–448 (1994)
67. Oudenaarden, A.V., Boxer, S.G.: Brownian ratchets: Molecular separations in lipid bilayers supported on patterned arrays. Science **285**, 1046–1048 (1999)
68. Kelly, T.R., Sestelo, J.P., Tellitu, I.: New molecular devices: in search of a molecular ratchet. J. Org. Chem. **63**, 3655–3665 (1998)
69. Pawin, G., Wong, K.L., Kwon, K.-Y., Frisbee, R.J., Rahman, T.S., Bartels, L.: Surface diffusive motion in a periodic and asymmetric potential. J. Am. Chem. Soc. **130**, 15244–15245 (2008)
70. Zhang, Y., Calupitan, J.P., Rojas, T., Tumbleson, R., Erbland, G., Kammerer, C., Ajayi, T.M., Wang, S., Curtiss, L.A., Ngo, A.T., Ulloa, S.E., Rapenne, G., Hla, S.W.: A chiral molecular propeller designed for unidirectional rotations on a surface. Nature Comm. **10**, 3742 (2019)
71. Stolz, S., Gröning, O., Prinz, J., Brune, H., Widmer, R.: Molecular motor crossing the frontier of classical to quantum tunneling motion. PNAS **117**, 14838–14842 (2020)
72. Astumian, R.D., Mukherjee, S., Warshel, A.: The physics and physical chemistry of molecular machines. ChemPhysChem **17**, 1719–1741 (2016)
73. Hänggi, P., Marchesoni, F.: Artificial Brownian motors: controlling transport on the nanoscale. Rev. Mod. Phys. **81**, 387–442 (2009)
74. Timm, M., Leung, L., Anggara, K., Polanyi, J.C.: Direct observation of knock-on reaction with umbrella inversion arising from zero-impact-parameter collision at a surface. Commun. Chem. **4**, 14 (2021)
75. Astumian, R.D.: Design principles for Brownian molecular machines: how to swim in molasses and walk in a hurricane. Phys. Chem. Chem. Phys **9**, 5067–5083 (2007)
76. M.G.L.v.d. Heuvel, C. Dekker, Motor proteins at work for nanotechnology, Science, 317 (2007) 333–336.
77. Kodera, N., Yamamoto, D., Ishikawa, R., Ando, T.: Video imaging of walking myosin V by high-speed atomic force microscopy. Nature **468**, 72–77 (2010)
78. Browne, W.R., Feringa, B.L.: Making molecular machines work. Nat. Nanotech. **1**, 25–35 (2006)
79. Erbas-Cakmak, S., Leigh, D.A., McTernan, C.T., Nussbaumer, A.L.: Artificial molecular machines. Chem. Rev. **115**, 10081–10206 (2015)
80. Baroncini, M., Silvi, S., Credi, A.: Photo- and redox-driven artificial molecular motors. Chem. Rev. **120**, 200–268 (2020)
81. García-López, V., Liu, D., Tour, J.M.: Light-activated organic molecular motors and their applications. Chem. Rev. **120**, 79–124 (2020)
82. Badjic, J.D., Balzani, V., Credi, A., Silvi, S., Stoddart, J.F.: A molecular elevator. Science **303**, 1845–1849 (2004)
83. Liu, Y., Flood, A.H., Bonvallet, P.A., Vignon, S.A., Northrop, B.H., Tseng, H.-R., Jeppesen, J.O., Huang, T.J., Brough, B., Baller, M., Magonov, S., Solares, S.D., Goddard, W.A., Ho, C.-M., Stoddart, J.F.: Linear artificial molecular muscles. J. Am. Chem. Soc. **127**, 9745–9759 (2005)
84. Eelkema, R., Pollard, M.M., Vicario, J., Katsonis, N., Ramon, B.S., Bastiaansen, C.W.M., Broer, D.J., Feringa, B.L.: Nanomotor rotates microscale objects. Nature **440**, 163 (2006)
85. Balzani, V., Clemente-Leon, M., Credi, A., Ferrer, B., Venturi, M., Flood, A.H., Stoddart, J.F.: Autonomous artificial nanomotor powered by sunlight. Proc. Natl. Acad. Sci. **103**, 1178–1183 (2006)
86. Klok, M., Boyle, N., Pryce, M.T., Meetsma, A., Browne, W.R., Feringa, B.L.: MHz unidirectional rotation of molecular rotary motors. J. Am. Chem. Soc. **130**, 10484–10485 (2008)

87. Conyard, J., Addison, K., Heisler, I.A., Cnossen, A., Browne, W.R., Feringa, B.L., Meech, S.R.: Ultrafast dynamics in the power stroke of a molecular rotary motor. Nature Chem. **4**, 547–551 (2012)
88. Stacko, P., Kistemaker, J.C.M., Leeuwen, T.V., Chang, M.-C., Otten, E., Feringa, B.L.: Locked synchronous rotor motion in a molecular motor. Science **356**, 964–968 (2017)
89. Kudernac, T., Ruangsupapichat, N., Parschau, M., Macia, B., Katsonis, N., Harutyunyan, S.R., Ernst, K.-H., Feringa, B.L.: Electrically driven directional motion of a four-wheeled molecule on a metal surface. Nature **479**, 208–211 (2011)
90. Augulis R., Klok, M., Feringa, B.L., Loosdrecht, P.H.M.V.: Light-driven rotary molecular motors: an ultrafast optical study. Phys. Stat. Sol. **6**(c), 181–184 (2009)
91. Chiang, P.-T., Mielke, J., Godoy, J., Guerrero, J.M., Alemany, L.B., Villagómez, C.J., Saywell, A., Grill, L., Tour, J.M.: Toward a light-driven motorized nanocar: synthesis and initial imaging of single molecules. ACS Nano **6**, 592–597 (2012)
92. Saywell, A., Bakker, A., Mielke, J., Kumagai, T., Wolf, M., García-López, V., Chiang, P.-T., Tour, J.M., Grill, L.: Light-induced translation of motorized molecules on a surface. ACS Nano **10**, 10945–10952 (2016)
93. Jacobson, P., Prezzi, D., Liu, D., Schied, M., Tour, J.M., Corni, S., Calzolari, A., Molinari, E., Grill, L.: Adsorption and motion of single molecular motors on TiO_2(110). J. Phys. Chem. C **124**, 24776–24785 (2020)
94. Schied, M., Prezzi, D., Liu, D., Jacobson, P., Corni, S., Tour, J.M., Grill, L.: Inverted conformation stability of a motor molecule on a metal surface. J. Phys. Chem. C **126**, 9034–9040 (2022)

DMBI—from n-Type Dopant to Molecular Machines

Oumaima Aiboudi and Franziska Lissel

Abstract Cationic benzimidazolium iodide salts are used in organic electronics to yield 2,3-dihydro-1*H*-benzimidazoles (DMBI-H), which are efficient n-type dopants. When brought onto a Au(111) surface, the derivative 2-(2-methoxyphenyl)-1,3-dimethyl-1*H*-benzoimidazol-3-ium iodide (*o*-OMe-DMBI-I) anchors in a highly stable fashion and subsequently rotates with high efficiency when excited with STM pulses: When voltage pulses are applied using a bias ranging between 300 and 400 mV, the molecule displays a sequential unidirectional rotational motion through six defined orientations with a probability higher than 95%. The exact binding mode of this molecular rotor could recently be elucidated and was found to be based on the cleavage of the methoxy group, which results in the formation of an alkoxy function able to bind to gold in a covalent fashion. Interestingly, the elongation of the rotator to a naphthalene unit prevents efficient binding, converting the rotor into a nanocar. Increasing the binding strength by substituting the -OMe with a -SMe group was not successful, as the required conversion to a cationic structure was not successful. Nonetheless, a structure combining the extended π-system of a naphthalene with the high addressability of the DMBI motor and a stable binding might be interesting to build more demanding molecular machinery, e.g. molecular gears.

Keywords Molecular machines · Molecular motor · Nano car · Molecular rotor

O. Aiboudi · F. Lissel (✉)
Institute of Macromolecular Chemistry (IMC), Leibniz Institute for Polymer Research Dresden (IPF), Hohe Str. 6, 01069 Dresden, Germany
e-mail: lissel@ipfdd.de

O. Aiboudi
Institute of Chemistry, Technical University Dresden, 01062 Dresden, Germany

F. Lissel
CFAED Center for Advancing Electronics Dresden, Technical University Dresden, 01062 Dresden, Germany

© The Author(s), under exclusive license to Springer Nature Switzerland AG 2023

F. Moresco and C. Joachim (eds.), *Single Molecule Mechanics on a Surface*,
Advances in Atom and Single Molecule Machines,
https://doi.org/10.1007/978-3-031-16930-4_2

1 Introduction

Molecular machines are multicomponent systems that perform mechanical-like work (output) in response to a defined external stimulus (energy input), e.g., thermal, chemical, and electrical energy [1]. Often, molecular machines are modelled on their macroscopic counterparts, e.g., nanocars: even as children, we have a clear idea of what a car looks like—tires connected by an axle carry a box, the chassis. Toy cars take this idea and introduce us to the most basic functions and limitations: After losing a wheel, the toy car runs slower and is harder to control. We can now follow these miniaturization steps further down to the molecular level, where our imagination of macroscopic cars becomes nanocars: molecules with a rigid inner chassis, for example an sp^2 hybridized vehicle chassis, which is supported by four round structures, for example fullerenes and is thus decoupled from the surface [2]. Richard Feynmann was the first to postulate the idea of infinitesimally small machines, which also includes molecular cars [3]. Nevertheless, it took years until James Tour finally synthesized the first nanocar in 2005 [2]. This molecule could be pulled off the tip of a scanning tunneling microscope (STM) like an infinitesimally small toy car. The group of Bernard Feringa was the first to build a molecular motor into a nanocar [4]: A double bond acts as a rotation axis and undergoes a trans-to-cis isomerization upon excitation by the STM tip, which pushes the nanocar forward. A distance of 6 nm can be covered with 10 STM pulses. Molecular rotors on the other hand do not move laterally, but instead show a rotational movement of one part of the molecule rotates against [5] Rotors consist of three parts: (i) a stator with high inertia—regarding surface mounted rotors, connected to the surface or the surface itself, (ii) a rotator with a small moment of inertia, and (iii) an atomic-scale axle connecting both components. The anchoring is of fundamental importance, as a reliable immobilization of the molecule is needed for experimental investigations of the rotor [6]. Ideally; the anchoring is sufficiently strong and robust under electrical operation, and favorable enough to bind reproducible. Fixing rotors on defined surface spaces is also prerequisite to build bigger molecular machinery, e.g. molecular gears [7]. In 2016, the Nobel Prize in Chemistry was awarded to B. Feringa along with Jean-Pierre Sauvage and J. Fraser Stoddart, “for the design and synthesis of molecular machines” [8].

From a chemical perspective, building molecular machinery is intriguing as it demands rigorous rational molecular design: e.g., the first nano car race in 2017 showed that the utilization of wheels in nanocar designs is not only superfluous, but can even detrimental.

2 1,3-Dimethyl-2-Phenyl-2,3-Dihydro-1*H*-Benzoimidazole (DMBI) as Building Block for Molecular Machinery

Two examples of these types of dopants that have been studied recently are the cationic benzimidazolium iodide salts (DMBI-I, Scheme 1), which release unidentified reactive intermediates during a high-temperature thermal deposition process, and the 2,3-dihydro-1*H*-benzimidazoles (DMBI-H, Scheme 1).

Benzoimidazoles like 1,3-dimethyl-2-phenyl-2,3-dihydro-1*H*-benzoimidazole (DMBI) have been mainly studied as easily deployed and comparably stable n-type dopants in organic electronics [9]. The synthesis is well accessible, as the cationic benzimidazolium iodide salts can be synthesized in a two-step process, and yield the targeted benzimidazoles during high temperature deposition processes [9]. In STM experiments, the derivative 2-(2-methoxyphenyl)-1,3-dimethyl-1*H*-benzoimidazol-3-ium iodide *o*-OMe-DMBI-I (Scheme 1) was found to anchor in a highly stable fashion to an Au(111) surface, and rotate with high efficiency when excited with STM pulses [10]. When voltage pulses are applied using a bias ranging between 300 and 400 mV, the molecule displays a sequential unidirectional rotational motion through six defined orientations with a probability higher than 95% [10]. Yet despite in-depth theoretical and experimental investigation of the rotation efficiency, the binding mode of the molecule to the gold surface was not clear. In general, the interaction of a molecule and a surface can be classified as (i) physisorption or (ii) chemisorption. The former describes weak (0.2–4 kJ/mo) [11] electrostatic interactions including *van der Waals* interactions, dipole–dipole and London forces. The latter encompasses the sharing of electrons between substrate and molecule, i.e. a formation of a chemical bond, and has a substantially higher interaction energy (e.g., 150–200 kJ/mol for the thiolate-Au bond [12]). This type of anchoring is possible by (i) radical adsorption and (ii) lone pair interaction [13]. Radical adsorption usually relies on the spontaneous dissociation of a molecule close to the metal surface, yielding unpaired electrons able to interact with unsaturated electronic metal states, or via a donor–acceptor bond (dative bond), i.e., the anchoring using a lone electron pair of the molecule that interacts with an under-coordinated metal atom.

Looking at the molecular structure of *o*-OMe-DMBI, several binding pathways are possible: (i) The cationic organic molecule is counterbalanced by a halide ion, and first experimental STM studies assumed the chemisorption of o-MeO-DMBI-I via the radical form obtained after such iodine dissociation [9]; (ii) the heteroleptic

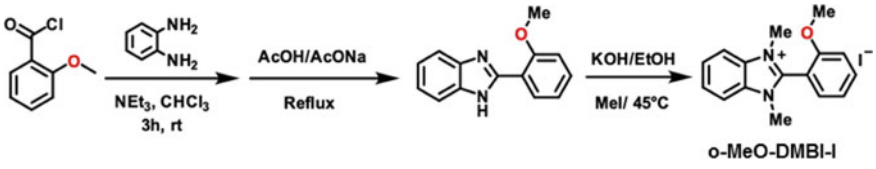

Scheme 1 Synthesis of *o*-MeO-DMBI-I

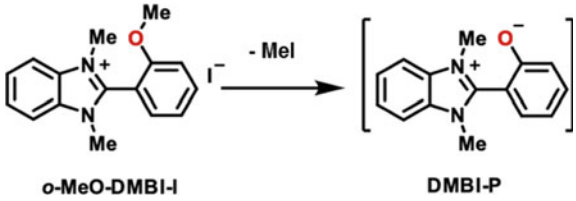

Fig. 1 2-(2-Methoxyphenyl)-1,3-dimethyl-1*H*-benzoimidazol-3-ium iodide (*o*-OMe-DMBI-I) yields 2-(1,3-dimethyl-1H-benzo[d]imidazol-3-ium-2-yl)-phenolate (DMBI-P) when methyl iodide is cleaved [10]

cleavage of the O–Me bond, which yield methyl iodide (MeI) and 2-(1,3-dimethyl-1H-benzo[d]imidazol-3-ium-2-yl)-phenolate (DMBI-P) (see Scheme 1) is an alternative intramolecular reaction observed by photoelectron spectroscopy. [14]. Binding via the resulting alkoxide is another possible pathway for stable binding to the gold surface (Fig. 1).

A mixed theoretical and experimental approach can be used to elucidate the binding mode. Thermal studies mimicking the deposition process can be carried out on sample sizes sufficient for applying different physico-chemical methods, i.e., proton nuclear magnetic resonance (^{1}H NMR) spectroscopy, headspace gas chromatography/mass spectrometry (GC/MS) and thermogravimetric analysis/infrared spectrometry (TGA/IR). Together with the results density functional theory (DFT) calculations of adsorption geometry and bonding energy of o-MeO-DMBI and DMBI-P on Au(111), they indicate the cleavage of the O–Me bond.

The molecule *o*-MeO-DMBI can be prepared in a two step reaction (Scheme 1) first proposed by Bao et al. [9] For the STM manipulation of *o*-MeO-DMBI-I and to observe the rotation on Au (111), the molecule is deposited by subliming at temperatures around 225 °C under ultra-high vacuum ($P \approx 1 \times 10^{-10}$ mbar). [10] Similar conditions are used for the deposition as n-dopant in organic electronics. [9] To understand the binding mode and whether *o*-OMe-DMBI or DMBI-P bind to the surface, thermal studies can be carried out. When a sample of *o*-MeO-DMBI-I is heated to 225 °C under vacuum ($P \approx 1 \times 10^{-3}$ mbar), a decomposition of the white compound can be observed, and a light-yellow compound is subliming to the upper part of the flask (see Fig. 2). [10]

The process taking place can be elucidated with different physico-chemical methods. ^{1}H NMR spectroscopy is extraordinary feasible, as the spectra reveal details about the chemical environment of the protons in the sample as well as the ratio of protons wit specific environments. The ^{1}H spectrum of pure *o*-MeO-DMBI-I has 7 proton signals with a total peak integration of 17 and specific chemical shifts (Figs. 3 and 4, bottom). The sample heated for 3 min shows the same peaks and peak pattern, but in addition revealed signals associated with an unknown species exhibiting 6 signals with a total peak integration of 14, i.e., three protons less than *o*-MeO-DMBI-I (Figs. 3 and 4, top) [10].

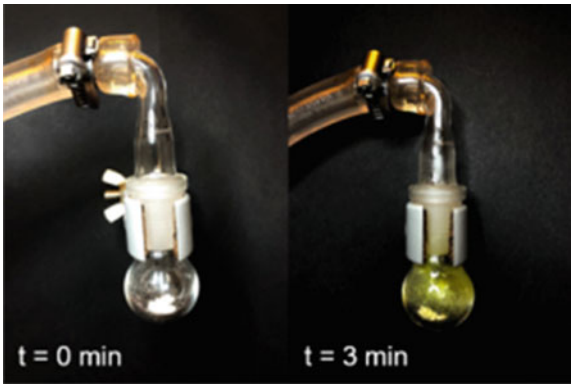

Fig. 2 Sublimation experiment—thermal transformation of *o*-MeO-DMBI-I at 225 °C. Reproduced/Adapted from Ref. [10] with permission from The Royal Society of Chemistry

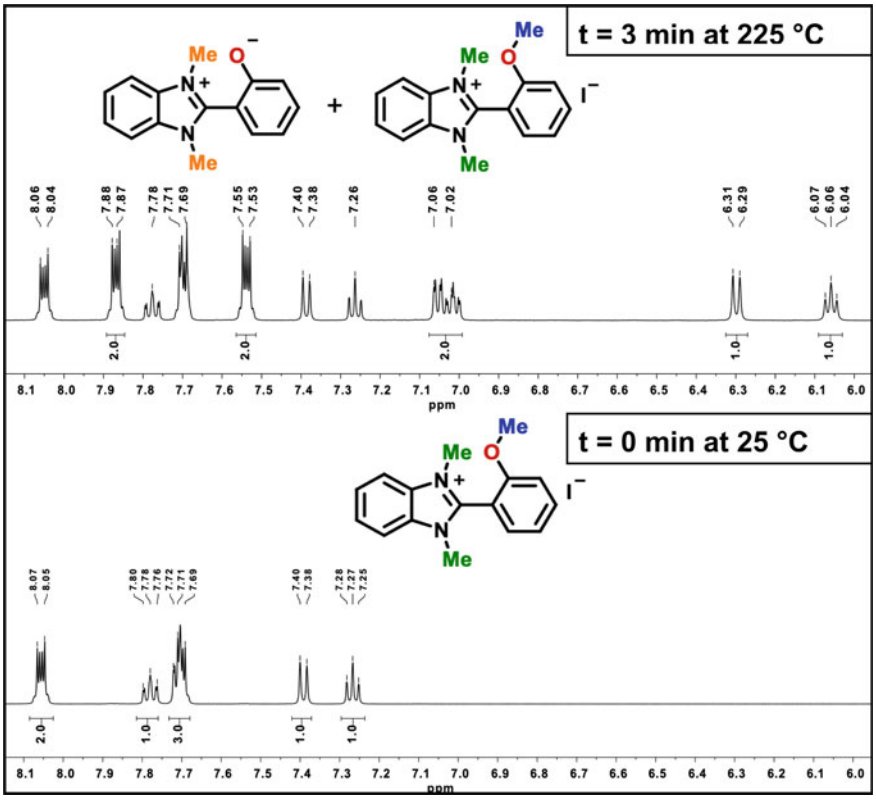

Fig. 3 ^{1}H NMR spectra of the aromatic region of a sample of *o*-MeO-DMBI-I at RT and after 3 min heating at 225 °C. Reproduced/Adapted from Ref. [10] with permission from The Royal Society of Chemistry

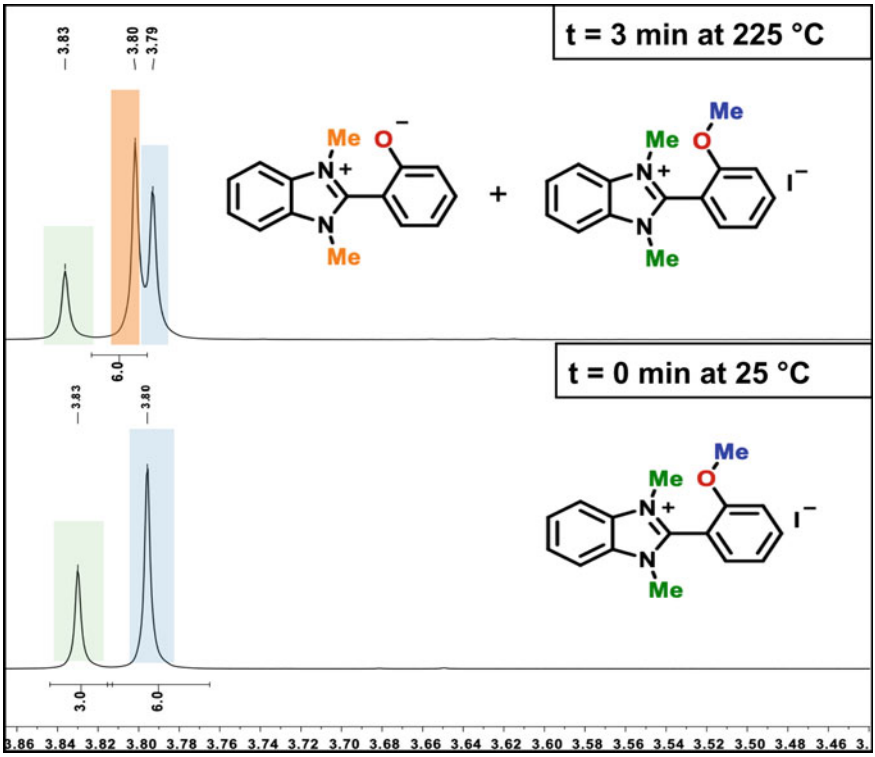

Fig. 4 Methyl region of the ^{1}H NMR spectra of a sample of *o*-MeO-DMBI-I before (bottom) and after (top) heating. Pure *o*-MeO-DMBI-I shows two peaks corresponding to N-Me and O-Me (colour coded in green and blue, respectively). After heating, a mixture of two species is observed: in addition the two signals of *o*-MeO-DMBI-I (colour coded in green and blue, respectively), a singlet (colour coded in orange) is observed. Reproduced/Adapted from Ref. [10] with permission from The Royal Society of Chemistry

In the aromatic region, *o*-MeO-DMBI-I and the decomposition product show similar signals with identical multiplicities and peak integration, but the peaks are shifted upfield (Fig. 4).

At the same time the methyl region shows a very insightful development: *o*-MeO-DMBI-I has two characteristic signals at chemical shifts of $\delta = 3.83$, and $\delta = 3.79$ ppm with a ratio of 1: 2 which correspond to the chemically equivalent N-Me groups and the O-Me group, respectively. The decomposition product shows only one signal (orange in Fig. 4)—i.e., the loss of one of the chemical groups. This is in agreement with the postulated cleavage of the O-Me group and the generation of DMBI-P, as a N-Me bond cleavage would reduce the molecular symmetry of the structure and result in two signals in a 1: 1 ratio, each corresponding to 3H of the O-Me and retained N-Me group, respectively. A cleavage of the O-Me group on the other hand should result into a singlet corresponding to the 6 H nuclei of the remaining two N-Me groups.

Investigations by GC/MS and TGA/IR further confirmed the cleavage of the methods group. In GC/MS, volatile (i.e., gaseous) fractions are separated on a stationary phase. The equation time depends on the their respective size and interaction with the stationary phase. The spirited products are then analysed in a mass spectrometer to pinpoint their molecular weight. *o*-Me-DMBI-I was heated in a sealed container, and the generated volatile fraction analysed. The obtained spectrum shows as major feature a sharp peak at a retention time of 1.8–1.9 min. Resolution in the mass spectrometer identified methyl iodide (m/z 141.9) as the volatile product.

For TGA, the sample is heated up under controlled conditions, and weightless is recorded. Again the evolved gaseous products can be further analyzed, e.g., with IR spectroscopy. The TGA spectrum of *o*-Me-DMBI-I shows a pronounced weight drop at 220 °C (Fig. 6, top). The weight loss of corresponds to 39 wt-%, which is again consistent with the loss of methyl iodide, i.e., the a decomposition of *o*-MeO-DMBI to DMBI-P via the cleavage of the H_3C-O bond. A second decomposition peak at 250 °C indicates a further degradation of DMBI-P at higher temperatures. The evolved gaseous products were analysed with IR spectroscopy (Fig. 5, bottom) and a clear succession of event can be followed: At 185 °C, only signals relating to water and CO_2 are detected. At 236 °C, i.e., the temperature of the pronounced weight loss, new bands are appearing at $\nu = 2971$, 3060 cm^{-1} and $\nu = 1250$, 1435 cm^{-1}. The former are associated with the -CH_3 stretching bands, while the latter denote the -CH_3 deformation. The occurrence of methyl-related bands is once more consistent with the loss of methyl iodide. At temperatures above 245 °C, the presence of aromatic fragments (700 cm^{-1}) indicate the thermal degradation of DMBI-P.

The used experimental methods indicate a partial thermal decomposition of *o*-MeO-DMBI, i.e., the cleavage of methyl iodide leading to DMBI-P. The resulting molecule can anchor to gold via the electron pairs of the alkoxy function (Fig. 6).

3 Varying the Molecular Structure of DMBI

The cleavage of methyl iodide makes *o*-MeO-DMBI-I an excellent molecular rotor that binds via the lone pairs of the oxygen. Yet already minor changes to the molecular structure have a pronounced impact on the efficiency of binding: e.g., the elongation of the aromatic core of the benzimidazole to a naphthalene seemingly prevents binding to the surface, maybe because of the interaction of the extended conjugated system with the metal surface. Interestingly, while the lack of reliable and pronounced binding to the surface prevents the application as *molecular rotors*, these molecules show defined lateral movement, i.e., are *nanocars* which show lateral movement when excited.

This raises another interesting question, i.e., what happens when an even stronger anchor group is used in combination with an extended conjugated system? One can assume that a sufficiently strong binding can anchor even an extended system, and that such a rotor might be a well controllable construction unit to build more complicated machinery, e.g., molecular gears.

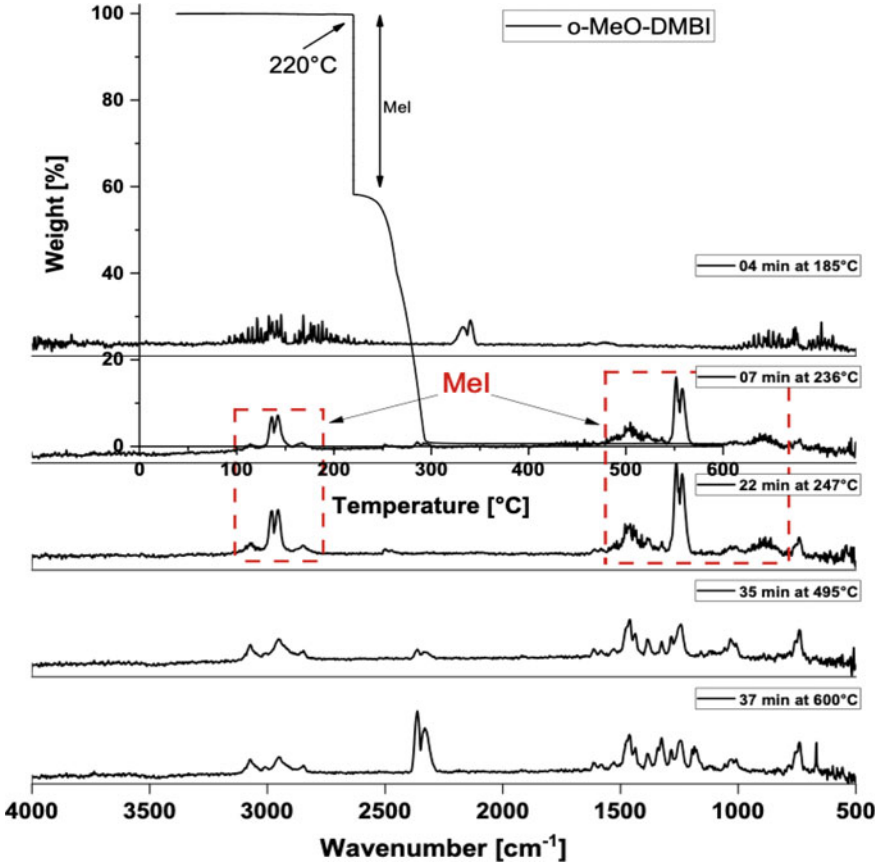

Fig. 5 Thermal gravimetric analysis (TGA) of *o*-Me-DMBI-I (top) shows a pronounced weight loss of 39 weight-% at 220 °C, consistent with MeI cleavage. IR spectroscopy of the gaseous products at different temperatures similarly shows bands associated with methyl stretching and deformation bands (bottom). Reproduced/Adapted from Ref. [10] with permission from The Royal Society of Chemistry

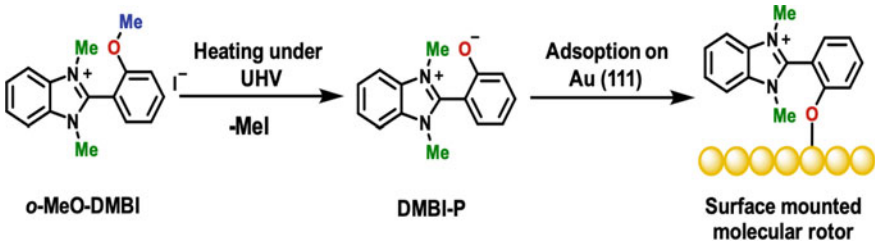

Fig. 6 Evaporation and adsorption process of *o*-MeO-DMBI leading to DMBI-P and binding to Au (111). Reproduced/Adapted from [10] with permission from The Royal Society of Chemistry

The cleavage of methyl iodide yields an alkoxy function, i.e., a classic oxygen based anchor groups. Together with other oxygen based anchoring groups, e.g., carboxylic acids (-COOH), carboxylic esters (-COOR), nitro groups (-NO_2), alkoxy groups (-O-R) are well studied—yet their stability and binding strength are weaker than organosulfur anchors [15]. Sulfur has a high affinity to gold, and sulfur-containing anchors chemisorb on Au surfaces with high binding energies (0.45–1.72 eV) [16]. Sulfur containing anchors, e.g. dialkylsulfides, methylsulfides and thioether bind and immobilize chemical compounds either via a lone pair or radical adsorption [17]. Replacing the oxygen of *o*-MeO-DMBI-I with a more robust thioether group might either allow direct biding via the lone pairs of the sulfur, or via cleavage of methyl iodide, leading to S-DMNI able to forma a strong covalent S–Au bond (Scheme 2).

The targeted MeS-DMNI should be achievable via a simple reaction scheme (Scheme 3): Thiobenzoic acid is commercially available, and can be S-methylated to achieve 2-(methylthio)benzoic acid (**10**). This acid can be converted to the corresponding acyl chloride (**11**), and the imidazole derivative (**12**) formed by condensation with diaminonaphtalene. Methylation should then yield the targeted iodide salt (**13**).

Scheme 2 Chemical structure of MeS-DMNI, expected cleaved S-DMNI, and postulated binding to Au (111) surface

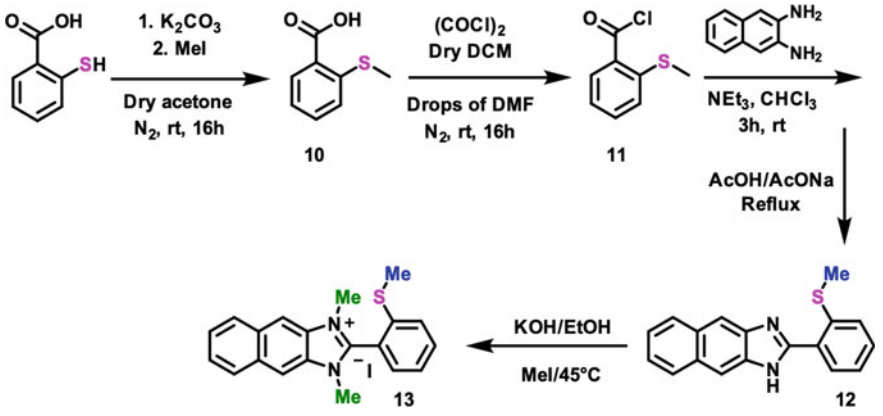

Scheme 3 Synthetic pathway targeting MeS-DMNI (**13**)

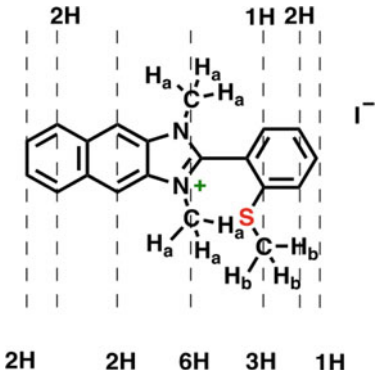

Fig. 7 Total protons of targeted compound **13**, and expected peak pattern

Yet while compounds **10**–**12** could be obtained and successfully characterized using proton and carbon NMR spectroscopy, the ^{1}H NMR spectrum of **13** is not consistent with the formation of the targeted molecule. Molecule **13** should display signals with a total integration of 19 (Fig. 7): Three signals in the down-field region (aromatic protons region, 8.79–7.50 ppm), corresponding to naphthalene unit, i.e. one singlet (2H) and two multiplets (2H). Like for *o*-MeO-DMBI, the two -N-CH_3 of the imidazolium are expected as singlet (6H) due to the symmetry of the molecule. The SCH_3 methyl group can be expected slightly shifted to high field compared to *o*-MeO-DMBI, as the sulfur has a lower electronegativity compared to oxygen.

The spectrum of **13** does not meet these expectations: most notably, proton signals with a total integration of 20 are found, i.e., one proton more than expected (Fig. 8). In the aromatic region, the naphthalene unit gives rise to 6 distinct signals: two singlets, two doublets and two triplets. In the high field, two singlets appear for the two N-CH_3 groups. The appearance of two signals in this region indicates a symmetry breaking within the molecule, which is also consistent with the number of signals in the aromatic region. The signal relating to the S-Me group, expected to be a singlet, is a doublet, while a new signal, a doublet ($1H$) appears at a chemical shift of $\delta =$ 6.66 ppm. Such a pattern might be explained by the generation of a double cation via sulfoxide formation or protonation of the sulfide group. Both of these structures should prevent the targeted cleavage and consequently the targeted binding. And indeed, no experimental proof of methyl iodide formation was found, and attempts to bind to gold surfaces and manipulate the molecule were unsuccessful. The of theIn this case, we would expect 20 protons in total, which is in agreement with the current NMR spectrum. However, one would expect 3 distinct signals (6H) for naphthalene instead of 6 signals as found in the spectrum we recorded.

While the inclusion of a sulfur-based anchor group was not successful, building elongated rotors might be possible with other anchors. One way to increase binding stability is the utilisation of more than one anchoring point, and one might easily imagine molecular structures containing DMBI cores and multiple binding points. Another possibility is the utilisation of a single bond that is stronger than the Au–S

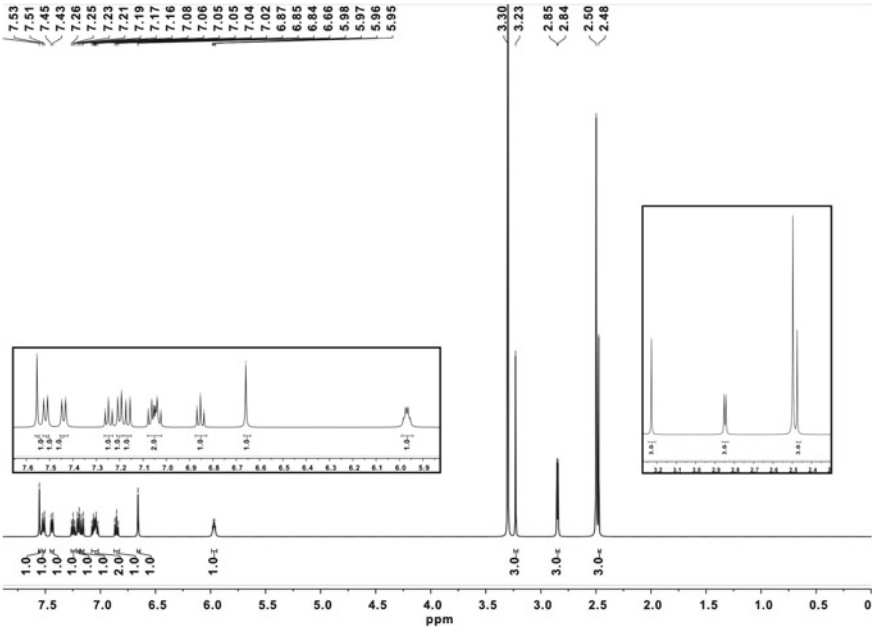

Fig. 8 ^{1}H NMR spectra of compound **13**

bond. In this regard, especially bonds between acetyl carbons and gold, or between carbenes and gold, are promising.

4 Summary

Molecular machinery seeks to build and manipulate molecules able to convert an external stimulus into defined motion, e.g. rotation (molecular rotors) or lateral movement (nano cars). To build advanced ensembles such as molecular gears to transporters, advanced molecular structures are needed. Cationic benzimidazolium iodide salts, known as efficient n-type dopants in organic electronics, are interesting building blocks for such applications: The derivative 2-(2-methoxyphenyl)-1,3-dimethyl-1*H*-benzoimidazol-3-ium iodide (*o*-OMe-DMBI-I) anchors to gold surfaces in a highly stable fashion and subsequently rotates in a unidirectional fashion when excited with STM pulses. The exact binding mode of the rotor to the surface was found to be based on the cleavage of the methoxy group, which results in the formation of an alkoxy function able to bind in a covalent fashion. Elongation of the rotator to a naphthalene unit prevents efficient binding, converting the rotor into a nano car. Increasing the bidding strength by substituting the -OMe with a -SMe group was not successful. Still, a structure combining the extended π-system of a naphthalene with the high addressability of the DMBI motor and a stable binding might be interesting to build

more demanding molecular machinery, e.g. molecular gears, and suitable groups are especially carbon-based anchors such as acetylides or carbenes.

Acknowledgments O.A. thanks the Helmholtz International Research School for Nanoelectronic Networks (NanoNet) for a Ph.D. fellowship, F.L. the Fonds der Chemischen Industrie (FCI) for a Liebig fellowship.

References

1. Ballardini, et al.: Acc. Chem. Res. **34**(6), 445 (2001)
2. Shirai, et al.: Nano Lett. **5**(11), 2330 (2005)
3. Feynman, presented in the framework of the yearly meeting of the "American Physical Society" at *California Institute of Technology (Caltech)* am 29 Dezember 1959, Eng. Sci. **23**(5), 22 (1960); Feynman, presented at *Jet Propulsion Laboratory* am 23 Februar 1983. J. Micromechanical Syst. **2**, 4 (1993)
4. Kudernac, R., et al.: Nature **497**, 208 (2011)
5. Kottas, et al.: Chemical Rev. **105**(4), 1281 (2005)
6. Aiboudi, O., Lissel, F.: Chemical anchoring of molecular rotors. In: Building and Probing Small for Mechanics, pp. 99–115, Part of the Advances in Atom and Single Molecule Machines book series (AASMM)
7. Manzano, et al.: Nat. Mater. **8**(7), 576 (2009); NPG Asia Mater. **1**(1), 13 (2009)
8. https://www.nobelprize.org/prizes/chemistry/2016/summary/. Accessed 20 May 2022
9. Wei, et al.: J. Am. Chem. Soc. **132**(26), 8852 (2010); Wei, et al.: J. Am. Chem. Soc. **134**(9), 3999 (2012)
10. Eisenhut, et al.: Nanoscale **13**, 16077 (2021)
11. Lippert, A.: Chem. **72**(16), 602 (1960)
12. Pensa, et al.: Acc. Chem. Res. **45**(8), 1183 (2012)
13. Olavarria-Contreras, et. al.: J. Am. Chem. Soc. **138**(27), 8465 (2016); Liu et al.: Beilstein J. Nanotechnol. **8**(1), 892ß (2017)
14. Schwarze, et al.: ACS Appl. Mater. Interfaces 10, 1340 (2018)
15. Reed, et al.: Science **278**(5336), 252 (1997); Lissel, et al.: J. Am. Chem. Soc. **136**(41), 14560 (2014); Schwarz, et al.: Nat. Nanotechnol. **11**, 170 (2016)
16. Ulman, C.: Rev. **96**(4), 1533 (1996)
17. Vericat, et al.: RSC Adv. **4**(53), 2773 (2014); Valášek, et al.: Beilstein J. Nanotechnol. **7**(1), 374 (2016)

Assembly, Diffusion and Rotation of Organic Molecules on a Gold Surface

Roberto Robles, Vladimír Zobač, and Nicolás Lorente

Abstract The interplay between molecules and surfaces has become a rich playground to study a wide variety of phenomena. Advances in deposition procedures, scanning probe techniques, and theoretical modeling and simulation have allowed us to explore many different avenues, like many-body effects, the on-surface synthesis of new molecules, or the motion of molecules on surfaces. Here, we study theoretically two different organic molecules on a gold (111) surface. For the first one, acetylbiphenyl (ABP), we show how after deposition the ABP molecule diffuses along the main directions of the Au(111) surface, revealing the directionality of the molecule-surface interactions driven just by van der Waals forces. This diffusion leads the molecules to form robust supramolecular assemblies stabilized by gold adatoms. For the second molecule, DMBI-P, we show how the molecule is dissociated after deposition, getting anchored to the surface and forming a molecule-rotor that presents a unidirectional motion at 5 K.

Keywords Molecular adsorption · Molecular assembly · Molecular deposition · On-surface synthesis · Supramolecular assemblies · Van der Waals forces · Molecule-rotor · Acetylbiphenyl · DMBI-P · Atomistic calculations · DFT · LT-UHV STM

1 Introduction

The question of how small a machine can be built has historically attracted a lot of attention. The award of the Nobel Prize in Chemistry to Sauvage, Stoddart and Feringa in 2016 for the design and synthesis of molecular machines exemplifies this

R. Robles · V. Zobač · N. Lorente (✉)
Centro de Física de Materiales CFM/MPC (CSIC-UPV/EHU), Paseo Manuel de Lardizabal 5, 20018 Donostia-San Sebastián, Spain
e-mail: nicolas.lorente@ehu.eus

N. Lorente
Donostia International Physics Center (DIPC), Paseo Manuel de Lardizabal 4, 20018 Donostia-San Sebastián, Spain

© The Author(s), under exclusive license to Springer Nature Switzerland AG 2023

F. Moresco and C. Joachim (eds.), *Single Molecule Mechanics on a Surface*,
Advances in Atom and Single Molecule Machines,
https://doi.org/10.1007/978-3-031-16930-4_3

interest [1]. The pursue in miniaturization has reached the limits of single atoms [2], but a lot of effort is still needed in order to understand the processes that rule these molecular machines. Particular interest deserves the machines formed by molecules adsorbed on surfaces, where they can be constructed and controlled by means of scanning probe microscopes [3, 4]. For example, the use of scanning tunneling microscopy (STM) tips allows us to translate molecules, which behave like "nanocars" [5], or to make them turn as molecular motors [6]. In addition, the presence of a surface opens the possibility of accessing new molecular compounds by applying on-surface synthesis techniques [7] or building supramolecular assemblies by molecular self-organization [8, 9]. The understanding of the processes behind the construction and manipulation of molecular machines is not straightforward and requires a lot of theoretical effort. An appropriated description of the different interactions at play between molecules, surfaces and scanning probe tips is paramount and the most powerful tool to achieve this description is the modeling of the systems by different theoretical methods. In this chapter, we will show how the use of first-principles calculations allows us to shed light on the assembly, diffusion and rotation of organic molecules on gold surfaces.

Based on previous experimental results, we will analyze the adsorption of acetylbiphenyl (Sect. 3), exploring its diffusion on Au(111) (Sect. 3.1) and the formation of robust supramolecular assemblies (Sect. 3.2). Then we will study the DMBI-P molecule also on Au(111), which behaves as a unidirectional molecular rotor (Sect. 4).

2 Theoretical Method

All the calculations were performed in the framework of the density functional theory (DFT) as implemented in the VASP code [10]. Core electrons were treated within the projected augmented-wave method [11], while valence electrons were described using a plane-wave basis set with an energy cutoff of 400 eV. The PBE flavor of GGA was used as exchange–correlation functional [12]. The long-range van der Waals (vdW) interactions are largely missing in this scheme. Since these forces are essential for the correct description of organic molecules on noble metal surfaces, we have completed the PBE functional following the Tkatchenko-Scheffler method [13] for the ABP molecules, and the DFT-D3 method [14] with Becke-Johnson damping [15] for the DMBI-P molecules. VASP is a periodic code that implements a periodic unit cell. This leads to representing molecules on surfaces as a periodic array, where the surface is represented by a finite slab separated by sufficient vacuum and each lateral unit cell is large enough to avoid interactions among molecules. The Au(111) surface was modeled using a slab of 4 Au layers and different unit cell sizes depending on the size of the deposited molecules to ensure the lack of interaction between the repeating images. The geometries of the molecules and the two upper Au layers were relaxed until all forces were smaller than 0.02 $eV \cdot Å^{-1}$. The transferred charge between molecule and substrate was calculated by performing the Bader analysis of

Ref. [16]. Finally, the nudged elastic band method (NEB method) [17] was used to compute the adiabatic minimum-energy paths between two molecular configurations on the surface.

For the comparison of theoretical results with experimental STM data we have simulated STM topographic and conductance images using the Tersoff and Hamann [18, 19] theory following the method described by Bocquet et al.[20] as implemented in the STMpw computer code [21]. Structural images have been represented using the program VESTA [22].

3 Adsorption of 4-acetylbiphenyl on Au(111)

The adsorption of 4-acetylbiphenyl on Au(111) was experimentally studied in different works [23–25]. It was shown that after adsorption, the ABP molecules lie flat on the surface either along the $[1\bar{1}0]$ or the $[11\bar{2}]$ directions. The molecules self-assemble to form different supramolecular structures which can be moved as single entities and in a controlled way by applying voltage pulses by a STM tip. More that 90% of the structures can be moved along the $[1\bar{1}0]$ direction, while the rest of the motion involves other directions or a combination of rotation plus translation. Another important point is that the molecules move along the $[1\bar{1}0]$ direction in discrete steps: 60% in steps of a single lattice unit and the rest in steps of two lattice units.

The above results show that the ABP-surface interaction has an important directionality and selectivity. In order to understand these results, we have performed extensive theoretical calculations using DFT.

In Sect. 3.1 we will explore the adsorption and diffusion of a single molecule on Au(111), while in Sect. 3.2 we will explore the formation of the supramolecular structures.

3.1 Diffusion of a Single Molecule on Au(111)

The 4-acetylbiphenyl molecule is formed by two phenyl rings and an acetyl group. The phenyl rings are joined by a single C–C bond that allows the rings to rotate with respect to each other. The final structure of the molecule is determined by the balance between the tendency of the molecule to be flat in order to maximize the π-conjugation between the phenyl rings, and the steric hindrance between the adjacent hydrogen atoms [26]. We have fully optimized the geometry of the ABP molecule in the gas phase and the results can be seen in Fig. 1. Our calculations confirm the existence of an angle $\alpha = 35.8^{\circ}$ between the phenyl rings. The acetyl group is located at the fourth carbon atom of one of the phenyl rings. This group allows the formation of hydrogen bonds with similar molecules, and induces an asymmetry in the molecule which is reflected in the formation of a dipole of 1.455 D.

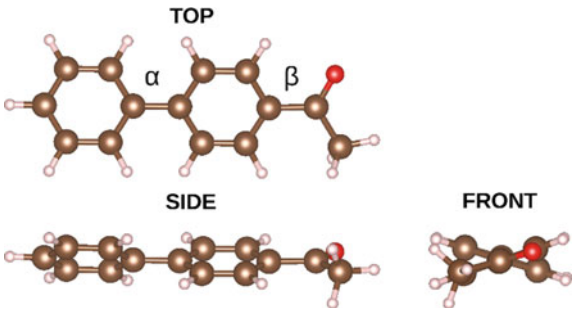

Fig. 1 Optimized gas-phase geometry of the ABP molecule. Both phenyl rings are rotated with respect to each other, forming an α angle of 35.8° (see front view). The β angle between the right-side phenyl ring and the acetyl group is around 0°

After determining the structure of the molecule in the gas-phase we have studied possible configurations of the molecule adsorbed on Au(111). In order to narrow down the exploration of the energy surface we have followed the experimental results from [23] and we have positioned the molecule with the two phenyl rings aligned along the $[1\bar{1}0]$ and the $[11\bar{2}]$ directions.

Then we have modified the adsorption site along both directions until finding the most stable configurations shown in Fig. 2. Comparing with the gas-phase geometry, the largest change after adsorption is the flattening of the molecule, as can be seen in the reduction of the α angle from 35.8° to 3.1° along the $[11\bar{2}]$ direction and to 0.8° along the $[11\bar{2}]$ one (see Table 1).

The reason for the flattening of the molecule is the effect of the van der Waals interaction, which is optimized for a large overlap between molecule and surface. As a consequence, the molecule presents a larger π-conjugation between the phenyl rings. We have also calculated the adsorption energy defined as $E_{ads} = E(Au111) + E(ABP) - E(ABP@Au111)$ (Table 1), where E(Au111) is the energy of the Au(111) surface, E(ABP) is the energy of the ABP molecule in the gas-phase and E(ABP@Au111) is the energy of the ABP molecule adsorbed on the Au(111) surface. The adsorption energy E_{ads} is quite strong, with a value around 1.7 eV. This energy is similar to the one found for other organic molecules, like naphtalene, adsorbed on densely packed noble metal surfaces [27]. The average height of the molecule over the surface (C_{aver}–Au) is around 3.3 Å (Table 1), also in agreement with previous results [27].

An analysis of the origins of the adsorption energy shows that the interaction with the substrate is due almost completely to the vdW forces, as it has been shown for other similar cases [27].

The adsorption of the molecule along both directions is largely the same, but some differences arise. The $[1\bar{1}0]$ conformation is 19 meV lower in energy than the $[11\bar{2}]$ one. The angle β formed between the acetyl group and the phenyl ring is higher along the $[11\bar{2}]$ direction, since the O atom is significantly closer to the surface (Table 1).

The above results point to a slightly different interaction of the O atom with the surface in the two cases. In order to confirm this finding, we have plotted the projected

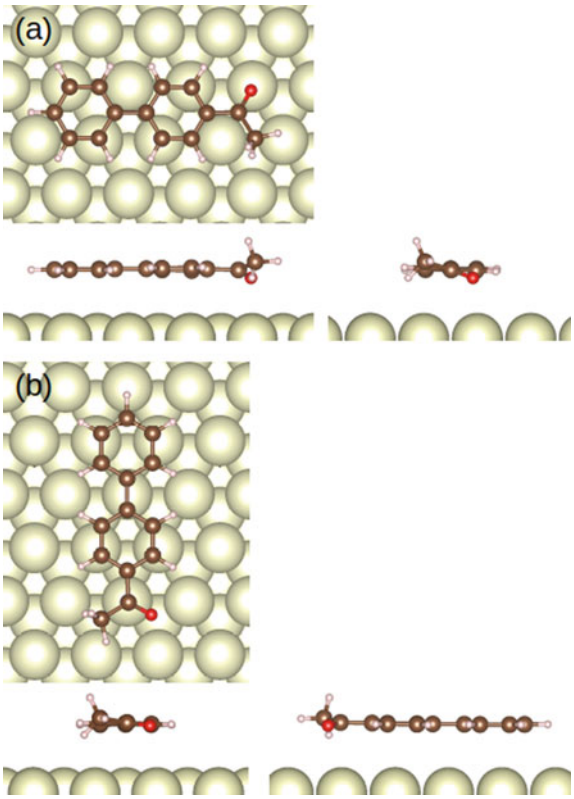

Fig. 2 Most stable structures of the ABP molecule adsorbed on Au(111) along [1$\bar{1}$0] (**a**) and [11$\bar{2}$] (**b**) directions. As can be seen in the lateral views, the molecule gets flattened with a significant reduction of the α angle

Table 1 Adsorption energies (E_{ads}) and geometrical properties of the ABP molecule in the gas-phase and supported configurations

	E_{ads} (eV)	d(O-Au)(Å)	d(C_{aver}-Au)(Å)	α (deg)	β (deg)
Gas-phase	–	–	–	35.8	1.4
[1$\bar{1}$0]	1.700	2.86	3.28	3.1	15.2
[11$\bar{2}$]	1.681	3.16	3.37	0.8	6.7

d(O-Au) is the distance between the oxygen atom and the closest Au atom from the first layer of the surface. d(C_{aver}-Au) was calculated as the difference of the average z coordinate of all C atoms and the average z coordinate of the Au atoms of the first atomic layer. α and β angles are shown in Fig. 1

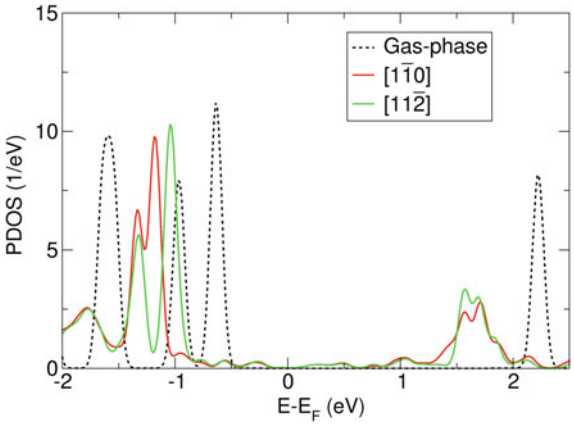

Fig. 3 Density of states projected on the states of the gas-phase ABP molecule (black dashed line), and on the molecule adsorbed along the [1$\bar{1}$0] (red) and [11$\bar{2}$] (green) directions. To make the comparison possible, we have aligned the vacuum levels of gas-phase and adsorbed molecules and we have applied a Gaussian broadening of 0.05 eV

density of states (PDOS) for the gas-phase molecule and for both adsorbed configurations (Fig. 3). We have aligned the gas-phase PDOS with the surface-supported one using their corresponding vacuum levels.

For the lowest unoccupied molecular orbital (LUMO), we observe a similar behavior for both orientations: a downshift of around 0.5 eV and a broadening of the molecular level as a consequence of the small hybridization with the surface.

The occupied levels (HOMO for highest occupied molecular orbital) show a different behavior. In the gas phase, HOMO and HOMO-1 are separated by 0.33 eV. On the [11$\bar{2}$] orientation, there is a downshift of the levels like for the LUMO, but the distance between HOMO and HOMO-1 is largely unchanged (0.28 eV). However, for the [1$\bar{1}$0] orientation, the downshift is larger and the separation between the levels is significantly closer (0.15 eV). We can rationalize this behavior by realizing that the HOMO has an important contribution from the oxygen p-orbital, which is largely absent from the other levels.

Finally, we can conclude that the stronger interaction of the O atom with the surface for the [1$\bar{1}$0] configuration is the origin of the different shift in energies of the HOMO, and the main electronic difference between both molecular conformations.

In the above discussion, we have seen that the ABP molecule binds almost exclusively due to vdW forces. However, the experimental results clearly show that the molecule diffuses on the Au(111), preferentially along the high-symmetry directions of the surface [23]. These results are somehow unexpected, since we expect the vdW bonding to show a very small corrugation along the surface, which should result in a quite-flat potential energy surface (PES). In order to rationalize this behavior, we have studied the energy barriers that the molecule encounters as it moves on the surface along certain directions.

First, we have looked at the molecule oriented along $[1\bar{1}0]$. When it moves in a direction forming 0° between the molecule axis and the path, the barrier is just 36 meV. This is much smaller than the adsorption energy of − 1.7 eV. If instead we move the molecule in a direction forming 60º with the orientation of the molecule, the barrier rises to 87 meV. Although this last value is still small compared to the adsorption energy, it shows that there is a corrugation of the PES of a few tens of meV. If we analyze the origin of the barrier, we can see that most of it originates in the vdW interactions (i.e. 80 meV of the 87 meV barrier is of van der Waals nature).

A similar scenario appears when we analyze the molecule adsorbed along the $[11\bar{2}]$ direction. Here, we have computed a small barrier of 19 meV when the molecule moves in a 60° direction with respect to the axis of the molecule. This barrier rises to 81 meV in a direction perpendicular to the molecule. As we can see, the size of the barriers is similar for both cases, but the final preferential direction depends on the orientation of the molecule.

In conclusion, our calculations show that the PES is flat compared with the binding energy, but it shows a corrugation of few tens of meV with different preferential directions depending on the orientation of the molecule. The main contribution to the corrugation comes from the vdW interactions. A deeper analysis of the PES can be found in [28].

3.2 Formation of Supramolecular Assemblies

After adsorption of the ABP molecules on the Au (111) surface, they self-organize to form supramolecular structures. In most cases, these supramolecular structures are just trimers and tetramers of ABP molecules [23]. These structures can be moved as one-single entity by applying pulses by the STM tip. This means that the molecules bind strongly enough to maintain the supramolecular structure.

Let us focus on the tetramer, dubbed "windmill" in Ref. [23]. By extensive DFT calculations we have explored different configurations of four ABP molecules which could result in the experimental conformations shown in [23]. Among all the possibilities the lowest energy configuration is shown in Fig. 4, together with a simulated STM image calculated using STMpw [21].

It is worth noting that an adsorbed ABP molecule is chiral, so we are just showing one of the possible chiralities of the supramolecular structure. Compared with the experimental images in [23], our model agrees in apparent size and height. However, there is a contrast depression at the center of the tetramer much deeper than the experimental one. In addition, the adsorption energy per ABP molecule is just 1.737 eV, only 37 meV stronger than the value for a single ABP molecule on Au(111). In other words, the energy gain due to the formation of the tetramer is just 37 meV per molecule. This value seems small to justify the experimentally observed integrity of the structure.

An extra ingredient to be considered in the explanation of the stability of the supramolecular structures is the existence of gold adatoms on the Au(111), which are

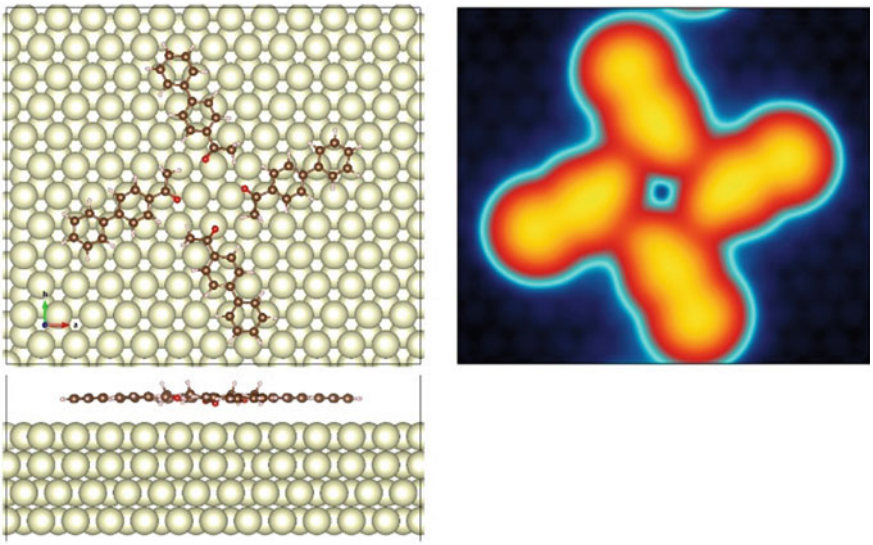

Fig. 4 (Left side) Top and side views of the most stable structure of the adsorbed tetramer found by DFT calculations. The four ABP molecules are oriented along the high-symmetry directions $[1\bar{1}0]$ (up and down molecules) and $[11\bar{2}]$ (left and right molecules). (Right side) Simulated topographic STM image at V = − 0.5 V of the structure in the left

known to diffuse at room temperature after, for example, detaching from step edges [29]. Gold adatoms are known to enhance the binding of organic molecules adsorbed on Au(111) [30–32]. They can also act as nucleation centers to start the self-assembly of molecular nanostructures [32]. In order to check this possibility, we have calculated the adsorption energy of a single ABP molecule to a gold adatom on Au(111). The adatom binds to the oxygen atom of the acetyl group. The obtained value is 2.077 eV, which represents an increase of 0.377 eV compared to the adsorption energy of a single ABP molecule on Au(111) (Table 1). After formation, an Au-ABP complex would randomly diffuse along the surface at room temperature and could work as a nucleation center for the supramolecular structures. In order to check this possibility, we have added an increasing number of gold adatoms to the structure in Fig. 4. Considering that the gold adatom binds to the oxygen atom for a single ABP molecule, we have added the adatoms to the central part of the tetramer. The obtained structures can be seen in Fig. 5 and the adsorption energies can be found in Fig. 6a. Already the addition of a single adatom represent a significant increase in the adsorption energy of 0.136 eV per molecule (1.873 eV/mol), and after the addition of 2 or more adatoms the adsorption energy stabilizes around 2 eV (Fig. 6a).

We can also study the plausibility of the involvement of gold adatoms in the formation of the tetramers from the point of view of thermodynamics. In Fig. 6b, we have estimated the change of the Gibbs free energy as a function of the chemical potential of the sources of adatoms. A negative change indicates that the gold adatoms

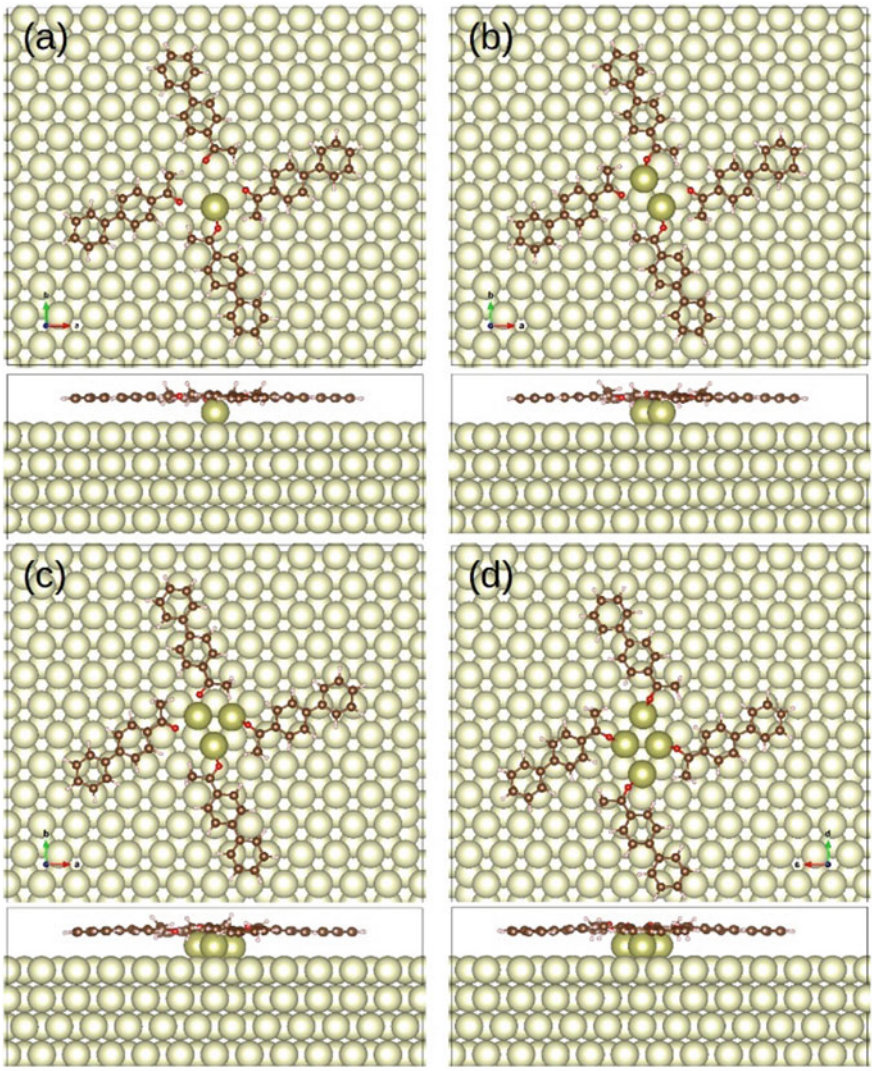

Fig. 5 Optimized structures of the tetramer containing an increasing number of gold adatoms, from one (**a**) to four (**d**). The gold adatoms adsorb at hollow positions of the Au(111) surface. The inclusion of the adatoms produces a modest distortion of the tetramer, which remains mainly planar like in the structure without adatoms (Fig. 4)

will be incorporated into the supramolecules, while a positive change would indicate that they will remain at the source.

There are different possible sources of gold atoms. We have assumed two probable limits depending on where the adatoms originates. The most-strongly-bound one would be a bulk-gold atom (left vertical blue line in Fig. 6b), while the least bounded

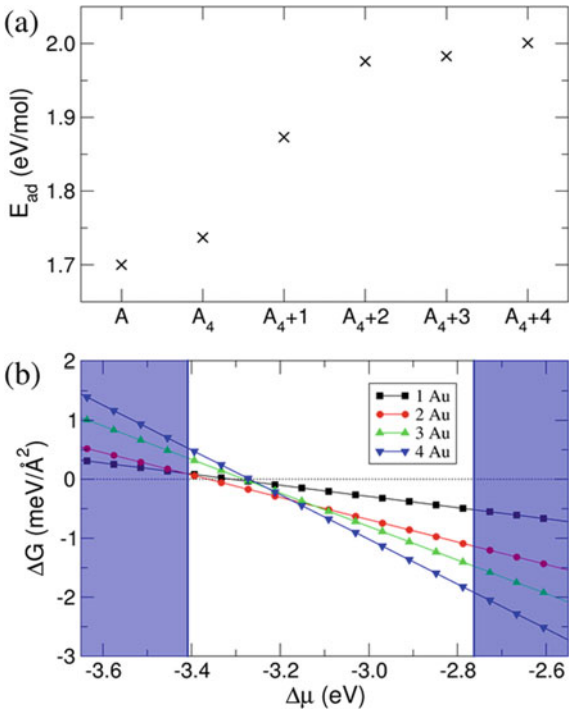

Fig. 6 **a** Adsorption energy per molecule of the tetramer as a function of the number of gold adatoms. **b** Estimation of the Gibbs free energy as a function the chemical potential of a source of adatoms. The accessible area is located at the middle of the plot between the blue shaded areas, and it is limited by the chemical potential of Au bulk (blue line at the left), and by the chemical potential of a gold adatom on the Au(111) surface (blue line at the right)

one would be a gold adatom diffusing on the Au(111) surface (right vertical blue line in the same figure). There are other possible sources of adatoms, like the herringbone reconstruction or step edges in the surface, but their chemical potentials will most likely be between these two limits.

In Fig. 6b, we can see that in the accessible region between the limiting chemical potentials there is a region where the change of free energy is negative and, therefore, the addition of adatoms to the tetramer would be favorable. In particular, the phase with two adatoms first, and then the phase with four adatoms have the most negative free energies. As a consequence, they are predicted to be the most stable situations at each particular chemical potential.

The presence of gold adatoms also helps to understand other experimental observations. In particular, the contrast depression at the center of the tetramer is reduced after the incorporation of adatoms, improving the comparison with the experimental result.

As mentioned before, the supramolecular structures can be manipulated by the STM tip using bias pulses [23–25]. The adatoms within the structure increase the

electronic density of states at empty and occupied states, increasing the tunneling current through the supramolecule and favoring the manipulation with the STM tip. On the other hand, there is a polarity dependence of the manipulations [23] that possibly indicates the existence of electrostatic interactions between the tip and the molecular structures. These interactions point out to a charge transfer in the supramolecules. Also in this respect the presence of adatoms is advantageous. Indeed, having gold adatoms increases the charge transfer, resulting in a much more positively charged structure than without adatoms. Finally, supramolecular structures move in discrete steps of a lattice unit. This is compatible with the movement of the gold adatom along the Au(111) surface. All these facts give strong support to the mediation of gold atoms in the formation of ABP supramolecular structures.

Additional data about tetramers and extra information about other structures as trimers can be found in [33].

4 Adsorption of DMBI-P on Au(111): Formation of a Unidirectional Molecular-Rotor

In the previous sections, we have studied the adsorption and diffusion of organic molecules on Au(111). However, it is also possible to have more complex movements on the surface like rotations. In particular, there are several examples of controlled rotation of organic molecules around a vertical axis [6, 34–36].

Here, we study one of such examples, where an organic molecule is deposited on Au(111) and it presents sequential and unidirectional rotational motion at a temperature of 5 K [37]. In that work they used the precursor 2-(2-Methoxyphenyl) − 1,3-dimethyl-1H-benzoimidazol-3-ium iodide (*o*-MeO-DMBI-I). This precursor is sublimated at 490 K and deposited on the Au(111) surface, where it chemisorbs. The binding energy to the gold surface is quite strong as it is shown by the fact that an attempt to remove the molecule typically results in pulling-out a gold atom from the surface together with the molecule. The adsorbed molecules show six preferred orientations rotated by 60º, corresponding to the high symmetry $[1\bar{1}0]$ directions of the hexagonal surface lattice.

At 5 K the STM tip can be positioned at a specific point over the molecule. Applying a voltage pulse of typically 400 mV the molecule suffers a rotation of 60º, clockwise or anticlockwise depending on the chirality of the molecule. This procedure can be repeated until a full 360º rotation is achieved. An analysis of the asymmetry of the geometry of the STM topographic images allows the authors to assign the anchoring point to an oxygen-gold bond.

If the temperature is increased to 11 K, random rotations start to be observed. Above 20 K, the molecule shows an hexagonal appearance, indicating that all six equivalent orientations are visited during the scanning time (~40 s) due to the thermally induced motion. An important point is the unidirectionality of the rotation:

depending of the chirality of the molecule on the surface, at 5 K the molecule always rotates in the same direction.

In order to study the experimental observations, we have performed extensive first-principles DFT calculations. The *o*-MeO-DMBI-I precursor is believed to undergo a reduction by the cleaving of iodine resulting in *o*-MeO-DMBI, as shown in [38]. Therefore, we have started the calculation by adsorbing this molecule on Au(111) and calculating the most stable configuration.

The optimized structure is shown in Fig. 7, together with a simulated topographic STM image. The comparison of this image with the experimental data in [37] shows poor agreement. In particular, the overall shape of the adsorbed molecule is quite different, with the simulated STM image presenting a rounder shape. In addition, the O atom is too far from the surface (3.03 Å) to present a strong O-Au bond, as suggested in the experiment. Other calculated configurations show even less resemblance with the experimental results.

Inspection of the simulated result suggests that a closer situation to the experimental results could be achieved if the methyl group is cleaved from the oxygen atom. Such reaction is known to occur starting from the o-MeO-DMBI-I precursor, forming a volatile methyl iodine (MeI) and 2-(1,3-dimethyl-1H-benzo[d]imidazol-3-ium-2-yl)-phenolate (DMBI-P). This reaction has been reported by photoelectron spectroscopy experiments [39]. A detailed chemical study of this process in gas phase

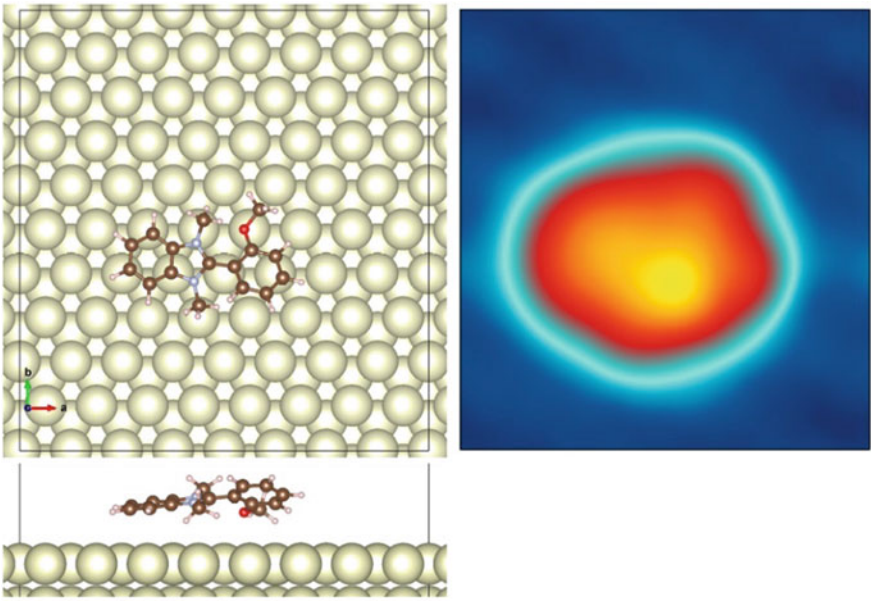

Fig. 7 (Left side) Top and side views of the calculated most stable structure of *o*-MeO-DMBI adsorbed on Au(111). (Right side) Simulated topographic STM image of the structure of the left at V = 0.5 V

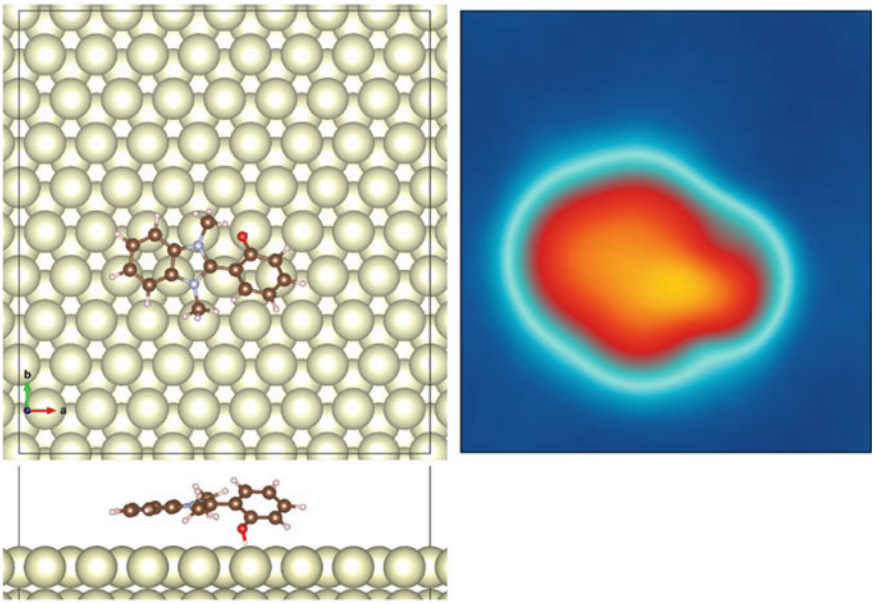

Fig. 8 (Left side) Top and side views of the calculated most stable structure of DMBI-P adsorbed on Au(111). (Right side) Simulated topographic STM image of the structure of the left at V = 0.5 V

by different methods was able to confirm that the reaction would take place at the experimental conditions of the sublimation [40].

Following the above results, we have studied the adsorption of DMBI-P on Au(111) by DFT calculations. The most stable configuration that we have found is shown in Fig. 8, together with a simulated STM image.

Now the result is much closer to the experimental data, with the STM image showing similar shape and asymmetry. The oxygen atom is on top a gold atom, in agreement with the experimental observations. In addition, the O-Au distance is now much shorter (2.29 Å) and compatible with a chemical O-Au bond. By Bader analysis we have calculated a charge transfer of 0.24 e-, transferred from the molecule to the surface. In order to have a clearer idea of the charge transfer and the effect of the O-Au bond, we have computed the induced charge density, defined as $\Delta\rho =$ ρ(DMBI-P@Au111) – ρ(DMBI-P) – ρ(Au111), where ρ(DMBI-P@Au111) is the charge density of the adsorbed molecule and the surface; ρ(DMBI-P) is the charge density of the molecule, and ρ(Au111) is the charge density of the Au(111) surface, the last two calculated using the geometry of the adsorbed case.

The result is shown in Fig. 9. From this image, we can see that there is a redistribution of charge between the oxygen atom and the nearby surface gold atoms, which indicates the nature of the O-Au bond responsible of the anchoring of the molecule.

The next step is to explore the rotation of the molecule. To that end, we have performed a Nudged Elastic Band (NEB) calculation in order to compute the rotational barriers as the molecule rotates on the surface. The result indicates a barrier

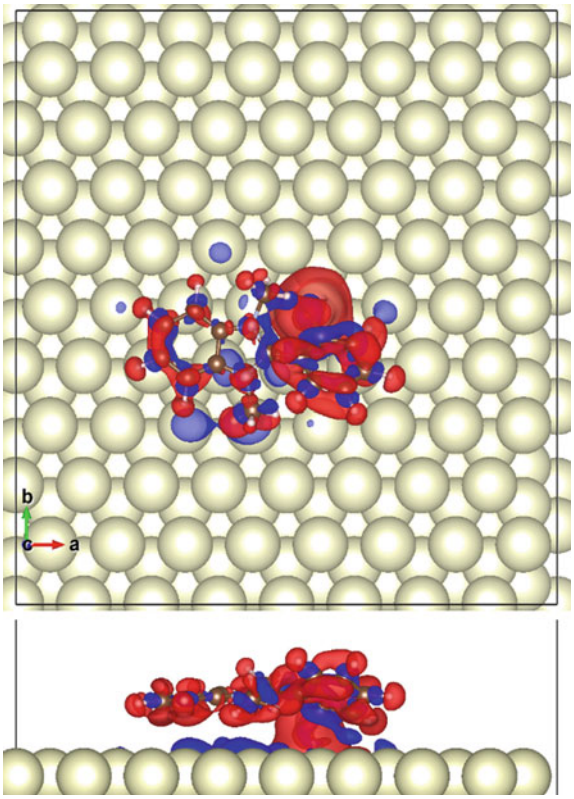

Fig. 9 Induced charge density of DMBI-P adsorbed on Au(111). Red (blue) areas indicate accumulation (depletion) of electrons

of around 50 meV, which is reduced to 11 meV if zero-point energies are included. Experimentally the random rotation of the molecule as a function of the temperature was explored. An analysis using an Arrhenius plot produced an effective barrier height of 5 meV, in qualitative good agreement with the calculated value [40].

Extra information on the rotation can be experimentally obtained by measuring the experimental yield for a single rotation step per electron as a function of the bias voltage.

The analysis of this so-called action spectra provides information about a possible vibrational origin of the excitations of the molecule [35, 41, 42].

For DMBI-P on Au(111) the fitting of the action spectra curves offers a threshold of 370 meV, which should correspond to the lowest energy vibrational mode that contributes to the excitation of the molecule. We have calculated the vibrational modes of the molecule on the surface.

The density of states of the modes is shown in Fig. 10. The calculated C-H stretch mode of the methyl group opposite to the O-Au bond is located at 371 meV, in agreement with the experimental threshold. Before this value, there is a 172-meV

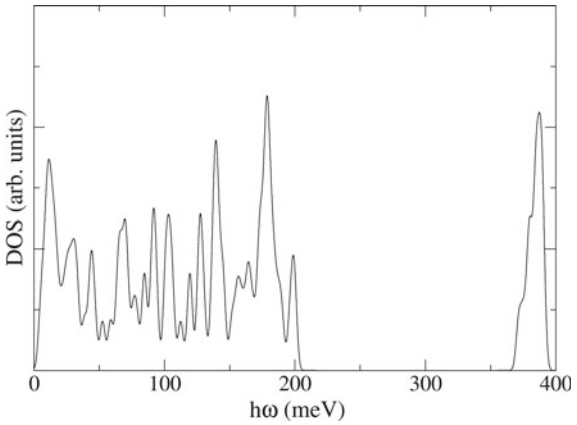

Fig. 10 Calculated vibrational modes of the DMBI-P molecule adsorbed on Au(111). The density of states shows the onset of the C-H strech modes at 371 meV. Before it, there is a 172 meV gap until the C-H rotation modes appear at 199 meV

gap with no available modes until the C-H rotational modes start at 199 meV. From these data, we can conclude that the energy is efficiently injected into the molecule by inelastic excitations of the C-H stretch modes.

5 Conclusions

Using first-principles calculations based on DFT with vdW corrections, we have studied the diffusion, assembly and rotation of organic molecules on Au(111). We have started by studying the adsorption of the 4-acetylbiphenyl molecule. We have determined that the molecule is adsorbed due to vdW forces whose main effect is the flattening of the molecule. Although the diffusion barriers are small compared to the binding energies, there is a corrugation of the vdW forces that explains why the molecule adsorbs aligned to the $[1\bar{1}0]$ and $[11\bar{2}]$ directions, and moves preferentially along particular directions. After deposition, the ABP molecules self-assemble and form robust supramolecular structures that can be manipulated in a controlled way by applying voltage pulses. We have studied the possible atomic structure of the supramolecules, proposing that they most likely incorporate gold adatoms that serve as stabilizing agents. The gold adatoms diffuse randomly at room temperature on Au(111) and they are reactive enough to bind to an ABP molecule. The Au-ABP compounds will then serve as nucleation centers for the assembly of the supramolecular structures. In addition, the presence of gold adatoms helps to understand several experimental facts, such as the movement of the supramolecules in discrete steps and their bias dependence.

In the last part of the present study, we have analyzed the deposition of the precursor *o*-MeO-DMBI-I on Au(111). We have shown that during the sublimation process the molecule dissociates into MeI and DMBI-P, which is actually adsorbed on the surface. This molecular fragment chemisorbs by the formation of an O-Au bond that works as an axle around which the molecule rotates step-by-step in one direction under the application of voltage pulses at low temperature (5 K). We have also shown that the injection of energy into the molecule is achieved by the inelastic excitation of the C-H stretch modes.

Finally, in this chapter we have presented examples of how first-principles calculations are an irreplaceable tool in the understanding of single-molecule mechanics. Using state-of-the art computational techniques, we can explore the processes at play that rule the interaction of molecules on surfaces, from the fundamentals of the vdW interactions, to the self-assembly of molecules to form supramolecules and the creation of molecule-rotors.

Acknowledgements We thank the European Union Horizon 2020 FET open project "Mechanics with Molecule(s)" (MEMO, grant 766864) for financial support during this work.

References

1. The Nobel Prize in Chemistry 2016, https://www.nobelprize.org/prizes/chemistry/2016/summary/
2. Roßnagel, J., Dawkins, S.T., Tolazzi, K.N., Abah, O., Lutz, E., Schmidt-Kaler, F., Singer, K.: A single-atom heat engine. Science **352**, 325–329 (2016). https://doi.org/10.1126/science.aad6320
3. Morgenstern, K., Lorente, N., Rieder, K.-H.: Controlled manipulation of single atoms and small molecules using the scanning tunnelling microscope. physica status solidi (b). **250**, 1671–1751 (2013). https://doi.org/10.1002/pssb.201248392
4. Pavliček, N., Gross, L.: Generation, manipulation and characterization of molecules by atomic force microscopy. Nat Rev Chem. **1**, 1–11 (2017). https://doi.org/10.1038/s41570-016-0005
5. Kudernac, T., Ruangsupapichat, N., Parschau, M., Maciá, B., Katsonis, N., Harutyunyan, S.R., Ernst, K.-H., Feringa, B.L.: Electrically driven directional motion of a four-wheeled molecule on a metal surface. Nature **479**, 208–211 (2011). https://doi.org/10.1038/nature10587
6. Stolz, S., Gröning, O., Prinz, J., Brune, H., Widmer, R.: Molecular motor crossing the frontier of classical to quantum tunneling motion. PNAS **117**, 14838–14842 (2020). https://doi.org/10.1073/pnas.1918654117
7. Clair, S., de Oteyza, D.G.: Controlling a chemical coupling reaction on a surface: tools and strategies for on-surface synthesis. Chem. Rev. **119**, 4717–4776 (2019). https://doi.org/10.1021/acs.chemrev.8b00601
8. Böhringer, M., Morgenstern, K., Schneider, W.D., Berndt, R., Mauri, F., De Vita, A., Car, R.: Two-dimensional self-assembly of supramolecular clusters and chains. Phys. Rev. Lett. **83**, 324–327 (1999)
9. Karan, S., Wang, Y., Robles, R., Lorente, N., Berndt, R.: Surface-Supported supramolecular pentamers. J. Am. Chem. Soc. **135**, 14004–14007 (2013). https://doi.org/10.1021/ja405456k
10. Kresse, G., Furthmüller, J.: Efficiency of ab-initio total energy calculations for metals and semiconductors using a plane-wave basis set. Comput. Mater. Sci. **6**, 15–50 (1996). https://doi.org/10.1016/0927-0256(96)00008-0

11. Kresse, G., Joubert, D.: From ultrasoft pseudopotentials to the projector augmented-wave method. Phys. Rev. B. **59**, 1758 (1999). https://doi.org/10.1103/PhysRevB.59.1758
12. Perdew, J.P., Burke, K., Ernzerhof, M.: Generalized gradient approximation made simple. Phys. Rev. Lett. **77**, 3865 (1996). https://doi.org/10.1103/PhysRevLett.77.3865
13. Tkatchenko, A., Scheffler, M.: Accurate molecular Van Der Waals interactions from ground-state electron density and free-atom reference data. Phys. Rev. Lett. **102**, 073005 (2009). https://doi.org/10.1103/PhysRevLett.102.073005
14. Grimme, S., Antony, J., Ehrlich, S., Krieg, H.: A consistent and accurate ab initio parametrization of density functional dispersion correction (DFT-D) for the 94 elements H-Pu. J. Chem. Phys. **132**, 154104 (2010). https://doi.org/10.1063/1.3382344
15. Grimme, S., Ehrlich, S., Goerigk, L.: Effect of the damping function in dispersion corrected density functional theory. J. Comput. Chem. **32**, 1456–1465 (2011). https://doi.org/10.1002/jcc.21759
16. Tang, W., Sanville, E., Henkelman, G.: A grid-based Bader analysis algorithm without lattice bias. J. Phys.: Condens. Matter. **21**, 084204 (2009). https://doi.org/10.1088/0953-8984/21/8/084204
17. Jónsson, H., Mills, G., Jacobsen, K.W.: Nudged elastic band method for finding minimum energy paths of transitions. In: Berne, B.J., Ciccotti, G., and Jacobsen, K.W. (eds.) Classical and Quantum Dynamics in Condensed Phase Simulations. p. 385. World Scientific, Singapore (1998)
18. Tersoff, J., Hamann, D.R.: Theory and application for the scanning tunneling microscope. Phys. Rev. Lett. **50**, 1998–2001 (1983). https://doi.org/10.1103/PhysRevLett.50.1998
19. Tersoff, J., Hamann, D.R.: Theory of the scanning tunneling microscope. Phys. Rev. B. **31**, 805–813 (1985). https://doi.org/10.1103/PhysRevB.31.805
20. Bocquet, M.-L., Lesnard, H., Monturet, S., Lorente, N.: Theory of Elastic and Inelastic Electron Tunneling. In: Santen, R.A. van and Sautet, P. (eds.) Computational Methods in Catalysis and Materials Science. pp. 199–219. Wiley-VCH Verlag GmbH & Co. KGaA (2009)
21. Lorente, N., Robles, R.: STMpw (v1.0b2), https://doi.org/10.5281/zenodo.3581159
22. Momma, K., Izumi, F.: VESTA 3 for three-dimensional visualization of crystal, volumetric and morphology data. J Appl Cryst. **44**, 1272–1276 (2011). https://doi.org/10.1107/S0021889811038970
23. Nickel, A., Ohmann, R., Meyer, J., Grisolia, M., Joachim, C., Moresco, F., Cuniberti, G.: Moving nanostructures: pulse-induced positioning of supramolecular assemblies. ACS Nano **7**, 191–197 (2013). https://doi.org/10.1021/nn303708h
24. Ohmann, R., Meyer, J., Nickel, A., Echeverria, J., Grisolia, M., Joachim, C., Moresco, F., Cuniberti, G.: Supramolecular rotor and translator at work: on-surface movement of single atoms. ACS Nano **9**, 8394–8400 (2015). https://doi.org/10.1021/acsnano.5b03131
25. Eisenhut, F., Durand, C., Moresco, F., Launay, J.-P., Joachim, C.: Training for the 1st international nano-car race: the Dresden molecule-vehicle. Eur. Phys. J. Appl. Phys. **76**, 10001 (2016). https://doi.org/10.1051/epjap/2016160259
26. Johansson, M.P., Olsen, J.: Torsional barriers and equilibrium angle of biphenyl: reconciling theory with experiment. J. Chem. Theory Comput. **4**, 1460–1471 (2008). https://doi.org/10.1021/ct800182e
27. Maurer, R.J., Ruiz, V.G., Camarillo-Cisneros, J., Liu, W., Ferri, N., Reuter, K., Tkatchenko, A.: Adsorption structures and energetics of molecules on metal surfaces: bridging experiment and theory. Prog. Surf. Sci. **91**, 72–100 (2016). https://doi.org/10.1016/j.progsurf.2016.05.001
28. Zobač, V., Robles, R., Lorente, N.: Directionality in van der Waals Interactions: the case of 4-Acetylbiphenyl Adsorbed on Au(111). J. Phys. Chem. C. **124**, 4545–4551 (2020). https://doi.org/10.1021/acs.jpcc.9b09599
29. Jaklevic, R.C., Elie, L.: Scanning-tunneling-microscope observation of surface diffusion on an atomic scale: Au on Au(111). Phys. Rev. Lett. **60**, 120–123 (1988). https://doi.org/10.1103/PhysRevLett.60.120
30. Maksymovych, P., Voznyy, O., Dougherty, D.B., Sorescu, D.C., Yates, J.T., Jr.: Gold adatom as a key structural component in self-assembled monolayers of organosulfur molecules on Au(1 1 1). Prog. Surf. Sci. **85**, 206–240 (2010). https://doi.org/10.1016/j.progsurf.2010.05.001

31. Yang, Z., Corso, M., Robles, R., Lotze, C., Fitzner, R., Mena-Osteritz, E., Bäuerle, P., Franke, K.J., Pascual, J.I.: Orbital redistribution in molecular nanostructures mediated by metal-organic bonds. ACS Nano **8**, 10715–10722 (2014). https://doi.org/10.1021/nn504431e
32. Meyer, J., Nickel, A., Ohmann, R., Lokamani, Toher, C., Ryndyk, D.A., Garmshausen, Y., Hecht, S., Moresco, F., Cuniberti, G.: Tuning the formation of discrete coordination nanostructures. Chem. Commun. 51, 12621–12624 (2015). https://doi.org/10.1039/C5CC02723C
33. Robles, R., Zobač, V., Yeung, K.H.A., Moresco, F., Joachim, C., Lorente, N.: Supramolecular chemistry based on 4-acetylbiphenyl on Au(111). Phys. Chem. Chem. Phys. **22**, 15208 (2020). https://doi.org/10.1039/D0CP01657H
34. Simpson, G.J., García-López, V., Daniel Boese, A., Tour, J.M., Grill, L.: How to control single-molecule rotation. Nat Commun. **10**, 4631 (2019). https://doi.org/10.1038/s41467-019-12605-8
35. Jasper-Toennies, T., Gruber, M., Johannsen, S., Frederiksen, T., Garcia-Lekue, A., Jäkel, T., Roehricht, F., Herges, R., Berndt, R.: Rotation of Ethoxy and Ethyl moieties on a molecular platform on Au(111). ACS Nano **14**, 3907–3916 (2020). https://doi.org/10.1021/acsnano.0c00029
36. Ren, J., Freitag, M., Schwermann, C., Bakker, A., Amirjalayer, S., Rühling, A., Gao, H.-Y., Doltsinis, N.L., Glorius, F., Fuchs, H.: A Unidirectional Surface-Anchored N-Heterocyclic Carbene Rotor. Nano Lett. **20**, 5922–5928 (2020). https://doi.org/10.1021/acs.nanolett.0c01884
37. Eisenhut, F., Meyer, J., Krüger, J., Ohmann, R., Cuniberti, G., Moresco, F.: Inducing the controlled rotation of single o-MeO-DMBI molecules anchored on Au(111). Surf. Sci. **678**, 177–182 (2018). https://doi.org/10.1016/j.susc.2018.05.003
38. Wei, P., Menke, T., Naab, B.D., Leo, K., Riede, M., Bao, Z.: 2-(2-Methoxyphenyl)-1,3-dimethyl-1H-benzoimidazol-3-ium Iodide as a New Air-Stable n-Type Dopant for Vacuum-Processed Organic Semiconductor Thin Films. J. Am. Chem. Soc. **134**, 3999–4002 (2012). https://doi.org/10.1021/ja211382x
39. Schwarze, M., Naab, B.D., Tietze, M.L., Scholz, R., Pahner, P., Bussolotti, F., Kera, S., Kasemann, D., Bao, Z., Leo, K.: Analyzing the n-doping mechanism of an air-stable small-molecule precursor. ACS Appl. Mater. Interfaces. **10**, 1340–1346 (2018). https://doi.org/10.1021/acsami.7b14034
40. Eisenhut, F., Kühne, T., Monsalve, J., Srivastava, S., Ryndyk, D.A., Cuniberti, G., Aiboudi, O., Lissel, F., Zobač, V., Robles, R., Lorente, N., Joachim, C., Moresco, F.: One-way rotation of a chemically anchored single molecule-rotor. Nanoscale **13**, 16077–16083 (2021). https://doi.org/10.1039/D1NR04583K
41. Kim, Y., Motobayashi, K., Frederiksen, T., Ueba, H., Kawai, M.: Action spectroscopy for single-molecule reactions—Experiments and theory. Prog. Surf. Sci. **90**, 85–143 (2015). https://doi.org/10.1016/j.progsurf.2014.12.001
42. Motobayashi, K., Kim, Y., Ueba, H., Kawai, M.: Insight into action spectroscopy for single molecule motion and reactions through inelastic electron tunneling. Phys. Rev. Lett. **105**, 076101 (2010). https://doi.org/10.1103/PhysRevLett.105.076101

From Early Prototypes to On-Surface Drivable Single Molecule Nano-vehicles

Henri-Pierre Jacquot de Rouville, Sonia Adrouche, Xavier Bouju, Jean-Pierre Launay, Gwénaël Rapenne, and Christian Joachim

Abstract From their early prototypes to their most recent versions, the history of on-surface molecule-vehicles is briefly presented. An emphasis on their mechanical properties upon different manipulation modes induced by the STM tip, namely constant current, constant height, STM voltage pulse and dipolar mode are discussed. In addition, the chemical structure/mechanical property relationship of those nano-vehicles is described with a highlight on the first edition of the Nanocar Race. Finally, perspectives of the field are given with the introduction of molecular motors in the design of nano-vehicles thus leading to the first prototypes of motorized molecular vehicles on a surface for the technomimetic approach.

Keywords Molecular mechanics · Nano-vehicles · STM manipulation · Tunneling current · Single molecule

H.-P. Jacquot de Rouville (✉) · S. Adrouche
Institut de Chimie de Strasbourg, CNRS UMR 7177, Université de Strasbourg, 4 rue Blaise Pascal, 67000 Strasbourg, France
e-mail: hpjacquot@unistra.fr

X. Bouju · J.-P. Launay · G. Rapenne · C. Joachim
Centre d'Elaboration de Matériaux Et d'Études Structurales (CEMES), Centre National de La Recherche Scientifique (CNRS), Université de Toulouse, 29 Rue J. Marvig, BP 4347, 31055 Toulouse Cedex, France

G. Rapenne
Division of Materials Science, Nara Institute of Science and Technology, Takayama, Ikoma, Nara 8916-5, Japan

C. Joachim
International Center for Materials Nanoarchitectonics (WPI-MANA), National Institute for Material Sciences (NIMS), 1-1 Namiki, Tsukuba 305-0044, Ibaraki, Japan

© The Author(s), under exclusive license to Springer Nature Switzerland AG 2023

F. Moresco and C. Joachim (eds.), *Single Molecule Mechanics on a Surface*,
Advances in Atom and Single Molecule Machines,
https://doi.org/10.1007/978-3-031-16930-4_4

1 Introduction

At the end of the year 1959 in a conference entitled "*There is plenty of room at the bottom*", R. Feynman pointed out the importance of going beyond different experimental limits such as temperature, pressure and also sample size to open new avenues in physics and in technology [1]. Later, he stated that if we "*consider any machine—for example, an automobile—and ask about the problems of making an infinitesimal machine […] I can see no reason why it can't be redesigned to work again*". Nowadays, optical and electron beam lithography can fabricate the mechanical pieces of a miniature automobile down to the scale of 100 μm. Indirectly resulting from the invention of the Scanning Tunneling Microscope (STM) by H. Rohrer and G. Binnig in 1981, the size limit of an automobile down to only one single molecule (a molecule car) was first discussed at the Loch Lomond NATO workshop "Nano-Age mechanics" in October 1995 [2]. In particular, using an STM working at its low temperature limits (300 mK $< T <$ 77 K) under ultra-high vacuum ($P \approx 10^{-11}$ mbars) allows the imaging of a single atom (or a single molecule) much better than using field ion (FIM) or field emission (FEM) microscopes. This new technique opened the way to the manipulation of atoms one at a time on a surface (or a single molecule) and then to probe single molecule mechanics on a surface.

Over the years, the thirst of knowledge led to an increasing complexity of the single molecule machineries with the monumentalization of their chemical structures [3]. One prominent class of molecules is called technomimetic molecules [4]. Technomimetic molecules are molecules mimicking the shape and the mechanical behavior of dailylife machines. Indeed, when comparing the shape of a bird and a plane, there are no doubts that a plane composed of a thin body and two wings can fly even if the flying propulsion is different than a bird. A molecule-vehicle is a single molecule of a few nanometers size having a molecular chassis chemically bonded to molecular wheels similarly to their pendant macroscopic counterparts (Fig. 1). In other words, their wheels can exhibit a rotation on a surface (with their rotation axis parallel to this surface) on account of the existing mechanical degrees of freedom between the subcomponents of the molecule. In Toulouse, this field of research began in 2001 with the design, the molecular mechanics calculations and then the chemical synthesis of a molecule-wheelbarrow [5]. Developed from the Lander molecule family [6], this early example of nano-vehicles was composed of a rigid polyaromatic chassis incorporating two front triptycene molecular groups acting as wheels (Fig. 1).

Another important contribution was made by the group of J. M. Tour with their nanocars built around a semi-rigid chassis connected to a variety of wheels, among them C_{60}, p-carborane, adamantane and $[Ru(C{\equiv}CH)_2(dppe)_2]$ can be cited [7]. The next important development in the field was the introduction of a molecular motor in the design of nano-vehicles. A particular attention was paid in incorporating the so-called Feringa's motor allowing in some cases a propelled motion on the STM surface upon using a series of STM voltage pulses. Finally, the new fashion is now

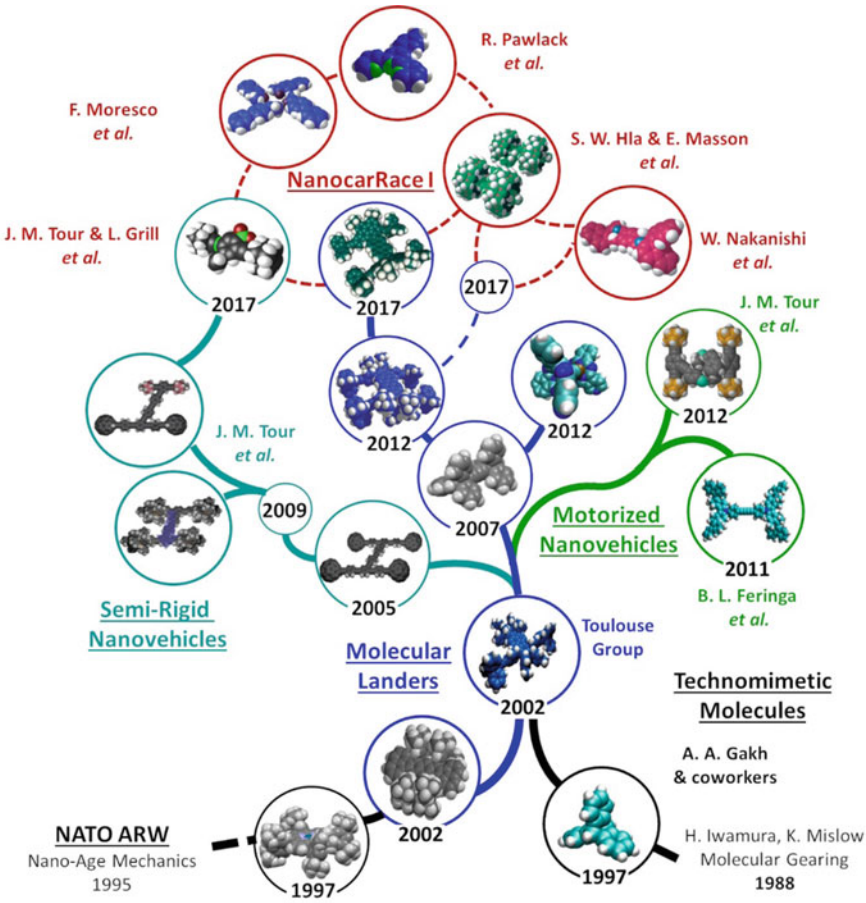

Fig. 1 Evolution tree of the nanocars coming from the molecular Landers to the incorporation of molecular motors in their design. On the bottom left and before 1995, STM small single molecule manipulation like CO was discovered by D. Eigler at the beginning of the 90's [8]. On the bottom right, molecular gearing studies in solid and solution emanated from a long tradition in organic chemistry [9] and organometallic chemistry [10]. A third direction not given on this graph is macromolecular proteins molecular motor exploration [11–13]. Molecular gearing effect was also advocated for understanding collective gearing effect inducing phase transition on 2D assembled PF_3 rotors on a metal surface as compared to NH_3 small molecular monolayer [14, 15]. At Loch Lomond, the mentioned NATO ARW was organized in 1995 under the patronage of H. Rohrer

in the incorporation of a donor–acceptor units (also called a push–pull unit) in the design of the chassis to induce a local dipolar moment.

In this book chapter, the concepts related to the manipulation of nano-vehicles will be depicted. First, basic principles related to manipulations using an STM tip will be developed. Then, the challenges of the manipulation of a complex molecular structure on a UHV atomically clean surface will be described. In addition, results obtained

from the French team during the 1st edition of the Nanocar Race in April 2017 will be presented as well as some comments on the results of the other competitors. Finally, a discussion of the motorized nano-vehicle of Feringa will also be given.

2 STM and Controlled Manipulations of Single Objects

An STM junction is composed of a sharp metallic tip apex (often made of W) facing the surface of a conductive substrate (usually Au, Ag, Cu) distant from each other of a few angstroms to one nanometer. A tunnel nanojunction is thus formed in which single atoms or molecules can be deposited and studied on the surface. The principle of the STM imaging is based on the tunnel effect. Once a bias voltage is applied in the tunnel junction, the electrons can flow between the tip apex and the surface without any electronic or mechanical contact between them. An image is simply obtained by sweeping the tip across the surface while maintaining constant the I(t) tunnel current. In consequence, the topography of the surface can be reconstructed from the change of the tip height while scanning the surface at a constant tunneling current intensity. The tip apex of the STM is not only utilized for imaging but also for the controlled lateral manipulation of the atoms, molecules and nanoscale objects adsorbed on the surface. In a seminal work, D. Eigler and coworkers have demonstrated in 1990 that the manipulation of a single xenon atom on a metal surface is possible [16]. Moving one by one 35 xenon atoms, he succeeded to write the three letters revealing the name of the IBM company. Slightly later, manipulations of diatomic molecules were performed and after, in 1996, the manipulation of larger molecules was also achieved even at room temperature [17]. It is worthwhile to note that imaging and manipulating using the STM tip cannot be done at the same time and these two processes are performed consecutively. Once a single molecule or atom is localized on the imaged area and is targeted to be manipulated, the manipulation procedure is triggered. It consists in approaching the STM tip to the adsorbate and then, either to translate the tip laterally (the mechanical manipulation mode) or to apply a voltage pulse at the good location on the adsorbate (local electric-field or inelastic current). During a manipulation process, the I(t) tunneling current intensity can be recorded giving a first indication of what happened for the adsorbate during the manipulation (see for example Figs. 2, 5, 6, 8 and 10). The interpretation of this signal is often delicate and requires large molecular mechanics calculations associated to the calculation of the I(t) tunnel current variations during a given manipulation sequence. Therefore, a new image is generally recorded to check whether the manipulation was successful or not.

The initial approach for manipulating a single adsorbate (such as an individual molecule) on a surface imposed a constant tip height during the manipulation while scanning the surface. In this way, the complex relation between the electronic structure of the adsorbate and its conductance is simplified by suppressing the dependence on the I(t) signal on the STM feedback loop. Three different manipulation modes have been explored depending on the atomic structure of the adsorbate: (i) the pulling

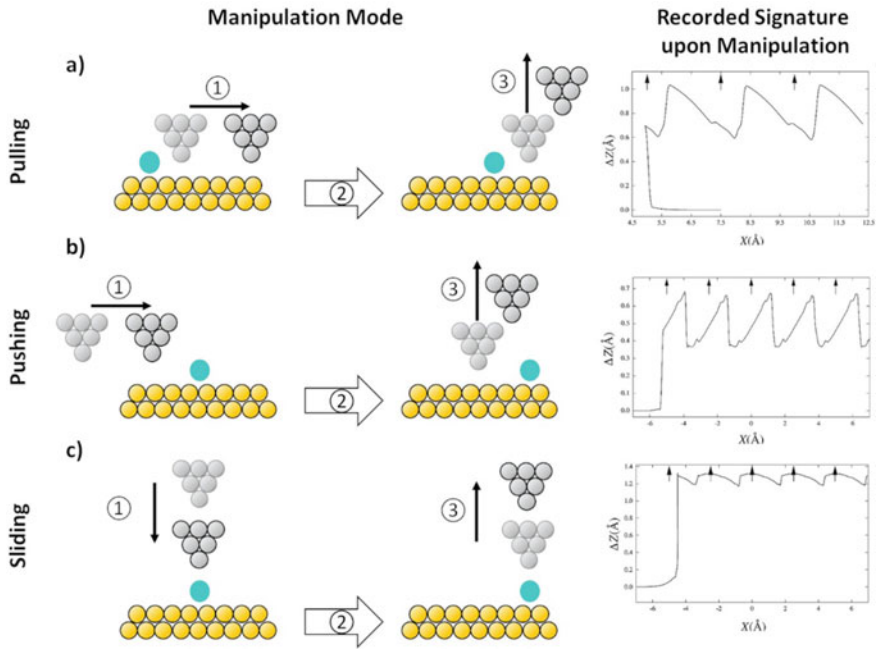

Fig. 2 The three manipulation modes (pulling, pushing and sliding) with their corresponding manipulation signals (right column) obtained with the STM feedback loop active leading to those constant current manipulation modes [18]

mode when the tip apex end atom is "in front" of the adsorbate while using attractive forces, (ii) the pushing mode when the apex is "behind" the adsorbate using repulsive forces and (iii) the sliding mode when the tip is "on top" of the adsorbate generating an attractive potential energy trap in between the tip apex and the surface (Fig. 2) [18]. As mentioned above and to avoid a blind manipulation process, the variation of the I(t) tunneling current can be recorded during the manipulation sequence in the constant height mode with the STM feedback-loop not activated.

Considering now the manipulation sequence of a single atom adsorbate in a constant current mode, the pulling mode is characterized by two main features (Fig. 2a): when the tip apex moves away laterally from the atom (①), the Δz signal exhibits a slow decrease, and then a sudden increase. This second event is due to the attractive interaction between the tip apex end atom and the atom itself leading to motion of the atom from its initial stable position on the surface to the next one (②). This change in position on the surface leads to a sudden increase of the tunneling current compensated by the STM feedback loop. The opposite situation occurs in the pushing mode leading to a reverse sawtooth profile of the Δz signal (Fig. 2b). Finally, just a small appreciable variation of the distance between the tip and the atom occurs when the atom is laterally displaced on the surface in a sliding mode (Fig. 2c).

Similar manipulation signal interpretations can be obtained for a manipulation of a single atom in a constant-height mode.

An alternative mode of manipulation of a single adsorbate on a surface uses a voltage pulse between the tip and the surface. While in the previous three manipulation modes, the changes in the potential energy of the adsorbate on the surface came from the mechanical interactions between the tip apex end and this adsorbate, now the STM tip apex is located above the adsorbate but relatively far away from the surface. Then, a bias voltage pulse is applied or superposed to the small bias voltage already applied and required for imaging. It results an increase of the local electric field in the STM junction and in the tunneling current intensity. In most cases, the electrons go through the adsorbate with no energy release (elastic process). However, interactions can also be inelastic between the transferred electrons through the adsorbate [19]. The probability of an inelastic effect is low and concerns typically one electron transferred over ten thousand. Since there are billions of electrons per second transferred to reach an average tunneling current intensity of 100 pA, a significant amount of energy can be transferred to the mechanical degrees of freedom of the adsorbate while increasing the bias voltage. Indeed, it is often admitted that the given energy in an inelastic scattering process is of the range of the vibrational energy of bonds within a molecular structure.

Besides the inelastic tunneling and when the molecular adsorbate is designed with a permanent dipolar moment, the bias voltage pulse applied on the STM junction can lead to electrostatic interactions. In consequence, it modifies the potential energy of the adsorbate on the surface. This dipolar-like manipulation mode is strongly dependent on the overall symmetry of the apex-adsorbate-surface tunnel junction. In particular, this symmetry determines the direction of motion (forward, backward, sideways, jump on the tip apex) and will be discussed in more detail in the Sect. 6 below. This approach consisting in stimulating an intramolecular conformation change in a single molecule through the tunneling current and/or the enhanced electric field is frequently used with photochromic molecule (e.g. azobenzene) [20]. These inelastic or dipolar-like manipulation modes were also favored during the 1st edition of the Nanocar Race in April 2017 (Sect. 5).

3 Evidence of a Lateral Translation Motion on a Surface

3.1 First Nano-vehicle on a Surface

The experimental certification of a controlled molecular motion on a surface is challenging. Indeed, an altitudinal rotational motion (i.e. rotation around an axis parallel to the surface) depends on the different mechanical chemical groups (chassis and wheels) forming the single molecule machinery [21]. Based on the design of molecular Landers [6], the Toulouse group designed in 2001 and synthesized in 2003 the first known nano-vehicle following a technomimetic approach (Fig. 1) built around a

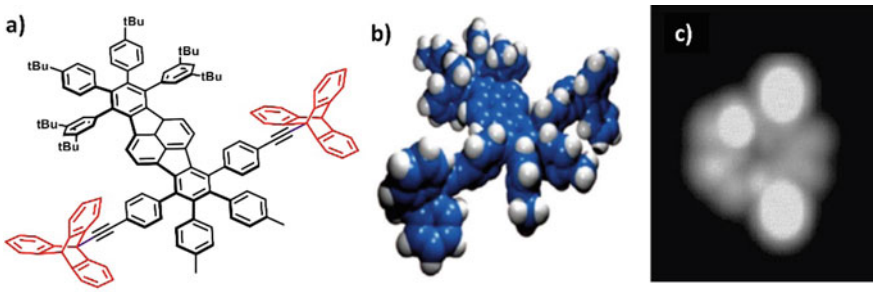

Fig. 3 **a** Chemical structure and **b** molecular model of the nano-vehicle after molecular mechanics optimization and **c** a low temperature constant current STM image of the molecule on a Cu(110) surface ($I = 0.3$ nA, $U = 0.5$ V) [5]

rigid polyaromatic chassis functionalized with two front triptycene wheels completed by two rear legs (Fig. 3a, b) [4, 5a]. It was designed to measure how the translation motion of a molecule on a surface can lead to the rotation motion of its front molecular wheels. The increase of the potential energy of the molecule-wheelbarrow on the surface was expected to be provided by a back repulsive push coming from the tip atomic apex of an STM. In consequence, the rotation of the front wheels was supposed to be directly measurable using the I(t) oscillation over time. Indeed, the front wheels having no tire, their rotation were supposed to induce an altitudinal oscillation on the front part of the chassis resulting in a measurable I(t) variations while the wheels would be rotating [5]. However, after deposition by sublimation on a Cu(100) surface (Fig. 3c), this molecule-wheelbarrow cannot be manipulated by the STM tip in any moderate mechanical manipulation modes [5b]. This behavior results from the strong electronic interactions between the π-system of the triptycene wheels and the Cu(100) surface. This experiment demonstrates how much the chemical structure of the subcomponents of a molecule is crucial in order to limit the wheel-surface interactions.

3.2 Translational Motion of a Nano-vehicle

In order to solve this adsorption problem, the group of J. M. Tour had then reported a series of nano-vehicles incorporating a semi-rigid polyaromatic chassis, namely an oligophenylacetylenyl fragment, connected to four robust wheels. In 2005, the first prototype was composed of a chassis equipped with four fullerene wheels (C_{60}) connected to the chassis by triple bonds. This design led to a low rotation energy barrier (4 kcal mol^{-1}) before adsorption on the surface (Fig. 4a) [22a]. It should be noted that C_{10} linear alkyl chains were also introduced in the design of the chassis in order to increase the solubility of the molecule during the synthesis. This molecule was studied by STM at variable temperature on a Au(111) surface. The images of the molecules revealed four lobes corresponding to the fullerene wheels. At room

temperature, the images showed that the nanocars were not moving on the Au(111) surface due to the strong van der Waals interactions between the 12 lateral alkyne chains, the four C_{60} wheels and the surface. Images at temperatures above 170 °C showed a random lateral translational motion of some molecules (Fig. 4b–d). The direction of the motion was perpendicular to those of the alkyne chains on the four axles. Some intramolecular contrast changes were also observed on the STM images (from Fig. 4b–d). These studies have led to the assumption that this directional linear motion was probably the result of a synchronized rotation of the four C_{60} wheels. However, there was no experimental evidence indicating how the C_{60} wheels were rotating.

The C_{60} molecular wheels have drawbacks related to both their lack of solubility as well as their strong physisorption on the surface. In order to overcome these problems, non-aromatic wheels (*p*-carboranes [22b], adamantanes [22c], trans-[Ru(C≡CH)$_2$(dppe)$_2$] [22d]) were introduced on the chassis. However, like the C_{60} fragments, these new units failed to show controlled rotational motions.

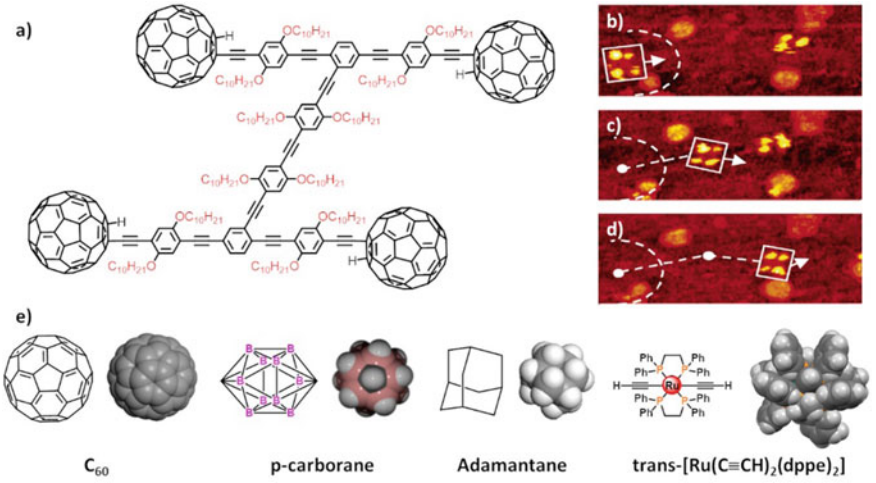

Fig. 4 **a** Chemical structure of a technomimetic like nanocar of the J. M. Tour group. **b–d** Series of constant current STM images ($I = 60$ pA, $U = 0.4$ V) showing the translational motion of this molecule-vehicle on a Au(111) surface after heating up the surface [22a]. **e** Chemical structures and space-filling models of a series of C_{60}, *p*-carborane, admantane and trans-[Ru(C≡CH)$_2$(dppe)$_2$] wheels

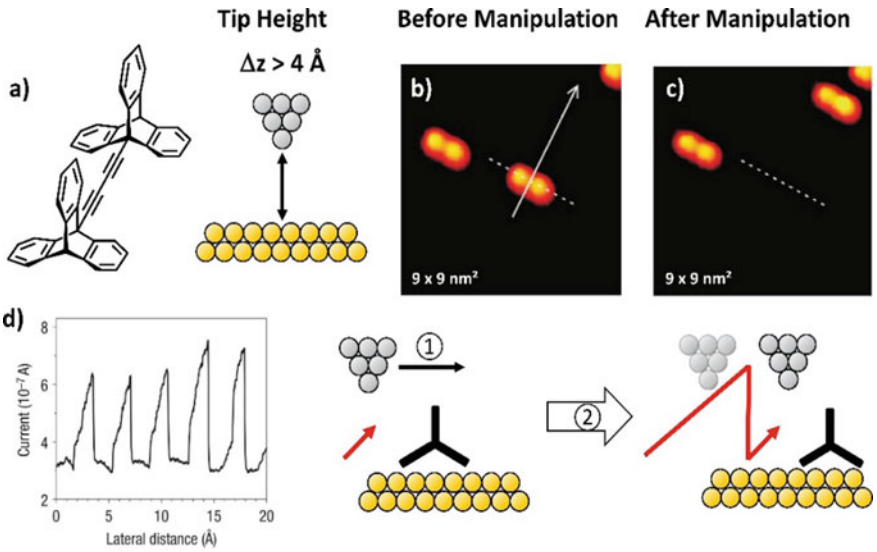

Fig. 5 **a** Chemical structure of the triptycene wheel dimer molecule. Low temperature constant current STM images ($I = 0.2$ nA, $U = 0.8$ V) **b** before and **c** after a manipulation sequence using a relative tip height (Δz) relative to the Cu(110) surface larger than 4 Å. **d** Recorded tunneling current during the manipulation and its interpretation demonstrating a pushing manipulation mode [23]

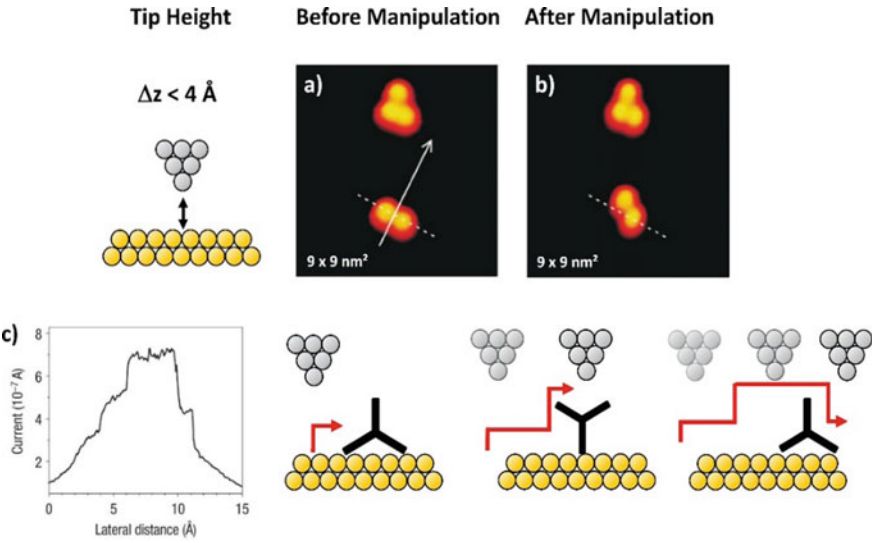

Fig. 6 Constant current low temperature STM images of the triptycene wheel dimer molecule ($I = 0.2$ nA, $U = 0.8$ V) **b** before and **c** after manipulation with a tip height (Δz) lower than 4 Å. **d** Recorded tunneling current intensity during the manipulation and its interpretation in term of intramolecular conformation change of the molecule [23]

4 Controlled Altitudinal Rotations and Wheel Dimers

4.1 Indirect Evidence of an Altitudinal Rotation

Starting from molecule-wheelbarrow chemical structure (Sect. 3.1), it was decided to simplify this technomimetic design and to keep only a wheel dimer composed of two triptycene wheels covalently connected to a 1,4-butadiyne axle (Fig. 5a) [23]. After sublimation on a Cu(110) surface, the STM low constant current images of this wheel dimer showed two lobes distant of 8.7 ± 0.3 Å (Fig. 5b). In a first STM manipulation experiment, the relative height of the STM tip apex end atom (Δz) was maintained at a distance high enough (> 4 Å) from the surface in order to push the complete molecule. After a manipulation sequence, the STM image revealed a translation of the molecule on the surface (Fig. 5c). The tunnel current recorded during this manipulation exhibited a sawtooth-like profile (Fig. 5d) with a periodicity corresponding to the distance between two Cu rows on the Cu(110) surface. A detailed analysis of this manipulation signal confirmed that the observed translation was the result of a sliding translation on the surface. It was triggered by the tip apex push and corresponded to a simple pushing mode as observed for a single atom STM manipulation (see Fig. 2b) without any signatures of a molecular wheel rotation. During this manipulation (Fig. 5b, c), the molecule moved on the Cu(110) surface in a series of successive jumps from one stable position to the next on the surface.

When repeating the experiment by positioning the tip apex end atom exactly in front of one of the two wheels and with a relative tip height (Δz) lower than 4 Å, the STM image of triptycene dimer after the manipulation showed a shift of 45° of the lobe of the targeted wheel (Fig. 6a, b). The tunnel current manipulation signal recorded during this manipulation (Fig. 6c) showed a different profile as compared to the current observed before (for $\Delta z > 4$ Å, Fig. 5d). The detailed analysis of this profile confirmed that the rotational motion of one wheel of the triptycene dimer took place. Indeed, the slow increase of the current corresponds to the tip apex end atom reaching a repulsive interaction with the targeted molecular wheel. Consequently, the potential energy of the molecule increased. At this stage, the release of this energy can lead either to the diffusion of the complete molecule to avoid this repulsion or to the rotation of the targeted wheel. In this experiment, the preferred energy release of the molecule was the rotation of the wheel. The distance between the tip apex and the wheel remained constant thus explaining the observed plateau in the tunneling current intensity. Finally, the tip slowly moved away from the molecule leading to a slow decrease of the recorded tunneling current intensity.

In this experiment, the proof of a controlled altitudinal rotation requires a fine analysis of the tunneling current manipulation signal. Indeed, detailed calculations of the tunneling current intensity variations as a function of the optimized conformation of the molecule on the surface are required while the tip apex end atom was interacting with the molecule. The direct way to gain direct evidence of the rotation of the wheel

is to chemically label some part of the wheels. It will cause a change of the STM contrast while comparing the images before and after the STM manipulation.

4.2 Direct Evidence of an Altitudinal Rotation

A chemical labelling strategy was first introduced in single molecule mechanics to follow the rotation of a single molecule-gear with its rotation axle perpendicular to the supporting surface [24]. This label can result from a chemical structure asymmetry (e.g. introduction of a bulky chemical group such as tBu) or from a dissymmetry in the electron cloud distribution of the molecule. At the rim of a phthalocyanine (SubPc) wheel dimer, one nitrogen atom per wheel was introduced to gently modify the local electronic structure of each wheel (Fig. 7a) [25a, b].

The SubPc wheels have a curved shape structure coming from the alternation of five- and six-membered rings in their chemical structure. The electronic labelling effect results of the different electronic transparency of the phenyl and pyridyl chemical groups of the wheel to tunneling electrons. After a sub-monolayer sublimation on a Au(111) surface, the STM images showed two conformations of the molecule (I

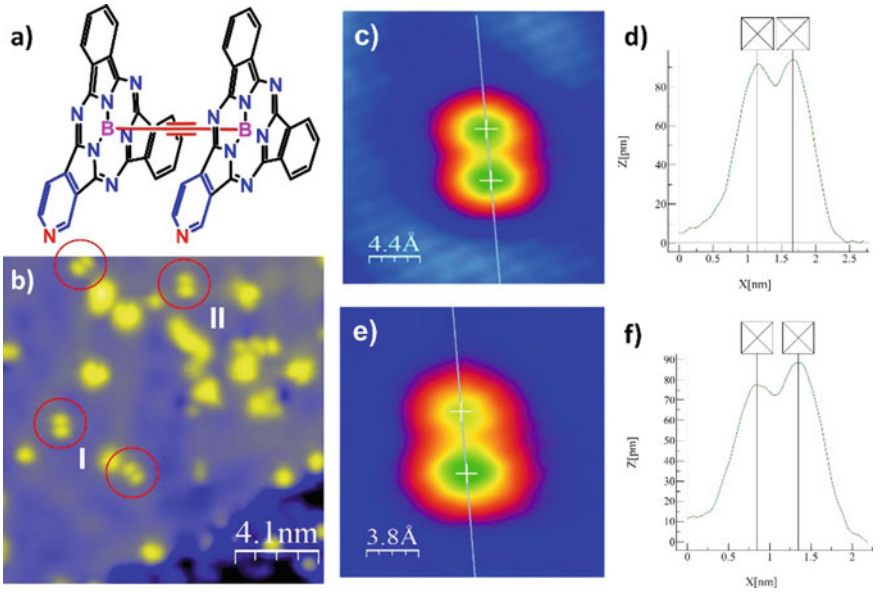

Fig. 7 **a** Chemical structure of the subphthalocyanine (SubPc) wheel dimer for the conformer (I) with the pyridine of each wheel pointing exactly in the same direction. **b** Constant current low temperature STM image on the Au(111) surface ($I = 50$ pA, $U = 0.01$ V) after the molecule sublimation revealing two conformers of the SubPc wheel dimer (I and II). STM images ($I = 50$ pA, $U = 0.01$ V) of the dimer of the **c** conformer I and **e** II with their corresponding apparent height (**d** and **f**) [25b]

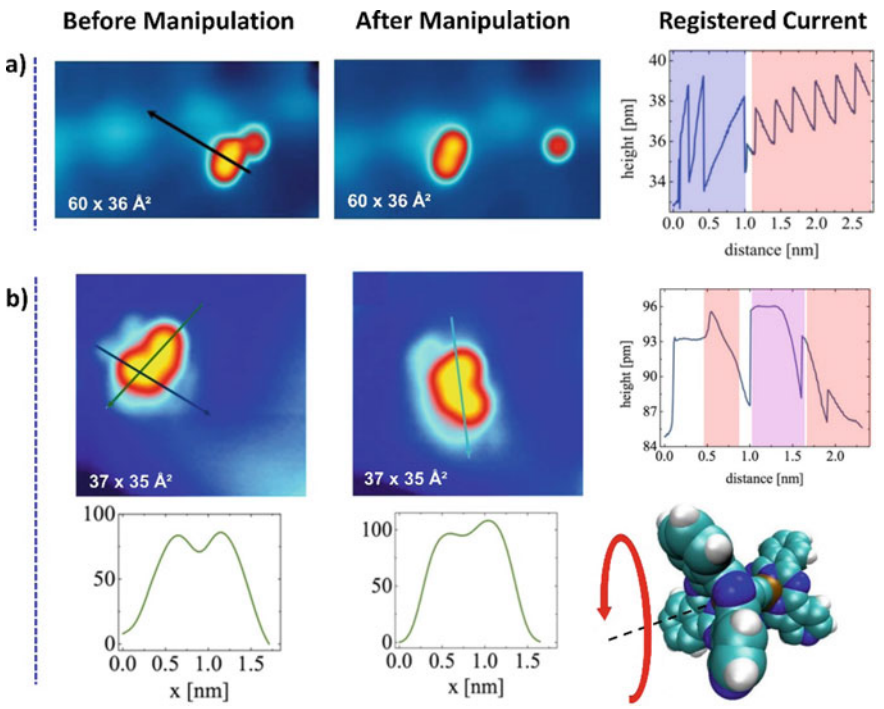

Fig. 8 **a** STM molecular manipulation in the direction of the black arrow leading to a translation of the SubPc wheel dimer on the Au(111) surface leading to a sequence of two different manipulation signals with first a pushing (blue) and between sliding and pulling (pink). **b** Manipulation in the direction of the black arrow leading to a rotation of one wheel of the SubPc wheel dimer on the Au(111) surface [25b]

and II) (Fig. 7b). The first has two symmetrical lobes corresponding to the positions of the nitrogen tags both pointing up or down in respect to the surface (Fig. 7c, d). The second conformation has an asymmetrical appearance of the two lobes (Fig. 7e, f). In this conformation, one nitrogen label is pointing up to the tip and the other down to the surface. This apparent height difference results from the different electronic coupling between the pyridine and the Au(111) surface as compared to the phenyl-surface coupling.

STM manipulation attempts were carried out in a standard pushing mode (Fig. 8a). Most of the experiments led to a translation of the molecule with no rotation of the wheels. This interpretation was further supported by analyzing the tunneling current manipulation signal which showed a standard sawtooth-like profile. In some cases, a rotational motion of one of the SubPc fragments of the dimer was observed (Fig. 8b). This motion was clearly identified in the image after manipulation by a change of the apparent height of one of the wheels. Finally, the profile of the tunnel current variation recorded during this manipulation presents an unusual profile different from a simple pushing or pulling mode signal. The complete interpretation of this

tunneling current signal proved to be challenging. While being pushed by the STM tip apex, the SubPc wheel dimer presents a complex mechanical behavior on the Au(111) surface involving a combination of a drifting and a rotational motion. These motions were accompanied by intramolecular conformation changes modifying the electronic tunneling conductance of the molecule at each STM tip apex position during the pushing manipulation.

Each nitrogen atom of the pyridyl fragments played their role as an electronic label and allowed the determination of an altitudinal rotation in a direct manner (image per image after a given manipulation sequence). However, the introduction of such SubPc wheels in more complex technomimetic chemical structures like a four-wheel molecule-vehicle was not considered due to the instability of the B–C_{sp} bond under the sublimation conditions as shown by the quantity of decomposed molecules which appeared on the surface after the sublimation step (Fig. 7b). The triangular-like molecules correspond to the SubPc wheels after breaking of the B–C_{sp} bond.

5 Nanocar Race I: Manipulation of Nano-vehicles

5.1 The French Nano-vehicle Engaged in the Race

In April 2017, the Nanocar Race (1st Edition) was the first international competition involving the driving of nano-vehicles for a long period (36 h non-stop). It gathered physicists, chemists and theorists from research groups of various countries (France, Germany, Swiss, Austria, United-States of America and Japan). The required propulsion mode involved either inelastic (relying on inelastic tunneling collisions) or dipolar (relying on the dipolar moment of the nano-vehicle) driving (see Sect. 2). The mechanical pushing, sliding and pulling manipulation modes as described above were forbidden which introduced new design constraints [26]. Each team of the contest went to Toulouse with its own challenges in a spirit of sharing information, their experience and their knowledge on the manipulation and on the driving of molecule-vehicle.

In the frame of this race, the Toulouse team has participated with a nano-vehicle having a rigid chassis built around a perylene core connected to four triptycene units normally acting as wheels. Remarkably, these nanocars were only composed of carbon and hydrogen atoms. A first design was tested incorporating four *tert*-butyl functional groups at the periphery of the chassis (Fig. 9a, b) [27a]. Despite its high molecular weight (MW = 2563 g mol^{-1}, $C_{200}H_{160}$), this molecule was deposited on a Cu(100) surface and the image revealed four lobes corresponding to the four triptycene fragments and also two protrusions coming from the *tert*-butyl (^{t}Bu) groups (Fig. 9c).

However, no soft manipulations of this molecule by an STM tip apex were possible since this molecule was stuck on the surface on account of important electronic

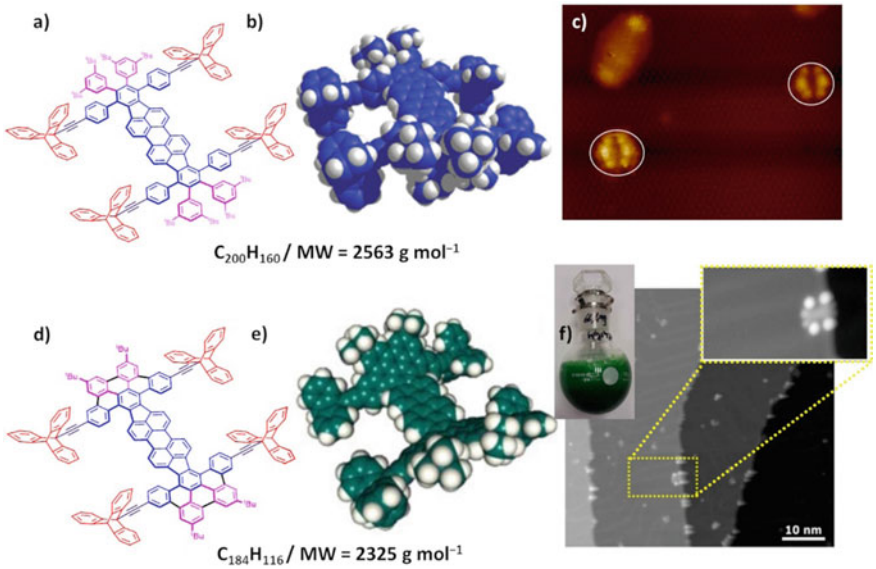

Fig. 9 **a** Chemical structure of the first French nano-vehicle, **b** its molecular model and **c** the corresponding low temperature constant current STM image ($I = 0.3$ nA, $U = 0.5$ V) of the molecule on a Cu(100) surface. **d** Chemical structure of the French nano-vehicle finally engaged in Nanocar Race I, **e** its molecular model and **f** the corresponding low temperature constant current STM image ($I = 10$ pA, $U = 0.2$ V) of the molecule on a Au(111) surface. Insert: zoom of the step edge showing one molecule with its four wheels STM imaged as four lobes corresponding to a large tunnel conductance of the molecule at the wheels location [27]

interactions between the four wheels and the Cu(100) surface. As already discussed with the wheelbarrow equipped with the same wheels, the large deformations of the triptycenes with the Cu(100) surface brings the central chassis down to the surface. As a consequence, the lateral diffusion potential energy barrier increased largely on the Cu(100) surface thus requiring a large repulsive interaction from the tip apex in order to bring this molecule out of its minimum energy potential well. In this case, different lateral ways out from this well appear on the Cu(100) surface and no controlled pushing direction were induced.

A fine tuning of the design of the four-wheel molecule and a change of the supporting surface to fulfill the Nanocar Race I rules led to a decrease of the adsorption energy of the four triptycene wheels. In addition, the introduction of only two ^{t}Bu groups allowed a pericyclization of the chassis during the synthesis (Fig. 9d). This new molecule (MW = 2325 g mol^{-1}, $C_{184}H_{116}$, nicknamed "green buggy" due to its powder color and to its highly curve structure) has a large π-system showing an alternance of five and six-membered rings (Fig. 9e). The resulting curvature of the chassis led to less interactions of the chassis with the Au(111) surface. This molecule appeared as four lobes on a Au(111) surface (Fig. 9f, insert: showing its aspect as a

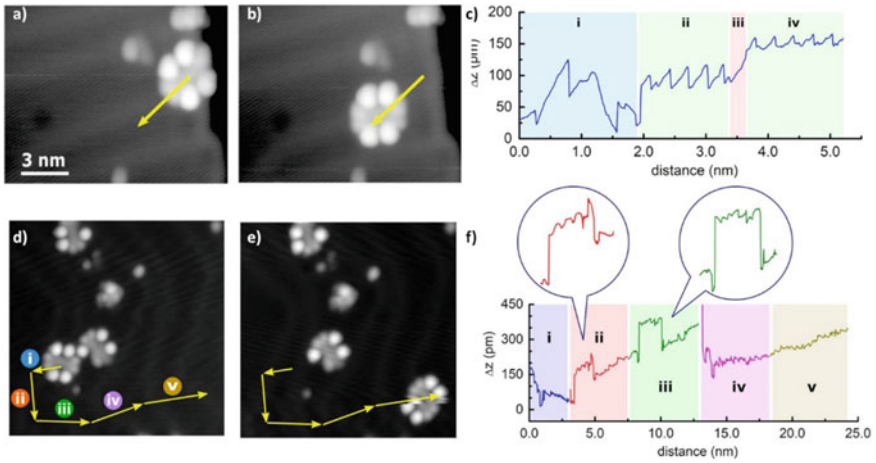

Fig. 10 Low temperature constant current STM images of the French Nano-vehicle ($I = 10$ pA, $U = 0.2$ V) **a** before and **b** after a manipulation sequence resulting in a translation of the molecule on the Au(111) surface. **c** Recorded tunneling current manipulation signal during this sequence. Low temperature constant current STM images of the French Nano-vehicle ($I = 10$ pA, $U = 0.2$ V) **d** before and **e** after a long driving passing over two Au(111) reconstruction. **f** Recorded tunneling current manipulation signal showing characteristics jumps in this constant current manipulation mode. Notice the positive Δz slop from (ii) to (iii) and from (iv) to (v) is characteristic of the non-planarity of the sample at the atomic scale

greenish powder in a round-bottom flask). It is the one which had participated to the 1st Nanocar Race [27].

Most of intact molecules (not destroyed by the flash sublimation protocol used) were located at a mono-atomic step edge at the junction of two Au(111) atomically flat terraces. The manipulation attempts using STM voltage pulses led to the decomposition of the molecule with the cleavage of one of its wheels [27b]. Mechanical low voltage manipulation using a constant height mode gave rise to the translation of the molecule on the surface as seen by the characteristic sawtooth-like manipulation signal (Fig. 10a–c).

The resulting manipulation signal was quite complex since the tip apex was located on top of the molecular chassis in between the four wheels. First, it was required to bring the nanocar out of the monoatomic step edge (Fig. 10c-i). Finally, an intramolecular pushing mode was used to drive the molecule along the Au(111) surface (Fig. 10c-ii and -iv).

On the long drive with five characteristic sequences (Fig. 10d, e), a constant current manipulation mode was used to moderate the repulsive interaction regime between the STM tip apex end atom and the wheels of the molecule. It is worthwhile to note that two other molecule-cars were imaged with one wheel missing indicating that the flash sublimation technique was quite destructive for these molecules. However, the molecule proved to be able to adapt its conformation to both the tip apex end atom

(placed ~~in~~ between the four wheels) and the different Au(111) surface reconstructions met during this drive. On the way, the two characteristics manipulation signal jumps (Fig. 10f-ii and c-iii) were the result of crossing one reconstruction. These jumps were attributed to the rotation of the triptycene wheels while passing over the surface reconstructions. Indeed, the Δz corresponded to the variation of the hub of a triptycene wheel upon rotation. However, this controlled rotation is only the result of mechanical manipulation by the STM and not to an inelastic tunneling effect. When possible and due to large inter-wheel lateral distance, pushing the molecule along the flat fcc direction (in between two Au(111) reconstructions) led to a silent manipulation signal sequences indicating a smooth translation almost like a sliding mode (Fig. 10f-iv, v).

5.2 The Five Other Nano-vehicles Engaged in the 1st Race

All together with the Toulouse team, five other teams were engaged in the 1st edition of the Nanocar Race with three of them competing on the same Au(111) surface, one in a remote control mode on its own Au(111) surface and the last one on its dedicated Ag(111) surface (Table 1). Some of them turned their attention on the use of supramolecular assemblies such as the teams from Ohio (team leaders: S. W. Hla and E. Masson) and Dresden (team leader: F. Moresco). During the race, it clearly appeared that these assemblies had some limitations. For instance, the "Ohio Bobcat" encountered deposition problems of its pre-assembled 3D architecture on account of the weak interactions holding the cucurbit[7]uril (CB[7]) wheels to the chassis. Another approach was exploited by TU Dresden researchers where the supramolecular assembly was made *in-situ* by putting together four identical molecular sub-units [28]. In both cases, these assemblies proved to collapse upon manipulation especially when they were stuck on a defect on the Au(111) surface. The instability of these supramolecular chemical structures easily rationalizes the low driving distance achieved (43 nm and 11 nm for Ohio and Dresden respectively).

On the other side, some fully covalent polyaromatic nano-vehicles proved to be unsuccessful for inelastic or dipolar driving. The Tsukuba team (team leader: W. Nakanishi) faced a strong physisorption of the rigid molecule on the surface as seen for the Toulouse team (Sect. 5.1) [29]. Indeed, the polyaromatic nature of their nano-vehicle increased the molecule-surface interactions thus increasing its lateral diffusion potential energy barrier height. In this case, the use of high voltage inelastic excitations pulses to create a quantum mixing between the ground and excited states of this molecule was not able to provide enough intramolecular energy to go over this energy barrier. The fastest nano-vehicle proved to be the smallest and most compact molecules was the one powered by the Basel team (team leader: R. Pawlack) [30] on a Au(111) surface and Rice-Graz team (team leaders: J. M. Tour and L. Grill) on a Ag(111) surface [31].

After this competition, J. M. Tour, L. Grill and their coworkers published a guide for designing a fast nano-vehicle [31]. Indeed, a fine balance between the mechanical

Table 1 The ranking of the first edition of the international Nanocar Race showing the chemical structures of the nano-vehicles of the different teams with the corresponding STM images, the team leaders and institutions, the surface used (shared means that the same surface was shared on the LT-UHV four-STM instrument of the CEMES-CNRS lab, Toulouse, France), the propulsion mechanism, the distance achieved, and the main encountered incidents during the driving

	Rice-Graz	Basel	Ohio	Dresden	Tsukuba	Toulouse
STM image						
Chemical structure	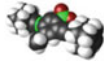		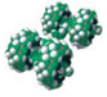		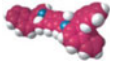	
Chemical formula	$C_{32}H_{36}N_2O_2$ (88 atoms)	$C_{22}H_{17}N_3$ (42 atoms)	$C_{244}H_{222}N_{120}O_{56}$ (642 atoms)	$C_{56}H_{48}O_4$ (108 atoms)	$C_{50}H_{34}O_4$ (88 atoms)	$C_{184}H_{116}$ (300 atoms)
Team leader(s) and universities	L. Grill & J. Tour Uni. Graz & Rice Uni.	R. Pawlack Uni. of Basel	S.W. Hla & E. Masson Ohio Uni.	F. Moresco TU Desden	W. Nakanishi MANA/NIMS	G. Rapenne CEMES/CNRS
Surface	Ag(111)	Au(111) (shared)	Au(111)	Au(111) (shared)	Au(111) (shared)	Au(111) (shared)
Propulsion mechanism	Dipolar	Inelastic	Dipolar	Inelastic	Inelastic	Inelastic
Driving distance	150 nm 1.5 hr	133 nm 6 hr	43 nm 29 hr	11 nm first hr	1 nm first hr	25 nm by pulling (not allowed)
Incidents	–	–	–	Molecule stuck on a defect	Motor blocked	Molecule jumped on the tip

structure of molecule and the nature of the surface has to be found. First, the molecule should have a low molecular weight to ease its deposition (often by sublimation using a crucible) and to minimize the molecule-surface interactions. A minimum of aliphatic wheels would be of interest here to lift the chassis off the surface in order to limit the adsorption energy of the molecule-car. A rigid structure should also be preferred in order to avoid the molecule sagging towards the surface. In addition, a robust molecule would survive the deposition conditions and would lead to its manipulation for a long run on a surface without breaking. Finally, the introduction of a dipolar moment in the design of the nano-vehicle seems to be of particular interest to avoid a manipulation though a mechanical pushing mode (see Sect. 2) which was not permitted by the rules issued by the Nanocar Race organization committee.

A dipolar moment on the molecular chassis allows the manipulation of this molecule by a strong local electric field (electrostatic forces) requiring the application of a relatively high bias voltage. This can be very effective for a straight line drive on an atomically ultra-flat surface but difficult to play with for a slalom such as on a Au(111) surface.

The 1st edition of the Nanocar Race in 2017 was a milestone for driving nano-vehicles since most contestants were competing on the same surface (Au(111)) thus allowing a direct comparison between the different chemical structures and giving rise to a deeper comprehension of the single-molecule manipulation protocols.

6 A Motorized Nano-vehicle

In the above examples, no chemical functional groups can be identified as a "motor" from a technomimetic point of view. The Basel, Dresden and Tsukuba nanocars are pertinent examples of molecular structures beneficiating of a quantum intramolecular motor. This quantum motor is in the form of an electronic structure having a dedicated excited state potential energy able to offer a directional translation on the Au(111) surface. A unidirectional motion, for instance forward versus backward, is also possible using a dipolar moment located on the molecular chassis as the Graz-Rice molecule-vehicle. During the pulse, the tip apex position imposes the symmetry of the STM tunnel junction resulting in an effective on-surface potential energy curve.

An alternative has been provided by the group of B. L. Feringa. They had developed a family of rotary molecular motors exhibiting a unidirectional rotation in solution. This rotation is the result of the isomerization of a C=C double bond [32a, b]. In the example presented below, the motor is composed of a thioxanthene group (stator) linked to a (2R)-methyl-2,3-dihydronaphthothiopyran group (rotor) (Fig. 11). The indicated starred asymmetric carbon refers to a defined chirality of this stereogenic center. The complete rotation cycle of the rotor part of this molecular structure can be explained in a four-step sequence. Upon light irradiation, the molecule undergoes the photoisomerization of its double bond ($\lambda_{max} = 365$ nm) from the (2'R)-(M)-trans form (①) to the (2'R)-(P)-cis form (②). This isomerization occurs preferably in one direction accounting for the asymmetric steric hindrance between the methyl group

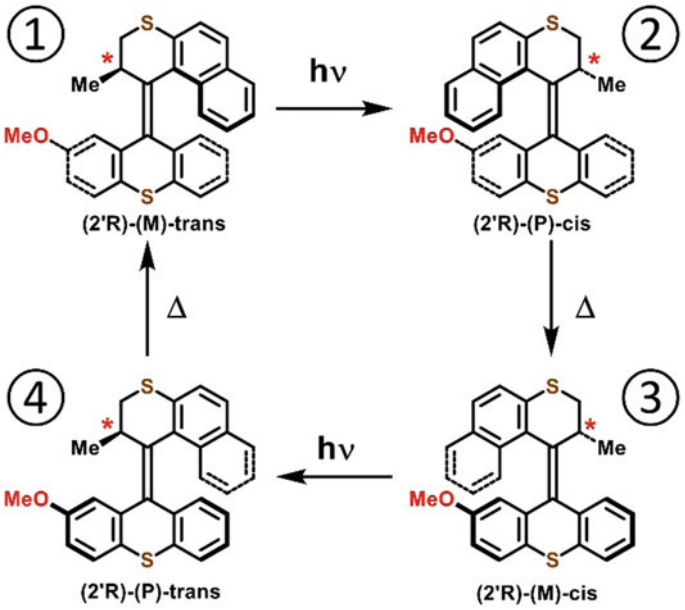

Fig. 11 The principle of the unidirectional rotation of the Feringa motor described with its light (hν) and thermal (Δ) cycles [32a, 34]

of the rotor and the methoxy group of the stator. A more stable conformation, (2'R)-(M)-cis (③), is reached by a thermal activated helix inversion (P to M isomer at T = 60 °C) thus causing the rotor to rotate 180°. A second cycle of irradiation led to the (2'R)-(P)-trans form (④) of the motor followed by a thermal inversion inducing a second rotation of 180°. It thus allows the complete and unidirectional rotation of the rotor part of this molecular structure.

This unidirectional rotation is rationalized by an energy diagram (Fig. 12) involving two states, namely the ground state (S_0) and the first excited state (S_1) [33, 34]. If thermal energy is the only source of energy for the motor, no unidirectional rotation can be achieved on the ground state potential energy curve (red) resulting from the microreversibility principle. Indeed, the steric hindrance is not supposed to lead to a one-way rotation since the potential energy gradient will be identical on both side of the saddle point. In consequence, an additional source of energy (here light) is necessary to overcome the energy barrier (E_{a21}) and to reach the well ② in a selective manner. The key factor of this photochemical isomerization process is the existence of a conical intersection (CI, only naively represented on Fig. 12). The CI makes the isomerization quantum yield markedly different from 50% at the saddle point thus leading to a one-way rotation. Then, thermal energy allows to pass the second energy barrier (E_{a23}). A similar sequence (light followed by heat) completes the rotation in one direction. Formally, the molecular design of the Basel, Dresden and Tsukuba molecule-vehicles were looking on a surface and

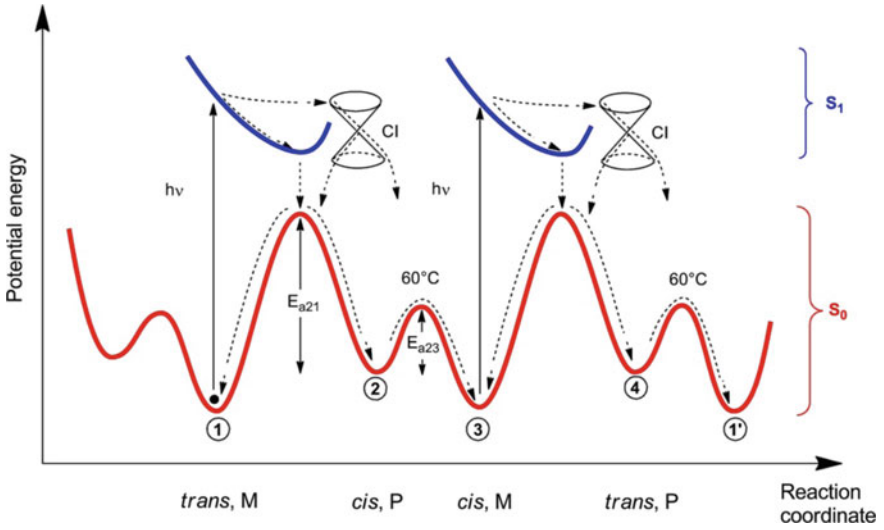

Fig. 12 The effective potential energy curve resulting from a projection of multi-dimensional potential energy surfaces of the ground and first excited states along the main reaction coordinate for a complete rotation. After the photochemical excitation from the ground S_0 state (in red), the system evolves towards a minimum of the excited state S_1 (in blue). However, it can also evolve in a perpendicular reaction coordinate towards a conical intersection (CI, thin black) privileging the evolution towards the right of the diagram

on a single molecule for such quantum design effect but without the subsequent molecular rotation observed by the Feringa group.

Using this molecular motor, the Feringa group has designed a nanocar. They mounted four motors with definite chiralities (R or S) as switchable legs on a semi-rigid scaffold chassis (Fig. 13a) [35]. The resulting molecule-car was imaged and manipulated at 7 K on a Cu(111) surface (Fig. 13). Different conformers exist for this molecule after adsorption on the Cu(111) surface because of the possible twisting around the central spar (Fig. 13a). A molecular model showed that only the meso-(R, S-R, S) isomer may lead to a combined action of the four legs molecular motors for the molecule to move on the Cu(111) surface after providing some energy using the STM tip apex. On a metallic surface, light cannot be used to trigger the S_0-S_1 isomerization of the switchable legs of this molecule-car since the excitation of a photochromic molecule is quenched on a metal surface. Therefore, the STM tip apex end atom was positioned at the center of the chassis and a voltage pulse was applied. The threshold of this voltage pulse for a motion was 500 mV. Selecting the right four-leg molecule isomer and after a series of ten voltage pulses, the molecule underwent an almost linear translational motion of 7 nm (Fig. 13b (1–6)). The action spectrum and the waiting time at each one-step motion on the Cu(111) can be interpreted by the fact that a quantum mixing of the ground and a virtually reduced molecular electronic states occurs at each individual electron transfer event through this molecule during each bias voltage pulse. The inelastic interactions mentioned above led certainly

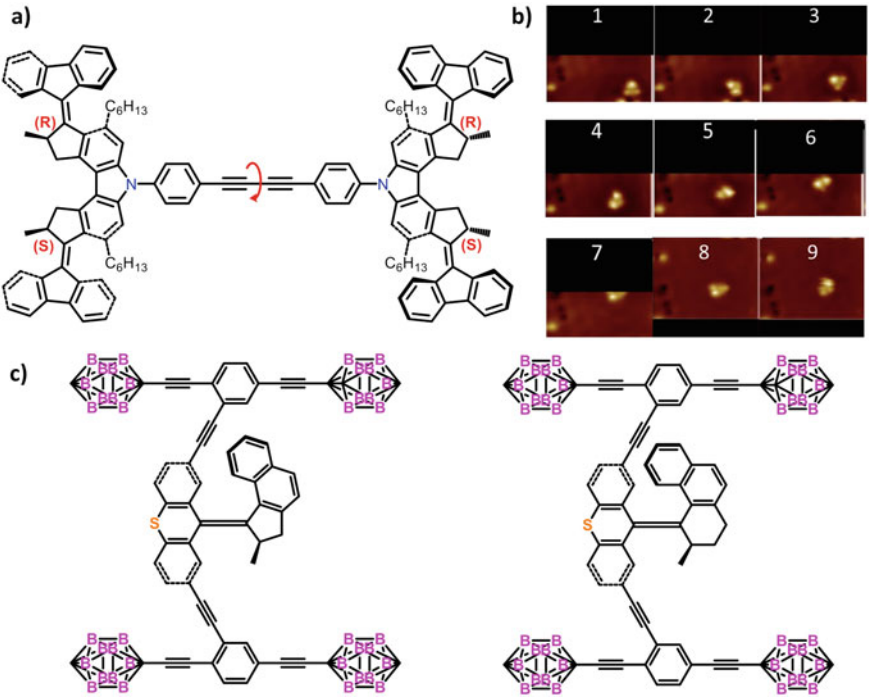

Fig. 13 **a** Chemical structure of the molecule-car of the Feringa group showing the four asymmetry switchable legs and the possibility of rotation around the central spar determining different molecular conformation on the Cu(111) surface during the sublimation process; **b**-1–**b**-10 STM images (I = 74 pA, U = 47 mV) showing the step by step motion of this molecule-car on the Cu(111) surface [35]; **c** Chemical structures of two nano-vehicles of the Tour group incorporating Feringa motor in their chassis [36]

to an intramolecular energy relaxation normally deserving at least one of the four switchable legs.

The complete interpretation of the motion, in particular the possible synchronization of the switching of the four motorized legs requires a detailed analysis. The dI/dV tunneling spectrum of the molecule-car had also not been recorded to understand the published action spectrum i.e. how the probability of motion develops as a function of the voltage pulse value. Furthermore, like in any such molecular mechanical motion with complex conformation, a detailed STM image calculations must be performed to extract the molecular conformation behind each recorded STM image. Much remains to be done to explain this behavior and to drive this molecule-car at a very long distance.

In 2012, the group of J. M. Tour incorporated one single Feringa's motor on the chassis of a molecule-car equipped with four *p*-carborane wheels (Fig. 13c). For this new technomimetic-like design, Feringa's motor was part of the chassis. The interaction of the central (2R)-methyl-2,3-dihydronaphthothiopyran group (rotor) with the

metal surface led to a down conformation of this propeller. In this conformation, it is no possible to switch it up using an STM bias voltage pulse to activate the supposed motor effect [36]. As a consequence, it was not possible to drive this molecule-car on a metal surface using an STM bias voltage pulse strategy.

7 Conclusion

Since the discovery of the STM and the first manipulation of xenon atoms (one at a time) on a metal surface, the field related to the study of the mechanics of a single molecule on a surface has evolved drastically. More complex molecular architectures have emerged in order to gain a deeper understanding on the mechanical properties in translation and rotation of a single molecule mechanical machinery. Each small step performed from the early studies of technomimetic-like molecules to motorized nano-vehicles has finally led to a giant leap to go beyond Feynman's initial vision. We now aim at targeting a functional single molecule machine.

The 1st edition of the Nanocar Race has clearly demonstrated that a long road has still to be taken to conceive, synthesize, study and understand the operating mechanisms of such molecule-machines on a metal surface. Here, transferred electrons through the molecule can act as a local energy source and the dissymmetry of the STM junction is provided by the position of tip apex end atom with respect to the molecule chemical structure. Nano-vehicles are now at the stage of the first ever "macroscopic" motorized automobile race in 1895 when Albert Lemaître reached the city of Rouen from Paris (a distance of 127 km) in 6 h and 48 min. Accordingly, the future of nano-vehicles (and synthetic molecular machines in general) looks bright with amazing perspectives ahead. The recent 2nd edition of the Nanocar Race (March 2022) pointed out the huge progresses in design, stability and drivability of a single molecule-vehicle on a surface accomplished in only five years.

Acknowledgements We thank the European Union Horizon 2020 FET open project "Mechanics with Molecules" (MEMO, grant 766864) for financial support.

References

1. Feynman, R.-P.: Eng. Sci. **23**, 22–36 (1959)
2. Schunack, M., Rosei, F., Naitoh, Y.: J. Chem. Phys. **117**, 6259–6265 (2002)
3. Molecular architectonics and nanoarchitectonics. In: Govindaraju, T., Ariga, K. (eds.) Nanostructure Science and Technology Series. Springer (2022)
4. (a) Gakh, A.A., Sachleben, R.A., Bryan, J.C.: ChemTech **27**, 26–33 (1997). (b) Jimenez-Bueno, G., Rapenne, G.: Tetrahedron Lett. **44**, 6261–6263 (2003)
5. (a) Joachim, C., Tang, H., Moresco, F., Rapenne, G., Meyer, G.: Nanotechnology **13**, 330–335 (2002). (b) Grill, L., Rieder, K.-H., Moresco, F., Jimenez-Bueno, G., Wang, C., Rapenne, G., Joachim, C.: Surf. Sci. **584**, L153–L158 (2005)

6. Schunack, M., Rosei, F., Naitoh, Y., Jiang, P., Gourdon, A., Lægsgaard, E., Stensgaard, I., Joachim, C., Besenbacher, F.: J. Chem. Phys. **117**, 6259–6265 (2002)
7. Vives, G., Tour, J.M.: Acc. Chem. Res. **42**(3), 473–487 (2009)
8. Zeppenfeld, P., Lutz, C.P., Eigler, D.M.: Ultramicroscopy **42–44**, 128–133 (1992)
9. Iwamura, H., Mislow, K.: Acc. Chem. Res. **21**, 175–182 (1988)
10. Livoreil, A., Dietrich-Buchecker, C.O., Sauvage, J.P.: J. Am. Chem. Soc. **116**, 9399–9400 (1994)
11. Kozlov, I.A., Skulachev, V.P.: Biochem. Biophys. Acta **463**, 29–89 (1977)
12. Noji, H., Yasuda, R., Yoshida, M., Kinosita, K.: Nature **386**, 299–302 (1997)
13. Boyer, P.D.: Annu. Rev. Biochem. **66**, 717–749 (1997)
14. Alvey, M.D., Yates, J.T., Jr., Uram, K.J.: J. Chem. Phys. **87**, 7221–7228 (1987)
15. Zwanzig, R.: J. Chem. Phys. **87**, 4870–4872 (1987)
16. Eigler, D.M., Schweizer, E.K.: Nature **344**, 524–526 (1990)
17. (a): Jung, T.A., Schlittler, R.R., Gimzewski, J.K., Tang, H., Joachim, C.: Science **271**, 181–184 (1996). (b) Moresco, F.: Phys. Rep. **399**, 175–225 (2004). (c) Hla, S.W.: J. Vac. Sci. Technol. B **23**, 1351–1360 (2005). (d) Hla, S.W.: Rep. Prog. Phys. **77**, 056502 (2014). (e) Wang, C., Chi, L., Ciesielski, A., Samorì, P.: Angew. Chem. Int. Ed. **58**, 18758–18775 (2019). (f) Khajetoorians, A.A., Wegner, D., Otte, A.F., Swart, I.: Nat. Rev. Phys. **12**, 703–715 (2019). (g) Li, Z., Gao, C.Y., Su, D., Jia, C., Guo, X.: ACS Mater. Lett. **3**, 1484–1502 (2021)
18. (a) Bouju, X., Joachim, C., Girard, C.: Phys. Rev. B **59**, R7845–R7848 (1999). (b) Bartels, L., Meyer, G., Rieder, K.-H.: Phys. Rev. Lett. **79**, 697–700 (1997). (c) Bouju, X., Girard, C., Tang, H., Joachim, C., Pizzagalli, L.: Phys. Rev. B **55**, 16498–16506 (1997). (d) Grill, L., Rieder, K.-H., Moresco, F.: Nano Lett. **6**, 2685–2689 (2006)
19. (a) Lee, H.J., Ho, W.: Science **286**, 1719–1723 (1999). (b) Hla, S.W., Bartels, L., Meyer, G., Rieder, K.-H.: Phys. Rev. Lett. **85**, 2777–2780 (2000). (c) Liljeroth, P., Repp, J., Meyer, G.: Science **317**, 1203–1206 (2007). (d) Lastapis, M., Martin, M., Riedel, D., Hellner, L., Comtet, G., Dujardin, G.: Science **308**, 1000–1003 (2005). (e) Henningsen, N., Franke, K.J., Torrente, I.F., Schulze, G., Priewisch, B., Rück-Braun, K., Dokić, J., Klamroth, T., Saalfrank, P., Pascual, J.I.: J. Phys. Chem. C **111**, 14843–14848 (2007). (f) Stone, I., Starr, R.L., Zang, Y., Nuckolls, C., Steigerwald, M.L., Lambert, T.H., Roy, X., Venkataraman, L.: Nat. Rev. Chem. **5**, 695–710 (2021)
20. (a) Qiu, X.H., Nazin, G.V., Ho, W.: Phys. Rev. Lett. **93**, 196806 (2004). (b) Alemani, M., Peters, M.V., Hecht, S., Rieder, K.-H., Moresco, F., Grill, L.: J. Am. Chem. Soc. **128**, 14446–14447 (2006). (c) Alemani, M., Selvanathan, S., Ample, F., Peters, M.V., Rieder, K.-H., Moresco, F., Joachim, C., Hecht, S., Grill, L.: J. Phys. Chem. C **28**, 10509–10514 (2008). (d) Scheil, K., Gopakumar, T.G., Bahrenburg, J., Temps, F., Maurer, R.J., Reuter, K., Berndt, R.: J. Phys. Chem. Lett. **7**, 2080–2084 (2016). (e) Nacci, C., Baroncini, M., Credi, A., Grill, L.: Angew. Chem. Int. Ed. **57**, 15034–15039 (2018). (f) Leoni, T., Lelaidier, T., Thomas, A., Ranguis, A., Siri, O., Attaccalite, C., Becker, C.: Nanoscale Adv. **3**, 5565–5569 (2021)
21. Joachim, C., Rapenne, G.: ACS Nano **7**, 11–14 (2013)
22. (a) Shirai, Y., Osgood, A.-J., Zhao, Y., Kelly, K.-F., Tour, J.M.: Nano Lett. **5**, 2330–2334 (2005). (b) Morin, J.-F., Sasaki, T., Shirai, Y., Guerrero, J.-M., Tour, J.M.: J. Org. Chem. **72**, 9481–9490 (2007). (c) Chu, P.L.E., Wang, L.-Y., Khatua, S., Kolomeisky, A.-B., Link, S., Tour, J.M.: ACS Nano **7**, 35–41 (2013). (d) Vives, G., Tour, J.M.: Tetrahedron Lett. **50**, 1427–1430 (2009)
23. Grill, L., Rieder, K.-H., Moresco, F., Rapenne, G., Stojkovic, S.-M., Bouju, X., Joachim, C.: Nat. Nanotechnol. **2**, 95–98 (2007)
24. Chiaravalloti, F., Gross, L., Stojkovic, S.M., Gourdon, A., Joachim, C., Moresco, F.: Nat. Mater. **6**, 30–33 (2007)
25. (a) Jacquot de Rouville, H.-P., Garbage, R., Ample, F., Nickel, A., Meyer, J., Moresco, F., Joachim, C., Rapenne, G.: Chem. Eur. J. **18**, 8925–8928 (2012). (b) Nickel, A., Meyer, J., Ohmann, R., Jacquot de Rouville, H.-P., Rapenne, G., Joachim, C., Cuniberti, G., Moresco, F.: J. Phys. Condens. Matter **24**, 404001 (2012)
26. Rapenne, G., Joachim, C.: Nat. Rev. Mater. **2**, 17040 (2017)

27. (a) Jacquot de Rouville, H.-P., Garbage, R., Cook, R.E., Pujol, A.R., Sirven, A.M., Rapenne, G.: Chem. Eur. J. **18**, 3023–3031 (2012). (b) Soe, W.-H., Durand, C., Guillermet, O., Gauthier, S., Jacquot de Rouville, H.-P., Srivastava, S., Kammerer, C., Rapenne, G., Joachim, C.: Nanotechnology **29**, 495401 (2018). (c) Jacquot de Rouville, H.-P., Kammerer, C., Rapenne, G.: Molecules **23**, 612 (2018)
28. (a) Nickel, A., Ohmann, R., Meyer, J., Grisolia, M., Joachim, C., Moresco, F., Cuniberti, G.: ACS Nano **7**, 191–197 (2013). (b) Eisenhut, F., Durand, C., Moresco, F., Launay, J.-P., Joachim, C.: Eur. Phys. J. Appl. Phys. **76**, 10001 (2016)
29. Soe, W.-H., Shirai, Y., Durand, C., Yonamine, Y., Minami, K., Bouju, X., Kolmer, M., Ariga, K., Joachim, C., Nakanishi, W.: ACS Nano **11**, 10357–10365 (2017)
30. (a) Pawlak, R., Meier, T., Renaud, N., Kisiel, M., Hinaut, A., Glatzel, T., Sordes, D., Durand, C., Soe, W.-H., Baratoff, A., Joachim, C., Housecroft, C.E., Constable, E.C., Meyer, E.: ACS Nano **11**, 9930−9940 (2017). (b) Pawlak, R., Meier, T.: Nat. Nanotechnol. **12**, 712 (2017)
31. Simpson, G.J., García-López, V., Petermeier, P., Grill, L., Tour, J.M.: Nat. Nanotechnol. **12**, 604–606 (2017)
32. (a) Feringa, B.-L.: Acc. Chem. Res. **34**, 504–513 (2001). (b) Koumura, N., Geertsema, E.M., van Gelder, M.-B., Meetsma, A., Feringa, B.L.: J. Am. Chem. Soc. **124**, 5037–5051 (2002)
33. Kazaryan, A., Kistemaker, J.C.M., Schäfer, L.V., Browne, W.R., Feringa, B.L., Filatov, M.: J. Phys. Chem. A **114**(15), 5058–5067 (2010)
34. Launay, J.-P., Verdaguer, M.: Electrons in Molecules, (Section 5.6.3.1) 2nd edn. Oxford University Press (2018)
35. Kudernac, T., Ruangsupapichat, N., Parschau, M., Macia, B., Katsonis, N., Harutyunyan, S.-R., Ernst, K.-H., Feringa, B.L.: Nature **479**, 208–211 (2011)
36. (a) Chiang, P.-T., Mielke, J., Godoy, J., Guerrero, J.M., Alemany, L.B., Villagómez, C.J., Saywell, A., Grill, L., Tour, J.M.: ACS Nano **6**, 592–597 (2012). (b) García-López, V., Chu, P.-L.E., Chiang, P.-T., Sun, J., Martí, A.A., Tour, J.M.: Asian J. Org. Chem. **4**, 1308−1314 (2015). (c) Saywell, A., Bakker, A., Mielke, J., Kumagai, T., Wolf, M., García-López, V., Chiang, P.-T., Tour, J.M., Grill, L.: ACS Nano **10**, 10945−10952 (2016). (d) García-López, V., Alemany, L.B., Chiang, P.-T., Sun, J., Chu, P.-L., Martí, A.A., Tour, J.M.: Tetrahedron **73**, 4864–4873 (2017)

On-Surface Translational Activity of Porphyrin Chromophore Molecules

Jonathan P. Hill, Daniel T. Payne, Kewei Sun, Yoshitaka Matsushita, Ayako Nakata, Puneet Mishra, Takashi Uchihashi, Waka Nakanishi, Katsuhiko Ariga, Tomonobu Nakayama, and Shigeki Kawai

Abstract Translational activity of molecules on a metal surface is an important area of study due to its relevance to the field of molecular motors and machines. Here, we study molecular motions of a planarized porphyrin molecule, a so-called 'nanocar', on a clean Au(111) surface, driven by applying a bias voltage from a tip of scanning tunneling microscopy (STM) at low temperature. The molecular design strategy involves on-surface cyclodehydrogenation to planarize the nanocar precursor molecule 5-(9-anthryl)-15-(9,9'-bianthryl)-10,20-bis(trifluoromethyl) porphyrinato-copper(II) under the concept of superlubricity leading us to assign the nickname 'Slider-Spider' to this nano-sportscar. The resulting planar nanocar molecule was

J. P. Hill (✉) · A. Nakata · P. Mishra · T. Uchihashi · K. Ariga · T. Nakayama
International Center for Materials Nanoarchitectonics (WPI-MANA), National Institute for Materials Science (NIMS), 1-1 Namiki, Tsukuba 305-0044, Ibaraki, Japan
e-mail: Jonathan.Hill@nims.go.jp

D. T. Payne
International Center for Young Scientists, National Institute for Materials Science (NIMS), 1-1 Namiki, Tsukuba 305-0044, Ibaraki, Japan

K. Sun · S. Kawai (✉)
Research Center for Advanced Measurement and Characterization, National Institute for Materials Science (NIMS), 1-2-1 Sengen, Tsukuba 305-0047, Ibaraki, Japan
e-mail: Kawai.Shigeki@nims.go.jp

Y. Matsushita
Research Network and Facility Services Division, National Institute for Materials Science (NIMS), 1-2-1 Sengen, Tsukuba 305-0047, Ibaraki, Japan

W. Nakanishi
Molecular Design and Function Group, National Institute for Materials Science (NIMS), 1-2-1 Sengen, Tsukuba 305-0047, Ibaraki, Japan

K. Ariga
Department of Advanced Materials Science, Graduate School of Frontier Sciences, The University of Tokyo, 5-1-5 Kashiwanoha, Kashiwa 277-8561, Chiba, Japan

S. Kawai
Graduate School of Pure and Applied Sciences, University of Tsukuba, 1-1-1 Tennodai, Tsukuba 305-8571, Ibaraki, Japan

© The Author(s), under exclusive license to Springer Nature Switzerland AG 2023

F. Moresco and C. Joachim (eds.), *Single Molecule Mechanics on a Surface*,
Advances in Atom and Single Molecule Machines,
https://doi.org/10.1007/978-3-031-16930-4_5

stimulated to move a distance of 1054 nm (including 54 turns) during a 24 h period leading to victory for the NIMS Tsukuba Team in the 2nd Nanocar Race. The molecule had excellent stability and could be operated as a nanocar for 24 h under remote control at 10,211 km (Toulouse in France–Tsukuba in Japan) by using a scanning probe system at subnanometer scale.

Keywords Porphyrin · On-surface synthesis · Superlubricity · Scanning tunneling microscopy

1 Introduction

Despite the great progress in molecular machines and molecular devices [1, 2], which has culminated in the awarding of the 2016 Nobel prize based on advances in this area, there remains a substantial requirement for advances in this field in order to further improve our understanding of the concept of molecular operations towards applications. Chemical nanotechnology might be able to provide operational devices in solution states or involving interfacial media [3, 4], but true molecular machines performing operations remain a fantasy. For this reason, it is important to investigate molecular operations in a range of different formats such as in self-assembled states [5], supramolecular systems [6] or individually at a suitable surface or interface [7]. This latter aspect might be aimed at allowing addressability of molecules contained within self-assembled lattices [8] or, as in the case described here, to assess the possibilities for the manipulation of molecules under a stimulus especially for a better understanding of molecular translational activity [9].

Previously, molecular motion at a metal surface has been studied under the competitive regime of a race where individual research teams have identified different paradigms for molecular motility [9, 10]. Our previous efforts involved the use of STM to manipulate molecules for translation and rotation [11]. In this paper, we will summarize some our activity in this field including a discussion of factors affecting the selection and manipulation of the molecules at surfaces. Molecular excitation using the tip of a scanning tunneling microscope (STM) has been applied for atomic-level manipulation since the pioneering work of Eigler and Schweizer [12], and the various mechanisms of single atom (and small molecule) mechanical translation have been studied [13, 14]. An STM tip can be used to maneuver single molecules at a surface [15, 16], and is a well-known method for the precise positioning of individual molecules for the study of molecular operations [17] or their electronic activity [18]. For the precise lateral translocation of a molecule situated on a metal surface involving no mechanical interference of STM tip and molecule (i.e., no touching), it is necessary that a bias be applied to excite the molecule at a lateral precision of a few picometers [19]. On the one hand, excitation might be inelastic caused by applied tunneling current or, on the other hand, might be due to an enhanced electric field at the tip/surface junction if an appropriately designed molecule bears a substantial dipole [20]. Inelastic excitation usually involves molecular low-lying electronic

states [18, 21]. Also, it is necessary to avoid the redistribution of any molecular excitation between the many available mechanical states of the molecule, and this might be achieved by considering the precise design of any potential molecules for study. This is an important matter to address in order to discriminate between any possible conformational variation of the molecule or its lateral displacement. Molecules might also be decomposed by the application of an inappropriate bias voltage pulse [22]. Energy intended for molecular excitation might also be redistributed to the substrate so that various suitable support moieties ('legs' or 'wheels') have already been identified. These effectively maintain distances between the substrate and the main body of the molecule (i.e., the chassis) [23–25].

In previous work (Nanocar Race I), we have designed and prepared the bisbinaphthyldurene (BBD) molecule (Fig. 1), observed its activity at a metal interface, and attempted single molecule manipulation including stepwise lateral translation using an STM tip. BBD contains two binaphthyl groups attached to a simple 1,2,4,5-substituted benzene chassis. The molecule is essentially planar and we applied low amplitude vibration modes of the 1,1′-binaphthyl groups [26, 27] through STM inelastic tunneling excitation to drive BBD on Au(111). The planar conformation of BBD does not exist in solution but is stable on Au(111) after lateral mechanical manipulation by STM. Lateral manipulation is necessary because the native state of BBD on Au(111) is a dimer with molecular plane perpendicular to the surface (see Fig. 2).

A nonplanar conformation (similar to its state in solution) is also available through excitation at the surface. BBD molecules in the planar conformation available on Au(111), were subjected to dI/dV molecular orbital mapping in order to find the optimum location for inelastic excitation and manipulation using the STM tip. It was found that the 1,1'-binaphthyl groups are not suitable for this purpose since BBD molecules treated in this way undergo strident conformational changes in competition with any stepwise translational activity. However, another location for excitation does exist, and can be used to excite the molecule without disrupting the planar conformation allowing consecutive molecular translations in 0.29 nm steps. The BBD molecule was used by the MANA-NIMS Japanese team during the first international Nanocar Race in Toulouse [11].

Although we have considered several classes of compound for use in the context of the current work, including pyrazinacenes [28–30], porphyrins [8, 31–33] and oxoporphyrinogens [34–36], porphyrin-type molecules were finally selected due to (1) the well-known synthetic methods, (2) ease of generating complexity in relatively few steps, (3) locking of the macrocycle made possible by the introduction of a transition metal cation, and (4) ease of sublimation for deposition at a metal interface for study using STM. Thus, the porphyrins already possess many of the features required in the preparation of molecules for study at interfaces as demonstrated by their long history of use in this field [37–40]. If the class of porphyrins is then selected, it only remains to identify which substituents ought to be introduced for the purpose at hand, i.e., to consider molecules moving at a surface. The molecules should be planar with a relatively rigid form, thus metalloporphyrins were selected. The molecule should also be of such dimensions that there exists a sufficient mismatch

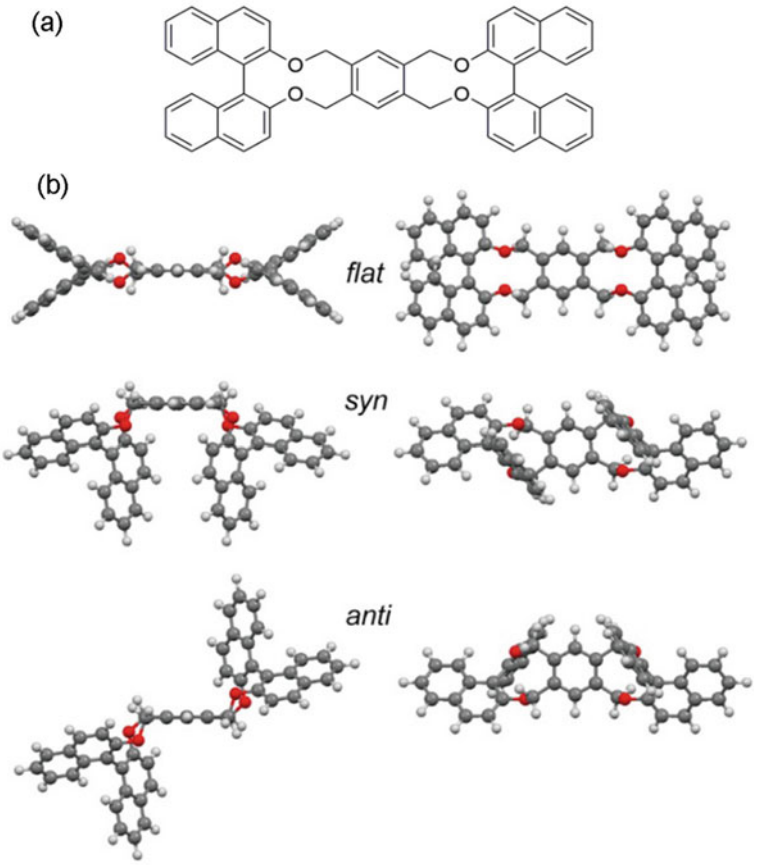

Fig. 1 **a** Chemical structure of the BBD molecule. **b** *Flat*, *syn*, and *anti* conformers of BBD obtained by DFT calculation at the B3LYP/6-31G(d,p) level. Their relative energies are respectively + 20, + 0.4, and 0.0 kcal/mol for their respective D_2, C_2, and C_2 symmetric structures. Torsion angles calculated for the binaphthyl unit are respectively $\theta = -61°$, $-64°$ and $-64°$. The *anti* and *syn* conformers are the only forms identified in solution. The flat conformer is only available by STM tip manipulation of BBD only when physisorbed at the Au(111) surface. Reproduced with permission from Soe et al. [11], Copyright 2017 American Chemical Society

between molecular vertices and those of the surface in order that the molecules do not 'stick' at particular locations. Finally, the molecule should be of sufficiently low symmetry that its direction of translation can be easily identified, with motion preferably occurring coincidental with one of the major molecular axes. If all these matters are considered, the analogy of the 'automobile' emerges naturally since it might be established that the notional molecule would be subjected to a stimulus such that it moves in the direction coinciding with its long axis, similarly to a car. Hence, we coin the term 'nanocar' [25, 41] to describe molecules where on-surface activity might be analogous with the activity of a motor car [42, 43]. Of course, principles

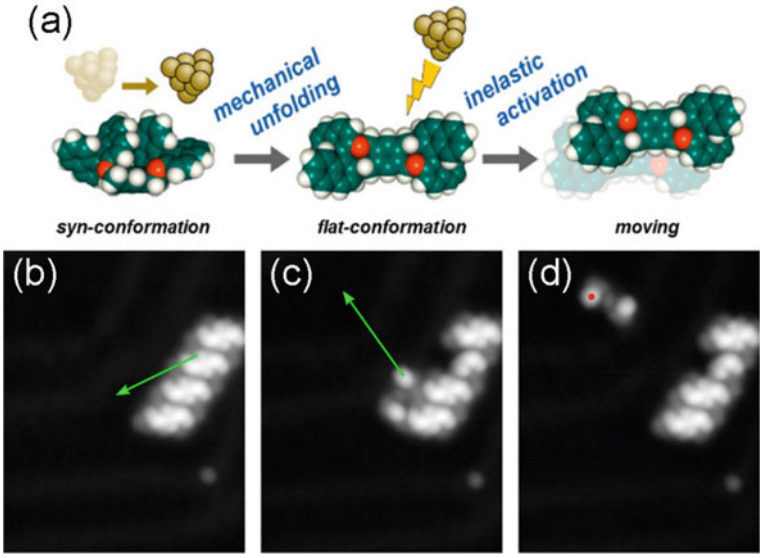

Fig. 2 **a** Schematic describing manipulation of the BBD molecules using an STM tip. **b–d** Forced molecular manipulation of BBD molecules initially contained in a self-assembled cluster. STM topology (b) prior to and (c) following manipulation: structure transforms from *syn* to *flat* conformer. **d** Flat conformer manipulated away from the original cluster using STM tip to isolate the molecule during subsequent dI/dV spectroscopic observations. Arrows in (**b**) and (**c**) indicate the tip trajectory for manipulation leading to the *flat* conformer. The red dot in (**d**) indicates the point at which spectra were collected [11]. Image sizes: 12 nm × 15 nm. Reproduced with permission from Soe et al. [11], Copyright 2017 American Chemical Society

involved in translational action of automobiles and nanocars differ based on the scales of action: macroscale versus nanoscale. While form and action might be similar for both, physical factors affecting the molecules at macro- and nanoscales are quite different [44]. In particular, friction has different connotations for the translational actions of macroscale objects and molecules at the nanoscale [45].

2 Molecular Design and Synthesis

Synthesis of the meso-substituted porphyrins selected as the most effective targets for study was according to existing methods [46]. Generally, these methods are referred to as the Lindsey method [47], or the Adler modification [48] of the Rothemund synthesis method [49], and are based on the condensation of pyrrole with aldehydes or dipyrrolylmethanes followed by oxidation of the resulting porphyrinogen (either in situ as in the Adler and Rothemund methods, or by applying an oxidation step involving a high potential quinone following the macrocyclization step). The methods give variable yields of the materials although, for STM study only

miniscule quantities of the target molecules are required. The method applied [50] can also be considered adaptations of the MacDonald 2 + 2 synthesis (also after Kawai et al. [51]) which facilitates the synthesis of unsymmetrical molecules suitable for nanocar directional detection. Precursors applied in the macrocyclization experiments were prepared according to similar acid-catalyzed procedures. General protocols for synthesis are shown in Schemes 1 and 2.

Several prototype molecules denoted **NC1**–**NC4** were studied prior to the final selection of molecule. While **NC1** is a relatively stable molecule expected to be deposited at surfaces as synthesized, the other compounds studied were selected for their propensity to undergo on-surface in-situ cyclodehydrogenation reactions yielding more highly planar species. The structures of the molecules obtained after synthesis and those of the compounds expected according to their on-surface dehydrogenation reactions (denoted by red dashed bonds) are shown in Scheme 3.

The compound **NC1** 5-(4-carboxymethylphenyl)-10,15–20-tris(3,5-di-t-butyl phenyl)porphyrin was prepared using the Adler modification of the Rothemund

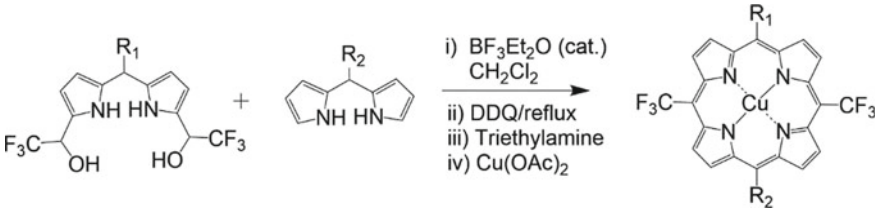

Scheme 1 Synthesis of unsymmetrically substituted porphyrins by mixed dipyrrolylmethane method. R = 2,4,6-trimethylbenzaldehyde (mesitaldehyde) or anthracene-9-carbaldehyde. In (iv) a solution of copper(II) acetate dihydrate in methanol was added to the porphyrin in refluxing chloroform

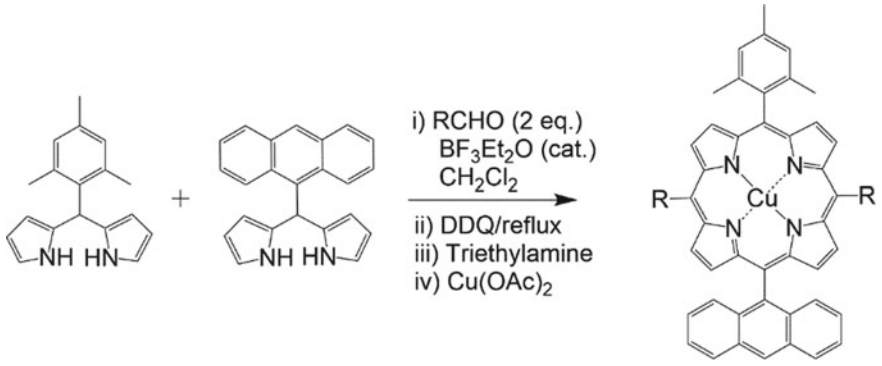

Scheme 2 Synthesis of unsymmetrically substituted porphyrins by mixed dipyrrolylmethane method similar to Macdonald 2 + 2 condensation. R_1 = 9-anthryl or 9,9'-bianthryl, R_2 = 2,4,6-trimethylphenyl or 9-anthryl. In (iv) a solution of copper(II) acetate dihydrate in methanol was added to the porphyrin in refluxing chloroform

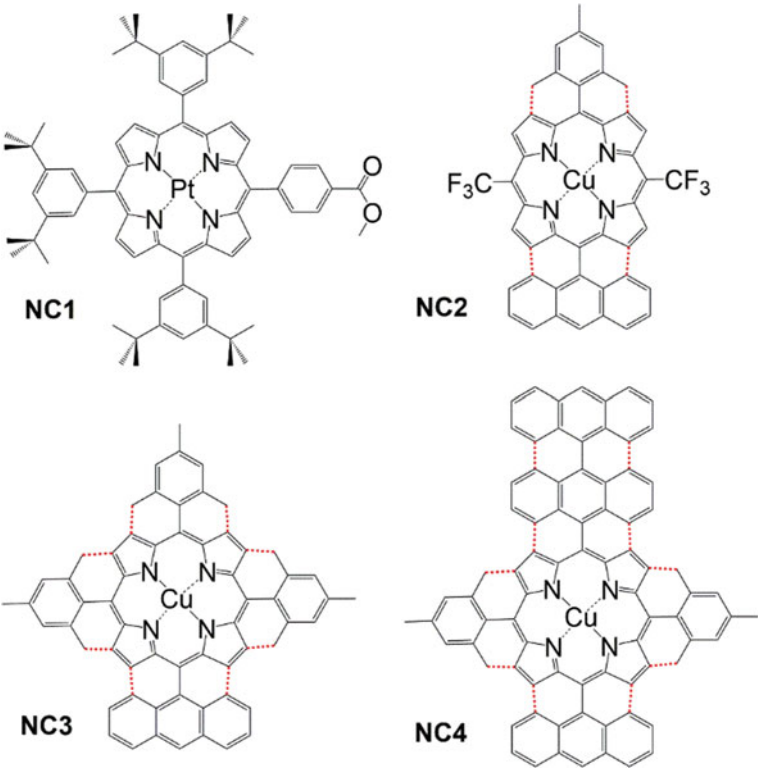

Scheme 3 Chemical structures of the molecules used as prototypes for molecular translation. **NC1**: 5-(4-carboxymethylphenyl)-10,15–20-tris(3,5-di-t-butylphenyl)porphyrinatoplatinum(II); **NC2**: (5-(9-anthryl)-15-(2,4,6-trimethyl phenyl)-10,20-bis(trifluoromethyl)porphyrinatocopper(II); **NC3**: 5-(9-anthryl)-10,15,20-tris(2,4,6-trimethylphenyl)porphyrinatocopper(II); **NC4**: 5-(9-anthryl)-15-(9,9'-bianthryl)-10,20-bis(2,4,6-trimethylphenyl)porphyrinato copper(II). Red dashed lines denote the expected sites of on-surface oxidative cyclodehydrogenation reactions (but vide infra) where fused six-membered rings are established in the final molecules with planar structures

procedure involving two different benzaldehydes and pyrrole in refluxing propionic acid followed by column chromatography and recrystallization. Pt(II) was inserted at the porphyrin macrocycle by treating this product with anhydrous platinum(II) chloride in refluxing benzonitrile [52] yielding **NC1** as an orange powder. (5-(2,4,6-Trimethylphenyl)-15-(9-anthryl)-10,20-bis(trifluoromethyl)porphyrin was prepared according to the reaction shown in Scheme 2 while (5-(9-anthryl)-10,15,20-tris(2,4,6-trimethylphenyl)porphyrin) and (5-(9-anthryl)-15-(9,9'-bianthryl)-10,20-bis(2,4,6-trimethylphenyl) porphyrin) were prepared according to the reaction shown in Scheme 1. Metal cation insertion was accomplished by adding copper(II) acetate solution in methanol to refluxing solutions of the respective porphyrins in chloroform yielding respectively **NC2–NC4**. For the reactions shown in Schemes 1 and 2, we note that significant scrambling of the substituents occurs (due to equilibration of the

porphyrinogen intermediates). Performing the reactions at lower temperature 0 °C helped alleviate this problem although isomerization persisted.

3 X-ray Crystallography

Since samples of high purity are required for the STM analyses, this improves the prospects for obtaining single crystals of the molecules suitable for X-ray crystallography. Molecules **NC2** and **NC3** could be characterized using this technique and molecular structures of the compounds are shown in Figs. 3 and 4, respectively. There are two interesting features in crystals of **NC2**, which is triclinic P-1 (a = 7.5610(2) Å, b = 14.8631(3) Å, c = 16.0660(8) Å; α = 83.907(3)°, β = 79.974(3)°, γ = 77.9456(19)°; V = 1734.54(10) Å^3, Z = 2). First, the 5-(9-anthryl) substituent is involved in extensive C–H…π and C–F…π interactions respectively with a 4-methyl group of the 15-(2,4,6,-trimethylphenyl) group and 10,20-trifluoromethyl groups (Fig. 3b). Second, a mutual coordinative interaction between F atoms of trifluoromethyl groups and Cu(II) cations in adjacent molecules establishes chains of molecules (Fig. 3c).

For compound **NC3** (Fig. 4a), crystals are also triclinic P-1 (a = 8.4630(2), b = 12.5598(3), c = 26.1247(7) Å; α = 95.796(2)°, β = 95.435(2)°, γ = 94.651(2)°; V =

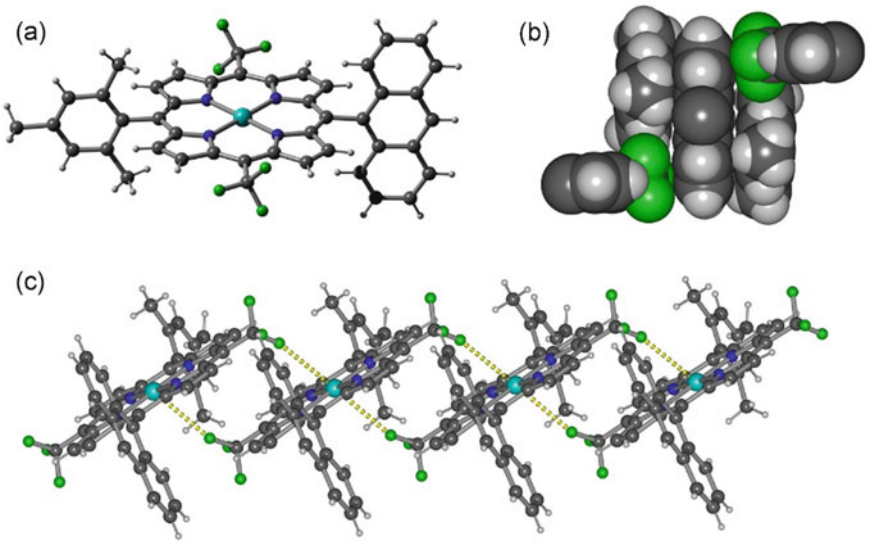

Fig. 3 X-ray crystal structure of **NC2**. **a** Molecular structure. **b** Interactions at the 9-anthryl unit include strong C–H…π (involving mesityl 4-methyl groups) and C–F…π (involving meso CF_3 groups). **c** Chain structure formed through mutual C–F…Cu interaction of pairs of the molecules. (Triclinic P-1; a = 7.5610(2) Å, b = 14.8631(3) Å, c = 16.0660(8) Å; α = 83.907(3)°, β = 79.974(3)°, γ = 77.9456(19)°; V = 1734.54(10) Å^3, Z = 2)

2738.73(12) $Å^3$, Z = 2). Two molecules in the unit cell are arranged in the structure so that 5-(9-anthryl) groups are contained in a layer, which alternates with a layer of the 15-(2,4,6,-trimethylphenyl) groups at the opposing position of the porphyrin. Planes of porphyrin and its 9-anthryl substituent subtend an angle of 80°, which is larger than that usually observed for meso-phenyl substituents (~60°), but is similar to that found for the other 2,4,6-trimethylphenyl substituents of **NC3** (78°). There is one notable interaction involving a partial π–π stacking between 9-anthryl moieties (Fig. 4b) with a closest distance of approach around 3.5 Å. Notably, there are no CH…π interactions.

4 Scanning Tunneling Microscopy of Prototype Molecules

NC1 was observed to undergo STM-tip induced translation on Ag(111) (Fig. 5), although this activity has proved difficult to reproduce. The molecules generally form large islands by self-assembly at the surface and individual molecules could only be made available for manipulation by the peeling off of a single molecule from smaller clusters of molecules. Single molecules could then be moved linearly by applying a positive bias sweep from + 0.1 to + 2.0 V corresponding to tunneling current injection. It should be noted that a similar procedure using a negative bias sweep did not result in molecular translation. Unfortunately, the tendency for self-assembly in **NC1** and a further preference for rotational activity even in small aggregates of the molecules made this compound unsuitable for further consideration for its linear translational activity.

Despite its poorly reproducible activity for linear motion, rotational activity of **NC1** introduced some interesting possibilities. A perceived preference for motion of the molecules in the direction of the small ester substituent and the tendency for self-assembly of the molecules led to the discovery of a self-assembled chiral rotor based on hydrogen-bonded dimers of **NC1** [53]. This dimer has an 'S'-shaped form establishing on-surface or planar chirality, and the dimer can be rotated as a whole based on stimulation applied through an STM tip (see Fig. 6).

Figure 6 shows that the **NC1** dimer unit (Fig. 6a, b) can be used to realize molecular rotary motion also being capable of *in-situ* chirality (or directional) switching according to variation of surface chirality (Figs. 6c–e). The 'S'-shaped dimer was formed by deposition of the **NC1** molecules onto the Au(111) surface at ultralow pressure. Dimer species are located preferentially at atomic defects of the Au(111) herringbone reconstruction with one molecule pinned as the rotor spindle and the other associated through hydrogen bonding forming the dimer. This formation can be rotated with almost exclusive directionality according to the chirality of the dimer by exciting the pinned molecule of the dimer through application of a tunneling current using the STM tip. The atomic defect and molecular centroid define the axis for rotation of the dimer [54, 55]. In this case, the Pt atom of the metalloporphyrin is located at this point. Surface chirality of the dimer is solely responsible for determining the rotation direction of the **NC1** dimer and, since chirality can be switched, so then

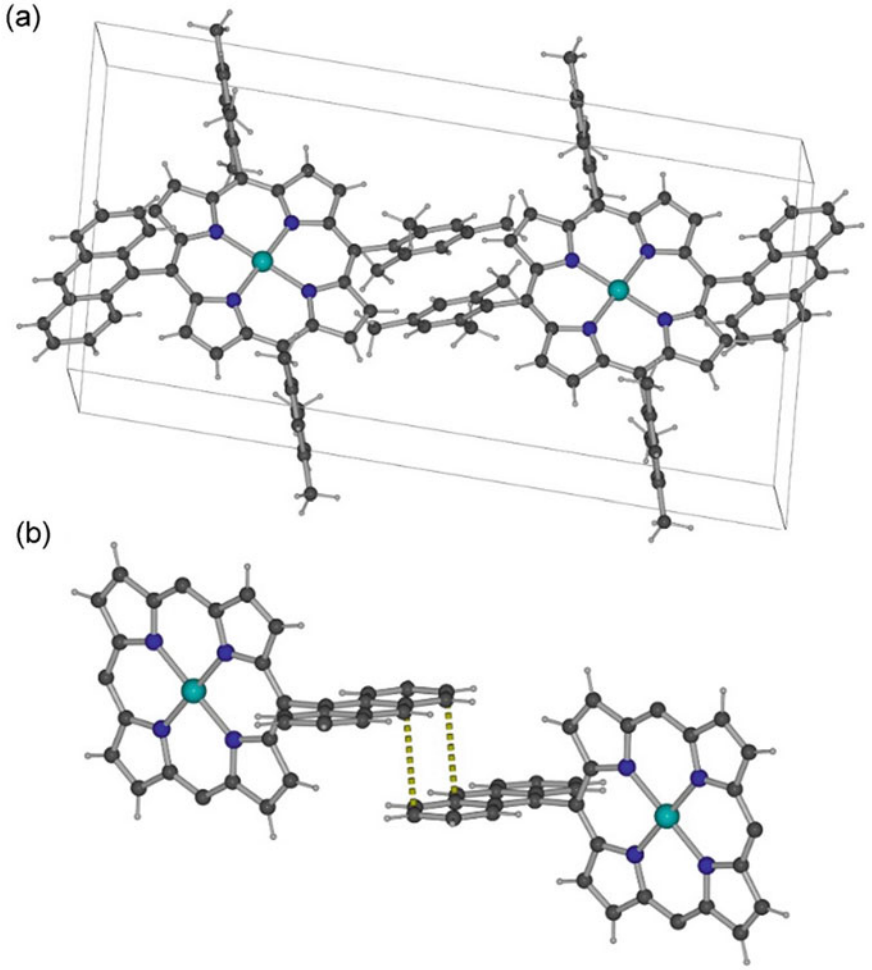

Fig. 4 X-ray crystal structure of **NC3**. **a** Two molecules contained in the unit cell. **b** Intermolecular π–π stacking at the 9-anthryl units (3.5037(36) Å). Dihedral angle between porphyrin and 9-anthryl planes is 80.288(27)°. Triclinic P-1 (a = 8.4630(2) Å, b = 12.5598(3) Å, c = 26.1247(7) Å; α = 95.796(2)°, β = 95.435(2)°, γ = 94.651(2)°; V = 2738.73(12) Å^3, Z = 2)

can be the direction of rotation. The switching process involves rearrangement of the dimer based on the application of an appropriate bias voltage. This phenomenon suggests the possibility of constructing complicated molecular machines similar to those found in biological systems [56–59] but at the nanometric scale at a solid surface.

Apart from the 'S'-shaped dimer, **NC1** self-assembles into other structures especially a trimer (with clover leaf morphology) and a tetramer, whose morphology defies analogy. Figure 7a shows as deposited molecules of **NC1** on Au(111).

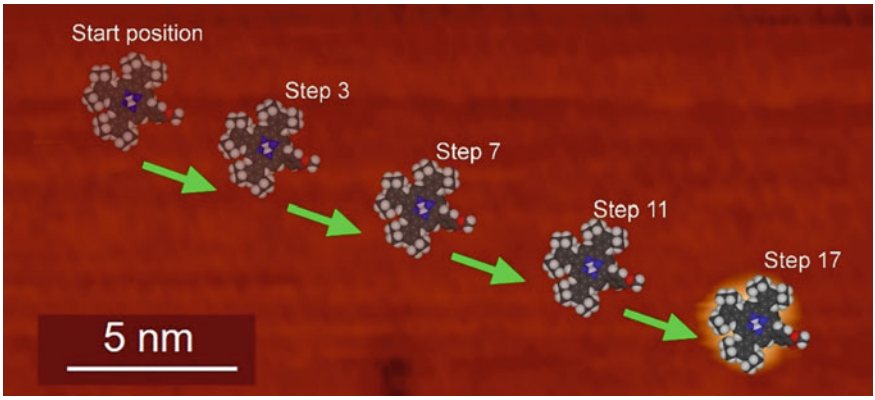

Fig. 5 Illustration of STM tip bias induced linear motion of **NC1** on Ag(111) surface. The STM tip was positioned above the centre of the molecule. With feedback turned off, bias voltage was swept from + 0.1 to + 2.0 V resulting in stepwise translation of the molecule in the direction of the non-*t*Bu-substituted phenyl group speculated to be the direction of least physical resistance to motion. During this experiment, a distance of 19 nm was traversed (approx. 0.9 nm per bias sweep)

Molecules are distributed individually (Fig. 7b, c) or as components of different self-assembled structures (Fig. 7d, e). Figure 7e shows three of the common self-assembled structures on Au(111) including the 'S'-shaped dimer, clover-leaf trimer, and an unusually structured tetrameric assembly. The structures appear to involve either mutual hydrogen bonding interactions between ester groups (trimer) or ester-tBu interactions presumably due to C–H…O hydrogen bonding, as has been observed for similarly structured porphyrin molecules [39].

In contrast to the study of **NC1**, molecules of other **NC**-designated structures have been annealed at 320 °C leading to oxidative cyclization processes occurring between the porphyrin pyrrole units and the meso-substituents. This is a common method for the planarization of the porphyrin core and has been used especially where graphene-like molecules have been required for study [60–62]. In the case of **NC3** (**NC2** behaves similarly to **NC3** and will not be described), molecules are similarly deposited at the corners of the zigzag surface reconstruction (Fig. 8a). Although the molecules tend not to aggregate, there are several features making this molecule unattractive for further study. First, there appears to be a mixture of different states of the molecule present on the surface (Fig. 8b). This is due to methyl group elimination occurring during thermal deposition and the subsequent on-surface annealing applied in this case although the 9-anthryl substituent can be clearly identified in the products (Fig. 8c). Second, where manipulation was attempted only rotational activity of the molecules was found (Fig. 8d). Figure 8e shows an STM image of a typical single with the expected structure of the molecule shown in space-filling form in Fig. 8f. In the case shown, oxidative cyclization between methyl groups at the 2,6-positions of two of the mesityl substituent appears to have occurred while, at the third such substituent, demethylation leads to cyclodehydrogenation directly between phenyl

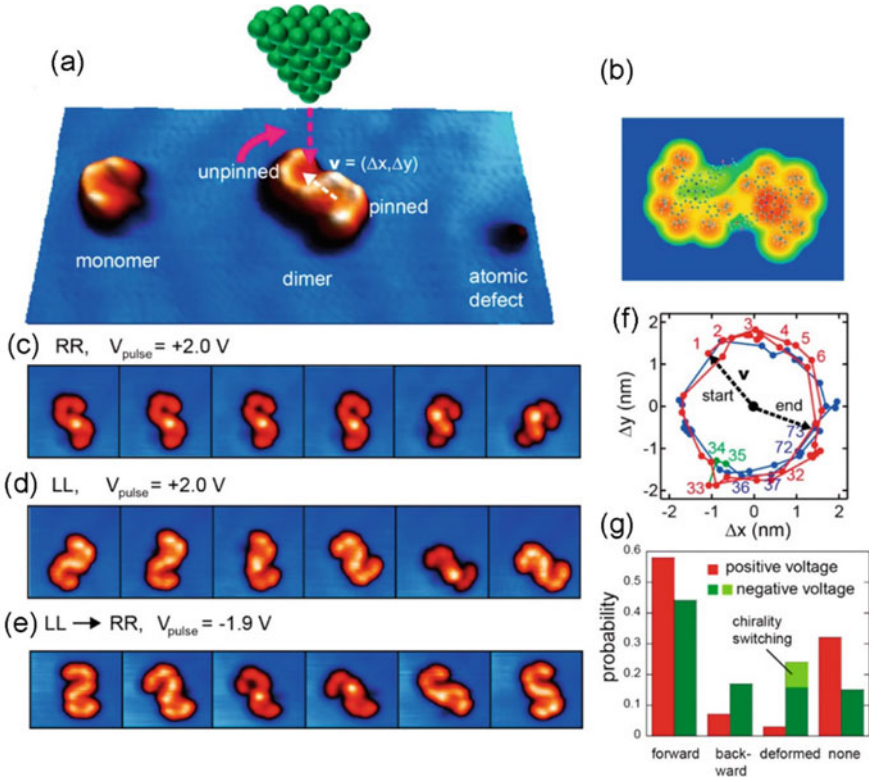

Fig. 6 Rotation of the **NC1** 'S'-shaped dimer under an applied current. **a** 3D STM image of the **NC1** dimer at 5 K illustrating tunnelling current injection from STM tip to centroid of the 'unpinned' molecule. Note monomer of **NC1** and an atomic defect. **b** Calculated (ESQC) constant current STM image of the **NC1** dimer on Au(111) at $I_t = 1$ pA, $V_s = 1$ V with blue to red corrugation = 0.35 nm. Centroid of one molecule of the dimer sits on an individual Au adatom. Image: 4.13 nm × 5.58 nm (**c**) (**d**) Directional rotation of an **NC1** dimers at $V_{pulse} = +2.0$ V. Conditions: $V_s = +0.3$ V, $I_t = 3$ pA; dimensions: 6.8 nm × 6.8 nm. Chirality of the dimers is RR and LL in (**c**) and (**d**), respectively. **e NC1** dimer undergoes chirality switching at $V_{pulse} = -1.9$ V. Conditions: $V_s = +0.1$ V, $I_t = 1$ pA; dimensions: 6 nm × 5 nm. **f** Trajectory of the centroid of the dimer unpinned molecule during rotation. Displacement vector $\mathbf{v} = (\Delta x, \Delta y)$ is plotted. Numbers indicate the pulse sequence: red (RR) and blue (LL) dots are the sequences of positive voltage pulses ($V_{pulse} = +2.0$ V) applied prior to and following chirality switching. Green dots indicate negative voltage pulse (chirality switching, $V_{pulse} = -1.9$ V). **g** Histogram of events (forward/reverse rotation, deformation, no action) for positive ($V_{pulse} = +2.0$ V) and negative ($V_{pulse} = -1.9$ V) pulses. Reproduced with permission from Mishra et al. [53], Copyright 2015 American Chemical Society

and porphyrin pyrrole units establishing an unsymmetrical structure as is clearly seen in Fig. 8e.

The final prototype molecule is **NC4** containing 9-anthryl, 9,9'-bianthryl and mesityl units intended for the preparation of a large π-electronic surface when subjected to thermally promoted oxidative cyclization reactions. This molecule

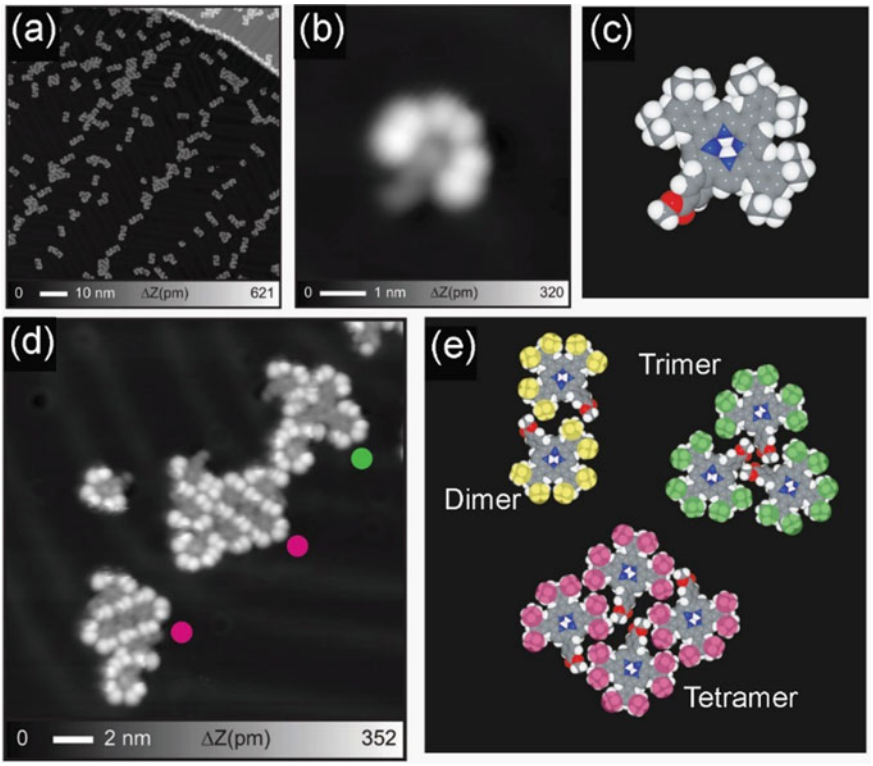

Fig. 7 STM images of **NC1** deposited on Au(111). **a** Molecules predominantly deposited at vertices of the Au(111) herringbone surface reconstruction (Bias voltage (V) = 200 mV, tunneling current (I) = 10 pA). **b** Single molecule clearly showing the position of the 4-carboxymethylphenyl group ('tail') and 6 t-butyl groups (bright spots) deflected to optimize surface contact (V = 100 mV, I = 10 pA). **c** Space-filling model of a single molecule highlights the substituent positions. **d** Higher magnification image shows the common forms of the self-assemblies (V = 200 mV, I = 10 pA). Colored spots indicate trimer and tetramer structures shown in (**e**). **e** Common self-assembly motifs for **NC1**: 'S'-shaped dimer (see Fig. 6), clover-leaf trimer, and tetramer. Colored spots highlight the positions of tBu groups in dimer (yellow), trimer (green) and tetramer (pink)

could be thermally evaporated onto a Au(111) surface as shown in Fig. 9a and was subjected to a thermal annealing process indeed promoting the planarization of the molecule (Fig. 9b). Figure 9c shows a space-filling model of a structure corresponding to the STM profile of the molecule, indicating that molecules of **NC4** undergo desymmetrization upon oxidative cyclization similarly to **NC3**.

Attempts to manipulate **NC4** led to some short distance translational activity but the molecule is again susceptible to tip-induced reaction, which result in the pinning of the molecule to the surface. Initial reaction leads to states where only rotation is permitted while subsequent reaction 'parks' the molecule permanently. With the experience gained by studying molecules **NC1**–**NC4** in mind, we could formulate some rules for the synthesis of molecules capable of on-surface translational activity

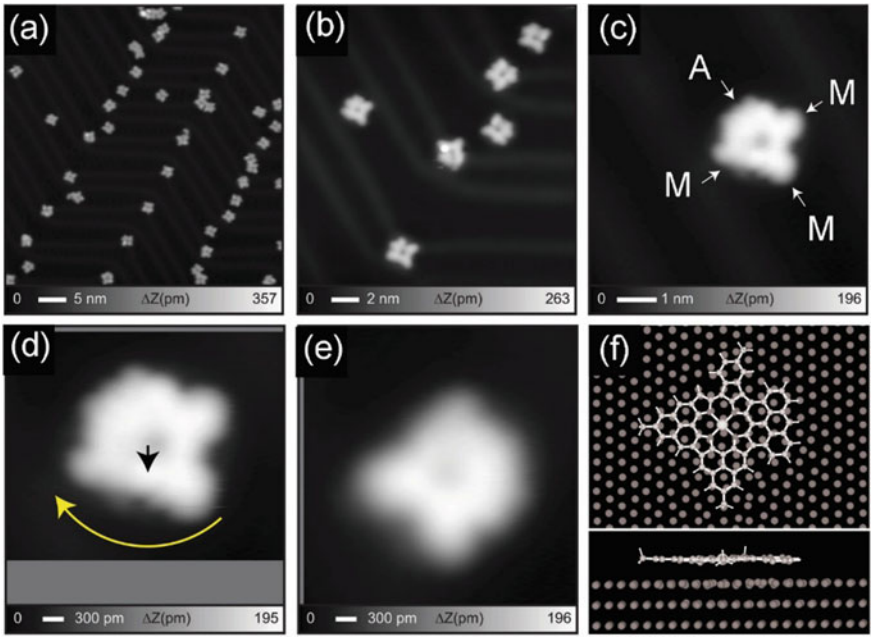

Fig. 8 STM images of **NC3** deposited on Au(111) and subsequently annealed at 320 °C. **a** Molecules mainly adsorbed at elbow sites of the herringbone structure (V = 200 mV, I = 10 pA). **b** Close-up view of the molecular products (V = 200 mV, I = 10 pA). **c** Assignment of the substituent (prior to cyclodehydrogenation): 'A' = 9-anthryl, M = 2,4,6-trimethylpphenyl (V = 200 mV, I = 5 pA). **d** Single molecules could be controlled but tend to rotate about the molecules centre (V = 200 mV, I = 5 pA) before and **e** after tip-induced manipulation. (V = 200 mV, I = 5 pA). **f** Structure optimized using DFT for a possible cyclodehydrogenated state of **NC3** on Au(111). Note the essentially flat molecular geometry with essentially exclusively van der Waals surface interactions and molecular form closely corresponding to the STM topography in (**e**)

based on excitation using an STM tip. First, t-butyl groups promote self-assembly making difficult the location and manipulation of any single molecules. Second, moieties involving mesityl (2,4,6-trimethylphenyl) units are not suitable for this purpose due to (a) inconsistent reaction in oxidative cyclization and (b) subsequent STM-tip-induced reactions which cause pinning of the molecules at fixed locations. Third, if low symmetry can be achieved using substituents in the 5,15 positions of the porphyrin, then simple unreactive substituents (e.g., trifluoromethyl) are suitable to occupy other (10,20) positions. Based on these, structure **NC5** (Fig. 10) has been proposed and synthesized. Details of the on-surface activity of this molecule are given in the next section.

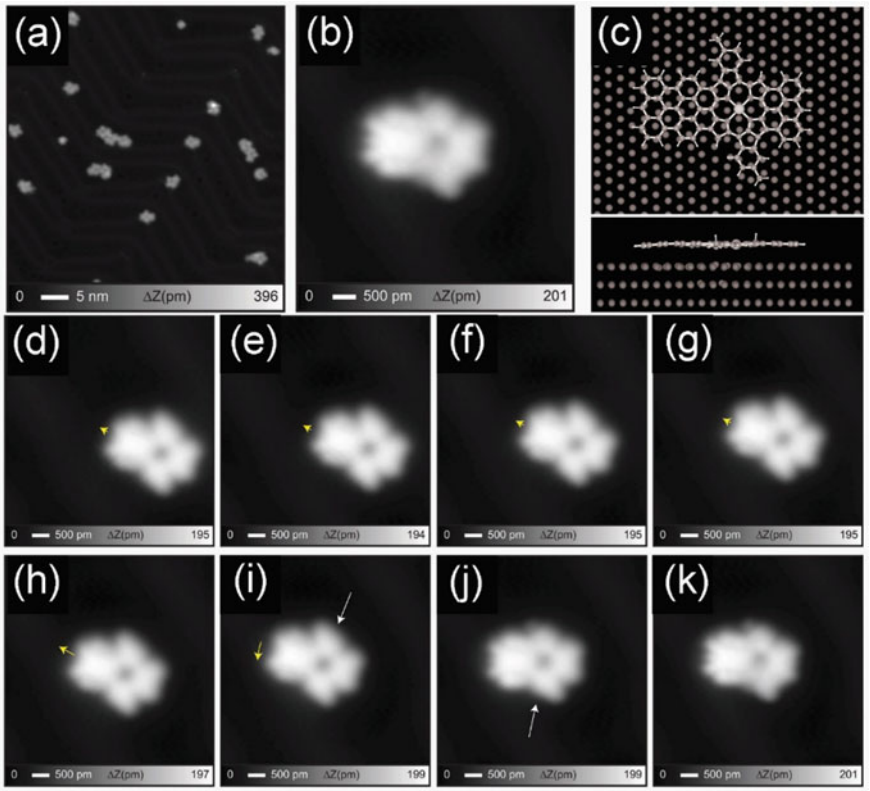

Fig. 9 **NC4** deposited on Au(111) with attempted manipulation using STM tip. **a** Molecules are distributed largely as single molecules (V = 200 mV, I = 10 pA). **b** Different morphologies of the molecular products of annealing are observed (V = 200 mV, I = 10 pA). **c** Structure optimized using DFT for a possible cyclodehydrogenated state of **NC4** on Au(111). Note the flat molecular geometry with essentially exclusively van der Waals surface interactions and molecular form closely corresponding to the STM topography in (**b**). **d**–**k** A series of STM topographies during manipulation of the molecule. It can be moved single lattice steps (**d**–**g**) and double lattice steps (**h**) but following some reaction (speculated to be methyl group cracking) the molecules is pinned and only rotation occurs (**i**). After both methyl groups have been cracked (**j**), the molecule is doubly pinned and no further manipulation (translation or rotation) is possible by using the STM tip (**k**)

5 Trajectory of NC5 During Nanocar Race II

NC5 was synthesized according to the method shown in Scheme 2. A crystal structure could not be obtained for this molecule due to its relatively poor solubility in organic solvents although STM imaging of the molecule at the surface confirms structure based on the expected rectangular morphology of molecule obtained following oxidative cyclodehydrogenation [60–62] of the synthetic precursor. Notably, the final synthetic step of **NC5** is the on-surface oxidation procedure. The shape of **NC5** is due to the fusion of 9-anthryl and 9,9'-bianthryl meso substituents at opposing positions

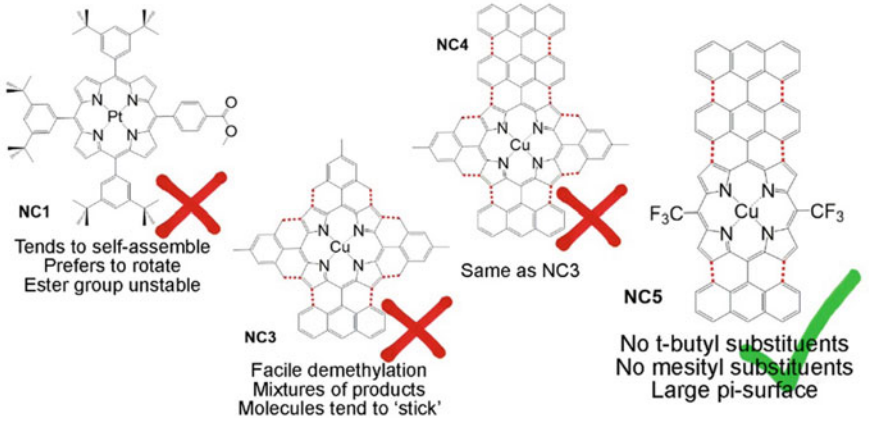

Fig. 10 Evolution of the molecular structure to establish facile translational activity of prospective molecular nanocars. Based on molecules available on-surface by oxidative cyclization reactions (idealized expected structures): **NC1**: Tends to self-assemble, prefers rotation, ester group unstable (not shown). **NC3**: unpredictable demethylation reactions during sublimation or cyclodehydrogenation (mixtures of products), molecules are pinned according to STM-tip-induced reactions. **NC4**: similar disadvantages to **NC3**. **NC5**: Problematic substituents eliminated, and only a single symmetrical product of oxidative cyclization at 9-anthyrl and 9,9'-bianthyrl groups is reasonably possible

of the planar metalloporphyrin macrocycle. This is illustrated in Fig. 11a, b. There are two critical aspects of this molecule formed at the Au(111) surface: (1) its multiple fused six-membered rings (like graphite) have atomic vertices increasingly incommensurate with the underlying Au(111) lattice to prevent 'pinning' of molecules, and (2) its large graphene like conjugated π-electronic chromophore, which promotes molecular stability under field-induced manipulations and also promotes molecular mobility according to superlubricity [63–65]. In the course of Nanocar Race II, STM data was collected that reveal the excellent mobility and sufficient stability of **NC5** during an extended period of manipulation over 24 h (see Fig. 11).

Nanocar Race II was performed under remote control by the different teams of their scanning probe microscopes in their home laboratories. For the NIMS Tsukuba Team, after some initial network connection difficulties had been overcome, scanning and selection of the molecule to act as nanocar was undertaken. The molecule selected is indicated in Fig. 11a where the circuit of the nanocar movements is also shown (highlighted with arrows). Other molecules present as obstructions in the course are indicated with red arrows. These were eliminated as obstacles by applying a tip-induced bias similar to that used to move the nanocar molecule. After clearing obstacles, the same circuit was used for movement of the molecule. During a 24 h period, approx. 4.3 circuits were completed leading to a total distance moved of 1054 nm with 54 turns also being completed including 2 'lane' changes per lap (indicated in Fig. 11a by green chevrons; lanes defined by the Au(111) reconstructed surface).

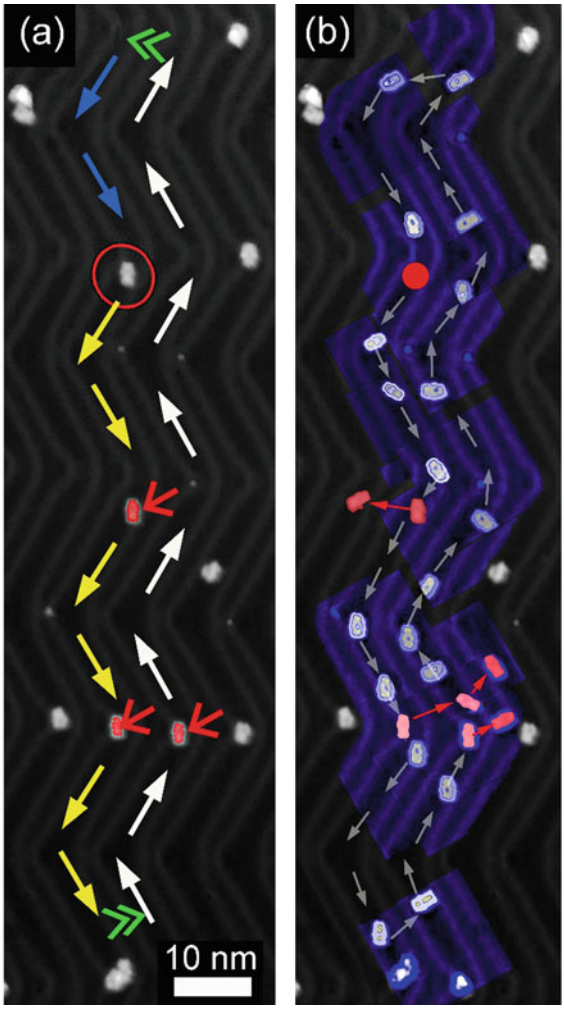

Fig. 11 Nanocar trajectory. **a** Nanocar circuit based on adjacent 'lanes' on the Au(111) reconstructed surface. Yellow arrows: front course; white arrows: back course; blue arrows: home straight. Obstructions (molecules) in the course are marked in red and indicated with red arrows. Positions for jumping to the adjacent track are indicated with green double chevrons. **b** First lap taken using the **NC5** molecule. Molecular obstructions indicated in red (these were absent in subsequent laps). Shifting of obstructions indicated by red arrows. Scale bar applies to both panels

Figure 11b shows the initial lap of the selected molecule including also the shifting of the obstructing molecules, again indicated in red with arrows showing their movement off-circuit. Except for the shifting of obstacles, subsequent laps were similar and are not shown. For the duration of the 4.3 lap distance the molecule remained largely intact until close to the end of the 24 h when some modifications appeared due to dehalogenation at the meso-trifluoromethyl substituents. However,

the nanocar remained mobile by applied tip-induced bias although rate of movement was attenuated.

6 Concluding Remarks

The molecular design strategy that we employed during our deliberations of the subject of nanovehicles eventually involved on-surface cyclodehydrogenation to planarize the nanocar precursor molecule **NC5** or 5-(9-anthryl)-15-(9,9'-bianthryl)-10,20-bis(trifluoromethyl)porphyrinato-copper(II) under the concept of superlubricity for smooth on-surface transport. These different aspects led us to assign the nickname 'Slider-Spider' to the resulting molecule. The planar nanocar molecule could be stimulated to move a distance of 1054 nm (including 54 turns) during a 24 h period leading to victory for the NIMS Tsukuba Team in the 2nd Nanocar Race. The molecule had excellent stability and could be operated as a nanocar for 24 h under remote control at 10,211 km (Toulouse in France – Tsukuba in Japan) by using a scanning probe system and under observation at subnanometer scale. The molecular design, synthesis work and probe manipulations not only present opportunities to gain insight into the effects of molecular structure on nanoscale translational activity but also can be seen as being not dissimilar from the macroscale automobile design process. For instance, an initial period of work (where vehicle utility and design philosophy are established) is followed by a regime of trial, error and troubleshooting before a final product is achieved (and subjected to additional optimization). Improvements are usually made in subsequent generations of products, a matter that remains to be seen in the case of nanocar racers of all the teams involved at Nanocar Race II.

Acknowledgements This work was partly supported by World Premier International Research Center Initiative (WPI Initiative), MEXT, Japan. S.K. thanks Shohei Saito (in Kyoto University) and Ernst Myer (in University of Basel) for valuable discussions of planarization and the diffusion on surface of 5,15-bis(10-bromoanthracen-9-yl)-10,20-bis(trifluoromethyl)porphyrin. This work was also supported in part by Japan Society for the Promotion of Science (JSPS) KAKENHI Grant Number 21K18885, 21F21058 and 22H00285. D.T.P is grateful to the International Center for Young Scientists, NIMS, Japan, for support. Financial support by the Toyota Motor Co. Ltd. (Japan) is gratefully acknowledged.

References

1. Aprahamian, I.: The future of molecular machines. ACS Cent. Sci. **6**, 347–358 (2020)
2. Chen, H., Stoddart, J.F.: From molecular to supramolecular electronics. Nat. Rev. Mater. **6**, 804–828 (2021)
3. Lancia, F., Ryabchun, A., Katsonis, N.: Life-like motion driven by artificial molecular machines. Nat. Rev. Chem. **3**, 536–551 (2019)

4. Ariga, K.: The evolution of molecular machines through interfacial nanoarchitectonics: from toys to tools. Chem. Sci. **11**, 10594–10604 (2020)
5. Moulin, E., Faour, L., Carmona-Vargas, C.C., Giuseppone, N.: From molecular machines to stimuli-responsive materials. Adv. Mater. **32**, 1906036 (2020)
6. Kassem, S., van Leeuwen, T., Lubbe, A.S., Wilson, M.R., Feringa, B.L., Leigh, D.A.: Artificial molecular motors. Chem. Soc. Rev. **46**, 2592–2621 (2017)
7. Kammerer, C., Erbland, G., Gisbert, Y., Nishino, T., Yasuhara, K., Rapenne, G.: Biomimetic and technomimetic single molecular machines. Chem. Lett. **48**, 299–308 (2019)
8. Wakayama, Y.: On-surface molecular nanoarchitectonics: from self-assembly to directed assembly. Jpn. J. Appl. Phys. **55**, 1102AA (2016)
9. Simpson, G.J., García-López, V., Petermeier, P., Grill, L., Tour, J.M.: How to build and race a fast nanocar. Nat. Nanotechnol. **12**, 604–606 (2017)
10. Rapenne, G., Joachim, C.: The first nanocar race. Nat. Rev. Mater. **2**, 17040 (2017)
11. Soe, W.-H., Shirai, Y., Durand, C., Yonamine, Y., Minami, K., Bouju, X., Kolmer, M., Ariga, K., Joachim, C., Nakanishi, W.: Conformation manipulation and motion of a double paddle molecule on an Au(111) surface. ACS Nano **11**, 10357–10365 (2017)
12. Eigler, D.M., Schweizer, E.K.: Positioning single atoms with a scanning tunnelling microscope. Nature **344**, 524–526 (1990)
13. Bartels, L., Meyer, G., Rieder, K.-H.: Basic steps of lateral manipulation of single atoms and diatomic clusters with a scanning tunneling microscope tip. Phys. Rev. Lett. **79**, 697–700 (1997)
14. Bouju, X., Joachim, C., Girard, C., Tang, H.: Mechanics of $(Xe)_N$ atomic chains under STM manipulation. Phys. Rev. B Condens. Matter Mater. Phys. **63**, 085415 (2001)
15. Jung, T.A., Schlittler, R.R., Gimzewski, J.K., Tang, H., Joachim, C.: Controlled room-temperature positioning of individual molecules: molecular flexure and motion. Science **271**, 181–184 (1996)
16. Grill, L., Rieder, K.-H., Moresco, F., Rapenne, G., Stojkovic, S., Bouju, X., Joachim, C.: Rolling a single molecular wheel at the atomic scale. Nat. Nanotechnol. **2**, 95–98 (2007)
17. Manzano, C., Soe, W.-H., Wong, H.S., Ample, F., Gourdon, A., Chandrasekhar, N., Joachim, C.: Step-by-step rotation of a molecule-gear mounted on an atomic-scale axis. Nat. Mater. **8**, 576–579 (2009)
18. Nickel, A., Ohmann, R., Meyer, J., Grisolia, M., Joachim, C., Moresco, F., Cuniberti, G.: Moving nanostructures: pulse-induced positioning of supramolecular assemblies. ACS Nano **7**, 191–197 (2013)
19. Lastapis, M., Martin, M., Riedel, D., Hellner, L., Comtet, G., Dujardin, G.: Picometer-scale electronic control of molecular dynamics inside a single molecule. Science **308**, 1000–1003 (2005)
20. Hla, S.-W.: Scanning tunneling microscope atom and molecule manipulations: realizing molecular switches and devices. Jpn. J. Appl. Phys. **47**, 6063–6069 (2008)
21. Stipe, B.C., Rezaei, M.A., Ho, W.: Inducing and viewing the rotational motion of a single molecule. Science **279**, 1907–1909 (1998)
22. Dujardin, G., Walkup, R.E., Avouris, P.: Dissociation of individual molecules with electrons from the tip of a scanning tunneling microscope. Science **255**, 1232–1235 (1992)
23. Langlais, V., Schlittler, R.R., Tang, H., Gourdon, A., Joachim, C., Gimzewski, J.K.: Spatially resolved tunneling along a molecular wire. Phys. Rev. Lett. **83**, 2809–2812 (1999)
24. Joachim, C., Tang, H., Moresco, F., Rapenne, G., Meyer, G.: The design of a nanoscale molecular barrow. Nanotechnology **13**, 330–335 (2002)
25. Shirai, Y., Osgood, A.J., Zhao, Y., Kelly, K.F., Tour, J.M.: Directional control in thermally driven single-molecule nanocars. Nano Lett. **5**, 2330–2334 (2005)
26. Fujiyoshi, S., Takeuchi, S., Tahara, T.: Time-resolved impulsive stimulated Raman studies of 1,1′-binaphthyl in the excited state: low-frequency vibrations and conformational relaxation. J. Phys. Chem. A **108**, 5938–5943 (2004)
27. Hochstrasser, R.M.: The effect of intramolecular twisting on the emission spectra of hindered aromatic molecules. Can. J. Chem. **39**, 459–470 (1961)
28. Richards, G.J., Hill, J.P.: The pyrazinacenes. Acc. Chem. Res. **54**, 3228–3240 (2021)

29. Miklík, D., Mousavi, S.F., Burešová, Z., Middleton, A., Matsushita, Y., Labuta, J., Ahsan, A., Buimaga-Iarinca, L., Karr, P.A., Bureš, F., Richards, G.J., Švec, P., Mori, T., Ariga, K., Wakayama, Y., Morari, C., D'Souza, F., Jung, T.A., Hill, J.P.: Pyrazinacenes exhibit on-surface oxidation-state-dependent conformational and self-assembly behaviours. Commun. Chem. **4**, 1–10 (2021)
30. Richards, G.J., Hill, J.P., Subbaiyan, N.K., D'Souza, F., Karr, P.A., Elsegood, M.R.J., Teat, S.J., Mori, T., Ariga, K.: Pyrazinacenes: Aza analogues of acenes. J. Org. Chem. **74**, 8914–8923 (2009)
31. Hill, J.P., Wakayama, Y., Schmitt, W., Tsuruoka, T., Nakanishi, T., Zandler, M.L., McCarty, A.L., D'Souza, F., Milgrom, L.R., Ariga, K.: Regulating the stability of 2D crystal structures using an oxidation state-dependent molecular conformation. Chem. Commun. **42**, 2320–2322 (2006)
32. Hill, J.P., Xie, Y., Shundo, A., Ariga, K., Schumacher, A.L., Karr, P.A., D'Souza, F.: Structure and properties of phenol-substituted porphyrins and oxoporphyrinogens. J. Porphyrins Phthalocyanines **13**, 60–69 (2008)
33. Hill, J.P., Wakayama, Y., Ariga, K.: How molecules accommodate a 2D crystal lattice mismatch: an unusual 'mixed' conformation of tetraphenylporphyrin. Phys. Chem. Chem. Phys. **8**, 5034–5037 (2006)
34. Hill, J.P., Hewitt, I.J., Anson, C.E., Powell, A.K., McCarty, A.L., Karr, P.A., Zandler, M.E., D'Souza, F.: Highly nonplanar, electron deficient, N-substituted tetra-oxocyclohexadienylidene porphyrinogens: structural, computational, and electrochemical investigations. J. Org. Chem. **69**, 5861–5869 (2004)
35. Geng, F., Gao, H., Meng, Q., Dong, Z., Wakayama, Y., Akada, M., Ariga, K., Hill, J.P.: Anchoring of self-assembled monolayers of unsymmetrically-substituted chromophores with an oxoporphyrinogen surface clamp. Chem. Commun. **47**, 8533–8535 (2011)
36. Stefani, D., Perrin, M., Gutiérrez-Cerón, C., Aragonès, A.C., Labra-Muñoz, J., Carrasco, R.D.C., Matsushita, Y., Futera, Z., Labuta, J., Ngo, T.H., Ariga, K., Díez-Pérez, I., van der Zant, H.S.J., Dulić, D., Hill, J.P.: Mechanical tuning of through-molecule conductance in a conjugated Calix[4]pyrrole. ChemistrySelect **3**, 6473–6478 (2018)
37. Jung, T.A., Schittler, R.R., Gimzewski, J.K.: Conformational identification of individual adsorbed molecules with the STM. Nature **386**, 696–698 (1997)
38. Wintjes, N., Hornung, J., Lobo-Checa, J., Voigt, T., Samuely, T., Thilgen, C., Stöhr, M., Diederich, F., Jung, T.A.: Supramolecular synthons on surfaces: controlling dimensionality and periodicity of tetraarylporphyrin assemblies by the interplay of cyano and alkoxy substituents. Chem. Eur. J. **14**, 5794–5802 (2008)
39. Yokoyama, T., Yokoyama, S., Kamikado, T., Okuno, Y., Mashiko, S.: Selective assembly on a surface of supramolecular aggregates with controlled size and shape. Nature **413**, 619–621 (2001)
40. Xie, Y., Akada, M., Hill, J.P., Ji, Q., Charvet, R., Ariga, K.: Real-time self-assembly and reassembly of molecular nanowires of trigeminal amphiphile porphyrins. Chem. Commun. **47**, 2285–2287 (2011)
41. Shirai, Y., Morin, J.-F., Sasaki, T., Guerrero, J.M., Tour, J.M.: Recent progress on nanovehicles. Chem. Soc. Rev. **35**, 1043–1055 (2006)
42. Kudernac, T., Ruangsupapichat, N., Parschau, M., Macia, B., Katsonis, N., Harutyunyan, S.R., Ernst, K.-H., Feringa, B.L.: Electrically driven directional motion of a four-wheeled molecule on a metal surface. Nature **479**, 208–211 (2011)
43. Van Venrooy, A., García-Lopez, V., Li, J.T., Tour, J.M., Dubrovskiy, A.V.: Nanocars with permanent dipoles: preparing for the second international nanocar race. J. Org. Chem. **85**, 13644–13654 (2020)
44. Ariga, K., Mori, T., Ishihara, S., Kawakami, K., Hill, J.P.: Bridging the difference to the billionth-of-a-meter length scale: how to operate nanoscopic machines and nanomaterials by using macroscopic actions. Chem. Mater. **26**, 519–532 (2014)
45. Vanossi, A., Dietzel, D., Schirmeisen, A., Meyer, E., Pawlak, R., Glatzel, T., Kisiel, M., Kawai, S., Manini, N.: Recent highlights in nanoscale and mesoscale friction. Beilstein J. Nanotechnol. **9**, 1995–2014 (2018)

46. Kadish, K.M., Smith, K.M., Guilard R. (eds.): Handbook of Porphyrin Science, vol. 2. World Scientific, Singapore (2010)
47. Lindsey, J.S., Schreiman, I.C., Hsu, H.C., Kearney, P.C., Marguerettaz, A.M.: Rothemund and Adler-Longo reactions revisited: synthesis of tetraphenylporphyrins under equilibrium conditions. J. Org. Chem. **52**, 827–836 (1987)
48. Adler, A.D., Longo, F.R., Finarelli, J.D., Goldmacher, J., Assour, J., Korsakoff, L.: A simplified synthesis for meso-tetraphenylporphine. J. Org. Chem. **32**, 476 (1967)
49. Rothemund, P.: A new porphyrin synthesis. The synthesis of porphin. J. Am. Chem. Soc. **58**, 625–627 (1936)
50. Sundharamurthi, S., Sudha, K., Karthikaikumar, S., Abinaya, K., Reddy, V.R., Kalimuthu, P.: Switching of inter-valence charge transfer in stimuli-responsive bis(ferrocenyl)porphyrin. New J. Chem. **42**, 4742–4747 (2018)
51. Kawai, S., Ishikawa, A., Ishida, S., Yamakado, T., Ma, Y., Sun, K., Tateyama, Y., Pawlak, R., Meyer, E., Saito, S., Osuka, A.: On-surface synthesis of porphyrin-complex multi-block co-oligomers by defluorinative coupling. Angew. Chem. Int. Ed. **61**, e202114697 (2022)
52. Jana, A., McKenzie, L., Wragg, A.B., Ishida, M., Hill, J.P., Weinstein, J.A., Baggaley, E., Ward, M.D.: Porphyrin/platinum (II) C^ N^ N acetylide complexes: synthesis, photophysical properties, and singlet oxygen generation. Chem. Eur. J. **22**, 4164–4174 (2016)
53. Mishra, P., Hill, J.P., Vijayaraghavan, S., Van Rossom, W., Yoshizawa, S., Grisolia, M., Echeverria, J., Ono, T., Ariga, K., Nakayama, T., Joachim, C., Uchihashi, T.: Current-driven supramolecular motor with in situ surface chiral directionality switching. Nano Lett. **15**, 4793–4798 (2015)
54. Gao, L., Liu, Q., Zhang, Y.Y., Jiang, N., Zhang, H.G., Cheng, Z.H., Qiu, W.F., Du, S.X., Liu, Y.Q., Hofer, W.A., Gao, H.J.: Constructing an array of single-molecule rotors on gold surfaces. Phys. Rev. Lett. **101**, 197209 (2008)
55. Manzano, C., Soe, W.H., Wong, H.S., Ample, F., Gourdon, A., Chandrasekhar, N., Joachim, C.: Step-by-step rotation of molecule gear mounted on an atomic-scale axis. Nat. Mater. **8**, 576–579 (2009)
56. Noji, H., Yasuda, R., Yoshida, M., Kinosita, K.: Direct observation of the rotation of F_1-ATPase. Nature **386**, 299–302 (1997)
57. Astumian, R.D.: Thermodynamics and kinetcis of a Brownian motor. Science **276**, 917–922 (1997)
58. Schliwa, M., Woehlke, G.: Molecular motors. Nature **422**, 759–765 (2003)
59. Ait-Haddou, R., Herzog, W.: Brownian Ratchet models of molecular motors. Cell Biochem. Biophys. **38**, 191–213 (2003)
60. Nakamura, K., Li, Q.-Q., Krejci, O., Foster, A.S., Sun, K., Kawai, S., Ito, S.: On-surface synthesis of a π-extended Diaza[8]circulene. J. Am. Chem. Soc. **142**, 11363–11369 (2020)
61. Sun, K., Sugawara, K., Lyalin, A., Ishigaki, Y., Uosaki, K., Taketsugu, T., Suzuki, T., Kawai, S.: Heterocyclic ring-opening of nanographene on Au(111). Angew. Chem. Int. Ed. **60**, 9427–9432 (2021)
62. Kong, H., Yang, S., Gao, H., Timmer, A., Hill, J.P., Arado, O.D., Mönig, H., Huang, X., Tang, Q., Ji, Q., Liu, W., Fuchs, H.: Substrate-mediated C–C and C–H coupling after dehalogenation. J. Am. Chem. Soc. **139**, 3669–3675 (2017)
63. Kawai, S., Benassi, A., Gnecco, E., Söde, H., Pawlak, R., Mullen, K., Passerone, D., Pignedoli, C., Ruffieux, P., Fasel, R., Meyer, E.: Superlubricity of graphene nanoribbons on gold surfaces. Science **351**, 957–961 (2016)
64. Kawai, S., Koch, M., Gnecco, E., Sadeghi, A., Pawlak, R., Glatzel, T., Schwarz, J., Goedecker, S., Hecht, S., Baratoff, A., Grill, L., Meyer, E.: Quantifying the atomic-level mechanics of single long physisorbed molecular chains. Proc. Natl. Acad. Sci. USA **111**, 3968–3972 (2014)
65. Gigli, L., Kawai, S., Guerra, R., Manini, N., Pawlak, R., Feng, X., Müllen, K., Ruffieux, P., Fasel, R., Tosatti, E., Meyer, E., Vanossi, A.: Detachment dynamics of graphene nanoribbons on gold. ACS Nano **13**, 689–697 (2019)

Controlled Driving of a Single-Molecule Anthracene-Based Nanocar on a Metal Surface

Ana Barragán, Koen Lauwaet, Tomás Nicolás-García, Ana Sánchez-Grande, José Ignacio Urgel, Jonas Björk, Emilio M. Pérez, and David Écija

Abstract We introduce the design of a compact and robust single-molecule nanocar and its controlled manipulation along a metal surface with the help of a CO-functionalized STM tip. The nanocar consists of an anthracene chassis and four phenyl derivatives as wheels, and it is easily sublimed and adsorbed on an Au(111) surface. This molecular design has been found to be ideal for racing, thanks to the easily polarization of the molecule by the STM tip, which creates an induced dipole that makes the nanocar susceptible to electric field gradients. Importantly, our STM tips were functionalized with CO molecules, which has been decisive for driving the nanocars without destroying or picking them up, allowing thousands of maneuvers. Our combined synthetic and operational strategy was successful to get the Nanocar Race II championship.

Keywords Single molecule · STM · Nanocars · Anthracene-based molecules · CO tip functionalization · STM manipulation

1 Introduction

There are many synthetic strategies to create a nanocar to be driven on a surface, and several of them were already showcased in the first Nanocar Race [1]. Different

A. Barragán · K. Lauwaet · T. Nicolás-García · A. Sánchez-Grande · J. I. Urgel · E. M. Pérez (✉) · D. Écija (✉)
IMDEA Nanoscience Institute, C/ Faraday 9, Campus de Cantoblanco, 28049 Madrid, Spain
e-mail: emilio.perez@imdea.org

D. Écija
e-mail: david.ecija@imdea.org

A. Sánchez-Grande
Institute of Physics of the Czech Academy of Science, 16253 Praha, Czech Republic

J. Björk (✉)
Department of Physics, Chemistry and Biology, IFM, Linköping University, 581 83 Linköping, Sweden
e-mail: jonas.bjork@liu.se

© The Author(s), under exclusive license to Springer Nature Switzerland AG 2023

F. Moresco and C. Joachim (eds.), *Single Molecule Mechanics on a Surface*,
Advances in Atom and Single Molecule Machines,
https://doi.org/10.1007/978-3-031-16930-4_6

approaches to obtain molecular-scale-controlled nanocars have been reported in the literature during the last years [2]. When restricting ourselves to the field of STM controlled motion, the vast majority of the nanocars were specifically designed to be adsorbed on a surface under ultra-high vacuum (UHV) conditions, as well as to be imaged and manipulated by an STM tip.

It is important to consider that a rational design of a nanocar does not necessarily imply that the different nanocomponents of the molecule look like the macroscopic components of a car, though for Nanocar Race II it was compulsory to design a nanocar with distinguishable front and rear.

For the participation in the second edition of the Nanocar race, we designed a family of minimalistic nanocars comprising an anthracene "chassis" and four aromatic rings as "wheels" (Fig. 1). The rear wheels of the nanocars could be synthesized with different substituents to fine-tune their properties and hence the response to the external electric field generated at the tunnel junction. Using such fine-tuning we managed to create a highly-controllable nanocar. The asymmetry between rear and front wheels equips the cars with a small built-in dipole moment that helps maneuver the nanocar with the STM tip due to electrostatic interactions. However, as we will explain below, the main mechanism of motion of our family of nanocars was the interaction between the STM tip and the induced dipole moment of the molecule by the STM tip when placed close to the nanocar with the appropiate tunnelling conditions.

During the design process, we ensured that our minimalist anthracene-based nanocars would accomplish the recommendations described by the winners of the first edition [3, 4]:

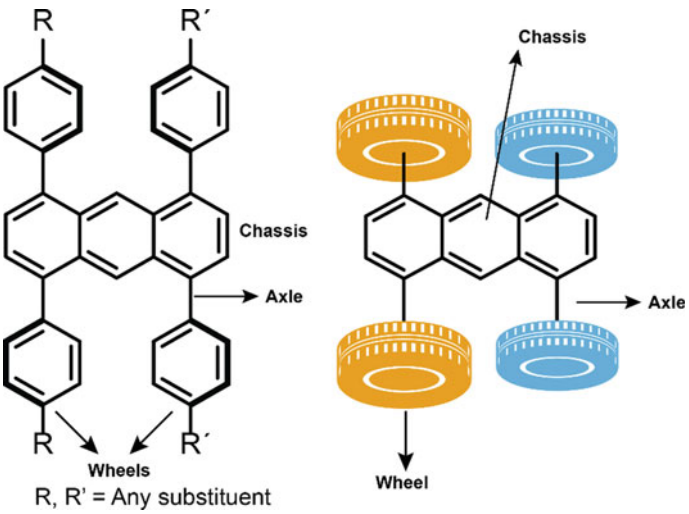

Fig. 1 Chemical structure of minimalistic anthracene-based nanocars (left) and nanocar sketch showing the different nanocomponents of a car: axle, chassis and wheels (right)

- Keep the molecular weight as low as possible. Our nanocars feature about 70–80 atoms and molecular weights about 500 g/mol.
- Minimize surface interactions. The external aromatic wheels keep the rigid anthracene chassis separated from the surface.
- Stability. The molecular structure comprises only strong C–C and C–H bonds, providing the nanocar enough stability to be deposited by thermal sublimation under UHV conditions without being broken.
- Propulsion mechanism without pushing. The electrostatic interaction between the induced dipole moment and the STM tip was enough to move the car along the surface.

On the driving side, we aimed to be able to create a sufficiently large electric field between sample and STM tip for enhanced driving, whilst minimizing direct interactions between our STM tip and the nanocar, in order to avoid any non-permitted "pick-up" event. With a metallic tip these two features are usually mutually exclusive, an effect that is employed in e.g. the lifting of graphene nanoribbons [3]. From our own unpublished lifting experiments and our experience with high-resolution STM imaging, we learnt that we could avoid picking-up the nanocar by employing carbon monoxide (CO) functionalized STM tips. By attaching a CO molecule to the tip apex, one can bring the tip much closer to an adsorbed molecule on the surface, without forming a strong bond between molecule and the STM tip. As a result, since the tip is closer to the surface and the electric field is inversely proportional to the tip-sample distance, such protocol leads to a higher electric field, without the fear of accidentally picking up the nanocar and ending the run for the race.

From a comprehensive study of this family of nanocars on surfaces, by combining theoretical calculations and STM manipulations, we could infer their mechanical behaviour under tip-induced stimuli, providing insights in surface science and synthetic chemistry for the design of future generations of nanocars.

2 Solution Synthesis of Anthracene-Based Nanocars

To make our design a reality, we based our synthetic strategy on the preparation of asymmetric arylated anthracenes with four different substituents through a set of [4 + 2] cycloadditions (Diels–Alder reaction) [5] between diphenylfuran derivatives and a bisaryne, as shown in the retrosynthetic analysis of Scheme 1. In a Diels–Alder reaction, two different components are required, a diene (a compound containing two C–C double bonds separated by a single C–C bond), which in our case would be the diphenylfuran derivatives, and a dienophile (the olefinic or acetylenic component that is "hungry" for the diene) which in our case would be the aryne. The key intermediates are the diphenylfuran derivatives, which are synthesized through Suzuki–Miyaura cross-coupling reactions between the correspondent boronic acids and dibromofuran. Thanks to this direct functionalization, we can decorate the wheels of the car with electron-donating or withdrawing groups. Since CsF is only slightly

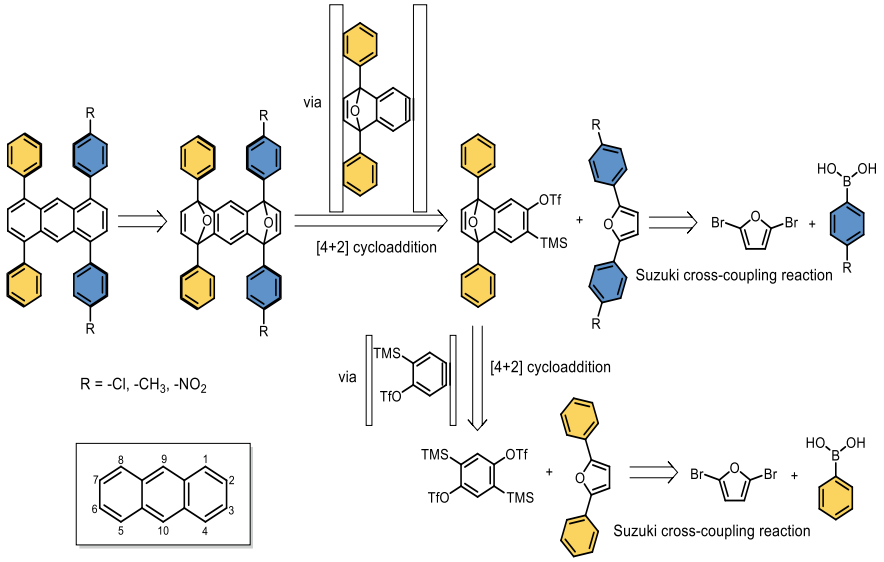

Scheme 1 Retrosynthetic analysis for the preparation of asymmetric anthracene-based nanocars. The chemical structure of anthracene, with its C numbering, is shown inside the black box

soluble in acetonitrile, we are able to control the generation of the aryne just in one half of the molecule [6]. In this way, we obtain anthracene derivatives asymmetrically functionalized in positions 1 and 4 or 5 and 8 of the anthracene backbone (see the black box in Scheme 1). Finally, we removed the oxygen bridges generated in the [4 + 2] cycloaddition adducts, to achieve the final planar anthracene chassis. This synthetic process can in principle be applied to introduce a vast range of functional groups both in the "front" (yellow aromatic rings in Scheme 1) and "rear" (blue aromatic rings in Scheme 1) wheels of the nanocar.

3 Preparing of the Race Track

Racing was performed in a custom-designed UHV system (base pressure below 4 $\times$ 10^{-10} mbar) hosting a commercial low-temperature microscope with STM/AFM capabilities from Scienta Omicron and located at IMDEA Nanoscience (Madrid, Spain) operated with Matrix control electronics. First, the Au(111) surface was prepared by cycles of Ar^+ ion sputtering (E = 1.5 keV, I = 10 μA) and subsequent annealing (740 K) under UHV conditions. Then, during the sublimation of the molecules, the surface was held at room temperature for molecular deposition. Deposition rates of the molecules were checked with a quartz micro-balance (LewVac). Nanocars were thermally deposited using a Kentax TCE-BSC evaporator. Once prepared, the sample was transferred within the UHV system to the microscope

where it was cooled down to 4.3 K for measurements. Before starting the STM experiments, CO molecules were dosed for few seconds at a pressure of 1 x 10^{-8} mbar in order to find CO molecules adsorbed on the Au(111) surface and prepare a CO functionalized tip. As the nanocar race forbids direct pushing and pulling, we did not use the Atom Manipulation routines in the Matrix software but measured with the STM Spectroscopy experiment. Racing was performed by manually going to the right tunnelling conditions and using tip relocation. We did use automatic substrate plane detection and subtraction when the feedback loop was turned off. The STM images were analyzed using WSxM [7].

4 Cl-Substituted Anthracene-Based Nanocar

First, we tested the chloride-substituted nanocar, which we could sublimate at 177 °C. Figure 2 shows the result of the adsorption of a submonolayer coverage of Cl-substituted anthracene molecules on Au(111). The molecules self-assemble into islands. Unfortunately, once the molecules are adsorbed on the Au(111) surface, most of them have lost their wheels.

Furthermore, for the manipulation of the few intact molecules found on the surface, the reactivity of the Cl atoms with the surface causes the wheels to come off, making controlled manipulation impossible. Therefore, we decided to go for a more inert version of our anthracene-based racer.

5 CH_3-Substituted Anthracene-Based Nanocar

Once the Cl atoms are replaced by CH_3 groups, the molecules are more stable after sublimation and deposition under UHV conditions. The sublimation temperature of this nanocar was 180 °C, very similar to the Cl-substituted one. As in the previous case, the small anthracene chassis keeps the weight at minimum, while, in this case the front wheels are benzene rings, and the rear wheels are toluenes. The solid-state structure of the nanocar had been solved by electron diffraction, depicted in Fig. 3, and shows that the steric interaction of the aromatic wheels in positions 1, 4, 5 y 8 of the anthracene backbone forces them to come out of planarity, separating the anthracene chassis from the Au(111) substrate, and thus decreasing the interaction with the surface, which promotes a highly-controllable manipulation.

Figure 4a shows the result of the deposition of a submonolayer coverage of CH_3-substituted molecules on Au(111) held at room temperature and then scanned at 4.3 K. We can find some decorated elbows, as well as a low coverage of self-assembled islands located along the FCC region of the herringbone reconstruction, where the nanocars are “parked” together in small starting grids. In between, and thanks to the low coverage, we have a large clean track for racing. A zoomed-in STM image allows us to notice that the molecules lie flat on the Au(111) surface, showing a

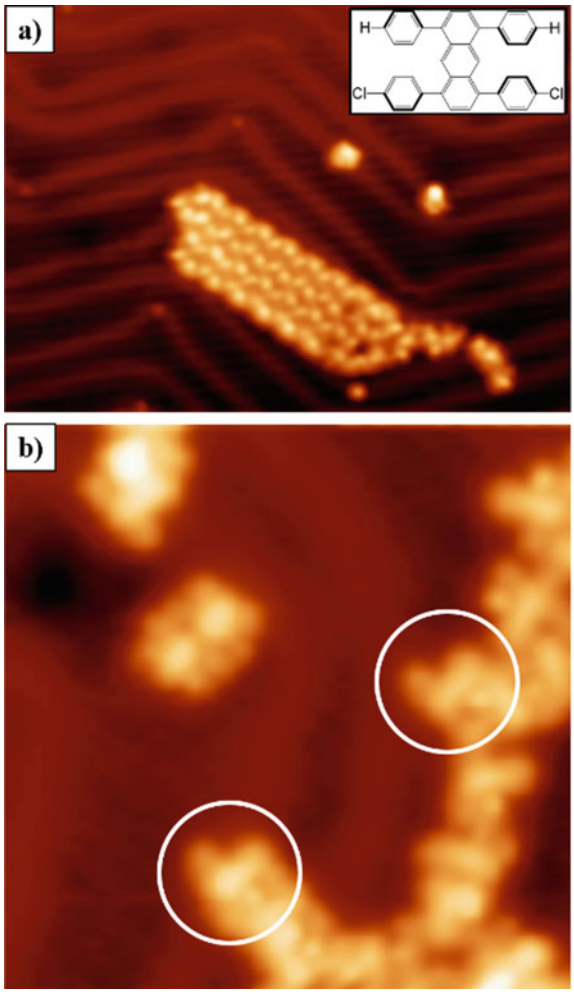

Fig. 2 Adsorption of Cl-substituted anthracene-based molecules on Au(111). **a** Long-range STM image showing the molecules self-assembled into islands. Scanning parameters: $V_b = -3.0$ V, $I_t = 150$ pA. Image size: 40 nm × 28 nm. The chemical drawing of the nanocar is shown in the inset. **b** High-resolution STM image where the two encircled molecules highlight nanocars with missing wheels. Scanning parameters: $V_b = 0.5$ V, $I_t = 5$ pA. Image size: 13 nm × 13 nm

perfect cartoon car-shape in the STM image (see Fig. 4c). Furthermore, we can distinguish an elongated central part, belonging to the anthracene chassis unit, and four characteristic lobes, which are assigned to the benzene derivative wheels. The comparison between the experimental and the theoretical STM image is excellent (Fig. 4c, d, respectively).

Several different adsorption configurations of the CH_3-substituted nanocar were considered in the DFT calculations, taking into account the direction of the anthracene

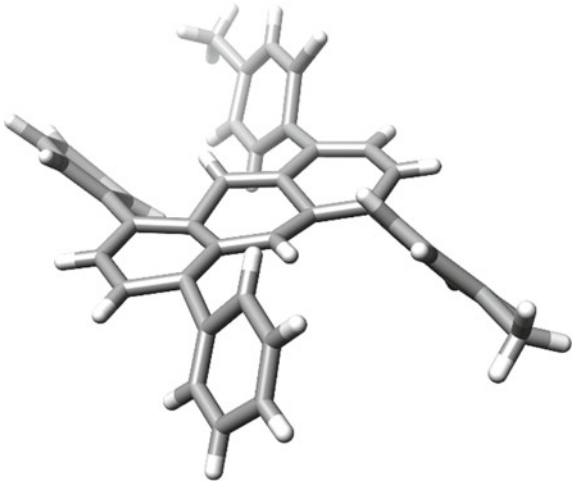

Fig. 3 Solid-state structure of CH_3-substituted anthracene-based nanocar solved by electron diffraction

chassis with respect to the surface, the adsorption site, and the orientation of the phenyl rings ("wheels"). The two most stable configurations have different orientations of the phenyl rings, being found within 2 meV (i.e. below the accuracy of the calculations). In Fig. 5 these two configurations are compared. Notably, the STM simulations of the configuration in Fig. 5b gives a better agreement with the contrast observed in the STM experiments, and it seems plausible this is the configuration imaged the experiments. The molecule adsorbs with the anthracene unit parallel to the surface while the phenyl rings have a slight tilt due to steric hindrance. It should be noted that most adsorption configurations considered are found within 10 meV, indicating that the molecule can move easily across the surface under week external stimuli. At the same time, it is expected that switching the orientations of the phenyl rings is difficult due to steric hindrance, and, thus, the phenyl rings will keep their orientation when maneuvering the car. Importantly, due to the interaction of the nanocar with the surface the final configuration of the phenyl rings is distinct, though still out the plane, as compared to the gas-phase conformation (see comparison between Figs. 3 and 5b).

Trying to maximize efficiency and time during the Nanocar Race II, the manipulation process is divided in two different steps, which will be described below: (i) the lateral manipulation to get the molecules out of the self-assembled grids, and (ii) the driving mechanism to bring the molecules to a selected spot.

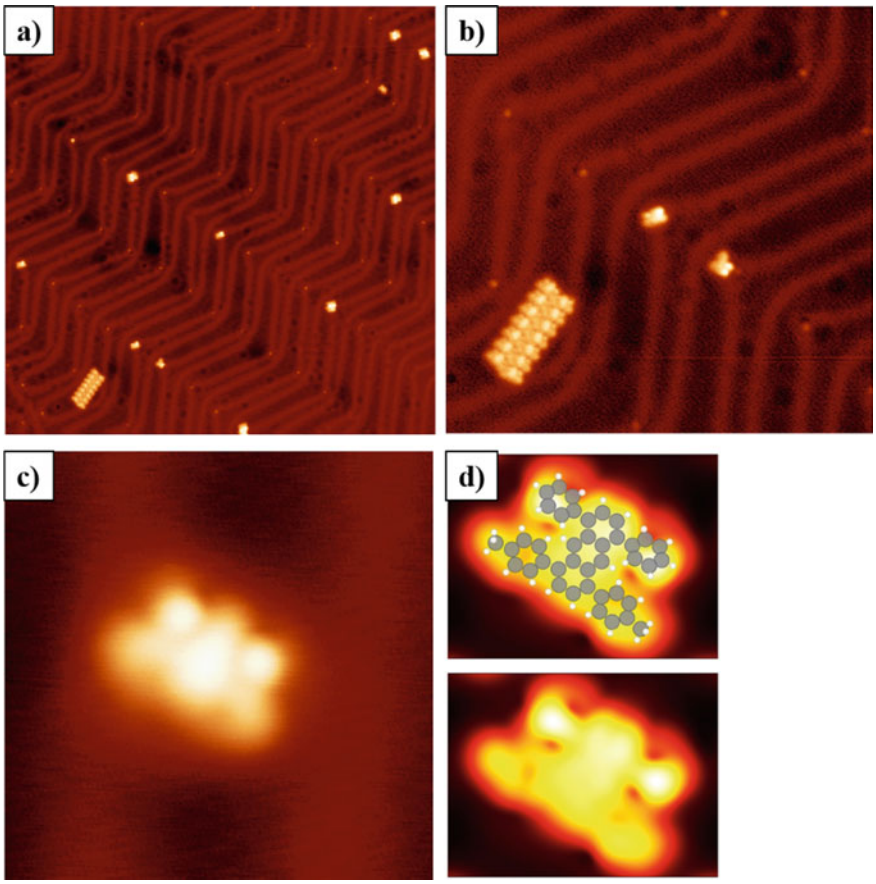

Fig. 4 **a** Overview STM image of the Au(111) surface showing some decorated elbows and a self-assembled island of CH_3-substituted anthracene-based nanocars. Scanning parameters: $V_b = 0.2$ V, $I_t = 10$ pA. Image size: 80 nm × 80 nm. **b** Zoomed-in image of a self-assembled starting grid. Scanning parameters: $V_b = 0.5$ V, $I_t = 40$ pA. Image size: 15 nm × 15 nm. **c** Isolated CH_3-substituted anthracene-based nanocar where the intramolecular features are distinguished. Scanning parameters: $V_b = 0.2$ V, $I_t = 5$ pA. Image size: 4 nm × 4 nm. **d** Simulated local density of states at the Fermi level, corresponding to an experimental constant current image at low bias

5.1 First Step: Getting off the Line (Lateral Manipulation)

Since isolated molecules are rarely found on the surface after deposition, as a first step, we need to separate the molecules from a self-assembled grid. In order to obtain individual molecules, we use a standard method, i.e. mechanical lateral manipulation. First, we take an STM image of the desired self-assembled nanoisland. Then, the lateral manipulation starts at the side of the molecule that one wants to move, as

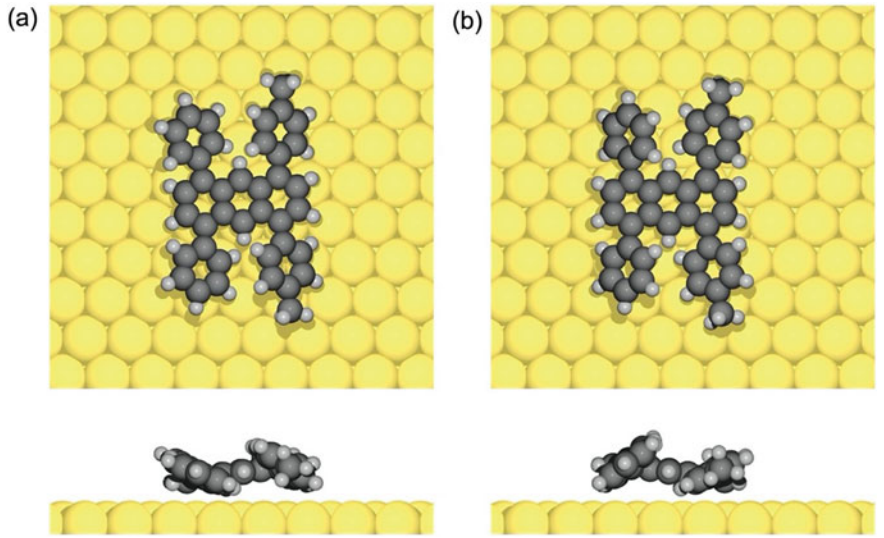

Fig. 5 The two most stable adsorption configurations of the CH_3-substituted anthracene-based nanocar on Au(111) as calculated with DFT. The configuration in (**a**) was found to be more stable by 2 meV than the configuration, but which is below the accuracy of the calculations. The STM simulation shown in Fig. 4d was obtained for the structure in (**b**), which gives a better fit to the contrast between the phenyl rings observed in the STM experiments

indicated by the white spot in Fig. 6b, and it is directed along its longest axis (see white arrow).

Specifically, once the CO-functionalized tip is located close to the molecule, the feedback loop is opened, and the tip is approached to the surface until a recorded current of approximately 0.5 nA is obtained. Then, the tip is laterally moved. In our STM, manipulation is successful if the current saturates when the pre-amplifier is in the 3.3 nA range. This high current arises from the presence of the molecule in the tunneling gap, meaning that the tip has controllably pushed the molecule. After closing the feedback loop, a new scan image with the initial scanning (and non-perturbative parameters) is performed to see the result of the manipulation (Fig. 6c).

5.2 An Insight: The Importance of the CO-Functionalized Tip

The CO-functionalized tip is important for getting an enhanced resolution and for maneuvering the nanocars. Figure 7a illustrates a nanoisland measured with a CO-functionalized tip, whereas Fig. 7b displays the same area, but with a purely metallic tungsten tip, clearly revealing a massive loss in resolution.

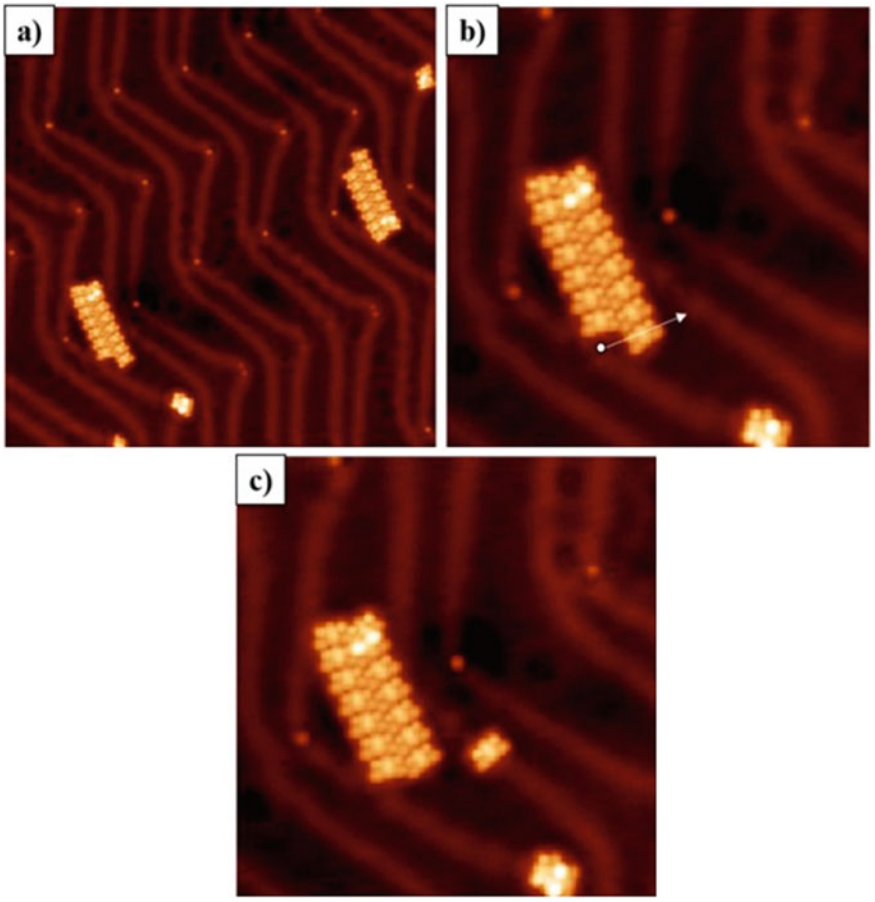

Fig. 6 First step: Getting off the line. a STM image showing a region with two self-assembled nanoislands. Scanning parameters: $V_b = 0.2$ V, $I_t = 10$ pA. Image size: 40 nm × 40 nm. **b** STM image before the lateral manipulation. Scanning parameters: $V_b = 0.2$ V, $I_t = 10$ pA. Image size: 20 nm × 20 nm. The white dot indicates the initial position of the tip, and the white arrow indicates the direction of the lateral manipulation. **c** STM image after the lateral manipulation. Scanning parameters: $V_b = 0.2$ V, $I_t = 10$ pA. Image size: 20 nm × 20 nm

When we try to move a single molecule out of the island with a metallic tip using the same procedure as previously described, we displace three molecules at once, some of which we see afterwards diffusing strongly on the surface outside of our control (see Fig. 7c). We could not reproduce a protocol for lateral manipulation to drag out this species from the nanoislands with a metallic tip.

As stable imaging conditions and high image quality are very important for the nanocar race due to outresearch, together with the enhanced capabilities for controlled manipulation, we consider that our choice for CO-functionalized tips is well motivated.

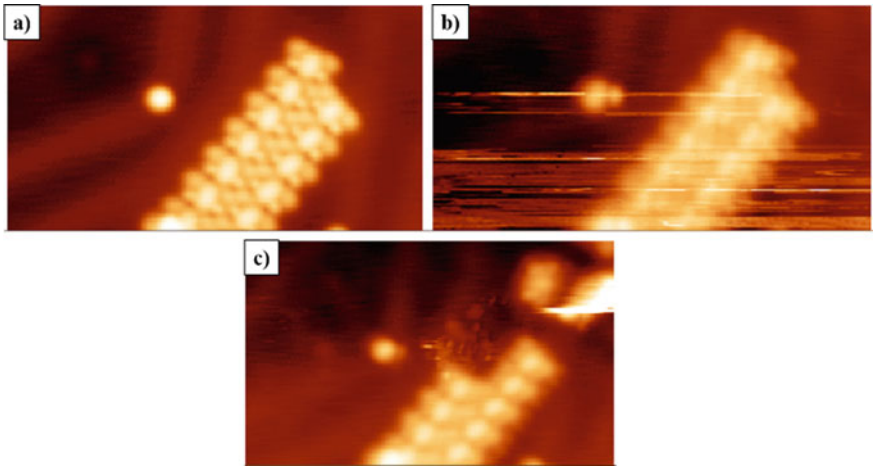

Fig. 7 Imaging with a metal tip. a CO-tip STM image showing an island of parked nanocars. Scanning parameters: $V_b = -0.5$ V, $I_t = 40$ pA. Image size: 13 nm × 7 nm, **b** Scanning the same area as in (**a**) with a metallic tip. Scanning parameters: $V_b = 0.2$ V, $I_t = 20$ pA. Image size: 13 nm × 7 nm, **c** The same area after trying to get a molecule from the starting grid with a metallic tip. Scanning parameters: $V_b = 0.6$ V, $I_t = 40$ pA. Image size: 13 nm × 7 nm

5.3 Second Step: Going Somewhere/Driving Mechanism

For the nanocar race itself, movement by direct mechanical pushing is forbidden. So, while we could use the pushing mechanism to prepare some molecules before the race, during the competition the propulsion mechanism had to be different. In our case, once we have obtained an isolated molecule, we developed a tip-induced electrical field gradient as the propulsion mechanism.

One step of movement is shown in Fig. 8 and proceeds as follows. After stopping the scanning of the STM, we place the CO-functionalized tip close to the molecule at a lateral tip-molecule distance of around 1.5 nm. At this location we open the feedback loop with standard conditions: $V_b = 0.2$ V, $I_t = 5$ pA. With the feedback loop opened, we progressively increase the bias applied to the tip from 0.2 to 2.2 V whilst monitoring the current versus time trace. We first start seeing instabilities in the tunneling current, followed by a sudden jump in current to a value of at least 2 nA (Fig. 8c), meaning that a translation event has taken place. The applied bias creates an electric field that induces a dipole on the molecule, which then is attracted towards the tip, being manifested by a sudden increase of the tunneling current. Finally, the tunneling parameters are set to non-perturbative scanning conditions and the feedback loop is closed to acquire the constant current STM image. Notably, after the attraction event, the tip is always located on top of one of the benzene wheels (see Fig. 8b).

By again positioning the tip around 1.5 nm away from the center of the molecule, and repeating the same process, the next step of displacement of the nanocar is done.

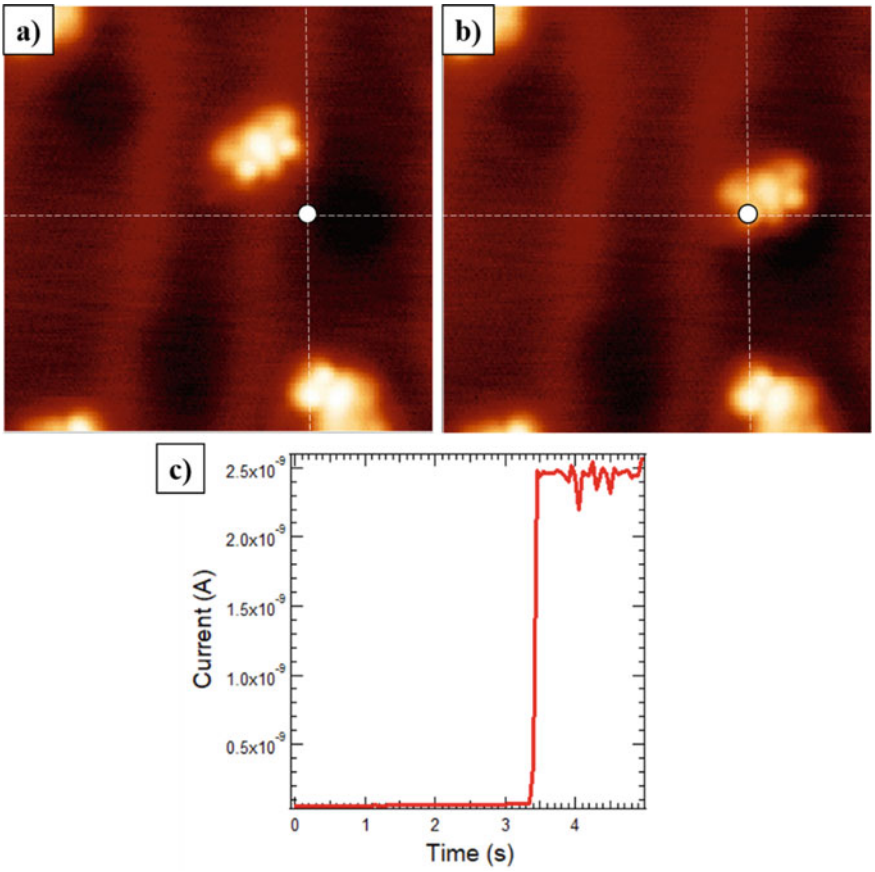

Fig. 8 Second step: Going somewhere/Driving mechanism. **a** and **b** STM images (Scanning parameters: $V_b = 0.2$ V, $I_t = 5$ pA. Images size: 8.5 nm × 8.5 nm) showing the positions of an isolated molecule before and after the translation event, respectively. The white dot indicates the position of the STM tip. **c** Current recorded as a function of the time while the feedback loop is open. The jump indicates the manipulation event

Notably, if the tip is moved too far from the nanocar for a reliable manipulation, no instabilities in the current are observed. As long as the current signal reflects these instabilities with sufficient intensity, the molecule will follow the tip. We observe this driving mechanism independently of the molecular adsorption position (FCC/HCP) or the moving direction (along/across the herringbone reconstruction, or any tip position around the molecule), as also shown in Figs. 9 and 10. Importantly, negative bias also produces translation events, which corroborates our interpretation of the attraction between STM tip and induced molecular dipole as the mechanism behind the maneuvering events.

Figures 9 and 10 shows a manipulation sequence of a nanocar around an obstacle that is adsorbed on an elbow and around a self-assembled island, respectively.

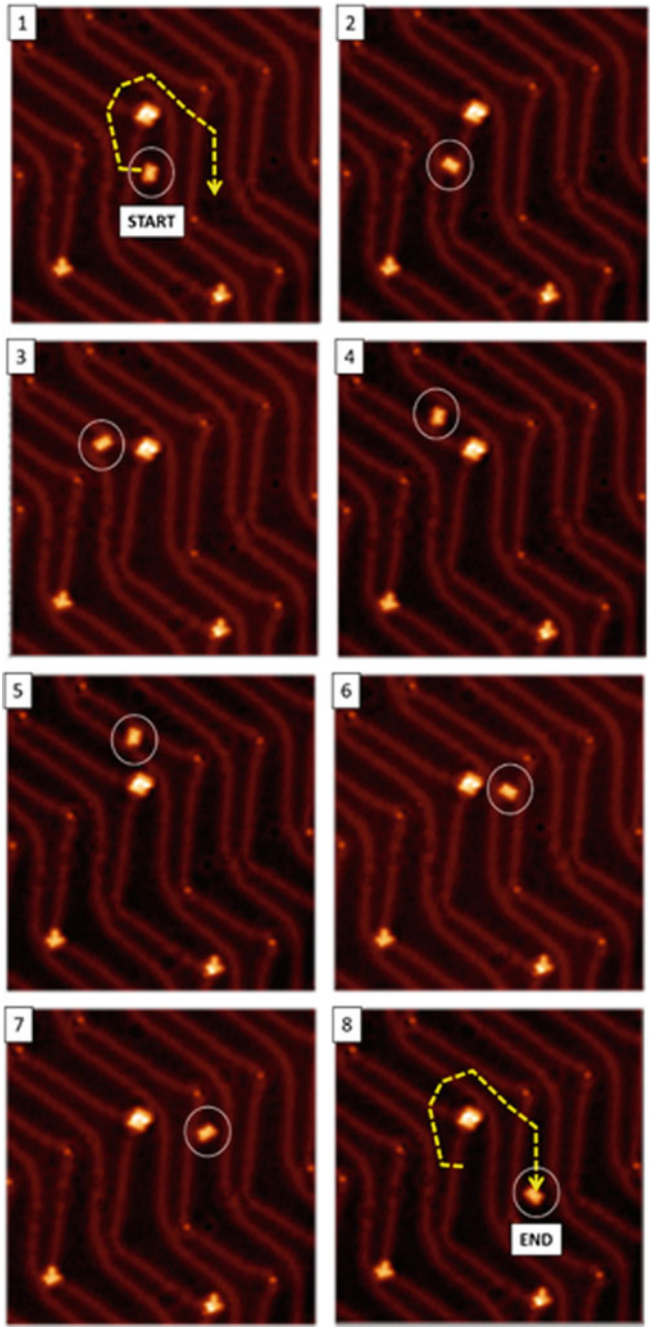

Fig. 9 Series of STM images showing the driving of an individual nanocar molecule around an obstacle. Scanning parameters: $V_b = 0.2$ V, $I_t = 5$ pA. Image size: 30 nm $\times$ 30 nm

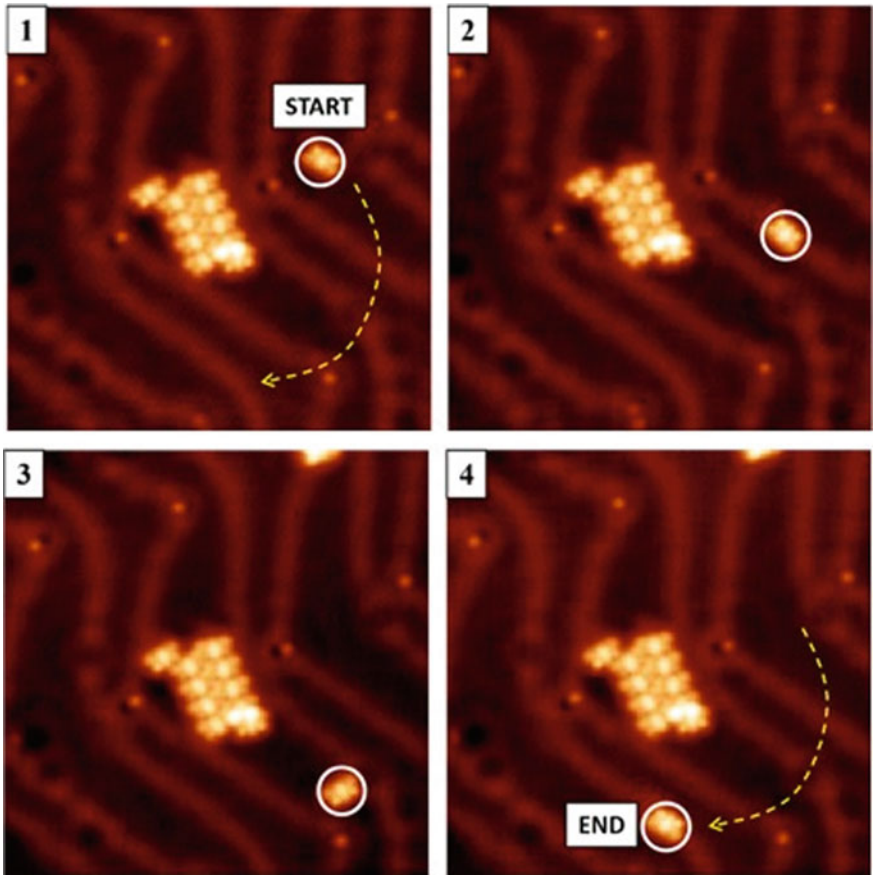

Fig. 10 Series of STM images showing the driving of an individual nanocar molecule around a self-assembled island. Scanning parameters: $V_b = 0.2$ V, $I_t = 5$ pA. Image size: 20 nm × 20 nm

Initially, the molecule is placed on a FCC region of the Au(111) herringbone reconstruction (Fig. 9-1). By following the pulse positions, the molecule is able to overcome the obstacles along the yellow track. The positions of the molecule in each panel are marked with a white circle. These two manipulation sequences show that we can drive the molecule following any desired track.

6 Conclusions

We have designed and synthesized a highly controllable nanocar that is able to be manipulated over the Au(111) surface following a STM tip. The design of the nanocar is minimalistic, featuring an anthracene chassis, benzene wheels at the front

and toluene wheels at the rear, thus displaying the shape of a car. We could control the manipulation and translation of the nanocars by taking advantage of the attraction between the STM tip and the electrical dipole induced at the nanocar by the CO-functionalized STM tip.

The second edition of the international Nanocar Race took place the past March 24th 2022 in Toulouse, and our team managed to cover 678 nm in 8 h and 17 min with the same molecule, completing 54 elbow turns along the FCC domain of the herringbone reconstruction. We took the first place in the competition, ex-aequo with the Japanese NIMS-MANA team, demonstrating an important progress in single-molecule predetermined manipulation for a very long period of time.

References

1. Rappene, G., Joachim, C.: The first nanocar race. Nat. Rev. Mater. **2**, 17040 (2017)
2. Joachim, C., Rapenne, G.: Molecule concept nanocars: chassis, wheels, and motors? ACS Nano **7**, 11–14 (2013)
3. Pawlak, R., Meier, T.: Fast and curious. Nat. Nanotechnol. **12**(7), 712–712 (2017)
4. Simpson, G.J., García-López, V., Petermeier, P., Grill, L., Tour, J.M.: How to build and race a fast nanocar. In: Nature Nanotechnology, vol. 12, pp. 604–606. Nature Publishing Group (2017)
5. (a) Suzuki, S., Segawa, Y., Itami, K., Yamaguchi, J.: Synthesis and characterization of hexaarylbenzenes with five or six different substituents enabled by programmed synthesis. Nat. Chem. **7**, 227–233 (2015). (b) Suzuki, S., Itami, K., Yamaguchi, J.: Synthesis of octaaryl naphthalenes and anthracenes with different substituents. Angew. Chem. Int. Ed. **56**, 15010–15013 (2017)
6. Rodríguez-Lojo, D., Peña, D., Pérez, D., Guitián, E.: Straightforward synthesis of novel acene-based aryne precursors. Synlett **26**(11), 1633–1637 (2015)
7. Horcas, I., Fernández, R., Gómez-Rodríguez, J.M., Colchero, J., Gómez-Herrero, J., Baro, A.M.: Rev. Sci. Instrum. **78**, 013705 (2007)

Azulene Based Nanocars

Tim Kühne, Kwan Ho Au-Yeung, Suchetana Sarkar, and Francesca Moresco

Abstract The precise design of Nanocars and single-molecule machines requires understanding the mechanisms of inducing and controlling molecular motion and hence allowing the conversion of electric power into controlled movement. We present a series of azulene-based Nanocars specifically designed to uncover the influence of several chemical groups on the movement performance. While the azulene core is characterized by a high dipole moment, the rational choice of lateral groups can further enhance the dipole moment and influence the interaction of the molecules with the Au(111) surface and with each other. First, we investigated the high electric dipole moment molecule di-*tert*-butyl 2-isocyanoazulene-1,3-dicarboxylate (BCA). While single molecules were immobile, a complex structure consisting of cleaved molecules and gold adatoms moved under STM voltage pulses. This structure could be driven along an arbitrarily chosen path. To investigate the influence of the different functional chemical groups and the impact of the manifold physical effects taking place, two modified molecules were investigated. The results of these experiments demonstrate the efficiency of the functional chemical groups attached to the azulene core and shed new light on design strategies for fast and controllably moving Nanocars in general.

Keywords Scanning tunneling microscope · STM manipulation · Nanocar · Dipole moment · Azulene

T. Kühne · K. H. Au-Yeung · S. Sarkar · F. Moresco (✉)
Center for Advancing Electronics Dresden, 01069 Dresden, TU, Germany
e-mail: francesca.moresco@tu-dresden.de

© The Author(s), under exclusive license to Springer Nature Switzerland AG 2023

F. Moresco and C. Joachim (eds.), *Single Molecule Mechanics on a Surface*,
Advances in Atom and Single Molecule Machines,
https://doi.org/10.1007/978-3-031-16930-4_7

1 Introduction

The idea of organizing a Nanocar Race "to boost molecular nanovehicle research" [1] was proposed in 2013 by Christian Joachim and Gwénaël Rapenne, with the aim of motivating the scientific community to design, manipulate with the tip of a scanning tunneling microscope (STM), and theoretically model novel single molecule-vehicles. The first Nanocar Race was organized in CEMES-CNRS Toulouse (France) in 2017 with the participation of six teams from Europe, USA and Japan [2].

Nanocars can be defined as single-molecule machines able to move efficiently in one direction on a surface at the nanoscale. They are driven by voltage pulses applied by the tip of an STM, transforming the energy coming from inelastically tunneling electrons and the electric field into controlled movement.

For the first Nanocar Race in 2017, the competing Nanocars were designed in very different ways, some of them based on a technomimetic strategy with a chassis connected to wheels [3], some others not resembling cars and without wheels at all [4] or based on smaller units self-assembled on the surface and connected by hydrogen bonds [5]. During this first edition, only two cars were able to drive more than 100 nm, while some of them could not move at all.

The Dresden Nanocar in 2017, in particular, was formed by four commercially available 4-acetylbiphenyl molecules self-assembled in a small structure resembling a windmill. The nanostructure was known to efficiently move by voltage pulses, thanks to inelastic tunneling electrons partially exciting molecular electronic states [5, 6]. Unfortunately, during the sample preparation in Toulouse prior to the race, the low amount of molecules on the surface allowed to form only trimers of molecules (see Fig. 1), showing a much lower mobility than the windmills during the race. In the final ranking, the Dresden team reached the fourth position and could drive the trimers along a distance of only 11 nm. According to the recent DFT calculations, both structures are stabilized by Au adatoms [7]. Even if the physical mechanisms allowing the movement of the windmills and hindering the movement of the trimers are still under investigation, the Dresden team decided to avoid self-assembled structures or on-surface synthesis for the future design of Nanocars.

A few years later, and with a significant delay due to the Covid 19 pandemic, Christian Joachim with the support of the European Union's Horizon 2020 FET Open Project Mechanics with Molecules (MEMO) organized the second edition of Nanocar Race. Nanocar Race II took place in March 2022 in CEMES CNRS Toulouse (France).

Eight teams from Europe, USA, and Japan registered for the race and, starting from the preregistration in 2018, had nearly four years time to design, synthetize, and test a Nanocar on the Au(111) surface moving under the STM tip.

Most teams started from the "dipolar racer" concept, considering that one of the winner of the first Nanocar Race, the dipolar racer from the Graz-Rice team, was successfully designed using the internal molecular dipolar moment to move in one direction under an applied electric field [8]. Most of the first molecules proposed for Nanocar Race II followed the common strategy to provide a dipole moment as high

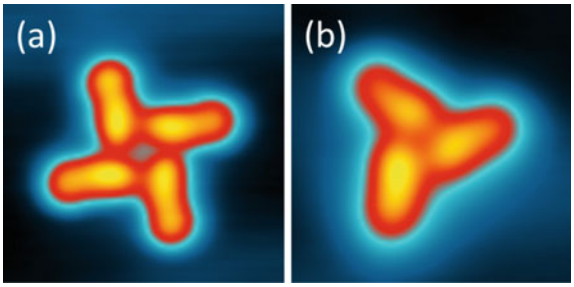

Fig. 1 STM images of supramolecular structures composed of 4-acetylbiphenyl molecules and stabilized by Au adatoms adsorbed on Au(111). **a** Windmill formed by four molecules and **b** trimer formed by three molecules. Image size: 3.9 nm × 3.9 nm; STM images recorded at V = 100 mV and I = 50 pA

as possible to the Nanocar. After the first experiments, however, it was clear that a successful strategy for a fast moving Nanocar should not underestimate the effects of inelastic electron tunneling and the excitation of electronic and vibrational modes. Similar to the rotational movement of single molecule motors and rotors [9–11], the directional translation of a molecule relies on many different factors and it is difficult to predict.

Figure 2 shows a graphical illustration of a STM tip that excites a molecule through tunneling current, which finally results in a lateral controlled motion of the molecule on the surface.

Nanocar Race II was not only a successful dissemination event, but also a unique long-time (24 h) experiment on the parallel molecular manipulation of eight Nanocars by voltage pulses, providing valuable knowledge about the mechanical properties of single molecules on a surface. During Nanocar Race II, molecules received voltage pulses varying from 500 mV to several volts, some of them survived more than 7000

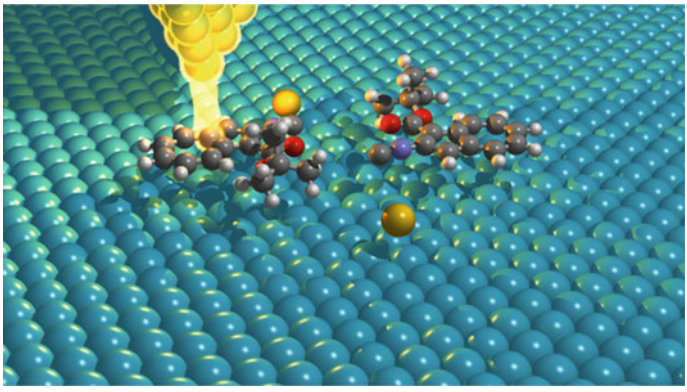

Fig. 2 Graphical illustration of a STM tip exciting an azulene-based molecular complex by tunneling electrons to move on the surface

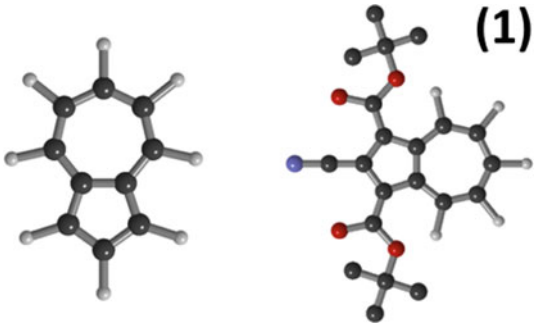

Fig. 3 Chemical structure of azulene and **(1)** di-*tert*-butyl 2-isocyanoazulene-1,3-dicarboxylate (BCA) used in this study. The intrinsic dipole moment of the azulene core is enhanced in **(1)** by adding a cyano group and carboxylate groups while *tert*-butyl groups decouple the molecule mechanically from the surface

excitations in about 8 h and moved over 1000 nm in a controlled way without being lost or destroyed.

The Dresden Team started to develop a Nanocar with high dipole moment in 2018, based on an azulene motor. Azulene (left structure in Fig. 3) is a non-benzoid isomer of naphthalene consisting of a 7- and a 5-membered ring. It presents a high dipole moment of 1.08 D [12, 13].

The present chapter reports the development and the testing of the first few examples of azulene-based Nanocars. Such Nanocar prototypes helped later to design the final German Azulene Explorer (GAzE) Nanocar, which participated to Nanocar Race II in March 2022.

Among the properties that qualify a molecule for movability, the electric dipole moment is currently in the focus of research [8, 14]. As already mentioned, in 2017 Simpson et al. [8] accounted the dipolar moment of a single molecule to be the decisive property. A basic understanding of the physical effects involved in inelastic electron tunneling manipulation and the influence of individual chemical groups and their electrical charge is however still missing. In other words, the present strategies for the design of Nanocars are still not completely successful or predictive. Hence, we investigated the influence of the dipole moment performing specific experiments on molecules featuring a high dipole moment. These experiments were performed using a low temperature STM at the temperature of 5 K and under ultra-high vacuum, where a Au(111) sample was used as substrate. In this environment, single molecule diffusion is hindered due to freezing and the surface remains clean.

This chapter presents a first design of an azulene based Nanocar, the on-surface formation of dimers allowing to vary the molecular dipole moment, as well as later designs obtained by adding specific lateral groups to the azulene core. The different compounds allowed us to investigate in detail the effect of the molecular dipole moment and of the side groups on the translation of the molecule on the Au(111) surface.

2 Moving Azulene-Based Nanostructures on the Au(111) Surface

In order to investigate the effect of the dipole moment on the mobility of molecules excited by voltage pulses with the STM tip, the molecule di-*tert*-butyl 2-isocyanoazulene-1,3-dicarboxylate (BCA) **(1)** shown in the right panel of Fig. 3 was synthesized in the group of Lissel [15]. The intrinsic dipole moment of the azulene core was specifically enhanced by a cyano group and carboxylate groups while *tert*-butyl groups were added to decouple the molecule mechanically from the surface. These modifications resulted in the comparably high dipole moment of 9.0 D with respect to 1.08 D for pure azulene.

The deposition of the BCA molecules by evaporation on the Au(111) surface at room temperature led to many different small complexes rather than single molecules, as one can see in in the overview STM image of Fig. 4.

Two structures were reproducibly found (see Fig. 4), indicated by black and red boxes. With the help of calculations [15] we concluded that the dimers are stabilized by gold adatoms, therefore forming metal–organic structures. Close-up STM images are shown in Fig. 5 for a single molecule **(1)**, an "asymmetric dimer" **(2)**, where *tert*-butyl carboxylate groups were cleaved in each molecule, resulting in only one high

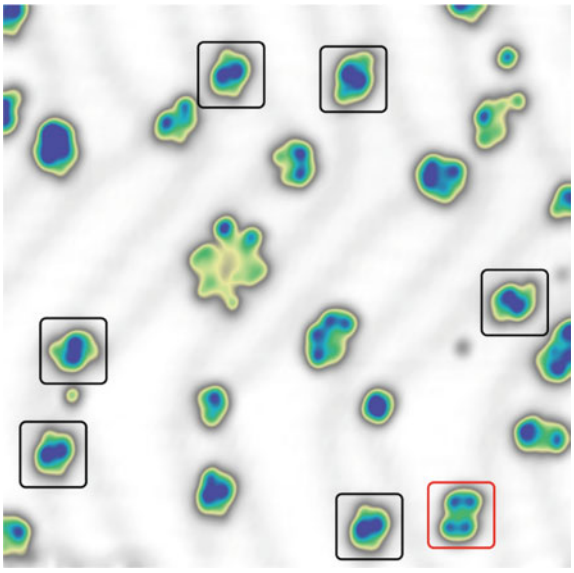

Fig. 4 Overview STM image of BCA molecules adsorbed on Au(111) after evaporation on the surface kept at room temperature. Different structures composed of intact (red square, "symmetric dimer") and cleaved molecules (black squares, "asymmetric dimer") as well as irregular structures are visible. Image parameters: V = 250 mV, I = 20pA, image size $(30\ \text{nm})^2$

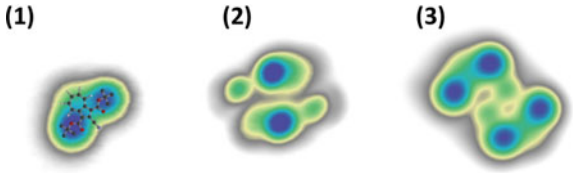

Fig. 5 **(1)** Single BCA molecule ((5 nm)^2, 1000 mV, 2 pA) with structure overlay atop, **(2)** "asymmetric dimer", consisting of two cleaved molecules and two gold adatoms ((5 nm)^2, 250 mV, 20 pA) and **(3)** "symmetric dimer" consisting of two pristine molecules and two gold adatoms ((5 nm)^2, 250 mV, 20 pA)

lobe remaining and the "symmetric dimer" **(3)**, consisting of two pristine molecules and two gold adatoms in the center.

Both dimers were found in the two possible chiral adsorptions, the symmetric dimer made up only 2% of the regular structures. Please note that only upon evaporation on a surface cooled with liquid nitrogen, single molecules as depicted in Fig. 4a could be found. To investigate the movement of the structures on the surface, voltage pulses were applied to both single molecules and dimers.

For inducing the movement of the molecule, the STM tip is positioned near to the chosen molecule or dimer, the feedback loop is kept open fixing the height of the tip with respect to the surface, and a voltage pulse, typically 1.2 V is applied between the sample and the tip. During the voltage pulse, a tunneling current is recorded, as shown in Fig. 6 for dimer **(2)**. After a short time, in this case about 0.05 s, the tunneling current suddenly increases, indicating that the molecule moved towards the tip. The result of the manipulation can be exactly imaged by recording a STM image after having applied the pulse.

The described manipulation procedure was tested on the different structures **(1)**, **(2)** and **(3)** of Fig. 5. Surprisingly, only the asymmetric dimers **(2)** could be controllably moved by voltage pulses, despite the fact that they have the lowest dipole moment among the observed structures: 9.0 D for the pristine BCA molecule **(1)**, 6.5 D for the symmetric dimer **(3)** and 2.3 D for the asymmetric dimer **(2)** [15]**.**

Figure 7 shows a sequence of images of the same 20 $\times$ 40 nm^2 Au(111) terrace. BCA molecules **(1)** were previously evaporated on the sample kept at room temperature. Similarly as previously discussed (Figs. 4 and 5), several dimers consisting of two cleaved molecules could be identified near to many irregular structures. This terrace was used as a background for demonstrating the controllable and reliable movements of the single dimers **(2)**. Black circles indicate the positions where a voltage pulse was applied in the vicinity of the chosen molecule. As can be seen from the track, the dimer could be controllably moved by voltage pulses in any direction and even be driven across the lines of the herringbone surface reconstruction, passing between the other structures on the surface. In this way, we could drive a single dimer over a distance of 35 nm by the consecutive application of 14 voltage pulses of 1.2 V and a current of roughly 700 pA each. The dimer moved within fractions of a second. We applied a pulse for a duration of one second, observing

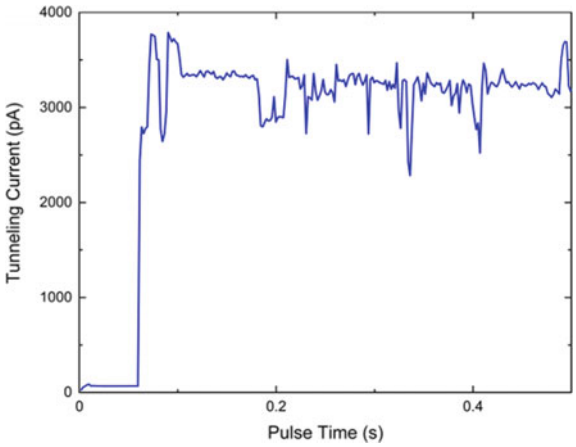

Fig. 6 Typical curve for the tunneling current during a voltage pulse inducing the movement of a BCA dimer **(2)** at 1.2 V. From the initial value of ~ 50 pA, the current within fractions of a second (here 0.06 s) raised to the 50-fold value, indicating that the structure moved below the tip, reducing the tunneling gap width and hence causing the current increase

a movement within this time in almost 100% of the cases (see Fig. 6 for a typical current curve). The most effective pulses were applied after positioning the STM tip-apex at a distance of up to 2 nm away from the center of the complex, independently from the orientation of the molecule with respect to the position of the tip. Hence, the dimer always moved towards the tip position, in steps of maximum 2 nm per pulse. It is important to note that the dimer always moved towards the tip position for a positive voltage pulse (applied to the surface with respect to the tip), while a negative bias during a pulse led to repulsive movement in not well defined directions. Figure 7 presents a complete sequence of manipulation of dimer **(2)**, which is composed by two cleaved molecules **(1)** and two gold adatoms, and shows that such dimer could be moved directionally in a controlled way along any arbitrary chosen path along the Au(111) surface. On the contrary, both dimers **(3)** and the single BCA molecule **(1)** could not be moved controllably by voltage pulses.

In order to investigate the physical effects driving the movement, pulse voltage and tunneling current (through tip height changes) were varied from pulse to pulse. In case of inelastic tunneling, a portion of the tunneling electrons loses energy to the target structure, finally resulting in motion. This is bias dependent, since a minimum energy is necessary to induce the excitation. The so called action spectra can be used to analyze the way of the energy transfer [16].

However, for large tip heights with vanishing tunneling current, excitation through inelastic tunneling would fail. In case of BCA dimers **(2)**, investigations using variable tunneling resistance showed a threshold voltage for movement linearly depending on the tip height. The results are reported in Fig. 8, where the graph shows the voltage threshold necessary to move the dimers depending on the tip height. For both positive and negative polarities of the bias voltage, the same linear dependence

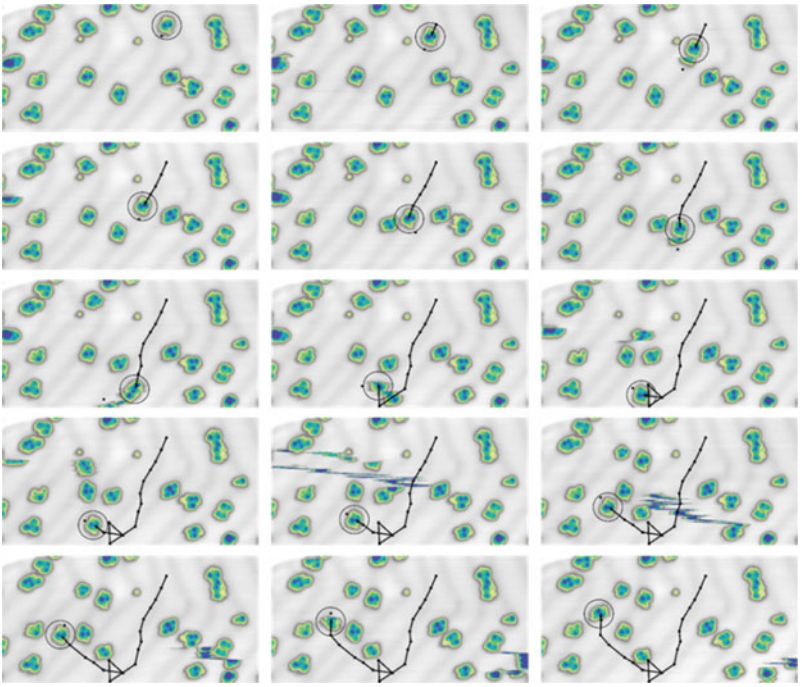

Fig. 7 (20×40) nm^2 STM topography images measured at 200 mV and 12 pA. The black circle marks a structure consisting of cleaved BCA molecules and gold adatoms. The black line depicts the track the structure has been moved along on the Au (111) surface where the dots indicate voltage pulse locations. Consecutive pulsing at a voltage of 1.2 V and a current of roughly 700 pA allowed moving the structure directionally and in a controlled way along the chosen path, for this track 35 nm within 14 consecutive steps

is observed. Additionally, even for very large tip heights of up to 1.9 nm, a movement of the asymmetric dimer was recorded. At this tip height, the tunneling current is practically zero (0.0004 electrons per second). The ratio between applied voltage and tip-surface distance provides an estimation of the electric field in the tunneling gap, i.e. the electric field applied to the molecular structure positioned between tip and metal surface. The experiments reveal therefore that the application of an electric field influences the observed motion of the dimers. Furthermore, the slope of the fit in the present experiment corresponds to 0.36 ± 0.01 V/Å, a value close to others reported in literature for comparable manipulation experiments [17].

Figure 9 shows the calculated charge distribution for an intact molecule and a cleaved one together with the gold adatoms as they appear in the dimers. They are intuitively quite similar apart from the cleaved side group. However, a crucial difference is the position of the gold adatom that, in case of the symmetric one, is located in the center while in the asymmetric dimer is at the edge.

Instead, a charge separation between center and periphery was identified as a necessary condition driving the movement with excitation by the electric field effect.

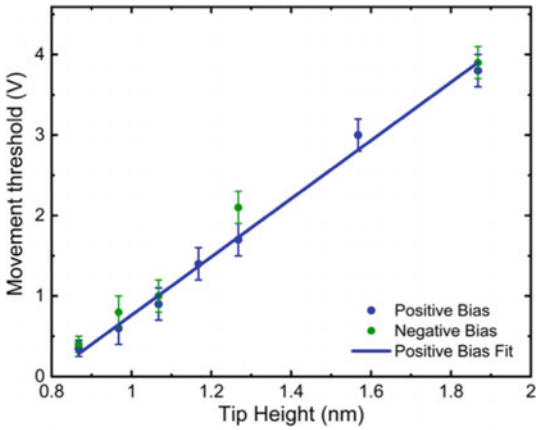

Fig. 8 Dependence of the movement threshold on the tip height for dBCA dimers (**2**). For both positive and negative polarity, a linear dependence can be deduced from the fit. The slope is 0.36 ± 0.01 V/Å which corresponds to the electric field in the tunneling gap

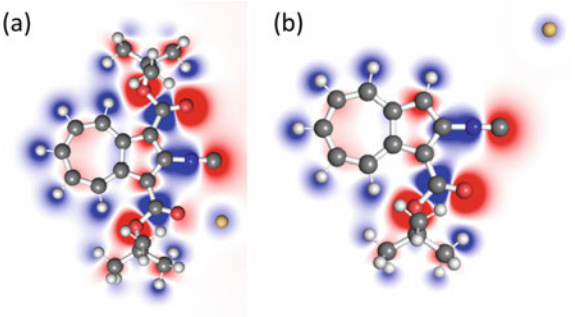

Fig. 9 Calculated charge distribution of pristine (**a**) and cleaved BCA (**b**) molecule as it is located in the dimers. The images show a cut in the plane of the molecule backbone through the three dimensional charge distribution with the structure atop. Red areas represent negatively charged regions, blue ones are charged positively. As one can see, in the pristine molecule case (**a**) the gold adatom close to the isonitrile group partially compensates the negative charging. This is not the case for the cleaved molecules since in the asymmetric dimer, the gold adatom is located at the edge of the structure

This charge separation can explain the fact that for positive bias the molecular structure always moved until its center met the tip location. This fact can be qualitatively explained the strongly negatively charged center is attracted to the tip location. On the other hand, a negative bias pulse leads to electrostatic repulsion and an uncontrolled movement away from the tip location. In order to develop a general model of the mobility of single molecules, it is crucial to understand the physical mechanisms beyond the molecular movement and to translate the results in chemical requirements leading to movable molecules. As a first step in this direction, we investigated similar

molecules with different lateral groups, gaining information about the influence of the different chemical substituents. Those experiments are presented in the next two sections.

3 Modifying the Lateral Groups Connected to the Azulene Core

As mentioned above, the molecules investigated in this chapter are based on the core component azulene, visible as combination of 5- and 7-membered ring in the core of the molecules as shown in Fig. 3. Through electron transfer from the 7-membered ring to the 5-membered ring in order to obtain aromaticity, the molecule gains a dipole moment. Figure 10 compares the initially designed molecule di-*tert*-butyl 2-isocyanoazulene-1,3-dicarboxylate (BCA) **(1)** introduced in Sect. 2, which is movable directionally in a controlled way in the form of dimers, with two new compounds. To disentangle the influence of the functional groups, the first compound di-*tert*-butyl azulene-1,3-dicarboxylate (BAC) **(4)** (Fig. 10) was synthesized in the group of F. Lissel. In particular, we aimed at investigating the influence of the cyano group on the dimer formation and the mobility on the surface. Such cyano group is present in **(1)** but not in **(4)**. Furthermore, the compound 1,3-bis(phenylethynyl)azulene (BEA) **(5)**, also depicted in Fig. 10, was synthesized in the group of F. Lissel to investigate the influence of the side group on the movability. While removing the carboxylate groups, the *tert*-butyl "arms" were replaced by phenyl rings coupled to the core by ethynyl linkers.

Apart from the possibility of tuning the mobility by changing the side groups, compounds **(4)** and **(5)** were designed to improve two further important properties of BCA **(1)**. First, the (thermal) stability of the molecules is desired, since BCA **(1)** easily cleaved upon evaporation losing a *tert*-butyl carboxylate group. And second, the formation of complexes and nanostructures on the surface had to be improved. As already discussed, BCA **(1)** formed metal–organic complexes on the Au(111) surface involving Au adatoms, which are always present and diffuse on the surface

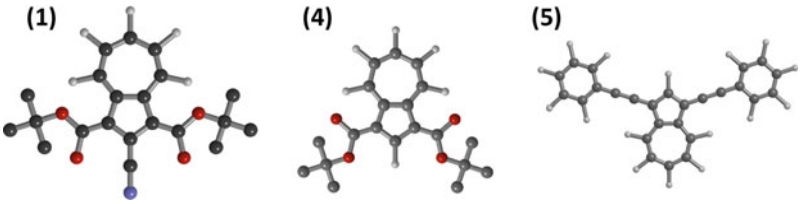

Fig. 10 Chemical structure of further azulene based compounds used in this study compared with the first **(1)** proposed and initially used molecule; **(4)** di-*tert*-butyl azulene-1,3-dicarboxylate (BAC) synthetized to learn about the functionality of the cyano group; **(5)** 1,3-bis(phenylethynyl)azulene (BEA) designed to investigate the surface decoupling effect of the *tert*-butyl groups

at room temperature. A large molecular dipole moment favors dimerization due to the reduction in the electric field through anti-parallel alignment. Looking for a protocol to get small movable structures, one possible solution was to reduce the overall dipole moment. Moreover, isonitrile groups are known to favor the formation of metal–organic structures with gold adatoms [18] (HCN is one of the few gold solvents). We therefore removed the CN group to minimize the dimer formation, aiming to investigate single molecules instead of complexes.

4 Influence of the Cyano Group

Reducing the electric dipole moment by removing the cyano group should intuitively reduce the movability of the molecule. Calculations show that CN enhances the natural dipole moment of azulene to 4.41 D, which is a quite strong change.

Compound **(4)** corresponds to compound **(1)** with the only difference of the absence of the cyano group, reducing the dipole moment but also the reactivity on the Au(111) surface.

Figure 11 shows the STM image of a single di-*tert*-butyl azulene-1,3-dicarboxylate (BAC) **(4)** molecule. Compared to BCA **(1)** (see Fig. 5), the STM image is nearly identical, meaning that the cyano group in **(1)** is probably shadowed by the relatively large *tert*-butyl groups. Please also note that no single **(1)** molecules were visible on the surface after deposition on the room temperature surface, indicating a strong molecule–molecule interaction and an easy decomposition. On the contrary, single intact **(4)** molecules are present after evaporation on the Au(111) surface in similar conditions.

Figure 12 shows an overview STM image of the Au(111) surface after evaporation of the BAC **(4)** molecules. Compared to BCA **(1)** (see Fig. 4), most of the molecules remain intact during the evaporation. Differently from the case of BCA **(1)**, molecules **(4)** form double stripes, where the BAC **(4)** molecules order alternatingly with the azulene "tail" pointing inwards. Thus, the dipole moments compensate each other.

Even if the molecules **(4)** seem much more stable than **(1)** after deposition on the surface, single high-lobe features can be observed at the ends of the double stripes formed by BAC **(4)** and in small separated clusters found at the herringbone kinks.

It was possible to separate the double molecular stripes of Fig. 12 by lateral manipulation with the STM tip, lowering the STM tip's height and thereby pushing a single molecule from the double stripe to the Au(111) terrace. A single BAC **(4)** molecule after its separation from the double stripe is shown in Fig. 13. Similarly to the case of BCA molecules **(1)** and dimers **(2)**, we applied voltage pulses in the vicinity to induce their movement. Figure 13 shows a series of three voltage pulses applied to the same molecule. The pulses were applied at the position of the red stars and the molecule moved towards the pulse position, denoted by the yellow dot in the next image. Similarly to the BCA asymmetric dimer **(2)**, the center of the molecule moves towards the tip position. The movement is however accompanied

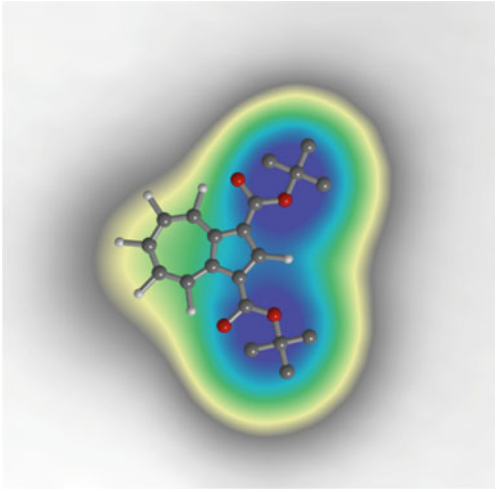

Fig. 11 STM topography image of a single di-*tert*-butyl azulene-1,3-dicarboxylate (BAC) **(4)** molecule, superposed with the molecular structure. The two *tert*-butyl groups define the two high lobes while the azulene "tail" extends the outline and the location on the surface. Image paramters: $(2.3\ \text{nm})^2$, 500 mV, 10 pA

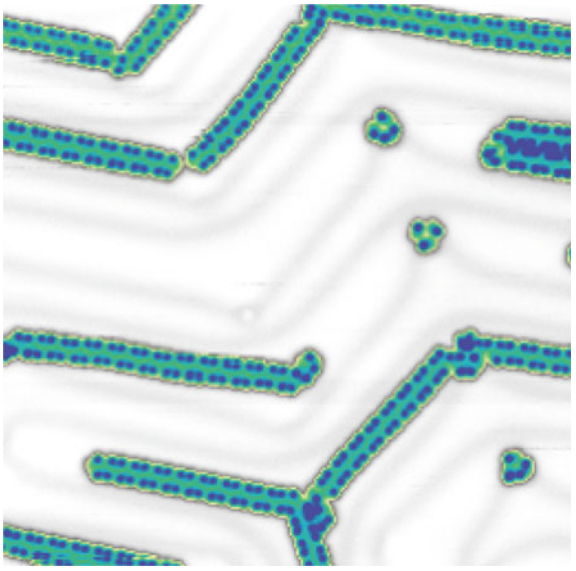

Fig. 12 STM topography $(40\ \text{nm})^2$, 500 mV, 10 pA image of di-*tert*-butyl azulene-1,3-dicarboxylate (BAC) **(4)**, where the cyano group was removed to decrease the dipole moment. Double molecule row stripes with alternating orientation can be seen, sometimes several stripes align next to each other. Most of the molecules remain intact during evaporation. Cleaved molecules are found in small structures or at the ends of the stripes

by a partial rotation of the molecule. Furthermore, different from the BCA dimers **(2)**, a comparably high voltage of at least 1.5 V is necessary to drive the molecule.

In the case of BAC **(4)**, dimers were observed only rarely. Hence, the stripe order excels the dimer formation. One example of dimers can be seen in Fig. 14. Noticeably, in both dimers of BCA **(1)** and the BAC **(4)** concerned here, the azulene "tail" points outwards. Contrary to the case of BCA dimers **(2)** and **(3)** however, no hint for gold adatoms as part of the observed structures was found for BAC **(4)**. This can be explained by the removal of the cyano groups, considering that these are known to facilitate the formation of metal–organic complexes with gold adatoms after adsorption on the Au(111) surface [18].

In order to obtain comparable results, the manipulation experiments were repeated for dimers of BAC molecules **(4)**, which were found rarely, naturally generated at the kinks of the Au(111) herringbone reconstruction.

Figure 14 shows a series of four voltage pulses applied to the same dimer. As previously described, the pulses were applied at the position of the red dots, while the yellow dots indicate the pulse position of the previous image, visualizing the movement of the dimer. In the case of the BAC **(4)** dimers shown here, the dimer moves towards the tip, irrespective of the pulse location. Occasionally, the dimer moves even further than the pulse location, indicating an excitation of motion going beyond simple attraction to the tip. This is remarkable and different from the single

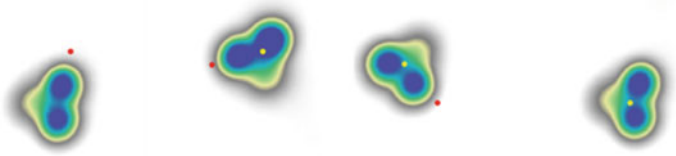

Fig. 13 STM images $(3.6\ \text{nm})^2$, 500 mV, 10 pA of a single BAC molecule that was removed from a double stripe. Voltage pulses of 1.7–2.0 V were applied at the positions of the red dots, leading to attractive movement and rotation of the molecule, yellow dots mark the position of the pulse applied before. The single molecule is attracted to the tip position

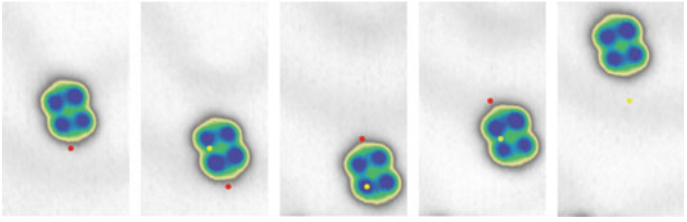

Fig. 14 Series of STM topography images $(8.5\ \text{nm})^2$, 500 mV, 2 pA that were consecutively taken after voltage pulses of 1500 mV and roughly 50 pA were applied at the positions of the red dots. Yellow dots indicate the position of the pulse applied before to elucidate its effect on the motion. The dimer is attracted towards the pulse location, following the pulse sequence in any direction and as visible in the last image sometimes even further than the pulse location

molecule movement shown in Fig. 13. Similarly to the case of the single molecule **(4)**, a threshold voltage of 1.5 V was observed to excite the movement. This may indicate that in case of BAC **(4)** the inelastic tunneling effect might have a larger influence on the movement compared to BCA **(1)** and that the electric field effect alone is not sufficient. Additionally, the directionality of the movement is much lower for BAC **(4)** molecules or dimers than for BCA dimers **(2)**, being near to a random movement. Hence, the dipole moment or charge separation is probably too low to achieve neither the same movement mechanism nor the control or directionality.

In conclusion, by removing the cyano group from molecule **(1)** obtaining molecule **(4)**, we improved significantly the stability of the molecule upon evaporation on the Au(111) surface. Furthermore, it was possible to manipulate single BAC **(4)** molecules and dimers by voltage pulses also if the dipole moment was partially reduced by the missing cyano group, however compensated by the carboxylate which is known to enhance the dipole moment, similarly to the isonitrile group in the original BCA **(1)** molecules. However, the directionality was lower and the threshold voltage for movement higher compared to BAC dimers **(2)**.

In the next step described in Sect. 5, the *tert*-butyl carboxylate groups were replaced to investigate their influence on the movement properties, both electronically and mechanically.

5 The Role of the Side Groups

The *tert*-butyl side groups of molecules **(1)** were designed to lift the azulene core above the Au(111) surface and thereby minimize the adsorption strength, making the molecules more mobile. After removing the cyano groups from molecules **(1)** di-*tert*-butyl azulene-1,3-dicarboxylate (BAC) **(4)** was obtained (Fig. 10), which can also partially decouple the azulene core from the metal surface.

In a second modification step, the *tert*-butyl groups were replaced by phenyl rings (compound **(5)** in Fig. 10), which are comparably flat and hence lack the decoupling effect. This is accompanied by a removal of the carboxylate groups and the use of ethynyl linkers to connect the phenyl rings, resulting in 1,3-bis(phenylethynyl)azulene (BEA) **(5)**.

Figure 15 shows a STM image of a single BEA **(5)** molecule after evaporation on the Au(111) surface with the chemical structure superposed. Its center part and side group lobes have the same apparent height. On the surface, the molecules locate well separated and do not favor the herringbone kinks.

Figure 16 presents a larger STM images of BEA **(5)** molecules adsorbed on the Au(111) surface keeping the substrate at room temperature. Similarly to the other molecules presented in this chapter, some elongated structures suggest a partial cleaving of a phenyl ring, resulting in molecules who consist of core and only one side group, but most of the structures that could be identified were single pristine molecules. This indicates that the low dipole moment in case of BEA reduces the molecule–molecule interaction below the level necessary to drive dimer- or (double-)

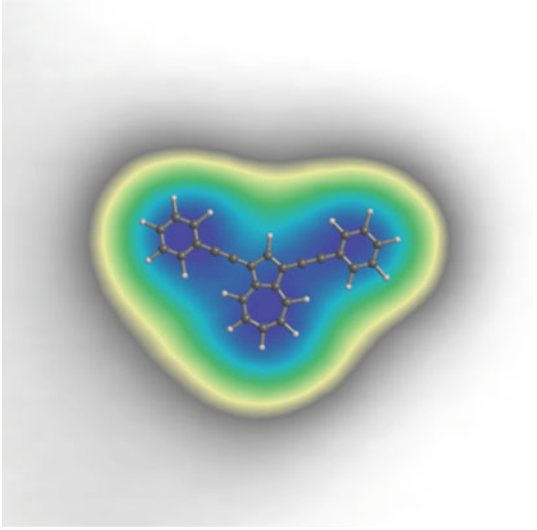

Fig. 15 STM topography image (3.5 nm)^2, 500 mV, 5 pA showing a single 1,3-bis(phenylethynyl)azulene (BEA) **(5)** molecule on the Au(111) surface. Center and side lobes for this molecule are of equal height since the phenyl rings are flat compared to the more three-dimensional *tert*-butyl groups

chain formation on the surface after evaporation. Furthermore, the molecule **(5)** is significantly more stable than **(1)**, probably due to the missing cyano group.

Similarly to the case of the molecules discussed in the previous sections, pulsing experiments were conducted in order to reveal the movement properties. Figures 17 and 18 show the behavior of a BEA molecule **(5)** upon application of voltage pulses at − 800 mV and 500 mV, respectively.

Following the same notation as described above, red starts denote the position of the pulse applied to the molecule, yellow dots the pulse leading to the current image. For both positive and negative voltage pulse polarities, the molecule is attracted towards the pulse position while the movement is accompanied by rotation. However, a larger current is needed (more than 1 nA) compared to the field-effect driven BCA dimers **(2)** that could be driven without measurable current. In the case of BEA **(5)**, the molecule is attracted towards the pulse location regardless of bias sign, but not always reaching it with its center or at all. Contrary to the immobile BCA single molecule, it can however be moved, but worse than the BCA dimer **(2)** structure. The lower movability can be explained by both the resulting lower charge separation and the modified side groups, where the flat phenyl ring has a higher interaction with the surface compared to the three-dimensional *tert*-butyl group used in the other molecules.

Figure 19 shows a heat map of the movement probability during a voltage pulse on a BEA **(5)** molecule. Depending on the pulse voltage and current, the color as third dimension encodes the probability that the target molecule moves during a

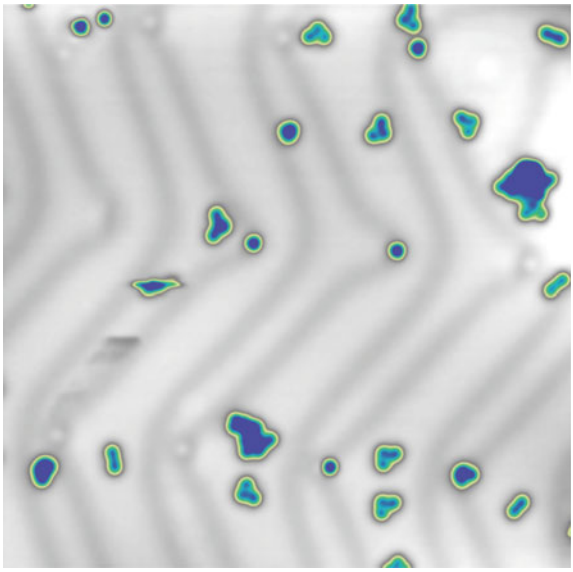

Fig. 16 STM topography image (40 nm)^2, 500 mV, 3 pA showing 1,3-bis(phenylethynyl)azulene (BEA) **(5)** molecules on the Au(111) surface. Single intact molecules are visible next to irregular structures and two-lobe elongated structures that most probably are molecules with a cleaved side group

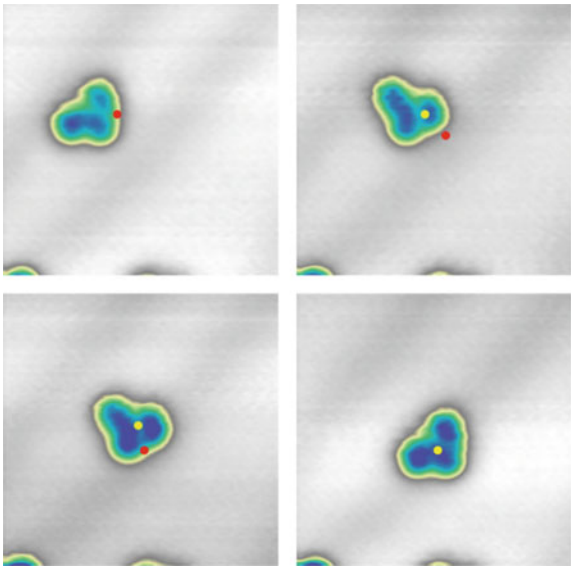

Fig. 17 STM topography images (8 nm)^2, 50 mV, 3 pA of a single BEA **(5)** molecule recorded consecutively while voltage pulses were applied at − 800 mV in the constant height mode reaching a current of roughly 1500 pA. The red dots indicate the location of the pulse applied after the image was taken, the yellow one the one from before. The molecule is attracted to the pulse location

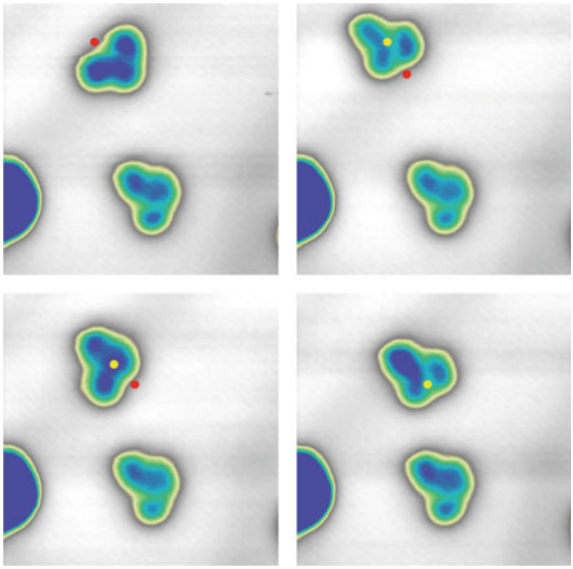

Fig. 18 Topography series of voltage pulse manipulation of a single BEA **(5)** molecule $(8\ \text{nm})^2$, 500 mV, 3 pA where voltage pulses with positive bias of 500 mV were applied to the red dot position reaching about 1300 pA. As for pulses with negative voltage, the molecule is tendentially attracted to the pulse location

voltage pulse. As the green/yellow/red sections show, a current of at least 500 pA is necessary to move the molecules. Motion is possible for a bias above 200 mV for currents larger than 1 nA or above 400 mV and for voltages below − 500 mV. This plot reveals two interesting information: even for higher voltages, where movement is triggered reproducibly, a current of at least 500 pA is necessary. This indicates that driving the molecule purely through the field effect as was observed for BCA dimers **(2)** can be excluded. Additionally, the voltage and current threshold values are different for positive and negative bias sign. The bias sign tells about whether occupied or unoccupied molecular states participate in the tunneling current. Taking this into consideration, it is another hint that the inelastic tunneling effect is the main mechanism for movement in case of BEA **(5)**: Since the electronic levels deviate between different bias signs, the energy transfer works at voltages of corresponding heights and with differing efficiency, called electronic yield. To summarize, for BEA **(5)** different measurement details indicate the inelastic tunneling effect as origin of the movement.

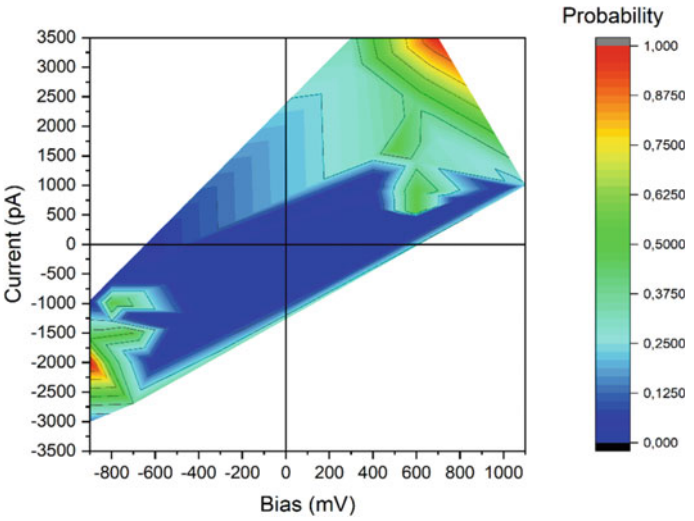

Fig. 19 Heat map plot for the movement probability of BEA **(5)** depending on both bias and current. A current of more than 500 pA is necessary to drive the molecules. Additionally, a bias threshold of − 500 mV or + 200 mV (for currents larger than 1 nA, else + 400 mV) delineates the minimum driving voltage. Remarkably, both current and different bias threshold depending on the voltage sign (occupied vs. unoccupied states) indicate that an inelastic tunneling process creates the excitations necessary to drive the motion instead of the field effect as in BCA

6 Summary and Outlook

The chapter presents three variations of a first design for an azulene-based Nanocar. While the azulene core with its 5- and 7-membered rings represents the motor of the Nanocar and is characterized by a high dipole moment, the lateral groups can further enhance dipole moment and charge separation. Such lateral groups also determine the interaction of the molecules with the Au(111) surface, the interaction with other molecules with the formation of dimers and metal–organic structures, as well as the stability of the molecule upon evaporation.

In the present study we have compared different azulene-core structures, investigating the adsorption on the Au(1111) surface, the formation of molecular structures and the reaction to voltage pulses applied from the STM tip.

This series of investigated molecules provide comparable information about inelastic tunneling electrons manipulation and the important parameters that must be considered for the design of a fast driving Nanocar. The results of the experiments presented in this chapter are qualitatively summarized in Table 1.

As one can see, the presence of a CN group clearly enhance the probability of dimer formation and decomposition. The decoupling from the surface due to the side groups improves the movement on the surface. Charge separation plays a role, however in the larger frame of inelastic tunneling electrons induced movement, where the role of excited electronic states cannot be neglected.

Table 1 Comparison between the different azulene-based structures presented in this chapter

Nanocar	Structure	Metal–organic (MO) dimer formation	Stability upon evaporation	Typical movement pulse parameters
BCA (**1**)	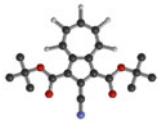	MO dimer formation	Not stable	No movement
BCA dimers (**2**)	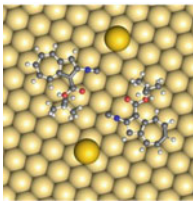	MO dimer formation after dissociation	Not stable	Controllable and reliable movement, V = 1.2 V I = 50 pA
BAC (**4**)	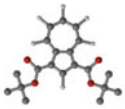	No MO, rare dimer formation	Stable	Translation with rotation V = 1.7 V I = 200 pA
BEA (**5**)	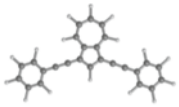	No dimer formation	Stable	Translation in short steps with rotation V = 0.5 V, I = 1.5 nA

The presence of the cyano group reduces the stability without significantly improving the mobility

While the initial hypothesis of maximum dipole moment falls short, a dipole moment increases the probability of dimer formation, where the complexes can be characterized by a strong charge separation. However, a too large dipole moment might favor the cleaving of the molecules during evaporation, since reducing the dipole moment yields an electrostatic energy gain.

Even if the formation of multiple nanostructures with different values of dipole moments can be useful for comparing the movability of similar structures, a successful strategy for Nanocar design should be based on stable compounds.

A delicate balance between stability, high dipole moment, and interaction with the surface should be taken into account for designing and testing novel controllably traveling Nanocars and for understanding the physics beyond the movement of molecules on a surface under the action of inelastic tunneling elections.

For participating to Nanocar Race II, the Dresden GAzE team took into account the results of the present study inserting azulene in a larger stable single molecule

vehicle, where charge separation was a key ingredient for the controlled movement [19].

Acknowledgements This work has received funding from the European Union's Horizon 2020 research and innovation program under the project MEMO, grant agreement No 766864.

The authors thank Oumaima Aiboudi and Franziska Lissel for synthetizing the molecules used in these studies.

References

1. Joachim, C., Rapenne, G.: Molecule concept Nanocars: chassis, wheels, and motors? ACS Nano **7**(1), 11–14 (2013)
2. Rapenne, G., Joachim, C.: The first nanocar race. Nat. Rev. Mater. **2**(6), 17040 (2017)
3. Jacquot de Rouville, H.-P., Kammerer, C., Rapenne, G.: From the synthesis of nanovehicles to participation in the first nanocar race—view from the french team. Molecules **23**(3), 612 (2018)
4. Pawlak, R., et al.: Design and characterization of an electrically powered single molecule on gold. ACS Nano **11**(10), 9930–9940 (2017)
5. Nickel, A., et al.: Moving nanostructures: pulse-induced positioning of supramolecular assemblies. ACS Nano **7**(1), 191–197 (2013)
6. Eisenhut, F., et al.: Training for the 1st international nano-car race: the Dresden molecule-vehicle. Eur. Phys. J. Appl. Phys. **76**(1), 10001 (2016)
7. Robles, R., et al.: Supramolecular chemistry based on 4-acetylbiphenyl on Au(111). Phys. Chem. Chem. Phys. **22**(27), 15208–15213 (2020)
8. Simpson, G.J., et al.: How to build and race a fast nanocar. Nat. Nanotechnol. **12**(7), 604–606 (2017)
9. Eisenhut, F., et al.: One-way rotation of a chemically anchored single molecule-rotor. Nanoscale **13**(38), 16077–16083 (2021)
10. Jasper-Toennies, T., et al.: Rotation of ethoxy and ethyl moieties on a molecular platform on Au(111). ACS Nano **14**(4), 3907–3916 (2020)
11. Stolz, S., et al.: Molecular motor crossing the frontier of classical to quantum tunneling motion. Proc. Natl. Acad. Sci. **117**(26), 14838–14842 (2020)
12. Anderson, A.G.J., Steckler B.M.: Azulene. VIII. A study of the visible absorption spectra and dipole moments of some 1- and 1,3-Substituted Azulenes1,2. J. Am. Chem. Soc. **81**, 4941–4946 (1959)
13. Shoji, T., Ito, S.: Chapter one—the preparation and properties of heteroarylazulenes and hetero-fused azulenes. In: Scriven, E.F.V., Ramsden, C.A., (eds) Advances in Heterocyclic Chemistry (pp. 1–54). Academic Press (2018)
14. Simpson, G.J., et al.: How to control single-molecule rotation. Nat. Commun. **10**(1), 4631 (2019)
15. Kühne, T., et al.: STM induced manipulation of azulene-based molecules and nanostructures: the role of the dipole moment. Nanoscale **12**(48), 24471–24476 (2020)
16. Kim, Y., et al.: Action spectroscopy for single-molecule reactions—experiments and theory. Prog. Surf. Sci. **90**(2), 85–143 (2015)
17. Alemani, M., et al.: Electric field-induced isomerization of Azobenzene by STM. J. Am. Chem. Soc. **128**(45), 14446–14447 (2006)
18. Meyer, J., et al.: Tuning the formation of discrete coordination nanostructures. Chem. Commun. **51**(63), 12621–12624 (2015)
19. Manuscript in preparation

Towards a Molecular Mechanical Calculator

We-Hyo Soe and Christian Joachim

Abstract A planar molecular Pascaline mechanical calculator design is presented based on existing molecule gears which have 6 teeth consisting each of a tert-butyl group at the end of a shaft consisting of a phenyl group. The central phenyl-core is mounted on a single copper ad-atom which is the physical rotation axle on the superconducting Pb(111) surface. In order to construct such a planar molecular calculator, it is essential to realize two key mechanisms: the gearing that is in our design the molecular interlock across a monoatomic step edge and the carry function. Experimental results using the atom/molecule manipulation capability of one low temperature scanning tunneling microscope (LT-STM) of a unique LT-UHV 4-STM instruments demonstrate the feasibility of the above two mechanisms. Experiments with 2.2 nm in diameter large molecule gears are also presented with the same tert-butyl end tooth. They confirm that mutual tert-butyl groups of molecule gears on a terrace with the different heights of the monoatomic step on Pb(111) interlock and gear across the step edge, even if it is imperfect. In addition, experiments using a carry molecule gear containing one shaft with one phenyl group extended also confirmed that the carry mechanism works on the same Pb(111) terrace.

Keywords Molecular Pascaline mechanical calculator · Molecule gear train · Carry molecule gear · Monoatomic stepped surface · LT-UHV 4-STM · Single molecule manipulation

W.-H. Soe · C. Joachim (✉)
Centre d'Elaboration de Matériaux et d'Études Structurales (CEMES), Centre National de la Recherche Scientifique (CNRS), Université de Toulouse, 29 Rue J. Marvig, BP 4347, 31055 Toulouse Cedex, France
e-mail: Christian.joachim@cemes.fr

International Center for Materials Nanoarchitectonics (WPI-MANA), National Institute for Material Sciences (NIMS), 1-1 Namiki, Tsukuba 305-0044, Ibaraki, Japan

© The Author(s), under exclusive license to Springer Nature Switzerland AG 2023

F. Moresco and C. Joachim (eds.), *Single Molecule Mechanics on a Surface*,
Advances in Atom and Single Molecule Machines,
https://doi.org/10.1007/978-3-031-16930-4_8

1 Introduction

Calculators were functioning mechanical and then electromechanical until the first electronic calculators appeared in the mid-1940s. The oldest true mechanical calculator is the Pascaline, built in 1642 by Blaise Pascal in France [1]. The Pascaline was able to perform addition and subtraction by turning a series of gears one after the other. The first quadrature calculator was the Stepped Reckoner (1672–1694), invented by the German mathematician Gottfried Leibniz, which was an improvement on the Pascaline, using the Leibniz wheel to allow also direct multiplications and divisions [2].

Calculating in basis ten, the Pascaline macroscopic mechanical calculator consists of a series of gears with a rachet and carry mechanism per digit to propagate the carry step by step along the machinery using gravity. A planar version of the Pascaline was invented by Jacob Auch in 1790 using a series of springs and a slider to propagate the carry instead of exploiting gravity [3].

To further miniaturize the Auch planar mechanical calculator down the molecular scale, it is very important to avoid gravity for the carry propagation because ultra-miniaturized gears and all the active required machinery to construct a mechanical calculator are becoming almost weightless from a classical mechanics point of view. To appreciate its detail functioning and as presented in Fig. 1, we have constructed the exact replica of the planar Auch calculator using the 3D printing modern technology [4]. The lesson from its good functioning and from the attempts to miniaturize it further using modern optical [5], electronic and He^+ focused ion beam nanolithography [6] is that the Auch slider concept to propagate the carry along the calculator board is not working even at the 100 nm mesoscopic scale.

As a consequence, we have designed first a planar macroscopic mechanical calculator where a slider is not required to propagate the carry along the board. Instead, a

Fig. 1 A planar 20 cm Auch 3-digits Pascaline mechanical calculator constructed using solid-state macroscopic mechanical parts and based on the original 1790 Jacob Auch design

stepped support is used to alternate periodically the calculating gear height relative to the surface in a way for the ratchet to play its role only to the nearest neighbor next gear. As presented in Fig. 2, we have also constructed this mechanical calculator using the 3D printing modern technology. It is working perfectly at the millimeter scale. We have not attempted to beneficiate from the modern optical, electronic and He^+ focused ion beam nanolithography to continue step by step the miniaturization of the Fig. 2 mechanical calculator and jumped directly to the molecular scale as described in this chapter.

Using the Fig. 2 stepped surface concept, we present in the following all the key molecular elements to what we believe will be the smallest possible size mechanical calculator with a carry propagation. Our atomic scale design is presented in Fig. 3. In Sect. 2, we detail the functioning of this Fig. 3 supramolecular machinery and

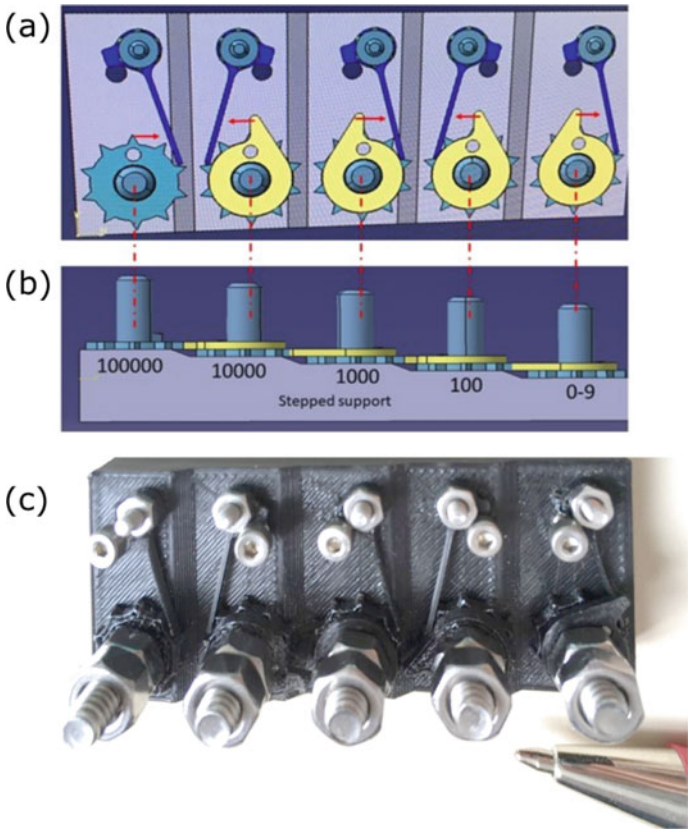

Fig. 2 A new version of the Auch Pascaline mechanical calculator constructed on a stepped support with one gear per stage to avoid the cumbersome miniaturized slider. **a** a top view with the rotation direction of each gear indicated by a red arrow, **b** a cross-section view. The carry is propagating from the right to the left and **c** the 3D printed experimental version of this stepped mechanical calculator 25 mm × 68 nm base dimension using 10 mm solid state gears with 10 teeth each

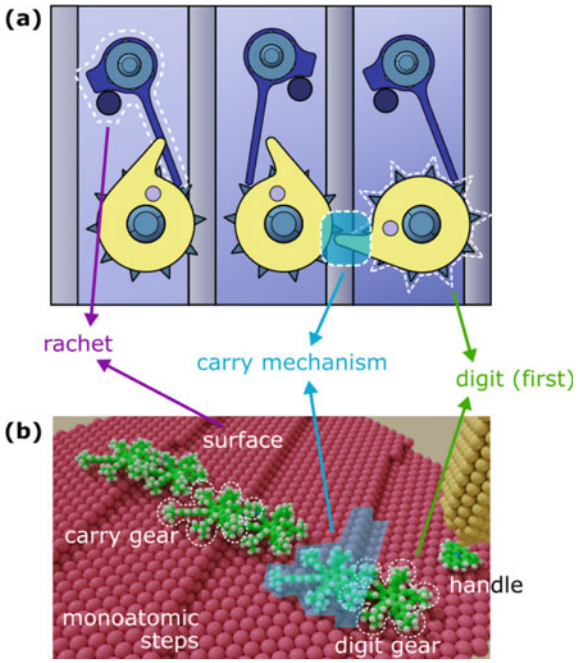

Fig. 3 A 3-digits Pascaline made by molecules on stepped surface. The carry gear molecules are driven in conjunction with the gear molecules of the digits that are entangled across the monatomic steps of the surface, and the carry-up operation is performed on the digit gear molecules that stay on the same terraces. This design is based on the Ref. [7] experimental results of molecule-gear rotation mechanics on a Pb(111) surface

our choice for the molecule-gears. In Sect. 3, we recall the important experimental results obtained recently on the transmission of rotation along a train of molecule-gears up to 3 gears in series on a flat Pb(111) surface. In Sect. 4, we demonstrate experimentally how this rotation propagation can be also obtained on a stepped Pb(111) surface by a good choice of molecule-gears teeth length as proposed in Fig. 3. In Sect. 5, we demonstrate experimentally the propagation of a carry on a flat surface as also required in the Fig. 3 design between each surface atomic step. We concluded by discussing the next steps required to construct a complete planar Pascaline like molecular mechanical calculator.

2 Mechanical Calculator Molecular Design on a Stepped Surface

The functioning on a stepped surface of the Fig. 3 supramolecular machinery for adding numbers decomposed on a basis 6 is as follows (see Fig. 4):

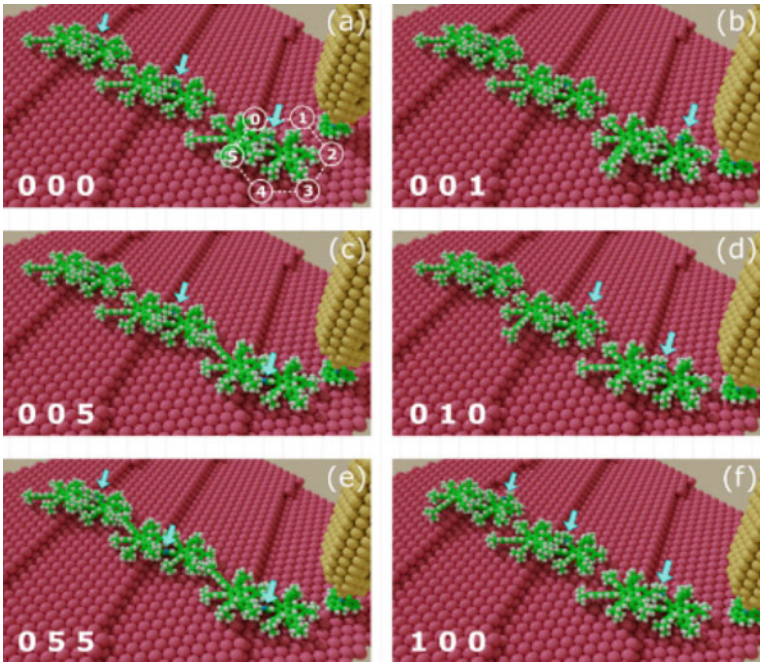

Fig. 4 Operating a molecular Pascaline in base 6. **a** all gear molecules are aligned on the "0" position giving a "000" encoding. The numbers indicated on the hexagon superposed drawing around the first on the right digit molecule are corresponding to the teeth embedded with pyrimidine indicated by light-blue arrows. **b** Encoding "001". Here, a 60° clockwise rotation increments the "1" and the carry molecule gear of the next nearest digit also rotates counterclockwise by 60°. **c–d** is the carry-up functioning passing from "005" to "010". **e–f** is the carry-up operation to reach the "100" result

(1) The molecule gear adsorbed on the lower terrace on the right Fig. 4a is the first digit. It is rotated step-by-step by STM tip molecular manipulations using a small handle molecule which is playing the role of the end of a stylus employed for example at the macroscopic scale to enter the number to be added on a planar J. Auch mechanical calculator [4].
(2) The step by step rotation of this first molecule gear transmits a 1 to 1 rotation to the carry molecule gear located near the step edge of the first upper terrace (see Fig. 4a, b). Here, we are using the experimental results (see below) that it is possible for individual molecule gears to rotate in different monoatomic planes parallel to each other, allowing the carry molecule gear to rotate completely without getting stuck on the surface an in the UHV.
(3) For each 360° revolution of the first digit molecule gear, the molecular tooth of the carry interacts with the second digit molecule gear, adding a "1". (Fig. 4c, d).
(4) Starting from the right, the second molecule gear in the train Fig. 4 connects to the next carry molecule gear located on the next surface atomic step edge. In

that case and for every 36 revolutions of the first digit molecule gear, the third digit molecule gear is rotated one step. (Fig. 4e, f).

In our molecular design, the mechanical ratchet effect (required not to ripple during a carry operation) is operating using a potential minimum per digit on the Pb(111) surface, i.e. a stable station met during the step by step rotation of the molecule gear. This avoids the introduction of a molecular spring per digit as it is required in a macroscopic design where the supporting surface is supposed to be flat to avoid friction (see Fig. 2). The key for the functioning of this planar molecular Pascaline is also the gearing effect across each monoatomic step edge. It is completed by the propagation of the carry between molecule gear belonging to the same terrace.

We have used a series of molecule gears synthesized on purpose and based on the hexa-tert-butyl-pyimidopentaphenylbenzene ($C_{64}N_2H_{76}$, HB-NPB) molecular structure listed in Table 1. We have selected Pb(111) superconducting surface to minimize the electronic friction during the gearing operation and single Cu ad-atoms for each gear-axle. All molecules were deposited at room temperature on the Pb(111) surface just after the UHV clean and atomically flat surface preparation process using multiple cycle of argon-ion sputtering and annealing. Only a small amount of Cu ad-atoms were deposited on the surface Pb(111). To prevent surface intermixing between the Cu ad-atoms and the Pb(111) surface atoms, the evaporation of the Cu atoms was performed after mounting the lead sample on the LT-UHV 4-STM sample stage maintained at LHe temperature. A small gate was installed on the LT-UHV 4-STM cryostat to be able to perform the Cu atoms evaporation.

3 A Molecule Gears Train: Experimental on the Terrace of the Pb(111) Surface

Before examining the key mechanisms of our planar molecular Pascaline, experimental results concerning small and large molecule gears on a Pb(111) surface terrace are recalled in this section. As already indicated in Table 1 (first and second molecules from the left), both molecule-gears can be easily manipulated molecule per molecule on the Pb(111) surface using the STM molecular manipulation technique. Each type of molecule-gears can be also mounted on a target single Cu ad-atom with its central phenyl-core centered on the Cu ad-atom.

As schematically depicted in the first row of Fig. 5, the gearing function is fully carried out only in the small gear molecule pair with an Cu ad-atom axle-to-axle distance of exactly 1.9 nm on the Pb(111) surface as demonstrated experimentally [8]. In Fig. 5 first row, the green molecule gear at the bottom of the train is the handle with no Cu ad-atom axle, the blue molecule gear in the middle is the enforced rotation molecule gear, and the blue molecule at the top end of this molecular train is molecule gear which is rotating as observed experimentally [8].

When now the large in diameter molecule gear are used to perform the same experiments, it leads to two different results depending on the distance between the

Table 1 Gear molecules used in this chapter. From left to right, they are named in the following small gear, large gear, rigid gear, and carry molecule gears. All of them can be manipulated on the Pb(111) surface by STM mechanical molecular manipulation technique. The atomic rotational axle can be constructed using a single Cu ad-atom axle only for molecules having a central phenyl like core. But the construction is much easy for small and carry molecule gears than for large molecule gears. Around a Cu single ad-atom axle, the molecular gearing effect on the Pb(111) surface can be achieved with small gear molecule with success. Conversely, large molecule gears are unable to transmit rotation (see Sect. 3 below). Carry operation is not yet perfect using this Table 1 carry molecule (see Sect. 5)

Pb(111) surface Cu-adatom axle				
manipulation	○	○	○	○
construction	○	○	×	○
easiness	○	△	—	○
gearing	○	×	—	△

Cu ad-atom axles but both of which are unsuccessful. On the Fig. 5 second row and when this axle-to-axle distance is 2.5 nm or less, two gearing molecules are too closed together and the handle molecule gear is simply rotating around the first molecule gear on the train like a "rack-and-pinon" machinery [7]. When now the distance Cu ad-atom axle distance is 2.6 nm or greater, the two molecule gears of this short train are too far to be engaged in a gearing effect and only the first gear molecule is rotated by the handle molecule gear as presented in the bottom row of Fig. 3 [7].

Notice that according to those results which guide us to select the best molecule gears for the on-terrace transfer of rotation (see Fig. 4), an axle-to-axle distance of 2.5 nm appears to be optimal for gearing between two large molecule gears. However, this reasoning is valid only for a rigid body machinery. Even physisorbed on the Pb(111) surface and due to the mechanical flexibility of the molecules, the gear tooth deform and slide before some potential energy can be transferred from one molecule gear to the other for a collective rotation. There is here a competition between the surface stabilization which is supposed to avoid such mechanical deformation and the fact that when a molecular tooth is starting to enter even in a van der Waals interactions with the teeth of the next molecule gear, part of the interaction energy is distributed to other internal mechanical degrees of freedom of both molecules instead of contributing to pass over the rotation barriers.

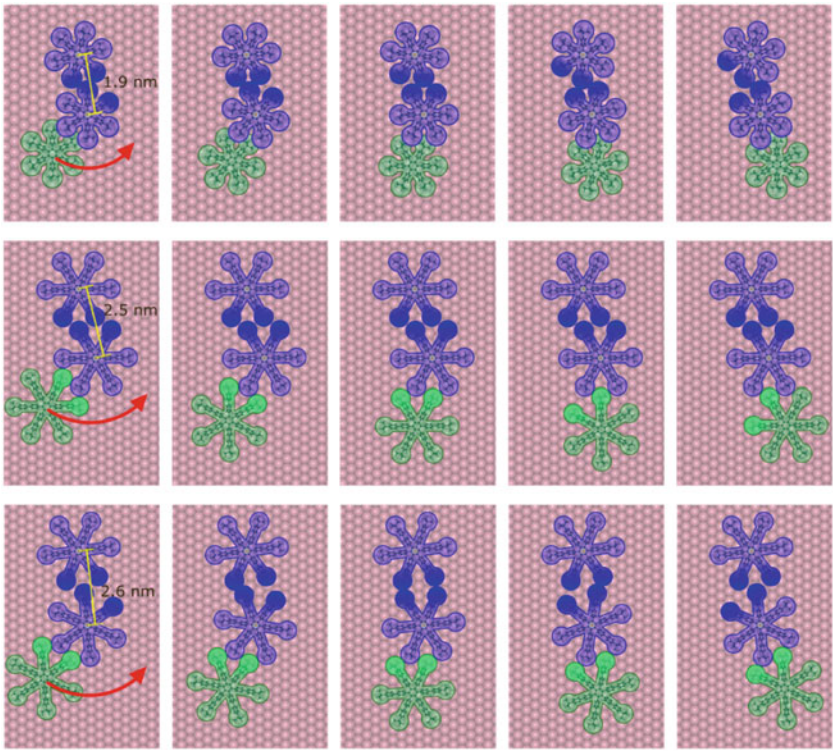

Fig. 5 A schematic overview of molecular gearing experimental results [7, 8]. The molecule gears colored in blue are mounted on their single Cu ad-atom axles, and the molecule gears colored in green are handles, driven directly by the STM tip to mechanically rotate the central first molecule gear. The first row shows the successful gearing rotation of the small gear system when the axle-to-axle distance of exactly 1.9 nm. The second and third rows present the case of the large molecule gear train. When the axle-to-axle distance is 2.5 nm (second row), the two-molecule gear train hook each other and the handle molecule rotates around the first molecule gear molecule. When the axle-to-axle distance is 2.6 nm (third row), the handle molecule rotates the first molecule gear, but the second one cannot be driven at this distance, so it stays in the same minimum potential energy state on the Pb(111) surface

One way to avoid this phenomenon is to use rigid molecule gears. We have for example tried molecule gears with a central HBC-core (3rd molecule from the left in Table 1). Unfortunately, those molecules were not able to be mounted centered on a single Cu ad-atom on the Pb(111) surface. With no success, we have also tried single Co ad-atom axles on a Ag(111) surface because of the lower Co adsorption height on the Ag(111) surface.

Our interpretation of the difficulties to use single metallic ad-atom as a rotation axle for an HBC core as compared to a phenyl core is that HBC is the first member of a series of molecules leading step by step to nanographene like molecules. In that case, the number of p_z orbitals of the core molecular skeleton is increasing the

molecule interactions with the metal surface as compared to a simple central phenyl core. As a consequence, the molecular core-surface distance is reduced for HBC as compared to phenyl leading to an adsorption minimum energy configuration with its metal axle ad-atom no more centered at the axle of rotation and very often positioned at the border of the core [9].

4 Experimental Molecular Gearing Effect Across a Monoatomic Step Edge

After having recall how the transmission of rotation between molecule gears on the same flat terrace (Fig. 4, from Fig. 4c, d and Fig. 5) was demonstrated experimentally using an adapted molecule gear size, the Fig. 3 proposed design requires also the transmission of rotation between two molecule gear one located on the lower and the other on the upper terrace of a monoatomic stepped surface. For this purpose, at least the tert-butyl part of the molecule gear on the upper terrace has to overhung the step edge to interact with teeth of the molecule gear positioned on the lower terrace.

As presented in Fig. 6 and when the smallest molecule gear given in Table 1 is employed for this construct with a van der Waals diameter of about 1.2 nm, the upper terrace Cu axle ad-atom has to be positioned just at the border of the step edge. At this location, the molecule gear is not sufficiently stable for a rotation. As a consequence, the Table 1 large molecule gear was used for demonstrating how a step by step rotation can be transferred across a monoatomic step edge on the Pb(111) surface.

As presented in Fig. 7a, b and after having located the required single Cu ad-atoms on the upper and lower terraces for the respective rotation axle to be well positioned, it is possible to construct by LT -STM molecular manipulation the Fig. 6 molecular machinery using 2 large molecule gears. In this configuration and as shown from Fig. 7e, f, the rotation of the first molecule gear of the train, located on the upper terrace, propagates to the second one located on the lower terrace with the help of a non-Cu mounted handle molecule for pushing on the upper terrace molecule gear. This is a generalization of the mechanics of gearing functioning used at the macroscopic scale (Fig. 2) even if the molecule-gears are here not perfectly rigid. It is the supporting surface which is stabilizing the step by step rotation across the monoatomic step edge.

5 Experimentations on the Carry Propagation

The next step to experimentally test the Fig. 3 planar design is the functioning of a molecular carry mechanics on an atomically flat terrace. Carry molecules are molecule gears with one tooth longer than the others: here a biphenyl as indicated in

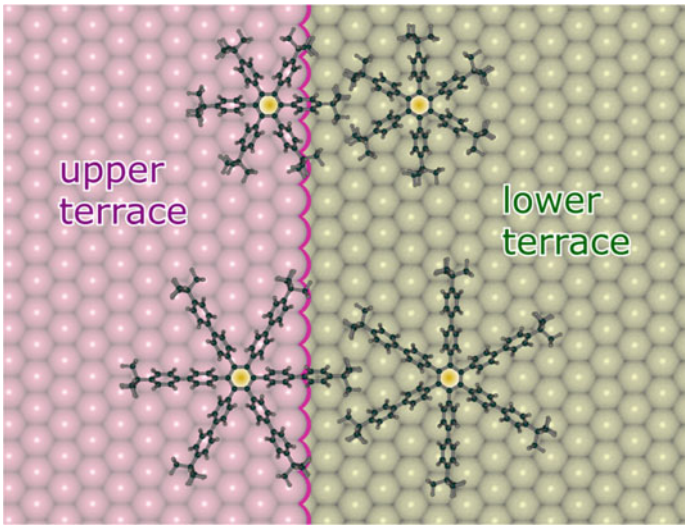

Fig. 6 Top view of gearing molecules across a monoatomic step edge. The size of the molecules and the lattice constant of the Pb(111) fcc surface are in the same ratio as the actual size. The positions of the center of the molecule gears, i.e. Cu ad-atom positions are chosen on the hollow-sites of the fcc surface. For the small molecule gear case, the Cu ad-atom axle is exactly at the last hollow site at the Pb(111) monoatomic step edge, a not very stable position for a centered rotation

Table 1 and presented in more details in Fig. 8. It must behave almost like a small molecule gear under STM molecular manipulations, i.e. easy to be LT-UHV STM tip manipulated on the Pb(111) surface and easy to be mounted on a single Cu ad-atom to ensure a stable rotation axle.

The carry movement must propagate from the biphenyl tooth of the carry molecule gear to the monophenyl teeth of the counting molecule gear. The optimum single Cu ad-atoms axle-to-axle distance for a carry operation to function properly is (2.5 nm + 1.9 nm)/2 = 2.2 nm because it is exactly halfway between the optimal gearing distance for large molecule gear and that of small molecule gears as presented in Fig. 8.

For a successful propagation of the carry and while the first carry molecule makes its one step carry rotation, the second molecule must not rotate except during its engagement with the biphenyl tooth of carry molecule. To test experimentally this functioning, the initial mechanical configuration was built as presented in Fig. 9a. Here, the Cu axle-to-axle distance is exactly 2.2 nm. The bottom-carry molecule is the molecule whose rotational motion is induced by STM molecule manipulation using the small handle molecule presented Fig. 9h. This handle molecule is necessary to prevent the direct interactions between the STM tip and this first molecule-gear. If not, there is a large probability that this first molecule gear goes off-axis.

Another carry molecule may have been used as an handle. But such a carry-carry supramolecular system is prone to instability because the biphenyl tooth (belonging either to the carry handle molecule or to the first carry molecule) can easily become

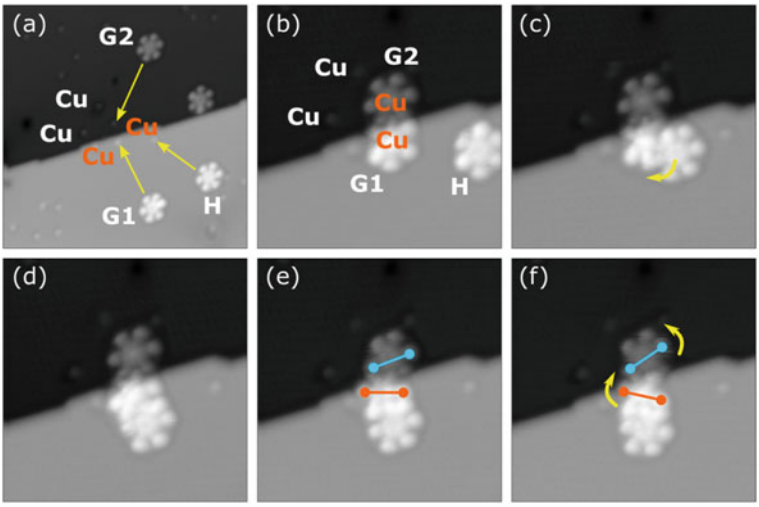

Fig. 7 The gearing experiments between the two large gear molecules across a monoatomic step edge on Pb(111). **a** and **b** LT-UHV STM construction sequence on the LT-UHV 4-STM along a Pb(111) monoatomic step edge. The machinery was constructed by first identifying two Cu adatoms with the adapted Cu-Cu interatomic distance relative to the step edge location. **c–d** only the first molecule (on the upper terrace near the step edge and previously on a Cu rotation axle) rotates and is then dismounted from its Cu axle. **d–e** second molecule (on the lower terrace) that is also dismounted from its Cu axle by the constraint of the first molecule rotation. **e–f** the first gear rotation on the upper terrace is transmitted to a second gear, whose angle of rotation is around 15° [7]. Image sizes: (**a**) 30 nm × 30 nm, and (**b–f**) 15 nm × 15 nm. Reused from our Ref. [7] with permission: copyright 2020, American Chemical Society

entangled with other molecules by van der Waals interactions. The presence of the biphenyl carry tooth also limits the flexibility of the mounting location for operating a three-carry molecular train. For these reasons, the small triangular nitrogen-centered polycyclic $C_{21}NH_{15}$ molecule (Fig. 7h) was employed as the molecular handle.

The first two operations coming from the first (bottom) carry molecule (Fig. 9 from a to b and from b to c) resulted in a rotation of 2 steps of 60° each without any rotation of the second (top) carry molecule. The third operation (Fig. 9c, d) results in a rotation of 90° of the first carry molecule. This is due to the fact that after a first 60° rotation, as in the first two rotation steps, the tert-butyl tooth at the end of the biphenyl shaft get close enough to the top second carry molecule to be van der Waals attracted by it which is inducing 30° more rotation of this first carry molecule.

The next rotation (Fig. 9 from d (also e) to f) leads to the carry operation. In the Fig. 9 presented case, the carry was successfully transferred to the next molecule gear. Here and as discussed above a small $C_{21}NH_{15}$ handle molecule was used to avoid any destabilization of this machinery induced by the STM tip apex.

However, and this stage, the tert-butyl tooth for carry transmission was trapped in a van der Waals well and blocked. As indicated in Fig. 9, even the usage again of the small $C_{21}NH_{15}$ handle molecule was not enough to go from Fig. 9f, g. In order

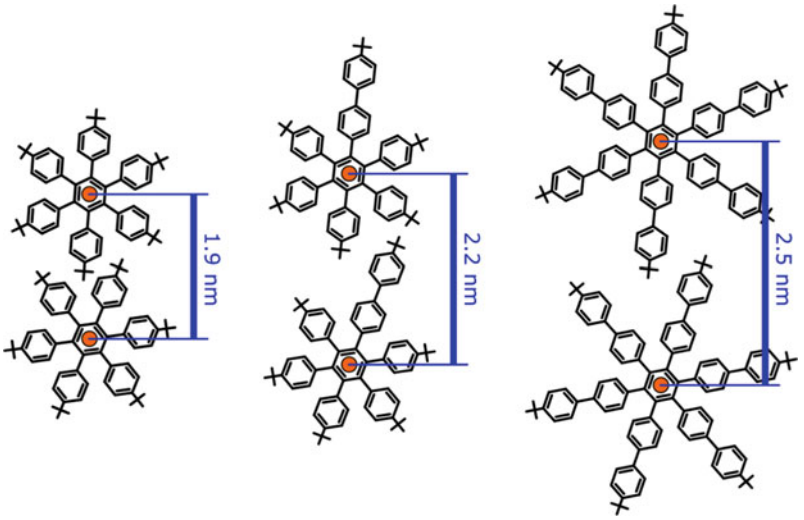

Fig. 8 Optimum Cu axle-to-axle distances for an intermolecular transmission of rotation. Distance for carry propagation (middle) was estimated from nearly C6 symmetric small (left) and large (right) molecule gears tested experimentally as discussed in Sect. 4

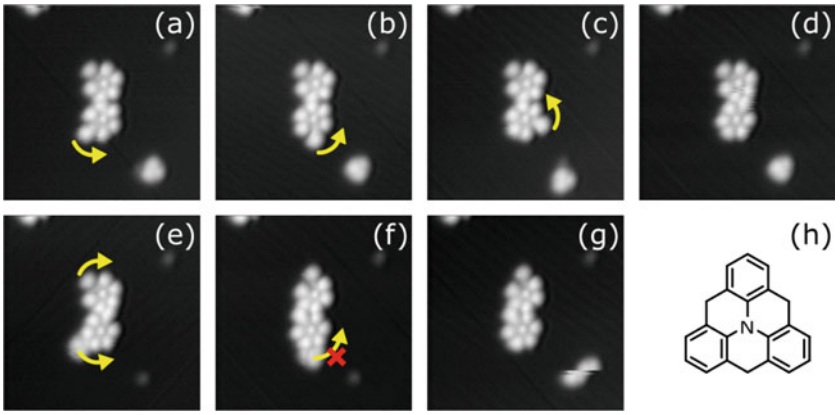

Fig. 9 A sequence of carry propagation operation in the carry molecules machinery with an inter-axle distance of 2.2 nm. Lower molecule was rotated using a small handle molecule by LT-UHV STM mechanical manipulation on Pb(111). The carry propagation to upper molecule can be verified between (**e**) and (**f**). All image sizes are 12 nm × 12 nm

to disentangle the carry tooth from the teeth of the second top carry molecule, this first carry molecule had to be rotated 90° at once.

To improve the carry propagation, we have also increased the axle-to-axle distance in a way to lower the van der Waals interactions between the carry molecules. Carry propagation experiments were conducted in the same way as presented in Fig. 9 but

with a larger 2.6 nm axle-to-axle distance. In this case, the 2 carry molecule gears appear to be too far apart to transmit a rotational movement from one to the next.

Notice that when imaging a molecule using an STM in constant current mode, the tip height is adjusted to consider not only the pixel-sized channel path perpendicular to the surface, but also the tunneling current flowing through the laterally open tunnel channels, especially when scanning at the border of the molecule. This leads to the fact that the image size of a molecule in STM is always larger (about 45%) as compared to its actual van der Waals lateral dimension. This is presented in Fig. 10a where the skeleton of carry molecules has been superposed to STM image.

Surprisingly and as presented in Fig. 10a, b, the biphenyl tooth of the first carry molecule is able to trigger the rotation of the second molecule gear due to the weak lateral van der Waals interactions, even though it was center to center 2.6 nm away from the second carry molecule-gear. Those interactions are not screened by the superconducting Pb(111) surface. As the molecular skeleton positioning is indicating in Fig. 10a, there is no direct physical (repulsive) contact between the 2 molecule gears. More important for the functioning our calculator, this is a one-way propagation working only when the first carry molecule gear is turned clockwise (a, b). It is not working while rotating counterclockwise (c–d).

Of course, the ground state potential energy surfaces governing the obtained rotations is multi-dimensional. The presented Fig. 11 one dimensional potential energy

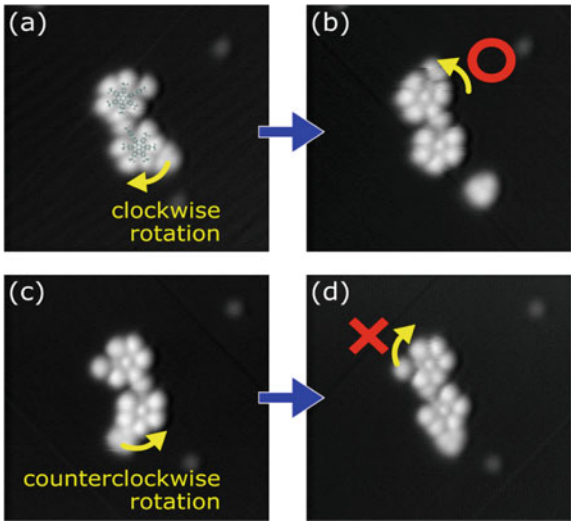

Fig. 10 Before and after the rotation expected carry propagation at the axle-to-axle distance of 2.6 nm. From (**a**) to (**b**), clockwise rotation was initiated in lower carry molecule and it was transmitted to upper carry molecule. On the other hand, counterclockwise rotation was not transferred as observed from (**c**) to (**d**). Skeleton molecular models adjusted its size to match image size are overlapped on each molecule image in (**a**). All image sizes are 12 nm × 12 nm

curves can be considered as the effective minimum energy path on those multi-dimensional surfaces. In Fig. 11 and to make it easier to illustrate the discussion, a molecule gear having a quasi-six-fold symmetry is considered instead of a carry molecule gear.

A first interpretation of the easy clockwise and not working counterclockwise rotation is that there is a difference in the slope of the effective potential energy curve governing this rotation while comparing the two rotation directions as illustrated in Fig. 11b. Even assuming that the tert-butyl teeth are symmetrical with respect to the surface vertical, each phenyl group on a shaft adopts a tilted conformation, still maintaining an almost horizontal orientation relative to the Pb(111) surface (Fig. 11a). Therefore, on an atomically rugged surface and when this phenyl group is slightly changing its orientation due to the rotation of the central phenyl, it is expected that its effective potential energy in the counterclockwise direction shows a deeper slope as a function the central phenyl rotation angle than in the clockwise direction leading to the observed ratchet effect. As a consequence, and in counterclockwise direction, the molecule gear is deformed and slip through before the applied force for rotation can result into a true rotational motion of the molecule gear round its central Cu adatom axle.

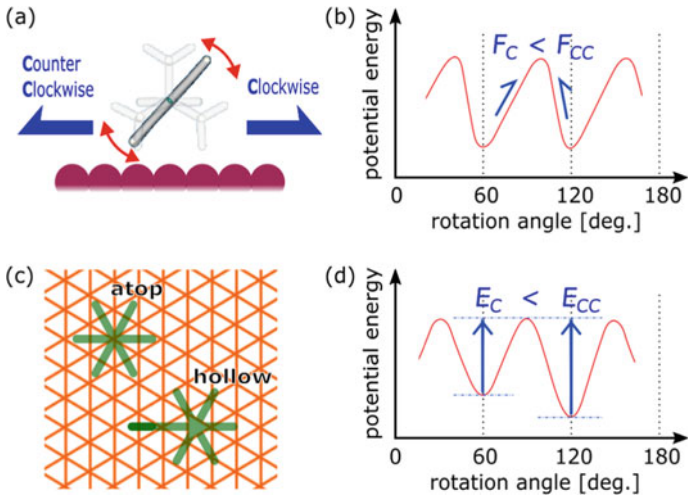

Fig. 11 Two possible interpretations of why carry works in only one direction. **a** Partial view of molecule conformation on the surface from the side. The phenyl groups on the shaft have a preferred deformation direction on the surface, which creates (**b**) a difference in effective one-dimensional potential energy curve gradient during its rotation. Difference in potential energy gradients appear as differences in driving forces, and direction that cannot be moved by van der Waals force appears. **c** Since the rotational axis of the gear consists of Cu ad-atom on the fcc(111) metallic surface, the molecule gears are adsorbed on a threefold symmetry surface location (hollow-site) on the six-fold Pb(111) symmetry surface. Therefore, each individual tooth and its shaft go through two different configurations every 60° of rotation. When the minimum potential energy of these two configurations are different, it results a different apparent potential energy barrier height (**d**)

A second possible explanation of this ratchet like effect is that the stable stations potential energy minima on the multi-dimensional ground state potential energy surface vary in energy depth depending on the orientation of the molecule gear on the Pb(111) surface. The molecule gear is flexible and tries to adopt a stable configuration as a function of the rotation angle of the central phenyl by slightly changing the position and angle of its tert-butyl teeth and its phenyl group on the shaft during this rotation. When a molecule gear with its six-fold symmetry is adsorbed on a six-fold symmetry central point of an fcc(111) surface, i.e. on an atop-site, it remains at a similar minimum potential energy value after a 60° rotation. This situation remains the same for a 1C symmetric molecule such as a carry molecule gear, since the effect is due to the symmetry of the surface. However, when a carry molecule gear adsorbs on a three-fold symmetry point of the surface, i.e. on a hollow-site, the carry tooth has to go through two different configurations for every 60° of rotation of the central phenyl as illustrated in Fig. 11c. In addition, two of the other five teeth are exploring two different configurations at the same time. The sum up of the potential energy changes of the individual teeth resulting from this difference in configuration leads to a difference in the effective 1D potential energy barrier as described in Fig. 11d.

Such a carry mechanism that works like a ratchet only in one direction is a very important property of our design for the functioning of a mechanical calculator. It opens the way to complete a simple summation of plus "11" in two operations only, one for first digit and one for tens digit, instead of repeating plus "1" 11 times for first digit. It also avoids the back rotation of the carry which at the macroscopic level is requiring specific supplementary mechanical elements per digit (see Figs. 1 and 2), supplementary element which will be very difficult to add up in a molecular design.

6 Conclusion

On a stepped atomic scale surface, we have first presented the design of a planar supramolecular machinery with its molecular structure constituted of a short train of molecule gears and carry molecule gears per digit able to add up numbers in basis six while the analogue inputs are performed on this structure using the tip apex of an STM as a stylus. We went a step further and explored experimentally how the different molecular mechanisms required for addition and carry transmission along this supramolecular train of gears are functioning mechanically. The basic chemical structure of the our elementary molecule gears is a 1.2 nm in diameter molecule with a central phenyl and 6 molecular teeth mounted on a single Cu ad-atom rotation axle. All the experiments were performed at very low temperature on a stepped atomically prepared Pb(111) surface using one STM of our very unique LT-UHV 4-STM. We have demonstrated that a carry can be transferred from one digit to the next but is rapidly stuck due to van dear Waals entanglements of the carry molecule molecular tooth. New molecule gears have now to be designed for the carry to propagate along the carry molecule gear train, a problem which have been solved by B. Pascal and

J. Auch in the seventeenth and eighteenth centuries at the macroscopic scale using millimeters in diameter wood and metal gears.

Acknowledgements We thank Dr. M. Kleinwächter, Y. Gisbert, C. Kammerer, and A. Gourdon for having kindly provided to us the molecules used in this study, and the European Union Horizon 2020 FET open project "Mechanics with Molecule(s)" (MEMO, grant 766864) for financial support during this work.

References

1. Martin, E.: The calculating machines. In: Charles Babbage Institute Reprint Series for the History of Computing (vol. XVI, pp. 33–38) (1992). ISBN 978-0-262-13278-7
2. Martin, E.: The calculating machines. In: Charles Babbage Institute reprint series for the History of Computing (vol. XVI, pp. 38–42) (1992). ISBN 978-0-262-13278-7
3. Martin, E.: The Calculating Machines. In: Charles Babbage Institute reprint series for the History of Computing (vol. XVI, pp. 52–53) (1992). ISBN 978-0-262-13278-7
4. Abheillou, P., Gatti, B., Froissard, K., Joachim, N., Joachim, C.: From the Pascaline to a 5-digits metallic and planner miniature mechanical calculator 1 cm in Lateral Size. In: Building and Probing for Mechanics (vol. XII, pp. 9–20). Springer Series: Advances in Atom and Single Molecule Machines (2020). ISBN 978-3-030-56776-7
5. Bourgerette, C., Noé, L., Pinaud, S., Joachim, C.: Photo-Microlithography fabrication of the parts of a micro-mechanical calculator. In: Building and Probing Small for Mechanics (vol. XII, pp. 21–39). Springer Series: Advances in Atom and Single Molecule Machines (2020). ISBN 978–3–030–56776–7.
6. Mailly, D., Faini, G.: Fabricating solid state gears at the Nanoscale: a top-down. In: Building and Probing Small for Mechanics (vol. XII, pp. 41–63). Springer Series: Advances in Atom and Single Molecule Machines (2020). ISBN 978–3–030–56776–7.
7. Soe, W.-H., Kleinwächter, M., Kammerer, C., Rapenne, G., Joachim, C.: Mechanics of molecule-gears with six long theeth. J. Phys. Chem. C **124**, 22625–22630 (2020)
8. Soe, W.-H., Srivastava, S., Joachim, C.: Train of single molecule-gears. J. Phys. Chem. Lett. **10**, 6462–6467 (2019)
9. Calmettes, B., Vernisse, L., Guillermet, O., Benjalal, Y., Bouju, X., Coudret, C., Coratger, R.: Observation and manipulation of hexa-adamantyl-hexa-benzocoronene molecules by low temperature scanning tunneling microscopy. Phys. Chem. Chem. Phys. **16**, 22903–22912 (2014)

Atomistic Modelling of Energy Dissipation in Nanoscale Gears

Huang-Hsiang Lin, Alexander Croy, Rafael Gutierrez, and Gianaurelio Cuniberti

Abstract Molecule- and solid-state gears build the elementary constituents of nanoscale mechanical machineries. Recent experimental advances in fabrication technologies in the field have strongly contributed to better delineate the roadmap towards the ultimate goal of engineering molecular-scale mechanical devices. To complement experimental studies, computer simulations play an invaluable role, since they allow to address, with atomistic resolution, various fundamental issues such as the transmission of angular momentum in nanoscale gear trains and the mechanisms of energy dissipation at such length scales. We review in this chapter our work addressing the latter problem. Our computational approach is based on classical atomistic Molecular Dynamics simulations. Two basic problems are discussed: (i) the dominant energy dissipation channels of a rotating solid-state nanogear adsorbed on a surface, and (ii) the transmission of rotational motion and frictional processes in a heterogeneous gear pair consisting of a graphene nanodisk and a molecular-scale gear.

Keywords Classical molecular dynamics · Molecule gears · Solid-state gears · Friction · Dissipation

1 Introduction

The increasing demands on the miniaturization of digital and analog devices has led to a proliferation of studies aiming at designing efficient strategies to reduce physical dimensions of the device's building blocks while still preserving their basic functionalities. While such approaches have been extensively developed and refined in the domain of electronic devices—following both top-down and bottom-up strategies—less work has been invested in the investigation of truly nanoscale mechanical systems

H.-H. Lin · A. Croy · R. Gutierrez (✉) · G. Cuniberti
Institute for Materials Science and Max Bergmann Center of Biomaterials, TU Dresden, 01069 Dresden, Germany
e-mail: rafael.gutierrez@tu-dresden.de

© The Author(s), under exclusive license to Springer Nature Switzerland AG 2023

F. Moresco and C. Joachim (eds.), *Single Molecule Mechanics on a Surface*,
Advances in Atom and Single Molecule Machines,
https://doi.org/10.1007/978-3-031-16930-4_9

with basic components consisting of molecular [1–3] or solid-state nanogears [4]. The most recent advances in fabrication techniques in this field, including bottom-up approaches [5, 6] as well as top-down methods such as focused ion beams [1] or electron beams [2, 7] point, however, in a very promising direction. In this context, there are several general issues, which play an important role in determining the feasibility of a roadmap leading to the fabrication of nanoscale analog devices based on gear trains: (1) the capability of transmitting angular momentum along gear trains, (2) the energy dissipation mechanisms from gear systems into the environment, (3) the atomistic features of the interface between solid-state nanogears and molecule gears, (4) the possible improvement of angular momentum transmission in nanoscale gear trains mediated by lubricants, and (5) the triggering of a rotation at the level of single molecule gears.

In this chapter we will focus on different aspects related to items (2) and (3) using representative nanogear systems. Studies related to item (1) in molecule gear trains have been previously presented in e.g. [8–12]. The influence of lubricants in nanoscale solid-state gears has been recently studied in [13, 14]. Work related to item (5) is, on the contrary, scarce, see e.g. Refs. [15, 16].

Concerning item (2), it is well-established that the friction laws known from macroscopic systems cannot, in general, be extrapolated to nanoscale systems [17–22], and this has lead to a large number of experimental [23–27] and model-based [28–31] investigations. In general terms, two qualitatively different friction regimes have been identified, which depend on the center-of-mass velocity: (a) a low-speed, stochastic regime ($v \ll 1000\,\mathrm{cm/s}$) [32], where the system is close to thermal equilibrium and friction is governed by Brownian motion, (b) a high-speed, viscous regime [31, 32], where the system is out of equilibrium and friction is proportional to the number of collisions with surface corrugations per unit time [31]. However, in the case of rotational motion, it is not immediately obvious if a clear separation of stochastic and viscous regimes is possible, since high tangential velocity (outer) and low tangential velocity (inner) atoms in a nanoscale gear are present at the same time and the motion of both sets is correlated. Additionally, for molecule gears as well as nanoscale solid-state gears, energy dissipation into internal degrees of freedom due to the larger conformational flexibility of the gears (compared with their macroscopic counterparts) can play a non-negligible role. For the development of truly nanoscale mechanical machines it is also of interest to address not only the transmission of rotational motion between gears of the same type (either solid-state or molecule gears), but also the interaction of gears with different sizes and different materials (item (3) above). A typical situation would be that of a solid-state nanogear coupled to a molecule gear. The transmission of rotational motion in such a situation is by far not obvious: molecule gears are rather flexible and energy can be dissipated into internal degrees of freedom. Moreover, the contact interface of both gears will have atomic resolution and, therefore, may require a very careful design to ensure good interlocking. Still, recent progress in the miniaturization of solid states gears down to the nanoscale [1–3, 7] is calling for the study of gear trains and of the transfer of rotation over different length scales. We may have been thus reaching the experimental stage where a single molecule gear (with diameter $\sim$1 nm)

[33] can be rotated by a solid state nanogear (diameter ∼10 nm) [2, 3]. Rotation of single molecule gears [33–37] or short molecule gear trains [38–40] has already been experimentally demonstrated. Building nanoscale devices where the transmission of angular momentum across gears with different sizes becomes feasible, poses many challenges to the experimentalist [4]: achieving gear thickness compatibility, the surface preservation with atomistic resolution after transferring the solid state nanogear on it, the mechanical stability of the rotational axle, and last but not least the triggering of the rotational motion and its transmission to gears of different size and composition.

This chapter is organized as follows: in Sect. 2, we describe briefly the basic Molecular Dynamics simulation details for the three different model systems we are going to discuss in Sect. 3. The latter includes, whenever necessary, more specific information on the simulation details. In Sect. 3.1, we study the energy dissipation mechanism in a setup consisting of a nanoscale solid-state gear adsorbed on different substrates. In Sect. 3.2 the rotational transmission between a graphene nanodisk and a molecule gear deposited on a Cu surface is addressed, together with an estimate of the vibrational and electronic contributions to rotational friction. The chapter ends with a summary of the results and an outlook in Sect. 4.

2 Simulation Methodology

For all the simulations presented here we have used the Large-scale Atomic/Molecular Massively Parallel Simulator (LAMMPS) software [41]. The choice of the corresponding classical force fields is, however, dependent on the specific system setup and is briefly described in the following:

1. For the solid-state diamond gear on SiO_2 substrates (Sect. 3.1), we use the Tersoff potential [42] in the SiO_2 bulk, whereas the adaptive intermolecular reactive empirical bond order (AIREBO) potential [43] was chosen for the carbon subsystem (gear). The coupling between both subsystems was assumed to be a non-bonding 12-6 Lennard-Jones type of potential. The corresponding parameters are given in Ref. [44]. When using a graphene substrate for comparison, the AIREBO potential was also used for the surface.
2. The interaction between a graphene nanodisk and a molecule gear on a Cu substrate (Sect. 3.2) was treated via the Reactive Force Field (ReaxFF) [41]. The upper two Cu layers were coupled to a Nosé-Hoover thermostat [45, 46] to fix a generic temperature $T = 10\,\mathrm{K}$, which is of similar order as that from low-temperature STM experiments. To define corresponding collective rotational variables out of the gear atomistic conformations we exploited the nearly rigid-body approximation (NRBA), see Refs. [8, 47] for technical details.

3 Results

3.1 Diamond Solid-State Gear on Substrates

In this section we will investigate a solid-state diamond nanogear physisorbed on different substrates. Our aim is to elucidate the dependence of the energy dissipation via friction on the type of substrate. Using classical MD simulations allow us to reach the relevant time scales in the range of 100 ps up to 1 ns [48]. In the first case, we consider a system consisting of a diamond-based solid state gear (radius $r = 5$ nm and thickness 9.8 Å) with involute profile [49] on top of an α-cristobalite $SiO_2(001)$ surface. The size of the substrate is 23.0 nm × 15.3 nm × 1.39 nm and we use periodic boundary conditions in x and y directions. The initial vertical separation between gear and substrate is 2.5 Å and, for preventing lateral and vertical motion the bottom layer of the substrate was fixed while the remaining part was allowed to structurally relax. For the sake of comparison, we have also used two additional substrates: amorphous SiO_2 and graphene.

Viscous dissipation limit.—We first address the typical time scales associated with the friction process. Taking into account that the atoms within a rotating gear have large tangential velocities, it is reasonable to expect that we are in the same frictional regime as for linear friction with high translation velocity [31]. Therefore, ignoring any applied external torque, the gear dynamics in the high friction limit will be described by a first order differential equation for the angular velocity ω:

$$I\dot{\omega} + \gamma\omega = 0, \tag{1}$$

where γ is the damping coefficient and I is the gear moment of inertia. From this equation we immediately obtain an exponential decay of the velocity with relaxation time given by $\tau_{rel} = \gamma/I$. In the frame of our MD simulations, we give an initial angular velocity to the gear and monitor its decay in time, expecting to find the exponential behavior obtained from Eq. (1), which in this case would result from the van-der-Waals interactions between the gear and the substrate at a given temperature. The results are displayed in Fig. 1 for different initial angular velocities $\omega_0 = 0.1$, 0.15 and 0.2 rad/ps and for an MD run of 100 ps. Notice that in the figure, we have plotted $\omega(t)$ scaled with the corresponding value of ω_0. It becomes apparent that the relaxation process does not sensitively depend on ω_0 and it displays (up to small fluctuations for small initial angular velocity) the expected exponential decay as a function of time. Fitting the obtained curves in the interval from 0 to 50 ps (highlighted in yellow in the figure) to a single exponential allows to obtain the corresponding relaxation times $\tau_{rel} = 59$, 55 and 56 ps for $\omega_0 = 0.1$, 0.15 and 0.2 rad/ps, respectively. Another interesting result is that for the used gear radius of 5 nm the dynamics is that of a deterministic rotor rather than a Brownian rotor, since stochastic fluctuations are increasingly suppressed with increasing gear size.

Substrate dependence of the angular velocity relaxation.—To better understand the influence of a specific substrate on the relaxation process, we carried out MD simu-

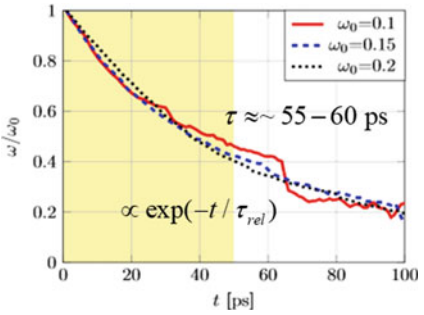

Fig. 1 The normalized angular velocity relaxation of a 5 nm diamond gear on top of α-cristobalite SiO_2. The initial angular velocities were $\omega = 0.1, 0.15$ and 0.2 rad/ps. The highlighted yellow region (from 0 to 50 ps) was used for extracting the velocity relaxation time τ by fitting to an exponential function $\propto e^{-t/\tau}$. Figure is reproduced from Ref. [50] Open Access under a CC BY 4.0 license, https://creativecommons.org/licenses/by/4.0/

lations over 100 ps at $T = 10$ K with initial angular velocity $\omega_0 = 0.2$ rad/ps on three different substrates: crystalline SiO_2, amorphous SiO_2, and graphene, see Fig. 2a–c. Besides the different substrates, we have also considered gears with three different diameters: 3, 4, and 5 nm. The results showing the relaxation of the angular velocity for different substrates and gear sizes are shown in Fig. 2d–f. It becomes clear from the figures that decreasing the gear radius leads in general to an increase of the angular velocity fluctuations, especially for α-cristobalite and amorphous SiO_2, although the effect is less pronounced for the graphene substrate. The origin of this behavior is that a reduction in gear size implies a reduction of the rotational kinetic energy, so that the gear will be more sensitive to surface vibrations, entering the low average tangential velocity dissipation regime where Brownian behavior becomes dominant. A further analysis of the relaxation times τ_{rel} [44] shows that for crystalline SiO_2 (and even more for graphene) τ_{rel} is approximately gear-size independent, while for amorphous SiO_2 τ_{rel} becomes smaller with decreasing gear size. This behavior is related to the decreasing degree of surface corrugation when going from amorphous SiO_2 to crystalline SiO_2 and to graphene.

Scrutinizing surface phonon excitations.—Although part of the rotational kinetic energy is dissipated into internal degrees of freedom of the gear [44], the major dissipation channel is related to the excitation of surface vibrations. It is, therefore, interesting to see how the energy dissipation is modified when the thickness d of the relaxed layer is changed (note that the overall thickness of the substrate in the simulations is always the same, only the thickness of the fixed layer is varied). The results for the crystalline SiO_2 substrate are shown in Fig. 3a. One can see that with increasing d the angular velocity relaxation time τ_{rel} becomes shorter (i.e., faster exponential decay). However, for larger d there is a tendency of the decay rate to saturate.

A deeper understanding of the energy dissipation process can be gained by analyzing the kinetic energy spectrum $K(\nu)$ [51, 52] as given by:

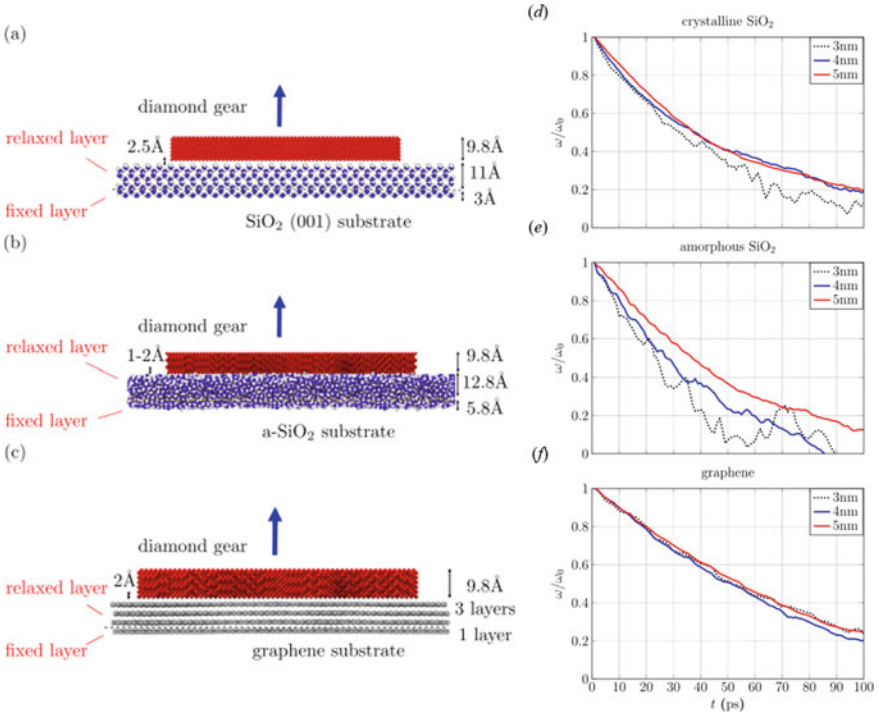

Fig. 2 Scheme of the 5 nm diamond-based solid-state gear on top of the **a** α-cristobalite SiO_2 with size 23.0 nm × 15.3 nm × 1.39 nm and gear-substrate distance 2.5 Å; **b** amorphous SiO_2 (28.2 nm × 16.9 nm × 1.86 nm) and gear-substrate distance ∼1–2 Å, and **c** 4-layer graphene (21.8 nm × 12.6 nm × 4 monolayers) and gear-substrate distance 2 Å. The normalized angular velocity of the diamond-based solid-state gear ($\omega_0 = 0.2$ rad/s) for different gear radius $r = 3$, 4 and 5 nm is shown in the right column for **d** crystalline SiO_2, **e** amorphous SiO_2 and **f** 4-layer graphene substrates, respectively. Reused from Ref. [44] with permission: copyright American Physical Society

$$K(\nu) = \sum_{i \in \mathrm{R}} K_i(\nu) = \sum_{i \in \mathrm{R}} \frac{1}{2} m_i |\mathbf{v}_i(\nu)|^2, \tag{2}$$

with $\mathbf{v}_i(\nu)$ being the Fourier transform of the velocity of the ith atom in the relaxed layer (R) and ν is the frequency. To identify the features arising purely from rotational dissipation, we show in Fig. 3b, d the kinetic energy spectra for the cases without and with gear rotation, respectively. For the case without rotation, Fig. 3b, as d increases a prominent spectral feature around 13 THz emerges, which is related to the well-known van-Hove singularity in the phonon density of states of crystalline SiO_2 [53].

When the gear rotational motion is allowed, then two main features can be observed in the kinetic energy spectral function, see Fig. 3e. First of all, the spectral feature at $\omega = 13$ THz gets strongly broadened (its lifetime is shorter) and loses intensity with decreasing d. This latter effect indicates that this peak is a bulk prop-

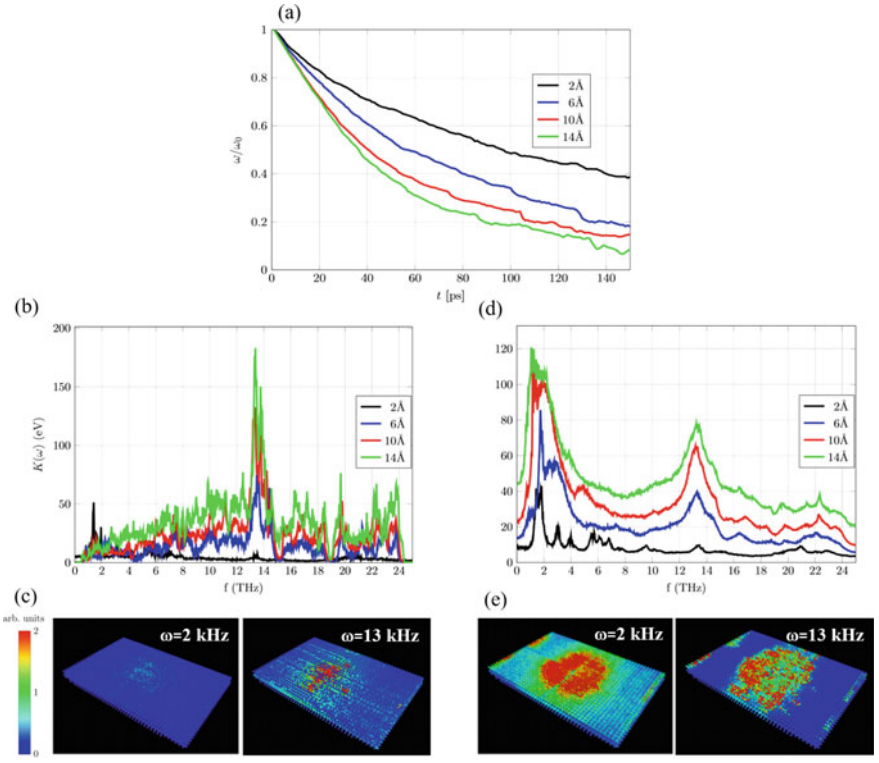

Fig. 3 **a** Substrate thickness dependence of the angular velocity relaxation. The kinetic energy spectra of the substrate **b** without and **d** with gear rotation within 50 ps. The heat maps in panels **c** and **e** present a real-space visualization of the kinetic energy spectrum $K_j(\nu_0)$ with contributions around the frequencies $\nu = 2$ THz and $\nu = 13$ THz **c** without and **e** with rotation of the solid-state gear. Modified from Ref. [44] with permission: copyright American Physical Society

erty rather than a surface property. The former effect hints at the increased energy dissipation into the substrate via phonon excitation. Secondly, a new spectral feature appears at $\omega \sim$1–2 THz. The corresponding peak intensity increases with increasing d, but the trend weakens for $d > 10$ Å, suggesting that only surface phonons are excited.

The bottom panels Fig. 3c, d provide a visualization of the spatial distribution of the two previously discussed spectral features at $\nu = 2$ THz and $\nu = 13$ THz. The calculation has been done by applying a band filter to the kinetic energy spectrum with bandwidth $\Gamma = 1$ THz [44].

Figure 3c shows that without gear rotation more atoms are excited at 13 THz than at $\omega = 2$ THz, which is consistent with the features found in the kinetic energy spectrum. In contrast, upon allowing for gear rotation (Fig. 3e) the mode at $\omega = 2$ THz has been strongly excited and localizes below the gear (the red region around the center), but also for $\omega = 13$ THz, there is also a visible pattern, which is apparently

due to the gear rotation. The conclusion from this analysis is that the low-frequency excitation is largely related to surface phonon modes excited by the gear rotation.

3.2 Graphene Nanodisk-Molecule Gear Interaction

As discussed in the Introduction, another interesting problem for the development and down scaling of gear systems is the possibility to couple gears with quite different sizes and to explore the efficiency of rotational transmission and energy dissipation. We have therefore studied in [54] a model system consisting of a graphene nanodisk and a single molecule gear, both adsorbed on a Cu(111) surface, see Fig. 6a). The molecule gear is a hexa-*tert*-butylphenylbenzene (HB-BPB) molecule with 6 *tert*-butylphenyl teeth. Further structural details as well as the rationale for choosing this molecule gear are provided in the next paragraphs.

In what follows, we will use a simple way to characterize the mechanical transmission of rotational motion between two gears by defining a locking coefficient as [8]:

$$L_\alpha = \frac{\langle \omega_\alpha \rangle}{\omega_{R\alpha}} \,, \tag{3}$$

where $\langle \omega_\alpha \rangle$ is the average angular velocity of gear α and $\omega_{R\alpha}$ is the terminal angular velocity of a rigid-body corresponding to this gear. For perfectly interlocked rigid gears, the coefficients L_α must be equal to unity. For soft gears or imperfect transmission, L_α will in general be much smaller than unity, since there will be dissipation into internal degrees of freedom.

Which molecule gear?—Our choice of the molecule gear has been based on the test of few similar candidates and on their capability to efficiently transfer angular momentum in a molecule gear pair. In Fig. 4 we show these molecules, which differ both in the compactness of their cores (alkyl groups or coronene cores) as well as on the shape of the teeth (adding one more phenyl ring).

To characterize the rotational transmission of the molecule gears we use the previously defined locking coefficient, Eq. (3), and plot it as a function of an external torque applied on the first gear. As previously shown in Ref. [8] for molecule gears, three different regimes can be identified (which do not necessarily appear simultaneously in each case), depending on the strength of the applied torque: (I) underdriving regime for which $|L_1| \approx |L_2| \approx 0$, i.e. the average angular velocities for both gears nearly vanish and there is no rotation; (II) driving regime with $0 < |L_1| \approx |L_2| < 1$, where transmission of rotation between the two gears takes place; (III) overdriving regime with $|L_1| > |L_2|$, where the driven gear cannot follow the driver. The goal is, therefore, to design a molecule gear where the driving regime is dominant over a broad range of applied torques. The corresponding phase diagrams for the four molecules (a)–(d) of Fig. 4 are shown in Fig. 5.

For molecule (a), the distance between gears is $d_{\mathrm{CM}} = 2.25\,\mathrm{nm}$ and only phases I and III were identified, so that no collective rotations take place. For molecule (b), the

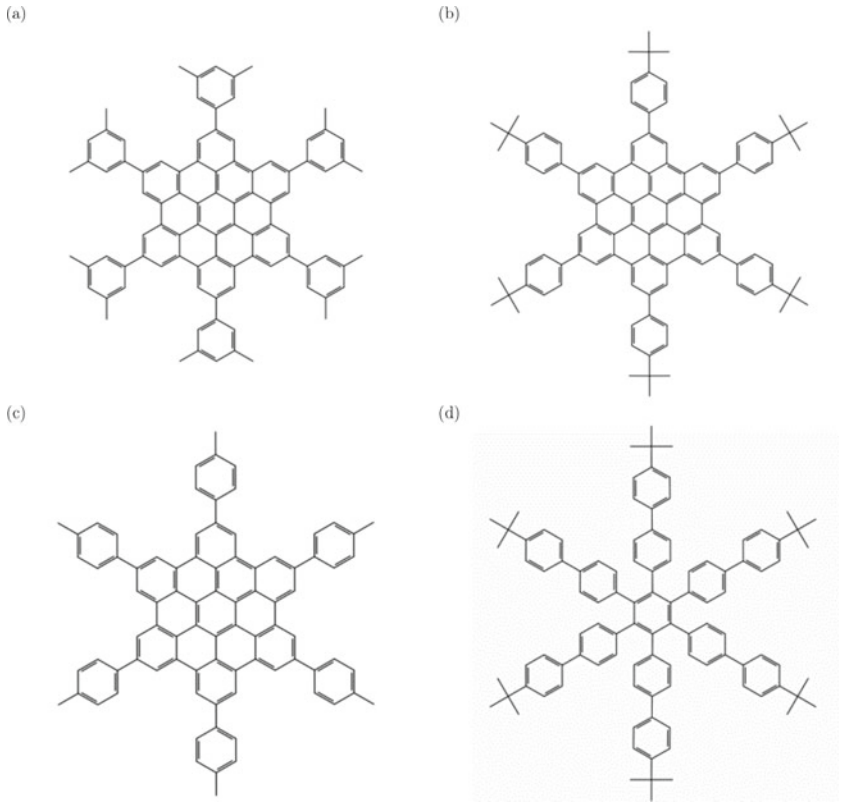

Fig. 4 Some possible candidates for the molecule gear in the heterogeneous graphene nanodisk-molecule gear system

distance is $d_{\mathrm{CM}} = 2.2\,\mathrm{nm}$, and now all three phases appear, meaning that collective rotations are possible. For the molecule (c), $d_{\mathrm{CM}} = 2\,\mathrm{nm}$ and we have again only regions I and III. Note that in the red region one can still see nonzero values for L_2 but the magnitude is relatively small compared with L_1. This implies that collective rotations are possible, but relative sliding between gears can happen as well. For molecule (d), $d_{\mathrm{CM}} = 2.2\,\mathrm{nm}$ and one can immediately see that there is a wider region II compared to the other molecule gears, which means collective rotations are robust in terms of external torque. This is why we have chosen case (d), the hexa-*tert*-butylbiphenylbenzene (HB-BPB) molecule, as our candidate to interface with the graphene nanodisk.

Heterogeneous gears: graphene nanodisk-molecule gear.—After the previous discussion for choosing an appropriate molecule gear, we address now the heterogeneous system made of a graphene disk with a diameter of 10 nm and a hexa-*tert*-butylphenylbenzene (HB-BPB) molecule with six *tert*-butylphenyl teeth. For the graphene nanodisk we tested different edge profiles such as irregular edges (rough-

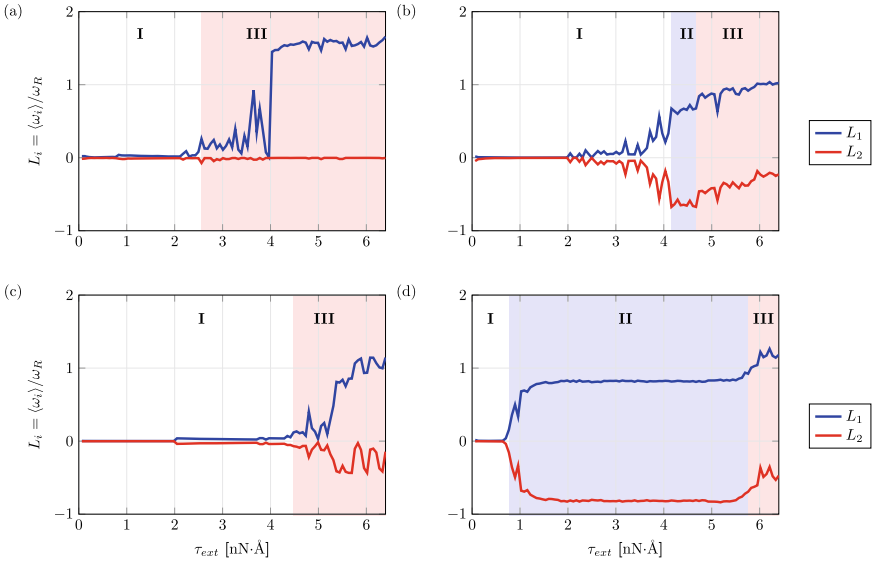

Fig. 5 Locking coefficients diagrams for two gears in a train of the molecules depicted in Fig. 4 with corresponding center-of-mass distances given by **a** $d_{\mathrm{CM}} = 2.25\,\mathrm{nm}$, **b** $d_{\mathrm{CM}} = 2.2\,\mathrm{nm}$ **c** $d_{\mathrm{CM}} = 2\,\mathrm{nm}$ and **d** $d_{\mathrm{CM}} = 2.2\,\mathrm{nm}$. Panels (**a**)–(**d**) correspond to the molecules in Fig. 4

ness), involute shape, and *tert*-butylphenyl teeth. Only in the latter case a correlated rotation of both gears for clockwise and anti-clockwise directions of rotation was obtained. Therefore, this is the atomistic model chosen for the following simulations. We remark that the thickness of the graphene nanodisk is compatible with the molecule gear chemical structure and with its physisorption height on the used Cu(111) surface. We have further found that using 20 *tert*-butylpheny chemical groups provides an optimal number of teeth to ensure a smooth transmission of rotational motion. Other master diameters will certainly require to adapt again its edge chemical structure. There is also a central 1.5 nm hole in the master Fig. 6a representing the location of the rotational axle, which is not explicitly modelled in this study. The optimized center-of-mass separation between the master (graphene disk) and the HB-BPB molecule gear was found to be 6.5 nm.

We now apply an external torque τ_{ext} on the master and monitor the angular momentum transfer to the HB-BPB molecule. The time dependence of the product $N_\alpha\theta_\alpha(t)$ for a small $\tau_{ext} = 12.8\,\mathrm{nN\,Å}$ and an intermediate $\tau_{ext} = 48\,\mathrm{nN\,Å}$ torques are presented in Fig. 6c, d, respectively, with $N_1 = 20$ and $N_2 = 6$. For a small torque only small amplitude oscillations of both gears around their equilibrium conformations are found, since τ_{ext} is not large enough to overcome the surface friction of the master on the substrate and to allow the molecule gear to overcome the energy barrier of the potential energy surface on Cu(111) at the simulation temperature of $T = 10\,\mathrm{K}$. For intermediate τ_{ext}, on the contrary, perfectly interlocked rotation is obtained, which satisfies the classical condition $N_1\theta_1 + N_2\theta_2 = 0$ [55]. In Fig. 6e we

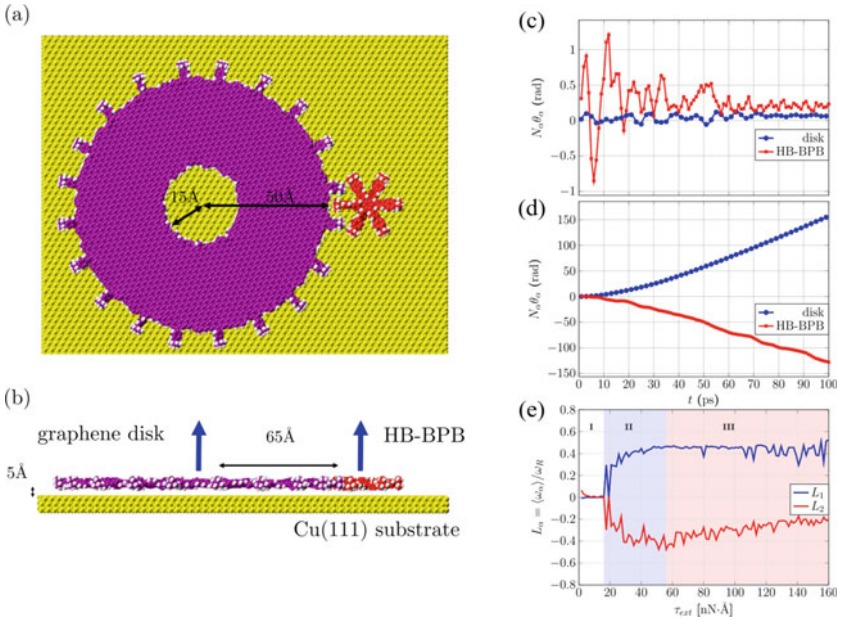

Fig. 6 A schematic illustration of the **a** top view **b** side view for a *tert*-butylbiphenyl functionalized graphene disk with radius 10 nm interacting with a hexa-*tert*-butylbiphenylbenzene molecule gear on a Cu(111) surface. Panels (**c**) and (**d**) show the time dependence of the angular displacement θ_α multiplied with the number of teeth N_α ($N_1 = 20$ for the graphene disk and $N_2 = 6$ for the HB-BPB molecule) for two applied external torques: **c** $\tau_{ext} = 12.8\,\text{nN Å}$ and **d** $\tau_{ext} = 48\,\text{nN Å}$. Panel (**e**) displays the locking coefficient $L_{1,2}$ as a function of the applied external torque in the range 0–160 nN Å. Regions I, II and III represent underdriving, driving and overdriving phases, respectively. Modified from Ref. [54] with permission: copyright Institute of Physics

plot the locking coefficient as a function of the applied torque using $\omega_{R1} = \frac{\tau_{ext}}{\gamma_1}$ with $\gamma_1 = 2.83 \times 10^{-29}\,\text{kg m}^2\,\text{s}^{-1}$ (extracted from $\tau_{ext}/\langle\omega_1\rangle$ in the same MD simulation) being the damping coefficient corresponding to a rigid disk on the Cu surface. For ω_{R2}, we then obtain $\omega_{R2} = -\frac{N_1\omega_1}{N_2}$. Interestingly, also for this heterogeneous two-gear system, we can still identify three typical different regimes (highlighted with different colors). In the (white) region I ($\tau_{ext} < 18\,\text{nN Å}$) the average angular velocities for both gears nearly vanish, and there is no rotation (underdriving regime). In the (blue) region II ($18 < \tau_{ext} < 58\,\text{nN Å}$) transmission of rotation between the two gears takes place (driving regime). Finally, in the (red) region III ($\tau_{ext} > 58\,\text{nN Å}$) the molecule gear cannot follow the master rotation (overdriving regime). Therefore, there is a relevant window in the applied torque (driving regime) where the interlocking of the two gears is largely favoured and the rotational transmission is optimal.

Nanodisk-molecule gear: Phononic dissipation channel.—In the previously described situation the main source of energy dissipation (friction), which requires the application of a large torque, is the interaction between the master and the Cu(111)

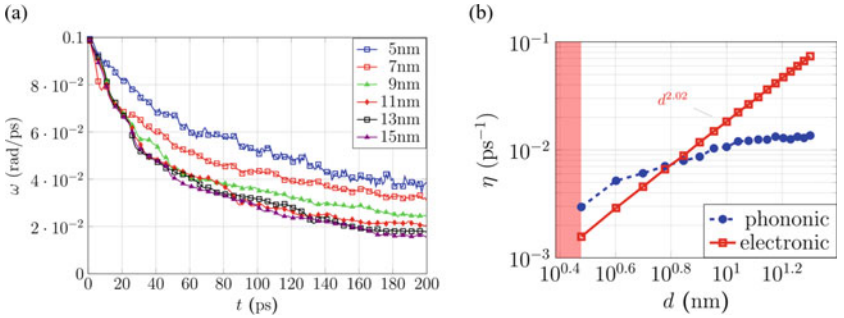

Fig. 7 **a** Viscous dissipation for graphene disks with initial angular velocity $\omega_0 = 0.1$ rad/ps on Cu(111) within 200 ps for different gear diameters ranging from 5 to 15 nm. **d** Nanodisk diameter dependence of the rotational friction coefficient $\eta = 1/\tau$ due to the phononic contribution (blue) and the electronic contribution according to Eq. (4) (red) for disk diameters d from 3 to 20 nm. The red region indicates that below 3 nm the motion becomes oscillatory due to confinement by rotational barriers. Modified from Ref. [54] with permission: copyright Institute of Physics

surface. To address in more detail this issue, we have considered graphene nanodisks with different diameters adsorbed on the Cu(111) surface, but without including the molecule gear. Then, by applying an initial angular velocity ω_0 we allow the graphene disk to slow down and eventually stop its rotation as a result of frictional dissipation to the substrate. The estimated tangential velocities indicate that the system is in the viscous dissipation regime [31]. Hence, by plotting the time-dependent angular velocity as a function of simulation time for the different diameters, we can fit each curve to a single exponential function and can extract the corresponding relaxation times. The function $\omega(t)$ is shown in Fig. 7a. As it may be expected, the relaxation time is longer for small diameters than for larger diameters as a result of the increased contact area with the surface.

The obtained inverse relaxation times τ_{rel}^{-1}, related to the friction coefficient $\eta = 1/\tau_{rel}$, are now displayed as a function of the nanodisk diameter as the blue curve in Fig. 7b. As seen in the figure, the friction increases with increasing diameter, but it becomes weakly dependent on d for values larger than 10 nm. Notice also that for $d < 3$ nm (highlighted by the vertical window in light red in Fig. 7b), the nanodisks no longer rotate but oscillate in a Brownian like motion. The reason for this transition is that the potential energy barrier height for rotation becomes in this domain larger that the initially imposed rotational kinetic energy, so that only fluctuations around equilibrium positions are feasible.

Nanodisk-molecule gear: Electronic dissipation channel.—Although our classical MD simulations do not allow to directly address dissipation processes involving the electronic system, we can try to obtain estimates of it by using mathematical relations available from quantum mechanical studies of model systems. In the case of van der Waals related electronic friction, estimates from second-order perturbation theory using a Jellium model were obtained in Refs. [56, 57]:

$$\eta_{el} = 1/\tau_{el} = \frac{e^2}{\hbar a_0} \frac{\left[k_F^3 \alpha(0)\right]^2}{(k_F z_0)^{10}} \frac{m_e}{M} \frac{\omega_F}{\omega_p} k_F z_0 I(z_0, r_s). \quad (4)$$

Here, e is the elementary charge, $\hbar$ is the reduced Planck constant, a_0 the Bohr radius, $\alpha(0)$ the static polarizability of the adsorbate, ω_p the plasma frequency of the metallic substrate, k_F the Fermi wave vector, ω_F the Fermi frequency, m_e the electron mass, M the mass of the graphene nanodisk and I is the parallel frictional integral as a function of the electron gas radius r_s and the distance z_0 between the graphene nanodisk and the substrate ($z_0 = 3.1$ Å in our case). For Cu(111), $\omega_p = 1.33 \times 10^{16}$ rad/s [58], $\omega_F = 1.06 \times 10^{16}$ rad/s [59], $k_F = 1.36 \times 10^{10}$ A $^{-1}$ [59] and $I(z_0, r_s) \approx 7$ [56] ($r_s = 2.67$ for Cu). For a monolayer graphene sheet, $\alpha(0) = 0.949$ Å^3 per unit cell [60]. To estimate $\alpha(0)$ for a graphene nanodisk, we assume that this disk is large enough such that $\alpha(0) \approx 0.949 \times N_c/2$ (one unit cell contains two carbon atoms) where N_c is the number of carbon atoms in the graphene nanodisk. Using these parameter values, we can estimate the electronic contribution to the frictional process as a function of the nanodisk diameter. This is shown as the dark red curve in Fig. 7b. According to Eq. (4), the electronic friction coefficient is roughly proportional to d^2 since the increase of polarizability is proportional to the number of carbon atoms and it grows faster than the increase of the mass of a graphene nanodisk ($\alpha(0)^2/M \propto d^2$). As it becomes clear from the figure, the electronic contribution to friction is dominant for larger disks whereas for smaller diameters the phononic dissipation channel dominates the process. As a consequence, a large (saturating phononic dissipation) graphene nanodisk of higher polarizability together with a substrate below the critical superconducting transition temperature (for suppressing the electronic dissipation channel) could provide an efficient starting setup where to build our modelled heterogeneous gear system.

Molecule gear trains based on HB-BPB: How efficient is the transmission of rotational motion?—The graphene nanodisk-molecule gear system can be considered to form the driving part of a molecule gear train with additional HB-BPB molecules. It is therefore of interest to look closely at the critical inter-gear separations in order to optimize the rotational transmission. In Fig. 8, we show the corresponding locking coefficients of two HB-BPB gears (see also the scheme in Fig. 8f) for different center-of-mass separations (a) $d_{\mathrm{CM}} = 2.1$ nm, (b) 2.2 nm, (c) 2.3 nm, (d) 2.4 nm and (e) 2.5 nm, respectively. One can see that gears with $d_{\mathrm{CM}} = 2.2$ nm give the optimal result for rotational transmission, since there is a wide range of applied torques corresponding to a driving phase (region II). This is also the separation used in Fig. 5. For $d_{\mathrm{CM}} = 2.4$ nm, on the contrary, the driving region II is already considerably narrowed. For $d_{\mathrm{CM}} = 2.5$ nm, there is largely only overdriving phase.

For this optimal separation $d_{\mathrm{CM}} = 2.2$ nm, we have then added additional gears to the train to see over how many gears rotational transmission is still feasible. In Fig. 9 we show the locking coefficients for $N = 2, 3, 4, 5$ HB-BPB gears.

First of all, we see that adding gears leads to a reduction in the values of the locking coefficients within the driving phase. If the locking coefficients decrease, this suggests additional energy dissipation during the rotational process. In fact,

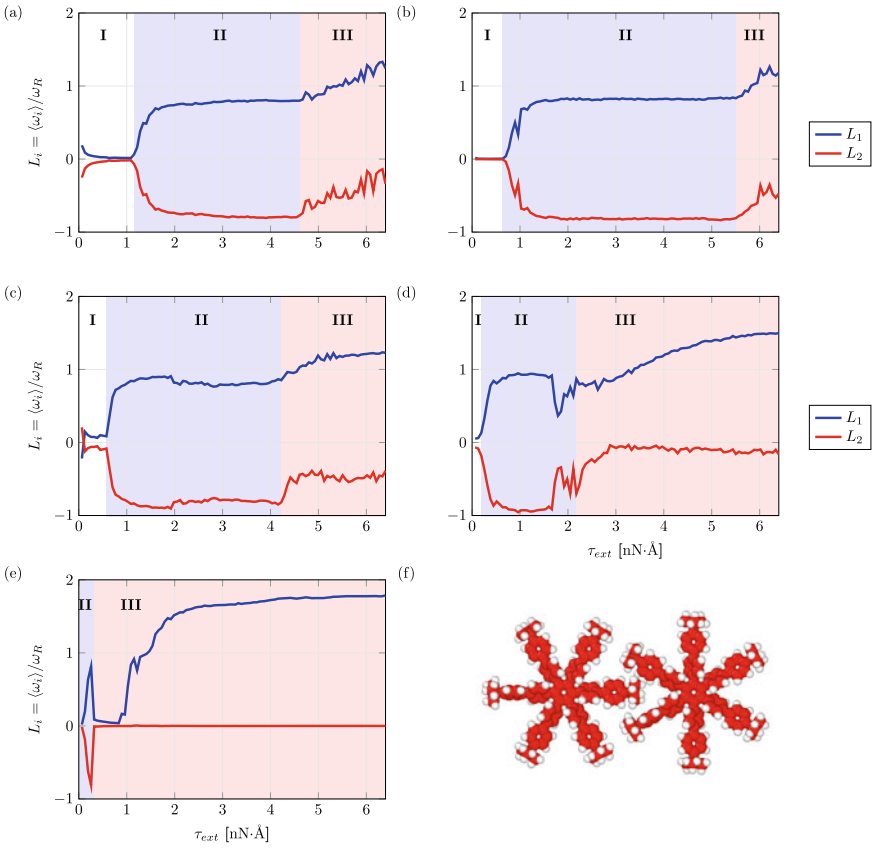

Fig. 8 Locking coefficients diagrams for two hexa-t-butylbiphenylbenzene (HB-BPB) gears in a train with center-of-mass distance **a** $d_{\mathrm{CM}} = 2.1\,\mathrm{nm}$, **b** $d_{\mathrm{CM}} = 2.2\,\mathrm{nm}$, **c** $d_{\mathrm{CM}} = 2.3\,\mathrm{nm}$, **d** $d_{\mathrm{CM}} = 2.4\,\mathrm{nm}$ and **e** $d_{\mathrm{CM}} = 2.5$. **f** Scheme of two HB-BPB gears. Figure is reproduced from Ref. [50] Open Access under a CC BY 4.0 license, https://creativecommons.org/licenses/by/4.0/

with increasing number of gears, a more detailed analysis of the MD simulations showed that collective rotations gradually become a set of internal torsional motions propagating among gears. In Fig. 9b, we can see that we have regions I, II, and III. Therefore, collective rotations for three gears are possible. On the other hand, in region III, we found that the locking coefficients satisfy $L_1 > |L_2| = |L_3|$. This means that one overdrives the first gear but the second and third gears are still interlocked and can sometimes still follow the first gear. For four gears (see Fig. 9c), collective rotations happen as well but in region III the locking coefficients satisfy $L_1 > |L_2| \gg |L_3| \approx |L_4| \approx 0$, meaning that the first gear is overdriven, but only the second gear can sometimes follow and the others stay still. For five gears (in Fig. 9d), region II completely vanishes, so that collective rotations are fully blocked. In region III, we have a similar situation as in the four gears case: $L_1 \gg |L_2| \gg |L_3| \approx |L_4| \approx$

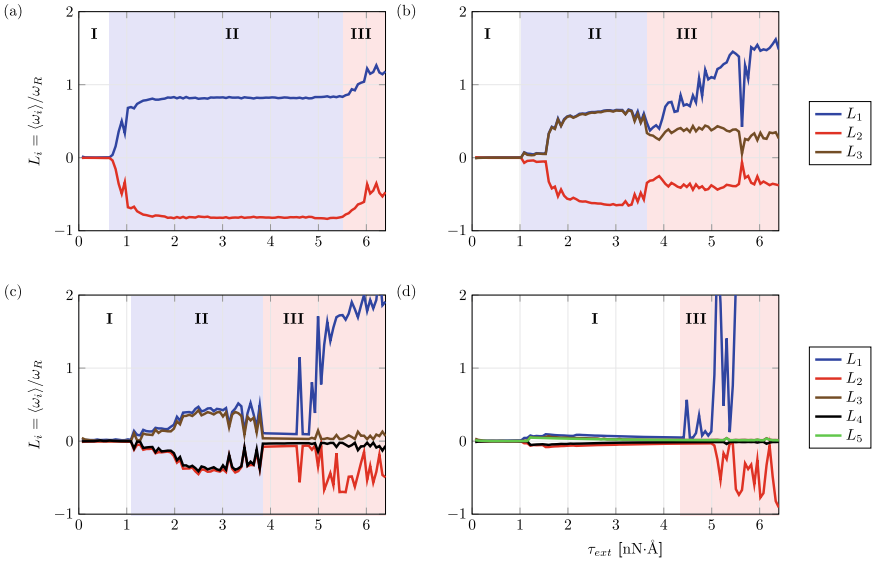

Fig. 9 Locking coefficients diagrams for N hexa-t-butylbiphenylbenzene (HB-BPB) gears in a train with center-of-mass distance $d_{\mathrm{CM}} = 2.2\,\mathrm{nm}$: **a** $N = 2$ **b** $N = 3$ **c** $N = 4$ and **d** $N = 5$. Figure is reproduced from Ref. [50] Open Access under a CC BY 4.0 license, https://creativecommons.org/licenses/by/4.0/

0, so that the first gear rotates very fast and only the second gear can follow at some point. Note also that in region I, we found very small nonzero values for all locking coefficients: $|L_1| \approx |L_2| \approx |L_3| \approx |L_4| \approx |L_5| \neq 0$. This is related to the fact that internal torsional motions are propagating from the first gear to the remaining gears, but the whole process is very slow and gets stuck eventually. Hence, the average angular velocity for all gears is nonzero but very small.

These results suggest that transmission of rotational motion may work up to $N = 4$ gears, but one needs to further investigate this issue by including e.g. a substrate and analyzing which dissipation channels become efficient in this case. The problem can be, however, very difficult since not only phononic dissipation is expected to occur, but also electronic friction, requiring a quantum mechanical treatment.

4 Conclusions and Outlook

In conclusion, we have shown how atomistic classical Molecular Dynamics simulations can contribute to shed light on different issues related to the dynamics of nanoscale gears. In the first part of this chapter we demonstrated that the regime of viscous dissipation can emerge out of van-der-Waals interactions between gears and substrates. The fitted exponential decay of the angular velocity allowed, additionally,

to obtain an estimate of the typical relaxation time scales associated with the process. Moreover, by changing the substrates and the gear sizes, we found out that the relaxation time monotonically decreases with decreasing gear size for amorphous SiO_2, but it is weakly dependent on size for crystalline SiO_2 and nearly size-independent for graphene, a result which correlates well with the differences in the degree of atomic-scale corrugation of these three substrates. We also identified the energy transfer between gear and substrate as the main energy dissipation channel involving the excitation of surface vibrational modes.

In the second part of the chapter, we investigated a heterogeneous pair of gears, consisting of a solid-state graphene nanodisk whose edge was regularly functionalized with chemical groups acting as atomic scale teeth. The latter were able to efficiently mediate the transfer of angular momentum to a single molecule gear upon the application of an external torque. Similar to previous studies on molecule gear trains [47] we could identify underdriving, driving and overdriving phases as a function of the applied torque. Moreover, we estimated the contribution of phononic and electronic energy dissipation channels leading eventually to a damping of the rotational motion of the master (graphene nanodisk). Our results support the use of superconducting surfaces in order to suppress electronic friction contributions [39]. We also showed that the locking coefficient is a reasonable descriptor not only to classify the different driving regimes but also to help in the selection of appropriate molecule gear candidates.

In relation to frictional effects, future research lines will need to address in more detail rotational energy dissipation at the single molecule gear level, which will involve dealing not only with excited vibrational modes on the substrate, but also (for metallic substrates) with electronic dissipation channels. This will require the use of more advanced first-principle methodologies or reactive force-fields (like ReaxFF) [61] (if MD simulations are the goal). From the more phenomenological perspective, it would be interesting to develop effective models to describe rotational damping along lines similar to the formulation of the Caldeira-Leggett and Rubin models [62], which are based in tracing out bath degrees of freedom and its inclusion in effective memory kernels, leading to a very rich physics.

One important point not covered in this short review and, in general, not well-understood is the mechanism for triggering the rotation of molecule gears. While the "mechanics" of pushing a molecule gear with an STM tip may be understood with the help of *ab initio* approaches and MD simulations, the excitation of a collective rotation via voltage pulses is considerably less clear [15, 16]. For instance, what breaks the rotational symmetry? Which molecular orbitals are involved? How the inelastic electronic excitation can be "converted" into the excitation of a collective coordinate leading to a concerted motion (rotation) of the molecular frame? The theoretical description of these effects may require the use of quantum master equation approaches or mixed quantum-classical methodologies.

Acknowledgements We would like to thank C. Joachim, J. Heinze, A. Mendez, A. Raptakis, T. Kühne, D. Bodesheim, S. Kampmann, R. Biele, D. Ryndyk, A. Dianat, and F. Moresco for very useful discussions and suggestions. This work has been supported by the International Max Planck

Research School (IMPRS) for “Many-Particle Systems in Structured Environments” and also by the European Union Horizon 2020 FET Open project “Mechanics with Molecules” (MEMO, grant nr. 766864).

References

1. Ju Yun, Y., Seong Ah, C., Kim, S., Soo Yun, W., Chon Park, B., Han Ha, D.: Nanotechnology **18**(50), 505304 (2007). https://doi.org/10.1088/0957-4484/18/50/505304
2. Yang, J., Deng, J., Troadec, C., Ondarçuhu, T., Joachim, C.: Nanotechnology **25**(46), 465305 (2014). https://doi.org/10.1088/0957-4484/25/46/465305
3. Mailly, D., Faini, G.: Building and Probing Small for Mechanics, pp. 41–63. Springer, Cham (2020) (Chapter 4). http://link.springer.com/10.1007/978-3-030-56777-4_4
4. Joachim, C. (ed.) Building and Probing Small for Mechanics. In: Advances in Atom and Single Molecule Machines. Springer International Publishing, Cham (2020). https://doi.org/10.1007/978-3-030-56777-4
5. Gisbert, Y., Abid, S., Bertrand, G., Saffon-Merceron, N., Kammerer, C., Rapenne, G.: Chem. Commun. **55**(97), 14689 (2019). https://doi.org/10.1039/C9CC08384G
6. Soong, R.K.: Science (80–). **290**(5496), 1555 (2000). https://doi.org/10.1126/science.290.5496.1555
7. Deng, J., Troadec, C., Ample, F., Joachim, C.: Nanotechnology **22**(27), 275307 (2011). https://doi.org/10.1088/0957-4484/22/27/275307
8. Lin, H.H., Heinze, J., Croy, A., Gutierrez, R., Cuniberti, G.: Building and Probing Small for Mechanics, pp. 165–180. Springer Nature Switzerland AG (2020) (Chapter 11). https://doi.org/10.1007/978-3-030-56777-4_11, http://arxiv.org/abs/2004.09857, http://link.springer.com/10.1007/978-3-030-56777-4_11
9. Lin, H.H., Croy, A., Gutierrez, R., Joachim, C., Cuniberti, G.: Phys. Rev. Appl. **13**, 034024 (2020). https://doi.org/10.1103/PhysRevApplied.13.034024
10. Zhao, R., Zhao, Y.L., Qi, F., Hermann, K.E., Zhang, R.Q., Van Hove, M.A.: ACS Nano **12**(3), 3020 (2018). https://doi.org/10.1021/acsnano.8b00784
11. Chen, L., Qi, F., Jitapunkul, K., Zhao, Y., Zhang, R., Van Hove, M.A.: J. Phys. Chem. A **122**(38), 7614 (2018). https://doi.org/10.1021/acs.jpca.8b04368
12. Zhao, R., Qi, F., Zhao, Y.L., Hermann, K.E., Zhang, R.Q., Van Hove, M.A.: J. Phys. Chem. Lett. **9**(10), 2611 (2018). https://doi.org/10.1021/acs.jpclett.8b00676
13. Lin, H.H., Heinze, J., Croy, A., Gutiérrez, R., Cuniberti, G.: Effect of lubricants on the rotational transmission between solid-state gears (2021)
14. Ahmed, S.B., Ullah, N., Zhao, Y., Zhang, R., Van Hove, M.A.: J. Phys. Chem. C **125**(32), 17612 (2021). https://doi.org/10.1021/acs.jpcc.1c04239
15. Echeverria, J., Monturet, S., Joachim, C.: Nanoscale **6**(5), 2793 (2014). https://doi.org/10.1039/c3nr05814j
16. Lin, H.H., Croy, A., Gutierrez, R., Joachim, C., Cuniberti, G.: J. Phys. Commun. **3**(2), 025011 (2019). https://doi.org/10.1088/2399-6528/ab0731
17. Vanossi, A., Manini, N., Urbakh, M., Zapperi, S., Tosatti, E.: Rev. Mod. Phys. **85**(2), 529 (2013). https://doi.org/10.1103/RevModPhys.85.529
18. Gnecco, E., Mayer, E.: Fundamentals of Friction and Wear. In: Nanoscience and Technology. Springer, Berlin, Heidelberg (2007). https://doi.org/10.1007/978-3-540-36807-6
19. Perssson, B., Tosatti, E.: Physics of Sliding Friction, vol. 311. Springer Netherlands, Dordrecht (1996). https://doi.org/10.1007/978-94-015-8705-1
20. Wen, S., Huang, P.: Principles of Tribology. Wiley, Singapore (2017). https://doi.org/10.1002/9781119214908

21. Manini, N., Braun, O.M., Tosatti, E., Guerra, R., Vanossi, A.: J. Phys. Condens. Matter **28**(29), 293001 (2016). https://doi.org/10.1088/0953-8984/28/29/293001
22. Sankar, K.M., Kakkar, D., Dubey, S., Garimella, S.V., Goyat, M., Joshi, S., Pandey, J.K.: Proc. Inst. Mech. Eng. Part J J. Eng. Tribol. **234**(3), 448 (2020). https://doi.org/10.1177/1350650119863993
23. Lodge, M.S., Tang, C., Blue, B.T., Hubbard, W.A., Martini, A., Dawson, B.D., Ishigami, M.: Sci. Rep. **6**(1), 31837 (2016). https://doi.org/10.1038/srep31837
24. Smith, E.D., Robbins, M.O., Cieplak, M.: Phys. Rev. B **54**(11), 8252 (1996). https://doi.org/10.1103/PhysRevB.54.8252
25. Walker, M., Jaye, C., Krim, J., Cole, M.W.: J. Phys. Condens. Matter **24**(42), 424201 (2012). https://doi.org/10.1088/0953-8984/24/42/424201
26. Binnig, G., Rohrer, H.: Rev. Mod. Phys. **59**(3), 615 (1987). https://doi.org/10.1103/RevModPhys.59.615
27. Balakrishna, S.G., de Wijn, A.S., Bennewitz, R.: Phys. Rev. B **89**(24), 245440 (2014). https://doi.org/10.1103/PhysRevB.89.245440
28. Tomlinson, G.: Lond. Edinb. Dublin Philos. Mag. J. Sci. **7**(46), 905 (1929). https://doi.org/10.1080/14786440608564819
29. Braun, O.M., Kivshar, Y.S.: The Frenkel-Kontorova Model. Springer, Berlin, Heidelberg (2004). https://doi.org/10.1007/978-3-662-10331-9
30. Panizon, E., Santoro, G.E., Tosatti, E., Riva, G., Manini, N.: Phys. Rev. B **97**(10), 104104 (2018). https://doi.org/10.1103/PhysRevB.97.104104
31. Guerra, R., Tartaglino, U., Vanossi, A., Tosatti, E.: Nat. Mater. **9**(8), 634 (2010). https://doi.org/10.1038/nmat2798
32. Tomassone, M.S., Sokoloff, J.B., Widom, A., Krim, J.: Phys. Rev. Lett. **79**(24), 4798 (1997). https://doi.org/10.1103/PhysRevLett.79.4798
33. Manzano, C., Soe, W.H., Wong, H.S., Ample, F., Gourdon, A., Chandrasekhar, N., Joachim, C.: Nat. Mater. **8**(7), 576 (2009). https://doi.org/10.1038/nmat2467
34. Chiaravalloti, F., Gross, L., Rieder, K.H., Stojkovic, S.M., Gourdon, A., Joachim, C., Moresco, F.: Nat. Mater. **6**(1), 30 (2007). https://doi.org/10.1038/nmat1802
35. Moresco, F.: Single Molecular Machines and Motors. In: Advances in Atom and Single Molecule Machines, pp. 165–186. Springer, Cham (2015). https://doi.org/10.1007/978-3-319-13872-5_10, http://link.springer.com/10.1007/978-3-319-13872-5_10
36. Mishra, P., Hill, J.P., Vijayaraghavan, S., Rossom, W.V., Yoshizawa, S., Grisolia, M., Echeverria, J., Ono, T., Ariga, K., Nakayama, T., Joachim, C., Uchihashi, T.: Nano Lett. **15**(7), 4793 (2015). https://doi.org/10.1021/acs.nanolett.5b01908
37. Perera, U.G.E., Ample, F., Kersell, H., Zhang, Y., Vives, G., Echeverria, J., Grisolia, M., Rapenne, G., Joachim, C., Hla, S.W.: Nat. Nanotechnol. **8**(1), 46 (2013). https://doi.org/10.1038/nnano.2012.218
38. Au Yeung, K.H., Kühne, T., Eisenhut, F., Kleinwächter, M., Gisbert, Y., Robles, R., Lorente, N., Cuniberti, G., Joachim, C., Rapenne, G., Kammerer, C., Moresco, F.: J. Phys. Chem. Lett. **111**, 6892 (2020). https://doi.org/10.1021/acs.jpclett.0c01747
39. Soe, W.H., Srivastava, S., Joachim, C.: J. Phys. Chem. Lett. **10**(21), 6462 (2019). https://doi.org/10.1021/acs.jpclett.9b02259
40. Zhang, Y., Kersell, H., Stefak, R., Echeverria, J., Iancu, V., Perera, U.G.E., Li, Y., Deshpande, A., Braun, K.F., Joachim, C., Rapenne, G., Hla, S.W.: Nat. Nanotechnol. **11**(8), 706 (2016). https://doi.org/10.1038/nnano.2016.69
41. Plimpton, S.: J. Comput. Phys. **117**(1), 1 (1995). https://doi.org/10.1006/jcph.1995.1039
42. Tersoff, J.: Phys. Rev. B **37**(12), 6991 (1988). https://doi.org/10.1103/PhysRevB.37.6991
43. Stuart, S.J., Tutein, A.B., Harrison, J.A.: J. Chem. Phys. **112**(14), 6472 (2000). https://doi.org/10.1063/1.481208
44. Lin, H.H., Croy, A., Gutierrez, R., Cuniberti, G.: Phys. Rev. Appl. **15**(2), 024053 (2021). https://doi.org/10.1103/PhysRevApplied.15.024053
45. Nosé, S.: J. Chem. Phys. **81**(1), 511 (1984). https://doi.org/10.1063/1.447334
46. Hoover, W.G.: Phys. Rev. A **31**(3), 1695 (1985). https://doi.org/10.1103/PhysRevA.31.1695

47. Lin, H.H., Croy, A., Gutierrez, R., Joachim, C., Cuniberti, G.: Phys. Rev. Appl. **13**(3), 034024 (2020). https://doi.org/10.1103/PhysRevApplied.13.034024
48. Persson, B., Nitzan, A.: Surf. Sci. **367**(3), 261 (1996). https://doi.org/10.1016/S0039-6028(96)00814-X
49. Norton, R.L.: Machine Design: An Integrated Approach, 4th edn. Prentice Hall (2010)
50. Lin, H.H.: Computational modelling of rotation, mechanical transmission and dissipation of nanoscale gears. Ph.D. thesis. Dresden University of Technology (2019). https://nbn-resolving.org/urn:nbn:de:bsz:14-qucosa2-764653
51. Meshkov, S.V.: Phys. Rev. B **55**(18), 12113 (1997). https://doi.org/10.1103/PhysRevB.55.12113
52. Lee, C., Vanderbilt, D., Laasonen, K., Car, R., Parrinello, M.: Phys. Rev. B **47**(9), 4863 (1993). https://doi.org/10.1103/PhysRevB.47.4863
53. Wehinger, B., Bosak, A., Refson, K., Mirone, A., Chumakov, A., Krisch, M.: J. Phys. Condens. Matter **27**(30), 305401 (2015). https://doi.org/10.1088/0953-8984/27/30/305401
54. Lin, H.H., Croy, A., Gutierrez, R., Joachim, C., Cuniberti, G.: Nanotechnology **33**(17), 175701 (2022). https://doi.org/10.1088/1361-6528/ac4b4b
55. MacKinnon, A.: Nanotechnology **13**(5), 678 (2002). https://doi.org/10.1088/0957-4484/13/5/328
56. Persson, B.N.J.: J. Chem. Phys. **113**(13), 5477 (2000). https://doi.org/10.1063/1.1290025
57. Persson, B.N.J., Volokitin, A.I.: J. Chem. Phys. **103**(19), 8679 (1995). https://doi.org/10.1063/1.470125
58. Ordal, M.A., Bell, R.J., Alexander, R.W., Long, L.L., Querry, M.R.: Appl. Opt. **24**(24), 4493 (1985). https://doi.org/10.1364/AO.24.004493
59. Ashcroft, N.W., Mermin, N.D.: Solid State Physics. Holt, Rinehart and Winston (1976)
60. Kumar, P., Chauhan, Y.S., Agarwal, A., Bhowmick, S.: J. Phys. Chem. C **120**(31), 17620 (2016). https://doi.org/10.1021/acs.jpcc.6b05805
61. Chenoweth, K., van Duin, A.C.T., Goddard, W.A.: J. Phys. Chem. A **112**(5), 1040 (2008). https://doi.org/10.1021/jp709896w
62. Weiss, U.: Quantum Dissipative Systems. World Scientific (2012). https://doi.org/10.1142/8334

Molecular Networks and Surface Engineering for Single Molecule Studies: From Spatial Separation to Emergent Properties

R. S. Koen Houtsma and Meike Stöhr

Abstract Functional molecules, among them artificial rotors, motors or gears, have been extensively studied over the past two decades with the aim to incorporate them into nanoscale devices, machines or factories. A plethora of studies have been conducted on functional molecules within a 3D (solution) environment while their investigation on atomically flat 2D surfaces despite being often a laborious effort has proven to add important insight. A less studied, but nevertheless important aspect is the (engineered) environment in which they operate, such as within the pore of a molecular network. Here, we review studies on the confinement of functional molecules within (porous) host–guest networks on atomically flat surfaces and discuss the effects this has on the operation of the functional molecule in question. To this end we will also provide a brief introduction to host–guest chemistry on surfaces. We will also present other methods to spatially arrange functional molecules, for instance through the use of specially engineered pre-patterned surfaces. Lastly, we will pay attention to the use of self-assembled networks to study emergent behavior of functional molecules.

Keywords Host–guest architectures · Porous networks · Molecular confinement · Single molecule manipulation · Scanning tunneling microscopy

1 Introduction

Over the past decades, machinery at the molecular and atomic level has garnered an increasing interest particularly within the fields of chemistry and surface science. The first artificial molecular motor exhibiting unidirectional rotation was built by Feringa et al. [1–3] This achievement earned Feringa the Nobel Prize in Chemistry in 2016 which he shared with J.-P. Sauvage and F. Stoddart for their design and production of molecular machines [2]. Inspired by biological systems, as well as

R. S. K. Houtsma · M. Stöhr (✉)
Zernike Institute for Advanced Materials, University of Groningen, Nijenborgh 4, 9747AG Groningen, The Netherlands
e-mail: m.a.stohr@rug.nl

© The Author(s), under exclusive license to Springer Nature Switzerland AG 2023

F. Moresco and C. Joachim (eds.), *Single Molecule Mechanics on a Surface*,
Advances in Atom and Single Molecule Machines,
https://doi.org/10.1007/978-3-031-16930-4_10

human inventions, great efforts were made to mimic and create molecular rotors and switches or more general 'functional molecules' [3]. The molecules may be actuated in a variety of ways such as through photons, electrons, thermal energy or mechanical force [1, 4–9]. Research has focused on both studying the molecular functionality within a 3D solution environment and on well-defined atomically flat surfaces and both topics have been reviewed recently [10–16]. The latter is on the one side of more fundamental nature but offers the possibility—because the powerful surface science toolkit is used—to track molecular motion in real-space with nanometer precision.

The work horse for this type of studies is the scanning tunneling microscope (STM) as it can be used to both image, manipulate and actuate functional molecules [17, 18]. In this way, a countless number of functional molecules have been successfully studied, among them molecular gears, rotors, motors, switches and nanocars [8, 19–24].

Up to now the interaction of functional molecules with their environment has been less studied while the purposeful design of such environments imparting the functional molecules novel properties offers the possibility to conduct studies on the single molecule level which yields important information on the molecule—environment interaction. This constitutes a promising pathway to spatially separate functional molecules—for instance in a host–guest network—and at the same time add functionality to the molecule through molecule–molecule and molecule–substrate interactions. This field was pioneered by Gimzewski et al. in their seminal work on a molecular bearing where they found that rotor-shaped molecules were "frozen" in a 2D self-assembled network, but could freely rotate within the vacancies of said network [25]. Here we will review efforts to study functional molecules on the single molecule level through means of host–guest networks and substrate engineering. To this end, we will also give a brief overview of host–guest architectures and porous networks on surfaces. On the other hand, we will explore how an assembly of functional molecules can do more than the sum of its parts.

2 Host–guest Architectures on Surfaces

Host–guest architectures were successfully used to trap and study individual molecules in solution [26–28]. Therefore, it is worthwhile to utilize 2D analogues of such host–guest architectures as molecular templates for studying single molecules on surfaces. Several aspects of on-surface 2D host–guest networks have been reviewed recently [29–32]. On surfaces, host–guest architectures are typically formed by first synthesizing a supramolecular nanoporous molecular network and subsequently depositing guest molecules in the pores. Therefore, we will expend special attention to 2D nanoporous molecular networks as well.

2.1 Nanoporous Networks

Surface-confined nanoporous networks, with a well-defined pore size, can be synthesized on a variety of substrates and conditions (UHV, ambient, solid–liquid interface) and through a variety of non-covalent interactions [33–37]. The most important interactions for such networks thus far have been hydrogen bonding [38, 39], metal–ligand coordination [40–42] and, especially at the solid–liquid interface, van der Waals interactions [43–45].

An early and well-studied example of a self-assembled nanoporous network is the one from 1,3,5-benzenetricarboxylic acid (trimesic acid, TMA) which was shown to form porous networks, stabilized by hydrogen bonds, on Cu(100) [46], HOPG [47–49], Ag/Si(111) [50], Ag(111) [51] and Au(111) [52, 53]. The pore size of these networks is approximately 1.1 nm. On Au(111) TMA was shown to exhibit an uncommon behavior in view of pore dimension. The interpore (pore-to-pore) distance was observed to be tunable upon varying the coverage of TMA on the Au(111) surface. At low molecular coverages, a chicken wire structure (Fig. 1a) is formed, while when coverage is increased, a flower structure (Fig. 1b) emerges with its pores spread further apart. Further coverage increase leads to the formation of a structure as in Fig. 1c. Upon increasing the coverage further, the pore to pore distance grows simultaneously. In this way the interpore distance can be effectively tuned between 1.6 nm and 8.2 nm, while the pore size remains constant [53]. In addition to a tunable interpore distance, the pore size may be varied by selecting molecules with a larger backbone but keeping the same functional groups and shape. For instance, 1,3,5-Tris(4-carboxyphenyl)benzene (BTB) has three carboxyphenyl groups instead of the carboxylic groups of TMA. Consequently, the porous network formed by BTB has a larger pore size of 2.9 nm [38, 54–57]. Similarly, adding further spacers between the central benzene ring and terminal carboxylic groups leads to a further increase in pore size (Fig. 1) [32, 58–60].

Robust porous molecular networks may also be constructed through metal–ligand interactions. Systems stabilized through metal–ligand interactions have the benefit of higher thermal stability due to the larger bond strength compared to the other bonding types mentioned. Importantly, the metal–ligand bond still allows for bond correction—for example through annealing at elevated temperatures—unlike covalently bonded networks [33, 35] . One of the first examples of porous networks formed through metal–ligand interactions are those made from dicarbonitrile-polyphenyl molecules (NC-Ph_n-CN). On Ag(111), NC-Ph_n-CN forms porous networks upon deposition of Co atoms. The carbonitrile groups are involved in threefold nodes with the Co adatoms, whereas the polyphenyl backbone acts as a spoke that connects the various nodes (Fig. 1) [41]. In this way, hexagonal pores of up to 6.7 nm in diameter have been demonstrated to be constructed using NC-Ph_6-CN [61].

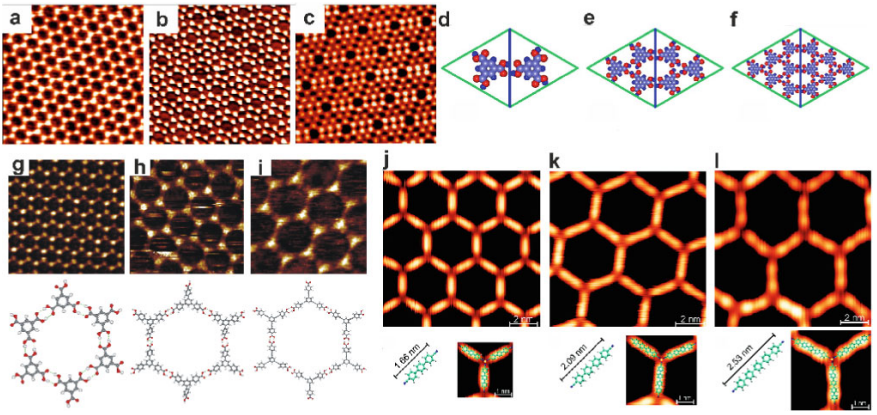

Fig. 1 **a**, **b**, **c** STM images of various porous molecular structures formed by TMA on Au(111) with varying interpore distance and **d**, **e**, **f** their corresponding molecular models. **a**–**f** Reprinted with permission from Ref. [53]. Copyright 2007 American Chemical Society (**g**, **h**, **i**) STM images of porous structures formed by various homologues of TMA exhibiting various pore dimensions together with their corresponding molecular models. Reprinted with permission from Ref. [58]. Copyright 2009 American Chemical Society. **j**, **k**, **l** STM images of porous networks formed by NC-Ph_n-CN and Co atoms on Ag(111). Reprinted with permission from Ref. [41]. Copyright 2007 American Chemical Society

2.2 *Host–guest Architectures Formed by TMA*

The networks formed by TMA and its homologues represent an excellent case study for host–guest chemistry in two dimensions. One early example of a host–guest architecture is that of TMA molecules embedded within the pores of the chicken-wire and flower phases of TMA. [47] Building upon this finding, C_{60} fullerenes [48], coronenes [49] and other circulenes [62] could be successfully trapped in the TMA pores at the solid–liquid interface. One particularly interesting example of using TMA in the framework of host–guest architectures is the work of Zhang et al. [63] They used the TMA networks with varying interpore distances to engineer a 2D lattice of Bi atoms on Au(111), using the TMA networks as molecular templates (Fig. 2).

In addition to TMA, also its larger homologues have been successfully used to fabricate host–guest architectures. For instance, BTB has been used to trap molecular macrocycles and several aromatic guest molecules [54, 57, 64]. The larger pore size of the BTB network compared to those made by TMA makes it possible to trap three coronenes in one BTB pore, compared to one for TMA. [57] In addition to the larger pore size of the BTB network when compared to TMA networks, BTB when self-assembled at the solid–liquid interface on HOPG can also be switched reversibly between a porous and close-packed structure, giving rise to the possibility of controllably adsorbing and desorbing guest molecules in the pores [56, 57].

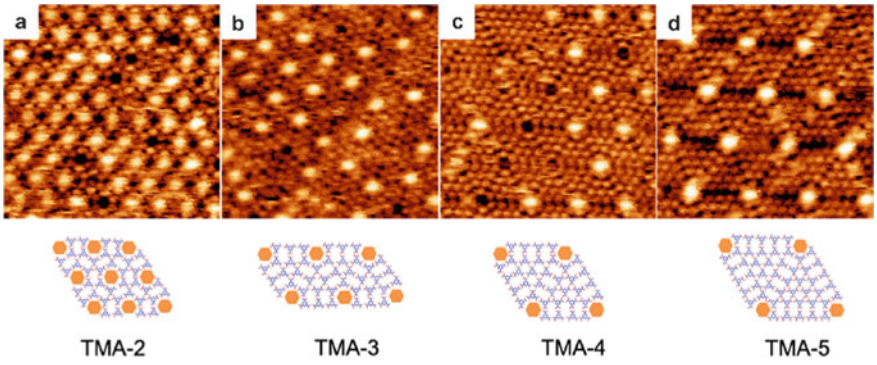

Fig. 2 **a–d** Superlattices from Bi atoms created with aid of TMA porous networks. TMA's variable interpore distance was utilized to controllably vary the spatial distance of the clusters. Reprinted with permission from Ref. [63]. Copyright 2015 American Chemical Society

3 Templates for Trapping and Studying Single Molecules

3.1 Porous Networks

Due to the success of porous networks as hosts for guest molecules and as templates for molecular growth, they are a natural candidate for trapping individual molecules for the purpose of single molecule studies in view of investigating the molecule´s mechanical, functional and further properties. The seminal work of Gimzewski et al. [25] showed that molecules are able to rotate within voids of molecular networks, creating a molecular bearing or a rotor–stator combination. So far, a few studies have managed to trap functional molecules, such as rotors, in a porous molecular network. One early example is the work of Charra and Cousty [65], who fabricated porous networks from hexakis-2,3,6,7,10,11-alkyloxytriphenylene (HnT, with varying alkyloxy side chain lengths) with single HnT molecules self-trapped in the network pores. The central HnT molecule were found to rapidly switch between different adsorption geometries. Similar results were found for other porous networks with other guest molecules [66, 67]. Such a random rotation of molecules within the pores is typified by a 'noisy' appearance in STM imaging if the rotational frequency of the molecule is much larger than the scan frequency of the STM. It is also possible, if the rotation rate is similar to the scan speed, that the molecules appear to have a higher symmetry than expected due to the STM simultaneously imaging all possible adsorption geometries (Fig. 3). In general, the STM will record a time-averaged pattern of the different adsorption position of the guest molecules [68]. The thermally induced rotation of molecules trapped in porous networks has been extensively studied. The rotation can be monitored by positioning the STM probe away from the center of rotation above the molecule and monitoring the tunneling current [5, 69]. A rotation of the molecule can then be observed either as a change in tip height or tunneling current, indicating that the molecule moved below the tip. By monitoring the rate at which

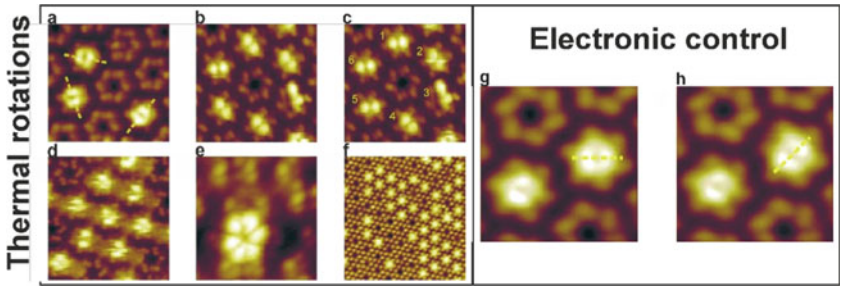

Fig. 3 **a**–**f** Porous porphyrin networks with porphyrin rotors embedded in its pores (imaged at 77 K, 112 K, 112 K, 115 K, 150 K and room temperature, respectively). Porphyrin rotors have varying appearances depending on sample temperature, ranging from two-fold symmetric at low temperatures to sixfold symmetric at 150 K to an apparently completely filled pore at room temperature. At 112 K thermal switching can be observed (structures 1 and 5). **g**, **h** Electronic control over the porphyrin position at low temperatures. A voltage pulse was able to rotate one porphyrin while keeping the neighboring porphyrins unaffected. **a**–**h** Reproduced with permission from Ref. [71]. Copyright 2007, Wiley–VCH

the changes in tip height/current occur at various temperatures, the activation barrier for thermal rotations can be extracted using an Arrhenius law [5, 69]. It was shown that the thermal rotation of molecules can be tuned via the interaction between STM tip and molecule: The lifetime of a molecular rotational position can be extended by moving the tip closer to the surface [70]. Similar to isolated functional molecules, guest molecules may also be manipulated through an STM voltage pulse as was demonstrated by Wintjes et al. (Fig. 3) [71].

An early example of control and manipulation of guest molecules inside a porous network is the work of Stöhr et al.[72] They used a porous network adsorbed on Cu(111) and deposited a combination of Zn-metalated porphyrin derivates and C_{60} molecules in the pores as guests. Stöhr et al. found that by mechanically pushing the C_{60} molecules with the STM probe, they could controllably be moved from one pore to the next. In addition, in this way the C_{60} could be placed on top of one of the porphyrin derivatives, creating a supramolecular bearing [25]. In addition, the C_{60} molecules could be vertically manipulated, picking one up with the STM probe and placing it back down in an empty pore. Earlier, it was found that C_{60} molecules were able to hop between pores through thermal fluctuations [73–75].

Porous networks can also serve as a template for the fabrication of supramolecular rotors as was first shown by Kühne et al. [76] They used NC-Ph_6-CN and Co atoms to create a honeycomb porous network on Ag(111) and found that some NC-Ph_6-CN molecules were self-trapped in the pores at low surface temperatures. The NC-Ph_6-CN self-assembled in chiral trimers inside the pores. Interestingly, the trimers were found to exhibit a thermally excited rotational hopping as one unit, i.e. all three molecules moved together. This system was also theoretically studied. [77, 78] Similar host-assisted self-assembly of molecular rotors was observed for various other systems and the interested reader is referred to the following references [79–81].

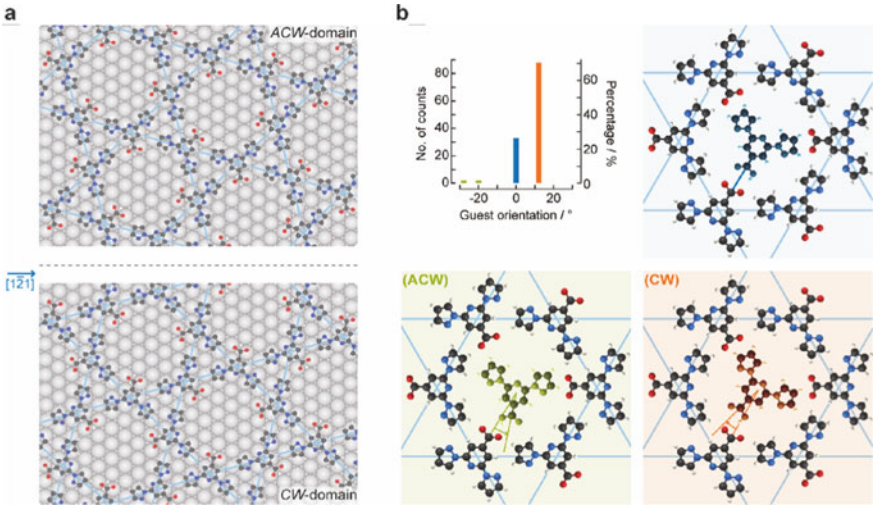

Fig. 4 Porous networks formed by bpp-COOH with embedded bpp-COOH rotors. **a** The two domains of porous networks formed by bpp-COOH. **b** Statistics of the guest orientation with respect to the host-molecules (for the ACW-domain). In the ACW-domain, the guest-molecules prefer to adsorb in the (CW) geometry (orange shaded molecule) with respect to the host-molecules. **a**, **b** Reproduced with permission from Ref. [104]. Copyright 2021, the Authors, published by Wiley–VCH. Provided under a Creative Commons CC BY 4.0 international license

Significantly, the pores do not only act as a physical barrier confining the rotors, but they also affect the potential energy landscape that the rotors reside in [82, 83] . When the porous networks are placed on substrates having a surface state, the porous networks can locally confine the surface electrons which has an up to now not extensively studied effect on the confined molecules [84–86]. On the other hand, the molecules that make up the porous network may interact directly with the confined rotors through their functional groups. A good example of this is the case of the prochiral molecule 2,6bis(1H-pyrazol-1-yl)pyridine-4-carboxylic acid (bpp-COOH) on Ag(111) (see Fig. 4). These molecules form a Kagome lattice (the stator) on Ag(111), which can host individual bpp-COOH molecules (the rotor) in its pores. Due to the formation of hydrogen bonds between the rotor and stator, together with surface registry effects, only one type of enantiomer was preferentially adsorbed in a given chiral domain of the porous networks (Fig. 4).

3.2 Pre-patterned Surfaces

Another way to create arrays of functional molecules and study them on an individual basis is the use of a pre-patterned surface. Here it is the goal to create a surface such that a molecular rotor or switch preferentially adsorbs either on only a single type of

site or that a switching or rotation event will only occur when the functional molecule is adsorbed on a specific site. A benefit of pre-patterning a surface compared to trapping a molecule in a porous network is that the molecules will neither be sterically hindered nor will they interact with the molecules forming the porous network. On the other hand, the ability to tune the behavior of the functional molecules through host–guest interactions is lost.

So far, only few examples have been reported in literature of pre-patterned surfaces being used for investigating functional molecules. Gao et al. [87]. observed the preferential adsorption of tetra-*tert*-butyl zinc phthalocyanine ((*t*-Bu)$_4$-ZnPc) on the elbow sites of the Au(111) herringbone reconstruction. In this way, a well-ordered array of molecular rotors was achieved, which is a desirable configuration for future applications. A more sophisticated approach is the intentional creation of a reconstructed surface. For example, deposition of tiny amounts of Ag on Cu(111) results in the creation of a hexagonal surface reconstruction. Subsequent deposition of molecular rotors (dibutyl sulfide) on this substrate led to the formation of a hexagonal array of rotors [88]. Molecules may also be used to pre-pattern a surface. A well-studied example is copper phthalocyanine (CuPc) on C_{60} on Au(111). The C_{60} molecules form a hexagonal monolayer on which individual CuPc were found to adsorb. Interestingly, the CuPc was found to sit slightly off-center with respect to the underlying C_{60} molecules, causing an eccentric thermally activated rotation [68, 89, 90].

For molecular switches it was shown that the interaction with the underlying substrate can result in a modification of the rotational/switching behavior. For instance, porphyrin derivatives that preferentially adsorb on the elbow sites of the Au(111) herringbone reconstruction were found to not act like a rotor, which is the case for similar molecules [70–72], but rather as a switch. The reduced symmetry at the elbow site allowed only two stable adsorption positions of the porphyrins between which they could thermally switch [91]. Similarly, azobenzene was found to adsorb on the elbow sites of Au(111) and it could be switched between two stable positions through voltage pulses [92].

4 Self-Assembled Networks for Single Molecule Studies and Cooperative Behavior

Self-assembled networks provide excellent opportunities for single molecule studies. The interest in self-assembled networks for such studies was sparked by the seminal work of Gimzewski et al. [25] who fabricated a molecular rotor and introduced the concept of a supramolecular bearing. Logic circuitry was demonstrated in simple bottom-up systems achieved through atomic manipulation, e.g. CO on Cu(111) [93], but these are time-intensive to construct. Interactions between individual molecules and their environment is an important stepping stone towards the realization of molecular machinery and cooperative behavior has already been demonstrated in, for instance, molecular gears [16, 19]. Where porous networks and pre-patterned

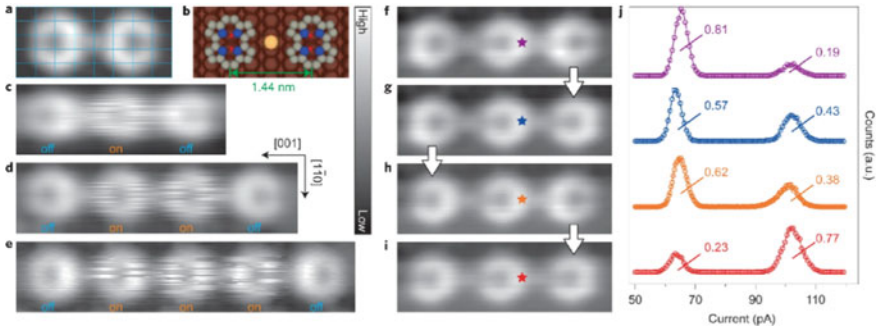

Fig. 5 **a**, **b** Porphycene dimer with quenched switching. **c**, **d**, **e** Trimers, tetramers and pentamers can be continuously switched. **f**–**i** Four possible porphycene trimer tautomer states. **j** Current histogram obtained by recording the switching behavior at the positions indicated in (f-i) showing the fractional occupation of the high and low state for the central porphycene. The occupation of these states can be controlled by the neighboring molecules. **a**–**j** Reprinted with permission from Ref. [95]. Copyright 2014, Springer Nature

surfaces are excellently suited towards spatially separating, confining and creating arrays of functional molecules, self-assembled networks are valued and established possibilities for studying emergent and cooperative behavior of functional molecules.

Up to now, a few examples of networks of rotors or switches with emergent behavior have been reported. An early example is the work of Liljeroth et al. [94] who found for a phthalocyanine derivative that switching could be initiated by current injection. In dependence of the distance/arrangement of the molecules switching either could be initiated for the molecule into which the current was injected or in a neighboring molecule. A similar effect was observed by Kumagai et al. [95] who found that the tautomerization (switching) rate of porphycenes was influenced by (1) nearby Cu adatoms and (2) nearby porphycenes, while for dimers switching was quenched and for longer porphycene chains continuous switching could be observed (Fig. 5).

A few cases were reported where multiple rotors or switches showed cooperative behavior. One example is a network of double-decker porphyrin derivatives, where the top porphyrin acts as a rotor and the bottom porphyrin as the stator. [96] When ramping the bias voltage they found that the rotors did not individually rotate, but rather all rotated in concert. This was explained by, among others, dipole–dipole interactions and an important role of defects in the network. Similarly, correlated switching was observed for a network of coupled molecular devices by Wasio et al. [97] Cooperative switching was also reported for photo-switched networks [98].

In addition, for some networks of molecular switches a significant interaction with the substrate was decisive allowing switching only when the molecule was adsorbed on a particular site. This causes molecular networks built up from such switches to exhibit a self-patterning behavior. Such an effect was first reported for azobenzene derivatives on Au(111) where a so-called ‘switching lattice’ was formed on the basis of the commensurability of the azobenzene derivative overlayer and

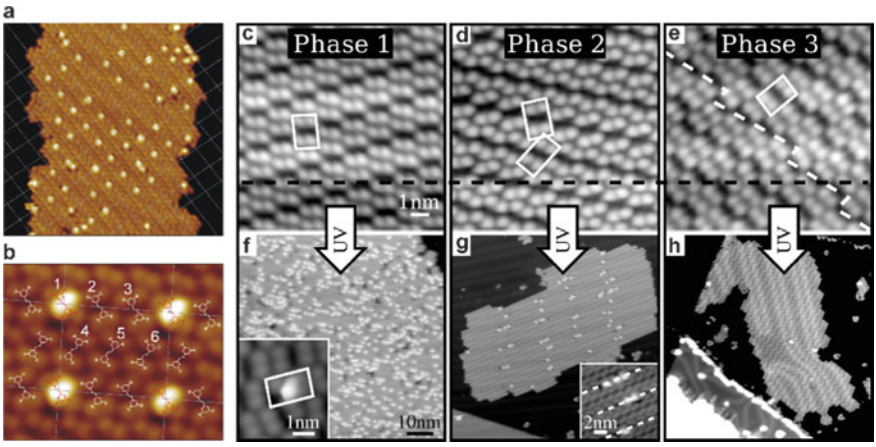

Fig. 6 Surface patterned switches. **a**, **b** STM images of self-patterned azobenzene-based molecular switches on Au(111). Switching is effected by applying a voltage pulse on the network. Reprinted with permission from Ref. [99]. Copyright 2008, Springer Nature. **c**–**h** Three different phases of azobenzene derivatives. Each network has different photo switching properties: phase 1 has an apparently random distribution of switched molecules, phase 2 has molecules switched in a striped pattern and phase 3 has switching almost completely quenched. Reprinted with permission from Ref. [100]. Copyright 2009, American Chemical Society

Au(111) [99]. When a voltage pulse was applied to the molecular overlayer, only molecules that were at the nodes of the switching lattice could reversibly be switched (Fig. 6). Different azobenzene derivatives were found to have a complex interplay of molecule–substrate and molecule–molecule interactions which enabled switching only for certain adsorption positions (Fig. 6) [100].

Lastly, self-assembled networks can act as templates for molecular translation–in essence creating nanometer scale roads [101–103]. For instance, a self-assembled network of methionine was shown to facilitate the confined motion of tetracene molecules.

5 Conclusion

The mechanisms and operation of numerous surface-confined functional molecules within self-assembled arrangements have been extensively studied over the past decades, but the number of studies on either confined or individual functional molecules is significantly less. However, the studies outlined in this review show that surface engineering is a promising way to further tune the properties of functional molecules. On the one hand, porous molecular networks can be used to spatially separate and confine molecular rotors and switches. On the other hand, those same networks can be used to adjust the potential energy landscape the molecules feel through the strategic selection of functional groups [104]. Since the use of porous

networks to tune the potential energy landscape is thus far underutilized further research is required that this concept can unfold its full power. More studies have been conducted on on-surface host–guest networks and thus, may serve as inspiration for this purpose [29–32]. Work on functional molecules confined within porous networks has so far focused mostly on self-accommodating systems and not on systems where the rotor is intentionally trapped in the pores. Moreover, more work should be done for researching confined functional molecules other than rotors, such as confined molecular switches within porous molecular networks.

So far, rotation motion often refers to a rotational hopping process for which the direction of rotation cannot be controlled whereas the directed, unidirectional motion of molecules on surfaces has been demonstrated only for free and only a few different molecules [4, 8, 105]. A similar result has yet to be shown for caged molecules warranting further research.

Similarly, the use of engineered surfaces—through the strategic use of surface reconstructions or the addition of metallic and molecular overlayers—shows potential to add functionality to molecules. Surface reconstructions can be used to spatially separate functional molecules and to create arrays in a facile manner [87, 91]. At the same time engineered surfaces can alter the function of functional molecules, for instance by changing the center of rotation or by hindering a full rotational motion—changing a rotor into a switch [91]. Compared to studies on trapped molecules in porous networks, the number of studies on functional molecules on engineered surfaces is so far small.

Networks of functional molecules can exhibit cooperative or emergent behavior which makes them an attractive option for mesoscopic applications: a scale at which single molecules cannot operate. Although relatively few examples exist in literature, this is also an encouraging prospect which requires more research.

Acknowledgements This work was supported by the Netherlands Organization for Scientific Research (NWO) (Vici grant 680-47-633) and the Zernike Institute for Advanced Materials of the University of Groningen.

References:

1. Koumura, N., Zijlstra, R.W.J., van Delden, R.A., Harada, N., Feringa, B.L.: Light-driven monodirectional molecular rotor. Nature **401**, 152–155 (1999)
2. Astumian, R.D.: How molecular motors work—insights from the molecular machinist's toolbox: the Nobel prize in Chemistry 2016. Chem. Sci. **8**, 840–845 (2017)
3. Iino, R., Kinbara, K., Bryant, Z.: Introduction: molecular motors. Chem. Rev. **120**, 1–4 (2020)
4. van Delden, R.A., ter Wiel, M.K.J., Pollard, M.M., Vicario, J., Koumura, N., Feringa, B.L.: Unidirectional molecular motor on a gold surface. Nature **437**, 1337–1340 (2005)
5. Stipe, B.C., Rezaei, M.A., Ho, W.: Coupling of vibrational excitation to the rotational motion of a single adsorbed molecule. Phys. Rev. Lett. **81**, 1263–1266 (1998)
6. Tierney, H.L., Baber, A.E., Jewell, A.D., Iski, E.V., Boucher, M.B., Sykes, E.C.H.: Mode-selective electrical excitation of a molecular rotor. Chem. Eur. J. **15**, 9678–9680 (2009)

7. Iancu, V., Hla, S.-W.: Realization of a four-step molecular switch in scanning tunneling microscope manipulation of single chlorophyll-a molecules. Proc. Natl. Acad. Sci. U.S.A. **103**, 13718–13721 (2006)
8. Tierney, H.L., Murphy, C.J., Jewell, A.D., Baber, A.E., Iski, E.V., Khodaverdian, H.Y., McGuire, A.F., Klebanov, N., Sykes, E.C.H.: Experimental demonstration of a single-molecule electric motor. Nat. Nanotechnol. **6**, 625–629 (2011)
9. Au Yeung, K.H., Kuhne, T., Eisenhut, F., Kleinwachter, M., Gisbert, Y., Robles, R., Lorente, N., Cuniberti, G., Joachim, C., Rapenne, G., Kammerer, C., Moresco, F.: Transmitting stepwise rotation among three molecule-gear on the Au(111) surface. J. Phys. Chem. Lett. **11**, 6892–6899 (2020)
10. Kay, E.R., Leigh, D.A., Zerbetto, F.: Synthetic molecular motors and mechanical machines. Angew. Chem. Int. Ed. **46**, 72–191 (2007)
11. Lensen, D., Elemans, J.A.A.W.: Artificial molecular rotors and motors on surfaces: STM reveals and triggers. Soft Matter **8**, 9053–9063 (2012)
12. Marbach, H., Steinrück, H.-P.: Studying the dynamic behaviour of porphyrins as prototype functional molecules by scanning tunnelling microscopy close to room temperature. Chem. Commun. **50**, 9034–9048 (2014)
13. Erbas-Cakmak, S., Leigh, D.A., McTernan, C.T., Nussbaumer, A.L.: Artificial molecular machines. Chem. Rev. **115**, 10081–10206 (2015)
14. Chérioux, F., Galangau, O., Palmino, F., Rapenne, G.: Controlled directional motions of molecular vehicles, rotors, and motors: from metallic to silicon surfaces, a strategy to operate at higher temperatures. ChemPhysChem **17**, 1742–1751 (2016)
15. Kassem, S., van Leeuwen, T., A.S. Lubbe, M.R. Wilson, B.L. Feringa, A. Leigh, D.: Artificial molecular motors. Chem. Soc. Rev. **46**, 2592–2621 (2017)
16. Gisbert, Y., Abid, S., Kammerer, C., Rapenne, G.: Molecular gears: from solution to surfaces. Chem. Eur. J. **27**, 12019–12031 (2021)
17. Stroscio, J.A., Eigler, D.M.: Atomic and molecular manipulation with the scanning tunneling microscope. Science **254**, 1319–1326 (1991)
18. Moresco, F., Meyer, G., Rieder, K.-H., Tang, H., Gourdon, A., Joachim, C.: Low temperature manipulation of big molecules in constant height mode. Appl. Phys. Lett. **78**, 306–308 (2001)
19. Chiaravalloti, F., Gross, L., Rieder, K.-H., Stojkovic, S.M., Gourdon, A., Joachim, C., Moresco, F.: A rack-and-pinion device at the molecular scale. Nature Mater. **6**, 30–33 (2007)
20. Manzano, C., Soe, W.-H., Wong, H.S., Ample, F., Gourdon, A., Chandrasekhar, N., Joachim, C.: Step-by-step rotation of a molecule-gear mounted on an atomic-scale axis. Nature Mater. **8**, 576–579 (2009)
21. Baber, A.E., Tierney, H.L., Sykes, E.C.H.: A quantitative single-molecule study of thioether molecular rotors. ACS Nano **2**, 2385–2391 (2008)
22. Simpson, G.J., García-López, V., Daniel Boese, A., Tour, J.M., Grill, L.: How to control single-molecule rotation. Nat. Commun. **10**, 1–6 (2019)
23. Moresco, F., Meyer, G., Rieder, K.H., Tang, H., Gourdon, A., Joachim, C.: Conformational changes of single molecules induced by scanning tunneling microscopy manipulation: a route to molecular switching. Phys. Rev. Lett. **86**, 672–675 (2001)
24. Auwärter, W., Seufert, K., Bischoff, F., Ecija, D., Vijayaraghavan, S., Joshi, S., Klappenberger, F., Samudrala, N., Barth, J.V.: A surface-anchored molecular four-level conductance switch based on single proton transfer. Nat. Nanotechnol. **7**, 41–46 (2012)
25. Gimzewski, J.K., Joachim, C., Schlittler, R.R., Langlais, V., Tang, H., Johannsen, I.: Rotation of a single molecule within a supramolecular bearing. Science **281**, 531–533 (1998)
26. Oshovsky, G.V., Reinhoudt, D.N., Verboom, W.: Supramolecular chemistry in water. Angew. Chem. Int. Ed. **46**, 2366–2393 (2007)
27. Stoffelen, C., Huskens, J.: Soft Supramolecular nanoparticles by noncovalent and host-guest interactions. Small **12**, 96–119 (2016)
28. Yang, X., Yuan, D., Hou, J., Sedgwick, A.C., Xu, S., James, T.D., Wang, L.: Organic/inorganic supramolecular nano-systems based on host/guest interactions. Coord. Chem. Rev. **428**, 213609 (2021)

29. Cicoira, F., Santato, C., Rosei, F.: Two-dimensional nanotemplates as surface cues for the controlled assembly of organic molecules. Top. Curr. Chem. **285**, 203–267 (2008)
30. Bonifazi, D., Mohnani, S., Llanes-Pallas, A.: Supramolecular chemistry at interfaces: molecular recognition on nanopatterned porous surfaces. Chem. Eur. J. **15**, 7004–7025 (2009)
31. Uemura, S., Tanoue, R., Yilmaz, N., Ohira, A., Kunitake, M.: Molecular dynamics in two-dimensional supramolecular systems observed by STM. Materials **3**, 4252–4276 (2010)
32. Teyssandier, J., Feyter, S.D., Mali, K.S.: Host-guest chemistry in two-dimensional supramolecular networks. Chem. Commun. **52**, 11465–11487 (2016)
33. Barth, J.V.: Molecular architectonic on metal surfaces. Ann. Rev. Phys. Chem. **58**, 375–407 (2007)
34. Kudernac, T., Lei, S., Elemans, J.A.A.W., De Feyter, S.: Two-dimensional supramolecular self-assembly: nanoporous networks on surfaces. Chem. Soc. Rev. **38**, 402–421 (2009)
35. Liang, H., He, Y., Ye, Y., Xu, X., Cheng, F., Sun, W., Shao, X., Wang, Y., Li, J., Wu, K.: Two-dimensional molecular porous networks constructed by surface assembling. Coord. Chem. Rev. **253**, 2959–2979 (2009)
36. Yang, Y., Wang, C.: Hierarchical construction of self-assembled low-dimensional molecular architectures observed by using scanning tunneling microscopy. Chem. Soc. Rev. **38**, 2576–2589 (2009)
37. Elemans, J.A.A.W., Lei, S., De Feyter, S.: Molecular and supramolecular networks on surfaces: from two-dimensional crystal engineering to reactivity. Angew. Chem. Int. Ed. **48**, 7298–7332 (2009)
38. Kampschulte, L., Lackinger, M., Maier, A.-K., Kishore, R.S.K., Griessl, S., Schmittel, M., Heckl, W.M.: Solvent induced polymorphism in supramolecular 1,3,5-Benzenetribenzoic acid monolayers. J. Phys. Chem. B. **110**, 10829–10836 (2006)
39. Stöhr, M., Wahl, M., Galka, C.H., Riehm, T., Jung, T.A., Gade, L.H.: Controlling molecular assembly in two dimensions: the concentration dependence of thermally induced 2D aggregation of molecules on a metal surface. Angew. Chem. Int. Ed. **44**, 7394–7398 (2005)
40. Stepanow, S., Lingenfelder, M., Dmitriev, A., Spillmann, H., Delvigne, E., Lin, N., Deng, X., Cai, C., Barth, J.V., Kern, K.: Steering molecular organization and host–guest interactions using two-dimensional nanoporous coordination systems. Nat. Mater. **3**, 229–233 (2004)
41. Schlickum, U., Decker, R., Klappenberger, F., Zoppellaro, G., Klyatskaya, S.: Metal—organic honeycomb nanomeshes with tunable cavity size. Nano Lett. **7**, 3813–3817 (2007)
42. Dmitriev, A., Spillmann, H., Lin, N., Barth, J.V., Kern, K.: Modular assembly of two-dimensional metal-organic coordination networks at a metal surface. Angew. Chem. Int. Ed. **115**, 2774–2777 (2003)
43. Lei, S., Tahara, K., De Schryver, F.C., Van der Auweraer, M., Tobe, Y., De Feyter, S.: One building block, two different supramolecular surface-confined patterns: concentration in control at the solid-liquid interface. Angew. Chem. Int. Ed. **47**, 2964–2968 (2008)
44. Tahara, K., Lei, S., Mössinger, D., Kozuma, H., Inukai, K., der Auweraer, M.V., Schryver, F.C.D., Höger, S., Tobe, Y., Feyter, S.D.: Giant molecular spoked wheels in giant voids: two-dimensional molecular self-assembly goes big. Chem. Commun. **33**, 3897–3899 (2008)
45. Destoop, I., Ghijsens, E., Katayama, K., Tahara, K., Mali, K.S., Tobe, Y., De Feyter, S.: Solvent-Induced homochirality in surface-confined low-density nanoporous molecular networks. J. Am. Chem. Soc. **134**, 19568–19571 (2012)
46. Dmitriev, A., Lin, N., Weckesser, J., Barth, J.V., Kern, K.: Supramolecular assemblies of trimesic acid on a Cu(100) surface. J. Phys. Chem. B. **106**, 6907–6912 (2002)
47. Griessl, S., Lackinger, M., Edelwirth, M., Hietschold, M., Heckl, W.M.: Self-assembled two-dimensional molecular host-guest architectures from trimesic acid. Single Mol. **3**, 25–31 (2002)
48. Griessl, S.J.H., Lackinger, M., Jamitzky, F., Markert, T., Hietschold, M., Heckl, W.M.: Room-Temperature scanning tunneling microscopy manipulation of single C60 molecules at the liquid−solid interface: playing nanosoccer. J. Phys. Chem. B. **108**, 11556–11560 (2004)
49. Griessl, S.J.H., Lackinger, M., Jamitzky, F., Markert, T., Hietschold, M., Heckl, W.M.: Incorporation and manipulation of coronene in an organic template structure. Langmuir **20**, 9403–9407 (2004)

50. Sheerin, G., Cafolla, A.A.: Self-assembled structures of trimesic acid on the Ag/Si(111)-($\sqrt{3}\times\sqrt{3}$)R30° surface. Surf. Sci. **577**, 211–219 (2005)
51. Payer, D., Comisso, A., Dmitriev, A., Strunskus, T., Lin, N., Wöll, C., DeVita, A., Barth, J.V., Kern, K.: Ionic hydrogen bonds controlling two-dimensional supramolecular systems at a metal surface. Chem. Eur. J. **13**, 3900–3906 (2007)
52. Su, G.-J., Zhang, H.-M., Wan, L.-J., Bai, C.-L., Wandlowski, T.: Potential-Induced phase transition of trimesic acid adlayer on Au(111). J. Phys. Chem. B **108**, 1931–1937 (2004)
53. Ye, Y., Sun, W., Wang, Y., Shao, X., Xu, X., Cheng, F., Li, J., Wu, K.: A unified model: self-assembly of trimesic acid on gold. J. Phys. Chem. C **111**, 10138–10141 (2007)
54. Ruben, M., Payer, D., Landa, A., Comisso, A., Gattinoni, C., Lin, N., Collin, J.-P., Sauvage, J.-P., De Vita, A., Kern, K.: 2D supramolecular assemblies of Benzene-1,3,5-triyl-tribenzoic Acid: temperature-induced phase transformations and hierarchical organization with macrocyclic molecules. J. Am. Chem. Soc. **128**, 15644–15651 (2006)
55. Silly, F.: Two-Dimensional 1,3,5-Tris(4-carboxyphenyl)benzene self-assembly at the 1-phenyloctane/graphite interface revisited. J. Phys. Chem. C. **116**, 10029–10032 (2012)
56. Cometto, F.P., Kern, K., Lingenfelder, M.: Local conformational switching of supramolecular networks at the solid/liquid interface. ACS Nano **9**, 5544–5550 (2015)
57. Lee, S.-L., Fang, Y., Velpula, G., Cometto, F.P., Lingenfelder, M., Müllen, K., Mali, K.S., De Feyter, S.: Reversible local and global switching in multicomponent supramolecular networks: controlled guest release and capture at the solution/solid interface. ACS Nano **9**, 11608–11617 (2015)
58. Lackinger, M., Heckl, W.M.: Carboxylic acids: versatile building blocks and mediators for two-dimensional supramolecular self-assembly. Langmuir **25**, 11307–11321 (2009)
59. Dienstmaier, J.F., Mahata, K., Walch, H., Heckl, W.M., Schmittel, M., Lackinger, M.: On the Scalability of supramolecular networks- high packing density vs optimized hydrogen bonds in tricarboxylic acid monolayers. Langmuir **26**, 10708–10716 (2010)
60. Gutzler, R., Lappe, S., Mahata, K., Schmittel, M., Heckl, W.M., Lackinger, M.: Aromatic interaction vs. hydrogen bonding in self-assembly at the liquid–solid interface. Chem. Commun. **6**, 680–682 (2009)
61. Kühne, D., Klappenberger, F., Decker, R., Schlickum, U., Brune, H., Klyatskaya, S., Ruben, M., Barth, J.V.: High-Quality 2D metal−organic coordination network providing giant cavities within mesoscale domains. J. Am. Chem. Soc. **131**, 3881–3883 (2009)
62. Ivasenko, O., MacLeod, J.M., Chernichenko, K.Y., Balenkova, E.S., Shpanchenko, R.V., Nenajdenko, V.G., Rosei, F., Perepichka, D.F.: Supramolecular assembly of heterocirculenes in 2D and 3D. Chem. Commun. **10**, 1192–1194 (2009)
63. Zhang, R., Lyu, G., Chen, C., Lin, T., Liu, J., Liu, P.N., Lin, N.: Two-Dimensional superlattices of Bi nanoclusters formed on a Au(111) surface using porous supramolecular templates. ACS Nano **9**, 8547–8553 (2015)
64. Lee, S.-L., Lin, C.-H., Cheng, K.-Y., Chen, Y.-C., Chen, C.: Stability of guest-incorporated 2D molecular networks. J. Phys. Chem. C. **120**, 25505–25510 (2016)
65. Charra, F., Cousty, J.: Surface-induced chirality in a self-assembled monolayer of discotic liquid crystal. Phys. Rev. Lett. **80**, 1682–1685 (1998)
66. Meier, C., Roos, M., Künzel, D., Breitruck, A., Hoster, H.E., Landfester, K., Gross, A., Behm, R.J., Ziener, U.: Concentration and coverage dependent adlayer structures: from two-dimensional networks to rotation in a bearing. J. Phys. Chem. C. **114**, 1268–1277 (2010)
67. Kalashnyk, N., Clair, S.: Self-Accommodating honeycomb networks from supramolecular self-assembly of *s* -indacene-tetrone on silver surfaces. Langmuir **38**, 1067–1071 (2022)
68. Stöhr, M., Wagner, T., Gabriel, M., Weyers, B., Möller, R.: Direct observation of hindered eccentric rotation of an individual molecule: Cu-phthalocyanine on (formula presented). Phys. Rev. B. Condens. Matter. **65**, 033404 (2001)
69. Stipe, B.C., Rezaei, M.A., Ho, W.: Inducing and viewing the rotational motion of a single molecule. Science **279**, 1907–1909 (1998)
70. Wahl, M., Stöhr, M., Spillmann, H., Jung, T.A., Gade, L.H.: Rotation-libration in a hierarchic supramolecular rotor-stator system: arrhenius activation and retardation by local interaction. Chem. Commun. **2**, 1349–1351 (2007)

71. Wintjes, N., Bonifazi, D., Cheng, F., Kiebele, A., Stöhr, M., Jung, T., Spillmann, H., Diederich, F.: A supramolecular multiposition rotary device. Angew. Chem. Int. Ed. **46**, 4089–4092 (2007)
72. Stöhr, M., Wahl, M., Spillmann, H., Gade, L.H., Jung, T.A.: Lateral manipulation for the positioning of molecular guests within the confinements of a highly stable self-assembled organic surface network. Small **3**, 1336–1340 (2007)
73. Spillmann, H., Kiebele, A., Stöhr, M., Jung, T.A., Bonifazi, D., Cheng, F., Diederich, F.: A two-dimensional porphyrin-based porous network featuring communicating cavities for the templated complexation of fullerenes. Adv. Mater. **18**, 275–279 (2006)
74. Kiebele, A., Bonifazi, D., Cheng, F., Stöhr, M., Diederich, F., Jung, T., Spillmann, H.: Adsorption and dynamics of long-range interacting fullerenes in a flexible, two-dimensional nanoporous porphyrin network. ChemPhysChem **7**, 1462–1470 (2006)
75. Pan, G.-B., Cheng, X.-H., Höger, S., Freyland, W.: 2D Supramolecular structures of a shape-persistent macrocycle and Co-deposition with fullerene on HOPG. J. Am. Chem. Soc. **128**, 4218–4219 (2006)
76. Kühne, D., Klappenberger, F., Krenner, W., Klyatskaya, S., Ruben, M., Barth, J.V.: Rotational and constitutional dynamics of caged supramolecules. Proc. Natl. Acad. Sci. U.S.A. **107**, 21332–21336 (2010)
77. Palma, C.A., Björk, J., Rao, F., Kühne, D., Klappenberger, F., Barth, J.V.: Topological dynamics in supramolecular rotors. Nano Lett. **14**, 4461–4468 (2014)
78. Palma, C.A., Björk, J., Klappenberger, F., Arras, E., Kühne, D., Stafström, S., Barth, J.V.: Visualization and thermodynamic encoding of single-molecule partition function projections. Nat. Commun. **6**, (2015)
79. Wang, T., Fan, Q., Feng, L., Tao, Z., Huang, J., Ju, H., Xu, Q., Hu, S., Zhu, J.: Chiral Kagome lattices from on-surface synthesized molecules. ChemPhysChem **18**, 3329–3333 (2017)
80. Lloyd, J.A., Papageorgiou, A.C., Fischer, S., Oh, S.C., Saŋlam, Ö., Diller, K., Duncan, D.A., Allegretti, F., Klappenberger, F., Stöhr, M., Maurer, R.J., Reuter, K., Reichert, J., Barth, J.V.: Dynamics of spatially confined bisphenol a trimers in a unimolecular network on Ag(111). Nano Lett. **16**, 1884–1889 (2016)
81. Jing, C., Zhang, B., Synkule, S., Ebrahimi, M., Riss, A., Auwärter, W., Jiang, L., Médard, G., Reichert, J., Barth, J.V., Papageorgiou, A.C.: Snapshots of dynamic adaptation: two-dimensional molecular architectonics with linear bis-hydroxamic acid Modules. Angew. Chem. Int. Ed. **58**, 18948–18956 (2019)
82. Guillermet, O., Mahmood, A., Yang, J., Echeverria, J., Jeannoutot, J., Gauthier, S., Joachim, C., Chérioux, F., Palmino, F.: Seeding molecular rotators on a passivated silicon surface. ChemPhysChem **15**, 271–275 (2014)
83. Xie, Z.-B., Wang, Y.-L., Tao, M.-L., Sun, K., Tu, Y.-B., Yuan, H.-K., Wang, J.-Z.: Ordered array of CoPc-vacancies filled with single-molecule rotors. Appl. Surf. Sci. **439**, 462–467 (2018)
84. Müller, K., Enache, M., Stöhr, M.: Confinement properties of 2D porous molecular networks on metal surfaces. J. Phys. Condens. Matter. **28**, 153003 (2016)
85. Yitamben, E.N., Niebergall, L., Rankin, R.B., Iski, E.V., Rosenberg, R.A., Greeley, J.P., Stepanyuk, V.S., Guisinger, N.P.: Tracking amino acids in chiral quantum corrals. J. Phys. Chem. C. **117**, 11757–11763 (2013)
86. Nowakowska, S., Wäckerlin, A., Piquero-Zulaica, I., Nowakowski, J., Kawai, S., Wäckerlin, C., Matena, M., Nijs, T., Fatayer, S., Popova, O., Ahsan, A., Mousavi, S.F., Ivas, T., Meyer, E., Stöhr, M., Ortega, J.E., Björk, J., Gade, L.H., Lobo-Checa, J., Jung, T.A.: Configuring electronic states in an atomically precise array of quantum boxes. Small **12**, 3757–3763 (2016)
87. Gao, L., Liu, Q., Zhang, Y.Y., Jiang, N., Zhang, H.G., Cheng, Z.H., Qiu, W.F., Du, S.X., Liu, Y.Q., Hofer, W.A., Gao, H.J.: Constructing an array of anchored single-molecule rotors on gold surfaces. Phys. Rev. Lett. **101**, 197209 (2008)
88. Bellisario, D.O., Baber, A.E., Tierney, H.L., Sykes, E.C.H.: Engineering dislocation networks for the directed assembly of two-dimensional rotor arrays. J. Phys. Chem. C. **113**, 5895–5898 (2009)

89. Stöhr, M., Wagner, T., Gabriel, M., Weyers, B., Möller, R.: Binary molecular layers of C60 and copper phthalocyanine on Au(111): self-organized nanostructuring. Adv. Funct. Mater. **11**, 175–178 (2001)
90. Fendrich, M., Wagner, T., Stöhr, M., Möller, R.: Hindered rotation of a copper phthalocyanine molecule on C60: experiments and molecular mechanics calculations. Phys. Rev. B Condens. Matter. **73**, 115433 (2006)
91. Suzuki, H., Yoshida, H., Sakaue, H., Takahagi, T., Tanaka, S., Kamikado, T., Otomo, A.: Flipping behavior of a porphyrin derivative molecule on a Au(111) reconstructed surface. J. Phys. Chem. C. **115**, 12414–12418 (2011)
92. Hao, D., Tang, X., An, Y., Sun, L., Li, J., Dong, A., Shan, X., Lu, X.: Orientation switching of single molecules on surface excited by tunneling electrons and ultrafast laser pulses. J. Phys. Chem. Lett. **12**, 2011–2016 (2021)
93. Heinrich, A.J., Lutz, C.P., Gupta, J.A., Eigler, D.M.: Molecule cascades. Science **298**, 1381–1387 (2002)
94. Liljeroth, P., Repp, J., Meyer, G.: Current-Induced hydrogen tautomerization and conductance switching of naphthalocyanine molecules. Science **317**, 1203–1206 (2007)
95. Kumagai, T., Hanke, F., Gawinkowski, S., Sharp, J., Kotsis, K., Waluk, J., Persson, M., Grill, L.: Controlling intramolecular hydrogen transfer in a porphycene molecule with single atoms or molecules located nearby. Nat. Chem. **6**, 41–46 (2014)
96. Zhang, Y., Kersell, H., Stefak, R., Echeverria, J., Iancu, V., Perera, U.G.E., Li, Y., Deshpande, A., Braun, K.F., Joachim, C., Rapenne, G., Hla, S.W.: Simultaneous and coordinated rotational switching of all molecular rotors in a network. Nat. Nanotechnol. **11**, 706–712 (2016)
97. Wasio, N.A., Slough, D.P., Smith, Z.C., Ivimey, C.J., Thomas, S.W., III., Lin, Y.-S., Sykes, E.C.H.: Correlated rotational switching in two-dimensional self-assembled molecular rotor arrays. Nat Commun. **8**, 16057 (2017)
98. Pace, G., Ferri, V., Grave, C., Elbing, M., von Hänisch, C., Zharnikov, M., Mayor, M., Rampi, M.A., Samorì, P.: Cooperative light-induced molecular movements of highly ordered azobenzene self-assembled monolayers. Proc. Natl. Acad. Sci. U.S.A. **104**, 9937–9942 (2007)
99. Dri, C., Peters, M.V., Schwarz, J., Hecht, S., Grill, L.: Spatial periodicity in molecular switching. Nat. Nanotechnol. **3**, 649–653 (2008)
100. Levy, N., Comstock, M.J., Cho, J., Berbil-Bautista, L., Kirakosian, A., Lauterwasser, F., Poulsen, D.A., Fréchet, J.M.J., Crommie, M.F.: Self-Patterned molecular photoswitching in nanoscale surface assemblies. Nano Lett. **9**, 935–939 (2009)
101. Urgel, J.I., Vijayaraghavan, S., Ecija, D., Auwärter, W., Barth, J.V.: Tetracene confinement in L-methionine gratings on the Ag(111) surface. Surf. Sci. **643**, 87–90 (2016)
102. Bonifazi, D., Spillmann, H., Kiebele, A., de Wild, M., Seiler, P., Cheng, F., Güntherodt, H.-J., Jung, T., Diederich, F.: Supramolecular patterned surfaces driven by cooperative assembly of C60 and porphyrins on metal substrates. Angew. Chem. Int. Ed. **43**, 4759–4763 (2004)
103. Haq, S., Wit, B., Sang, H., Floris, A., Wang, Y., Wang, J., Pérez-García, L., Kantorovitch, L., Amabilino, D.B., Raval, R.: A small molecule walks along a surface between porphyrin fences that are assembled in situ. Angew. Chem. Int. Ed. **54**, 7101–7105 (2015)
104. Meier, D., Adak, A.K., Knecht, P., Reichert, J., Mondal, S., Suryadevara, N., Kuppusamy, S.K., Eguchi, K., Muntwiler, M.K., Allegretti, F., Ruben, M., Barth, J.V., Narasimhan, S., Papageorgiou, A.C.: Rotation in an enantiospecific self-assembled array of molecular raffle wheels. Angew. Chem. Int. Ed. **133**, 27138–27144 (2021)
105. Perera, U.G.E., Ample, F., Kersell, H., Zhang, Y., Vives, G., Echeverria, J., Grisolia, M., Rapenne, G., Joachim, C., Hla, S.-W.: Controlled clockwise and anticlockwise rotational switching of a molecular motor. Nat. Nanotechnol. **8**, 46–51 (2013)